

Dissertation zur Erlangung des Doktorgrades
der Fakultät für Chemie und Pharmazie
der Ludwig-Maximilians-Universität München



Proton-sponge activity and receptor-targeting of
sequence-defined nucleic acid carriers

Ulrich Benjamin Lächelt

aus

Bad Saulgau, Deutschland

2014

Erklärung

Diese Dissertation wurde im Sinne von § 7 der Promotionsordnung vom 28. November 2011 von Herrn Prof. Dr. Ernst Wagner betreut.

Eidesstattliche Versicherung

Diese Dissertation wurde eigenständig und ohne unerlaubte Hilfe erarbeitet.

München, 21.10.2014

.....
Ulrich Lächelt

Dissertation eingereicht am 21.10.2014

1. Gutachter: Prof. Dr. Ernst Wagner

2. Gutachter: Prof. Dr. Wolfgang Frieß

Mündliche Prüfung am 04.12.2014

Meiner Familie

**“We learn wisdom from failure much more than from success.
We often discover what will do, by finding out what will not do;
and probably he who never made a mistake never made a discovery.”**

Samuel Smiles

Table of Contents

1	Introduction	1
1.1	Nucleic acid therapeutics.....	1
1.2	The delivery pathway of non-viral nucleic acid carriers.....	4
1.2.1	Nucleic acid complexation	4
1.2.2	Cellular uptake	6
1.2.3	Endosomal escape.....	7
1.2.4	Intracellular trafficking and cargo release	9
1.3	Sequence-defined nucleic acid carriers	10
1.4	Aims of the thesis	13
2	Materials and Methods	15
2.1	Materials	15
2.1.1	Solvents and reagents.....	15
2.1.2	Buffers.....	18
2.1.3	Equipment for solid-phase synthesis.....	18
2.1.4	Proteins	18
2.1.5	Nucleic acids	19
2.1.6	Cell culture	19
2.2	Methods.....	20
2.2.1	Synthesis of polyamino acid building blocks	20
2.2.2	Resin loading.....	27
2.2.3	Standard solid-phase synthesis conditions	29

2.2.4	Oligomer synthesis.....	33
2.2.5	Oligomer purification	39
2.2.6	Analytics.....	40
2.2.7	Alkalimetric titrations	41
2.2.8	Polyplex formation.....	42
2.2.9	Ethidium bromide exclusion assay	42
2.2.10	Electrophoretic mobility shift assay	43
2.2.11	Particle size and zeta Potential	43
2.2.12	Luciferase reporter gene expression <i>in vitro</i>	44
2.2.13	Luciferase reporter gene expression <i>in vivo</i>	44
2.2.14	Flow cytometry	45
2.2.15	Metabolic activity assay (MTT)	47
2.2.16	Dihydrofolate reductase activity assay	48
2.2.17	Fluorescence microscopy.....	49
2.2.18	Statistical analysis	50
3	Results	51
3.1	The modulation of proton-sponge activity in oligo(ethanamino)amides	51
3.1.1	The protonation of basic polymers and polyamines	51
3.1.2	The proton-sponge activity of different polyamino acids and their combinations with histidine.....	56
3.1.3	The combination of TETA and TEPA based polyamino acids	73
3.1.4	The influence of pyridyl amino acids on the proton-sponge activity.....	79
3.1.5	Iminodiacetic acid derived polyamino acids.....	86

3.2	Targeted and shielded oligo(ethanamino)amides for receptor-specific nucleic acid delivery.....	93
3.2.1	c-Met binding peptides for receptor-specific gene transfer by oligo(ethanamino)amides <i>in vitro</i> and <i>in vivo</i>	96
3.2.2	EGF receptor directed cellular uptake of pDNA polyplexes mediated by mEGF-oligo(ethanamino)amide conjugates	104
3.2.3	Multivalent carbohydrate ligands for asialoglycoprotein receptor directed gene transfer by oligo(ethanamino)amides	110
3.2.4	Methotrexate polyglutamates as dual-functional ligands in oligo(ethanamino)amides for cytotoxic poly(I:C) delivery	116
4	Discussion	127
4.1	The modulation of proton-sponge activity in oligo(ethanamino)amides ..	127
4.2	Targeted and shielded oligo(ethanamino)amides for receptor-specific nucleic acid delivery.....	132
5	Summary	138
6	Appendix	140
6.1	Abbreviations.....	140
6.2	Sequences of peptidic targeting ligands	143
6.3	Summary of SPS derived oligomers.....	143
6.4	Analytical Data.....	145
6.4.1	Building blocks	145
6.4.2	Oligomers.....	150
7	References	169
8	Publications	185
9	Acknowledgements.....	189

1 Introduction

This chapter is intended to give a brief introduction into the research field and to put the experimental data of the following chapters into a broader context. It is not considered to be a complete review of the whole scientific area.

1.1 Nucleic acid therapeutics

Since the elucidation of the molecular structure of nucleic acids by Francis Crick, James Watson, Maurice Wilkins and Rosalind Franklin [1-3] and the realization of their role in encoding, transfer and translation of genetic information [4-6], the knowledge about nucleic acid biology has increased continuously. The decryption of the human genome and the development of new sequencing technologies enabled the identification of disease causative or associated genes and thereby had enormous impact on the biomedical research [7-9]. The classical gene therapy, in terms of the substitution of deficient genes by transfer of genetical material, was the first concept for the therapeutic usage of nucleic acids [10, 11]. After two decades with over 2000 completed, ongoing or approved clinical gene therapy trials worldwide ([12], June 2014), finally the first gene therapeutic treatment (alipogene tiparvovec, Glybera[®]) got marketing authorization by the European Commission in 2012 [13]. In addition, more and more biological roles of RNA, beyond the central dogma of molecular biology, have been identified [14, 15]. Non-coding RNA, such as miRNA, siRNA, piRNA, snRNA, riboswitches, self-cleaving ribozymes or antisense transcripts, serve as specific endogenous regulators of gene expression [16-22], whereas species such as rRNA, snoRNA, telomeric RNA [23-25] and many more play important roles in several other cellular processes. The increasing knowledge about the diverse biological functions of RNA on the one hand represents an additional level for the understanding of cellular homeostasis and disease associated malfunctions, on the other hand opens new possibilities for precise therapeutic interventions by using nucleic acids as drugs. For that reason, RNA therapeutics have attracted much attention in the medical research and drug development. An alternative approach to the delivery of DNA, for the restoration or extension of the proteome, represents direct transfer of mRNA, which does not require transport and

transcription in the nucleus [26-28]. The complementary effect on protein expression can be achieved by the use of antisense oligonucleotides, which suppress translation of the target mRNA by either steric-blocking or RNase H dependent degradation [29]. Fomivirsen (Vitravene[®]), a 21-mer oligonucleotide with complementary sequence to the mRNA transcript of a cytomegalovirus (CMV) gene, represents the first marketed antisense therapeutic, which received FDA approval for the local treatment of CMV retinitis in 1998 [29]. In contrast to the antisense mechanism, based on the equimolar annealing of single-stranded oligonucleotides, double-stranded RNA (dsRNA) can mediate degradation of target RNA in a catalytic fashion by activation of the RNA-induced silencing complex (RISC). The underlying mechanism of RNA interference (RNAi), first discovered with rather long dsRNA in *C. elegans* [30], was transferred to the silencing of target genes in human cells by introduction of the small interfering RNA (siRNA) [31]. The highly efficient gene knock-down by RNAi opened the possibility of a specific modulation of gene expression and therefore raised great expectations for the usage in molecular medicine [32]. Other examples of nucleic acid species with great therapeutic potential are splice-switching oligonucleotides (SSOs), which entered clinical trials for the treatment of Duchenne muscular dystrophy [33] and immunostimulatory nucleic acids, such as cytosine-phosphate-guanosine (CpG) oligodeoxynucleotides [34, 35] or polyinosinic-polycytidylic acid poly(I:C) [36, 37]. The intracellular delivery of the synthetic dsRNA poly(I:C) simulates a viral infection and mediates immune response by activation of membrane-bound and cytosolic pattern recognition receptors, such as the dsRNA dependent protein kinase (PKR), Toll-like receptor 3 (TLR3), retinoic acid-inducible gene 1 (RIG-I) and melanoma differentiation-associated gene 5 (MDA5) [38]. A great potential of poly(I:C) for apoptosis induction and tumor cell killing in cancer immunotherapy approaches has been shown in several cases [39-41]. Another remarkable nucleic acid class is represented by aptamers, which bind target molecules with affinities comparable to antibodies, but can be engineered *in vitro* using evolutionary selection processes [42, 43] and are readily accessible by chemical synthesis [44]. The PEGylated anti-vascular endothelial growth factor (VEGF) aptamer pegaptanib (Macugen[®]), which received FDA approval for the treatment of age-related macular degeneration (ARMD) in 2004, represents the first aptamer based therapeutic on the market, and several more are in preclinical or clinical development stages currently [45]. Since RNA exhibits a very low chemical and enzymatic stability, numerous

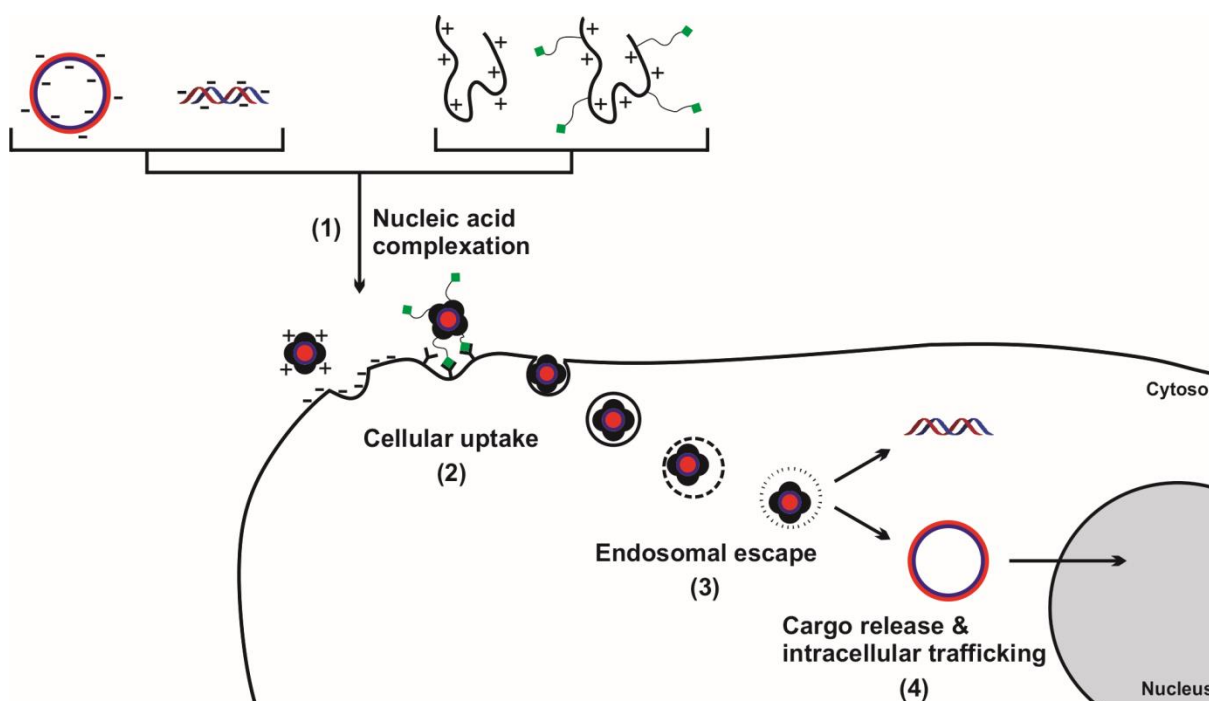
chemical modifications have been developed in order to improve the pharmacokinetic and pharmacodynamic properties or to reduce immunogenicity [46]. Prevalent strategies include phosphorothioate backbone modification, 2'-O-methyl, 2'-O-methoxyethyl or 2'-fluoro sugar modifications, 2'-O, 4'-C-methylene bridges (locked nucleic acid, LNA) and L-ribose oligonucleotides (spiegelmers) [33, 46, 47]. In addition, neutral nucleic acid analogs, such as peptide nucleic acid (PNA) or phosphorodiamidate morpholino oligomer (PMO) are used for antisense or splice-correction therapy approaches [48, 49].

Although the drug-like properties of nucleic acids can be adjusted by chemical modifications, the efficient and specific intracellular delivery of these macromolecular compounds remains a major limitation for therapeutic applications and therefore requires appropriate carrier systems. Viruses, which have been optimized by nature for the purpose of nucleic acid transfer into host cells, currently are the most investigated vectors for gene therapy. Over two-thirds of the clinical trials worldwide are based on viral delivery systems [12, 50]. However, despite their high efficiency, viral vectors also exhibit some serious drawbacks, such as immunogenicity, limited cargo capacity, virus-type depending cell tropism, sophisticated production and the inherent risk of reversion to wild-type or replication-competent virions [51, 52]. The complementary approach, to the modification of natural viruses, is based on the bottom-up development of 'artificial viruses' by synthetic chemistry [53, 54]. The high design flexibility, without restriction to natural building units, offers the possibility to engineer synthetic nucleic acid carriers with tailor-made properties. Moreover, scalable chemical strategies and drug formulation technologies can be used for the production [55-58]. However, the efficiency of current synthetic delivery systems is still low, compared to the viral counterparts. In order to develop improved nucleic acid carriers, the delivery pathway and the individual hurdles have to be considered in detail.

1.2 The delivery pathway of non-viral nucleic acid carriers

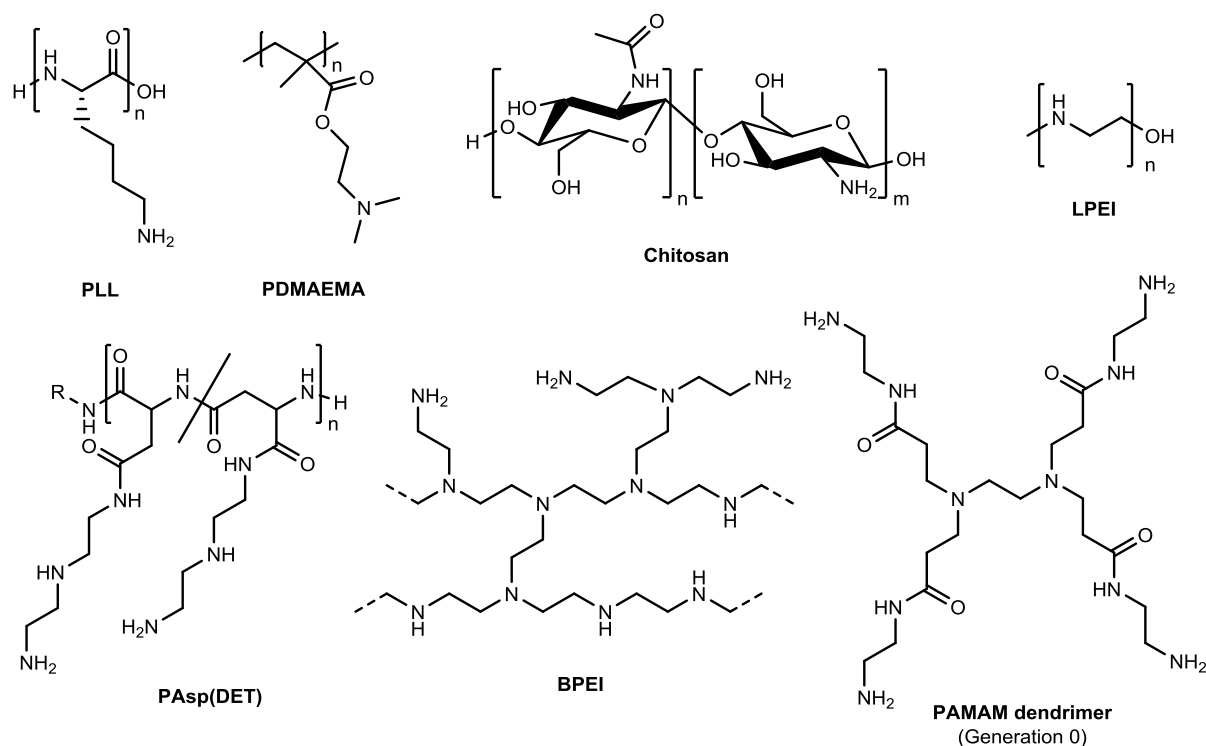
Several barriers are faced and have to be overcome by non-viral nucleic acid carriers for efficient intracellular delivery. Scheme 1.1 shows a simplified illustration of the rather complex delivery pathway passed by polymer-based systems. In the following chapters, the particularly critical steps, nucleic acid complexation (1), (specific) cellular uptake (2), endosomal escape (3), cargo release and intracellular trafficking (4), are described and discussed individually.

Scheme 1.1 The cellular delivery pathway of polymer-based nucleic acid carriers



1.2.1 Nucleic acid complexation

Since free nucleic acids are rapidly cleared from the blood stream, they have to be complexed and condensed to form particles, which increase the circulation time and protect the payload against nucleases. A convenient and frequently used mechanism is based on the ionic interaction between the negatively charged nucleic acid and multivalent cations. The nucleic acid condensation by positively charged polymers is an entropy driven process and produces nanosized complexes, called 'polyplexes' [59, 60]. Scheme 1.2 shows some examples of nucleic acid binding polymers.

Scheme 1.2 Basic polymers used for nucleic acid complexation and delivery

PLL, poly-L-lysine [61]; PDMAEMA, poly[(2-dimethylamino)ethyl methacrylate] [62]; chitosan, (partially) deacetylated chitin [63]; LPEI, linear polyethylenimine prepared by hydrolysis of poly(2-ethyl-2-oxazoline) [64]; PAsp(DET), diethylene triamine *N*-substituted polyaspartamide [65]; BPEI, branched polyethylenimine [66], PAMAM, poly(amido)amine dendrimer [67].

The size of nanoparticles for a systemic administration is a critical parameter with big impact on the pharmacokinetics and biodistribution. Particles with a hydrodynamic diameter of 5.5 nm and below are rapidly cleared by the kidneys [68]. Particle sizes of up to 400 nm can facilitate accumulation in highly vascularized solid tumors, as a result of the enhanced permeability and retention (EPR) effect based on particle passage through leaky vessels in the tumor tissue [69]. However, the extent of passive accumulation and the size-threshold of the porous tumor vasculature depend on the certain type of cancer [70, 71]. As reported by Cabral et al., within a set of polymeric micelles with hydrodynamic diameters ranging from 30 to 100 nm, only the smallest were able to accumulate in poorly permeable pancreatic tumors, whereas all micelles showed comparable penetration in another tumor model. The polyplex stability in biological fluids is an additional serious issue, since the interaction with proteins and electrolytes can cause polyplex dissociation due to counter ion

exchange. Stable packaging predominantly depends on the size and charge density of the cationic polymer, but can be improved by crosslinking or the introduction of hydrophobic elements [72-79].

1.2.2 Cellular uptake

Although it has been shown that the injection of naked nucleic acids under hydrodynamic pressure can mediate *in vivo* transfection [80, 81], in general the cellular uptake of free DNA and RNA is very low. The nucleic acid complexation by cationic polymers produces particles with positive surface potential, which can induce internalization by electrostatic interaction with the negatively charged cell membrane (cf. Scheme 1.1). However, this adsorptive endocytosis mechanism is rather unspecific and less efficient than a receptor-mediated uptake route [82, 83]. Therefore, the attachment of targeting ligands to exposed parts of the polyplexes is a convenient approach to enhance cellular internalization in a receptor-specific fashion. The selection of appropriate target-receptors depends on the individual expression of the target-cells. Since oncogenic transformation generally is accompanied by excessive proliferation and a high metabolic activity [84], transport proteins for the uptake of nutrients and cofactors, such as the folate receptor (FR) and transferrin receptor (TfR), are frequently overexpressed in various types of cancer and can be used for a receptor-mediated uptake into tumor cells [61, 85-88]. Other receptors for tumor-targeted delivery are represented by growth factor receptors [39, 40, 83, 89, 90] or integrins [91-93]. In addition, the physiological tissue-specific expression of membrane proteins, such as the asialoglycoprotein receptor (ASGPR), which is exclusively expressed by parenchymal hepatocytes [94], can be used for the targeted delivery to cells without malignant transformation [95-97]. The parameter predominantly determining the potency of a homing ligand is its affinity toward the target receptor. However, ligands can also vary in the triggered uptake mechanism, efficiency and kinetic, e.g. depending on simple receptor binding or additional activation of a signaling cascade [83, 98]. The cell binding potency can be strongly increased by the exposure of multiple ligands on the nanoparticle surface, which results in an avidity due to multivalent interactions [99-101]. Moreover, the combination of different ligands, binding to different surface-receptors of the target-

cells, can enhance both the internalization rate as well as the selectivity of the delivery devices [102-104].

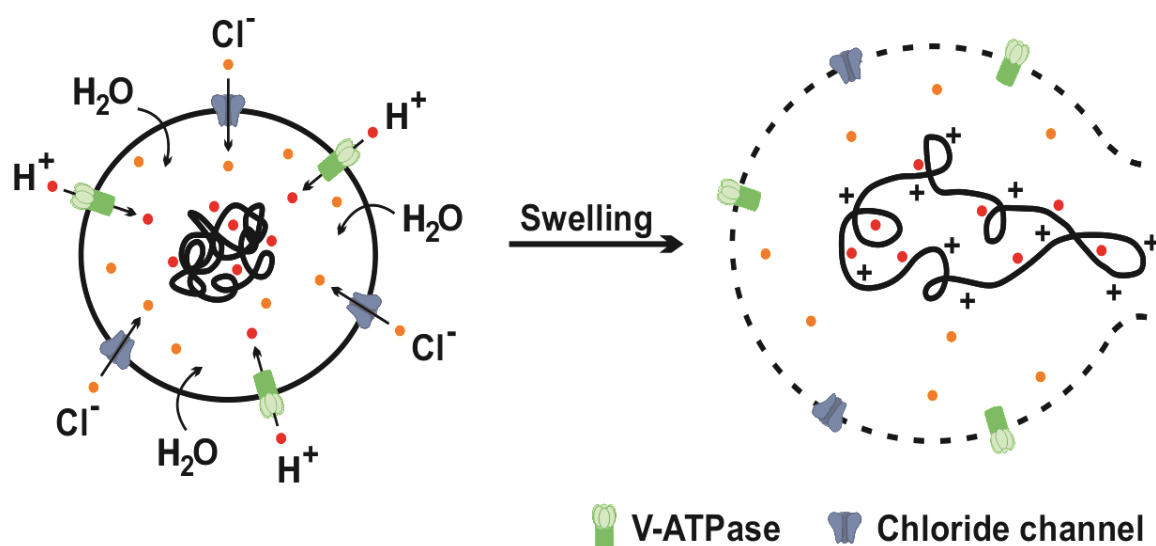
In case of positively charged polyplexes, the selectivity due to the usage of targeting ligands can partly be impaired by unspecific ionic interactions. Therefore, the introduction of targeting ligands is frequently combined with the attachment of hydrophilic molecules, which shield the surface potential from the exterior environment. The most common shielding agent is polyethylene glycol (PEG), which efficiently reduces unspecific interactions with non-target cells or blood components and increases the circulation time of nanoparticles [105]. However, some safety concerns about the use of PEG in repeatedly administered drug formulations have been raised. The non-biodegradability and tissue accumulation of PEG, as well as the formation of anti-PEG antibodies [106, 107] gave reason for the investigation of alternatives. Examples for alternative hydrophilic polymers, used in the context of nucleic acid delivery, are hydroxyethyl starch (HES), polysarcosine or poly[*N*-(2-hydroxypropyl) methacrylamide] (polyHPMA) [108-110].

1.2.3 Endosomal escape

After cellular uptake by an endocytic process, the next barrier within the delivery pathway is represented by endosomes. These intracellular vesicles are the major site for the sorting, trafficking and recycling of endocytosed material [111, 112]. Vacuolar ATPases (V-ATPases) generate a proton gradient with a luminal pH between approx. 5.9 and 6.5 of early endosomes (sorting endosomes and endocytic recycling compartment) and down to pH 5.0 of late endosomes and lysosomes [112]. The entrapped polyplexes have to be released from the vesicles to reach the site of action and to evade recycling to the cell membrane or degradation in late endo- and lysosomes. The endosomal escape is considered to be a major limitation for the intracellular delivery of macromolecules. Several strategies have been exploited in order to improve the endosomal escape of non-viral nucleic acid carriers, such as the conjugation of endosome-disruptive adenovirus [113], incorporation of lytic or fusogenic peptides (e.g. hemagglutinin derived Inf7 [114, 115], melittin from apitoxin [116, 117], synthetic KALA or GALA [118-120]), hydrophobic membrane destabilization [121] or photochemical internalization [122, 123]. Lysosomotropic

chloroquine is widely used as an endosomolytic cell culture agent to enforce the endosomal escape *in vitro* [124-126]. However, nucleic acid delivery systems containing chloroquine or other quinolone derivatives as an integral part have also been developed [127, 128]. The rather weak and hydrophobic base chloroquine can enter endo- and lysosomes, gets protonated and thereby accumulates in the acidic vesicles. Hypothesized mechanisms for the enhanced endosomal escape are the generation of osmotic pressure and vesicle swelling as well as the inhibition of endosome maturation due to pH buffering [111, 129]. In contrast to several other basic, nucleic acid binding polymers, polyethylenimine (PEI) exhibits a potent intrinsic endosomal escape performance and high transfection efficiency. The proposed mechanism relies on the presence of unprotonated basic groups at physiological pH, which generate a buffer capacity in the acidic endosomal environment. Buffering of the endosomal pH triggers an intensified active transport of protons by V-ATPases, accompanied by the passive diffusion of chloride counterions. In consequence of the increased osmotic pressure, water flows into the vesicles, causes endosome swelling and finally rupture. A simplified illustration of the described 'proton-sponge' mechanism, first proposed by Jean-Paul Behr [130], is shown in Scheme 1.3.

Scheme 1.3 The hypothesized proton-sponge effect, facilitating endosomal escape due to osmotic pressure and vesicle burst



Mechanistic studies, supporting the proton-sponge hypothesis, have been reported. Kichler et al. investigated the impact of endosome acidification on PEI mediated gene transfer [131]. The use of V-ATPase inhibitors during PEI-transfections displayed a clear dependency of reporter gene expression on endosomal acidification. Moreover, since PEI did not exhibit a hemolytic activity in erythrocyte leakage assays at neutral or acidic pH, the underlying mechanism indeed seems to be different from those of lytic or fusogenic peptides. Various reports about beneficial effects of an increased endosomal buffer capacity on endosomal escape and transfection efficiency can be found in the literature [65, 132-134]. Histidines or other imidazole derivatives with a pK_a around 6 have been shown to be useful motifs for an increase of endosomal buffer capacity [132-134]. However, there is also some debate about mechanistic details of the proton-sponge hypothesis [135-138]. Alternative mechanisms suggest a protonation-dependent membrane permeabilisation due to the interaction with cationized polyplexes, rather than complete osmotic burst of the vesicles [136, 137]. But also in this case a proton-sponge driven increase of osmotic pressure and membrane tension could be part of the mechanism [136].

1.2.4 Intracellular trafficking and cargo release

Depending on the type of transported nucleic acid, the site of action differs. Delivery of pDNA or splice-correcting oligonucleotides has its destination in the nucleus, whereas the targets of antisense therapeutics, siRNA or miRNA are located in the cytosol. Capecchi reported that transgene expression can be observed in 50-100 % of cells treated with a direct intranuclear microinjection of DNA, whereas the efficiency of cytoplasmic injections was less than 0.1 % [139]. This makes clear that DNA has to be guided to the nucleus. Fortunately, polyplexes can mediate nuclear uptake of DNA with efficiencies depending on the individual transfecting agents [140-142]. In addition, there have been several attempts to further enhance the DNA transfection efficiency by the conjugation of nuclear localization signal (NLS) peptides [143, 144]. However, the detailed mechanisms of intracellular trafficking and peptide directed nuclear entry are not entirely clear and the benefit of NLS peptides on gene transfer is controversial [145-147].

As mentioned in chapter 1.2.1, the polyplex stability is a critical issue - also in context of intracellular trafficking and cargo release. Since the nucleic acid has to be liberated at the target site, high stability and strong binding does not necessarily correlate with transfection efficiency. Itaka et al. reported intracellular trafficking studies of pDNA polyplexes with poly-L-lysine (PLL), linear PEI (LPEI) or branched PEI (BPEI). In contrast to PLL, both LPEI and BPEI were capable of mediating endosomal escape, but differed in the subsequent pDNA release. The disintegration of LPEI polyplexes correlated with a higher and faster transgene expression compared to the BPEI polyplexes with restricted cargo release [148]. For this reason, the particle firmness has to be balanced between a sufficient extracellular polyplex stability, but fast and complete nucleic acid release at the target site. An elaborate approach to combine these opposing prerequisites is represented by 'smart' delivery vehicles with dynamic response to environmental changes, such as the translocation into the cell. The approx. 100- to 1000-fold elevated intracellular glutathione (GSH) levels generate a reduction potential, which can serve as a stimulus for a redox-driven disassembly of nucleic acid carriers [149]. Widely used structural motifs for this purpose are bio-reducible disulfide-crosslinks [149-151]. It has been shown in numerous cases that the integration of thiols or disulfide-bridges can offer several advantages, such as polyplex stabilization, redox-triggered disassembly and a reduction of cytotoxicity due to the biodegradability into smaller units [74-76, 152-155].

1.3 Sequence-defined nucleic acid carriers

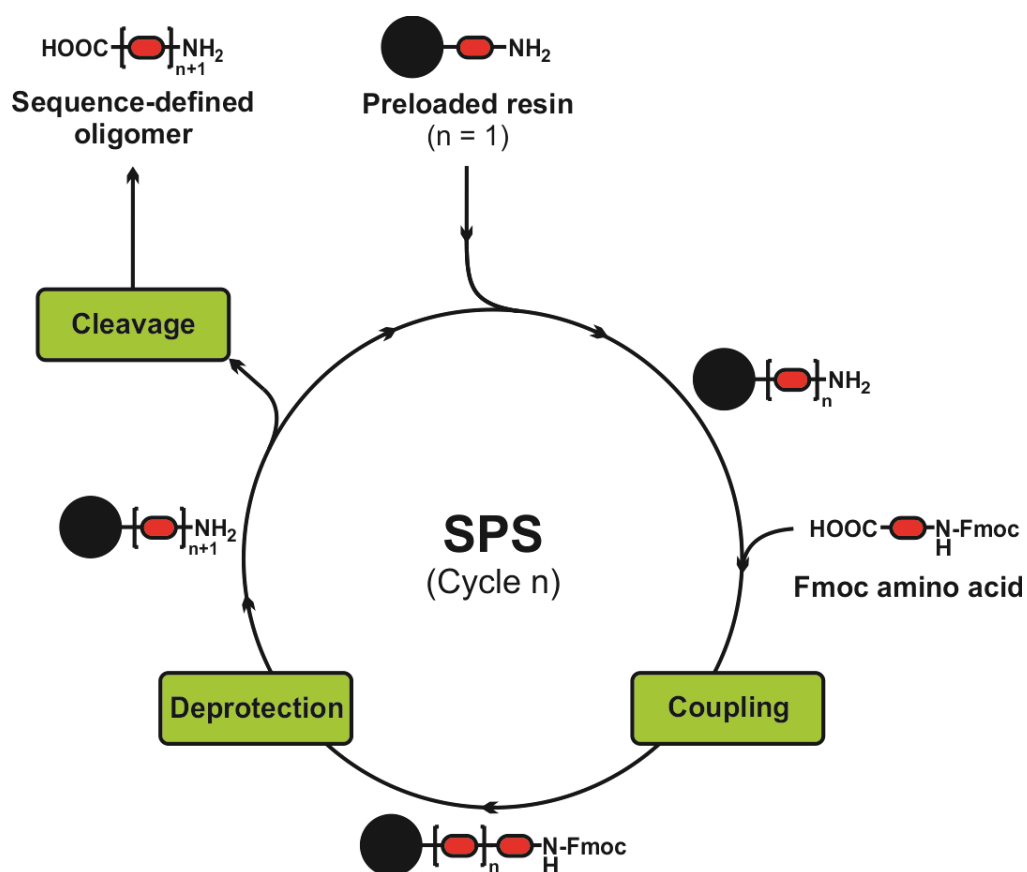
As described in chapter 1.2, several barriers have to be overcome within the nucleic acid delivery pathway. Just like natural viruses, artificial nucleic acid carriers have to be multifunctional, bio-responsive to a changing environment and precise [55]. However, the production of multifunctional materials and the investigation of clear-cut structure-activity relationships require a precise synthetic strategy and definite compound identification. The properties of a macromolecular compound are not necessarily determined alone by the presence of certain subunits. The exact size, topology (linear, branched, comb, dendrimeric, etc.) and order of subunits can play additional important roles for the biological activity [156-159]. In case of oligomers with multiple different subunits, a maximal degree of precision is achieved by

'sequence-definition', where a sequence can be used for the unique compound identification and definite discrimination between isomers. It provides all compound information and descriptive parameters, such as the monodisperse molecular weight, exact monomer order, orientation and topology. Especially in context of synthetic materials for clinical application and their regulatory compliance, this high degree of precision, reproducibility and compound identification is desirable.

New polymerization strategies have shown their applicability for the production of multifunctional, 'well-defined' polymers for nucleic acid delivery [160-163]. This high degree of definition generally implies a narrow size-distribution, low polydispersity, controlled architecture and subunit composition. Nevertheless, microstructures, such as the exact order of monomers and subunits, are still hard to control in statistical polymerization reactions [164]. Therefore, the expression 'sequence-defined' suggests a sequential assembly of the compounds. Recently, an intriguing concept of template-assisted synthesis has been reported, where monomers are converted into sequence-defined oligomers in a single step due to a sequence-specific pre-arrangement at a DNA template [165]. But also here, at least the template, which provides the sequence information, has to be prepared in a sequential manner. Solid-phase peptides synthesis, invented by Robert Bruce Merrifield [166], is a famous example of a highly efficient sequential oligomer synthesis. Hartmann et al. developed a solid-phase supported synthesis of sequence-defined oligo(amidoamines) by alternating coupling of diacids and diamines [167, 168]. Schaffert et al. extended this strategy by establishing artificial polyamino acids (PAA) with appropriate protecting groups for complete compatibility with common Fmoc solid-phase synthesis (SPS) [169]. Scheme 1.4 shows the chemical structures of the polyamino acids in protected and unprotected form; scheme 1.5 represents a simplified illustration of the SPS approach.

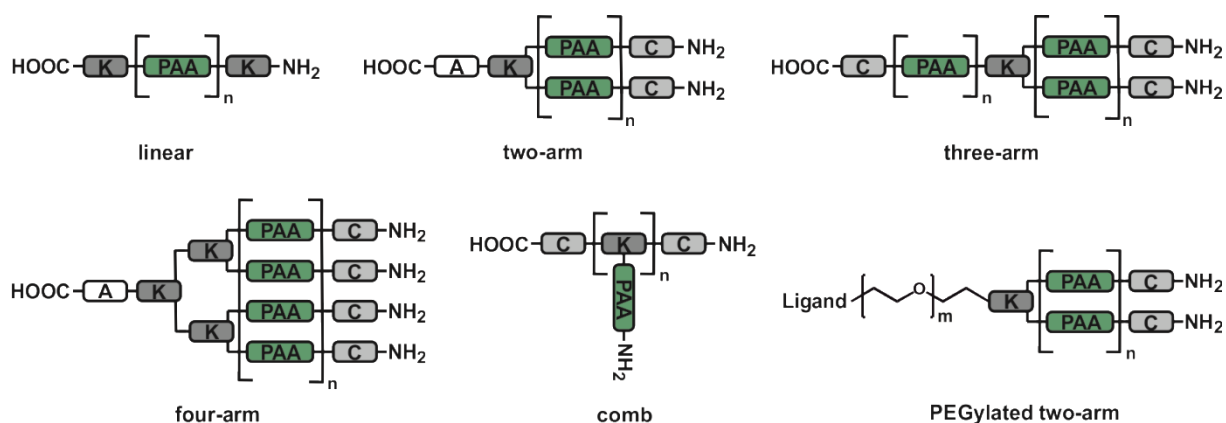
Scheme 1.4 Artificial polyamino acids for the SPS of sequence-defined oligo(ethan-amino)amides**Fmoc-Gtt(Boc₂)-OH** (n=2, m=3)**Fmoc-Stp(Boc₃)-OH** (n=3, m=2)**Fmoc-Gtp(Boc₃)-OH** (n=3, m=3)**Fmoc-Sph(Boc₄)-OH** (n=4, m=2)**Gtt** (n=2, m=3)**Stp** (n=3, m=2)**Gtp** (n=3, m=3)**Sph** (n=4, m=2)

Gtt, glutaryl-triethylene tetramine; Stp, succinyl-tetraethylene pentamine; Gtp, glutaryl-tetraethylene pentamine; Sph, succinyl-pentaethylene hexamine.

Scheme 1.5 Illustration of the Fmoc SPS approach

Using the artificial PAA building blocks together with commercially available Fmoc α -amino acids, a multitude of sequence-defined oligo(ethan-amino)amides has been synthesized. Scheme 1.6 shows examples of some published oligomer architectures. Reported topologies, which were realized with the SPS strategy, include oligomers with linear [154, 170], two-arm [115], three-arm [170], four-arm [155] and comb architectures [159] as well as PEGylated two-arm compounds with targeting ligands [115, 126]. Branching points were introduced by lysines, which provide two amines after deprotection during synthesis. Additional cysteines served for the lateral polyplex stabilization based on the formation of bio-reducible disulfides.

Scheme 1.6 Examples of published oligomer topologies realized by the SPS strategy



PAA, polyamino acid; A, alanine; C, cysteine; K, lysine.

1.4 Aims of the thesis

Despite expectations that therapeutic nucleic acids will be innovative biopharmaceuticals with diverse clinical applications, only a few examples have so far received marketing authorization. A major hurdle for the development of nucleic acid based drugs is the safe and efficient intracellular delivery. Polymer-based nucleic acid carriers face several barriers within their delivery pathway. Particularly critical steps are stable nucleic acid complexation, cellular uptake, endosomal escape and intracellular cargo release at the target site. Therefore, efficient nucleic acid carriers have to combine multiple functionalities, which are optimized to overcome each of the separate hurdles. The recently established solid-phase synthesis platform

for the assembly of sequence-defined oligo(ethanamino)amides allows the design of nucleic acid carriers with precise architectures, containing different modules and functionalities. Using this modular assembly approach, the thesis focuses on the optimization of the proton-sponge activity and specific receptor-mediated uptake of polyplexes.

The first aim of the thesis was the development of strategies to modulate the endosomal buffering of oligo(ethanamino)amides and the investigation of their impact on gene transfer efficiency. For this purpose, the individual protonation characteristics of different polyamino acid building blocks and the influence of additional heterocyclic amino acids with low pK_a , such as histidine and pyridylalanine, had to be examined. The oligomer basicity and endosomal protonation was to be correlated with the activity in different stages of pDNA delivery, especially the endosomal escape. The structure-activity relationship studies aimed at the identification of important parameters and suitable strategies to achieve a beneficial endosomal buffering and enhanced proton-sponge activity of pDNA polyplexes *in vitro* and *in vivo*.

The second aim was the combination of the sequence-defined oligo(ethanamino)amides with a set of heterogeneous receptor-targeting ligands to investigate the compatibility of the nucleic acid carrier platform with ligands of diverse chemical nature. Peptides, a protein, multivalent carbohydrates and small molecules were to be used as ligands. After establishment of required synthetic strategies, the most potent candidate within each group had to be identified in structure-activity relationship studies.

As a final aim, the results of the two separate optimization processes were to be combined in selected cases to generate efficient nucleic acid carriers with improved proton-sponge activity and a receptor-specific targeting.

2 Materials and Methods

2.1 Materials

2.1.1 Solvents and reagents

For all experimental procedures solvents and reagents in high quality were used. Table 2.1 and 2.2 summarize the used solvents and reagents together with their unique CAS numbers and the sources of supply.

Table 2.1 Solvents used for experimental procedures

Solvent	CAS-No.	Source
1,4-Dioxane ¹	123-91-1	BASF (Ludwigshafen a. Rh., Germany) ^a
Acetonitrile ²	75-05-8	VWR Int. (Darmstadt, Germany)
Chloroform ³	67-66-3	VWR Int. (Darmstadt, Germany)
Chloroform-d ⁴	865-49-6	Euriso-Top (Saint-Aubin Cedex, France)
Deuterium oxide ⁴	7789-20-0	Euriso-Top (Saint-Aubin Cedex, France)
Dichloromethane ⁵	75-09-2	Bernd Kraft (Duisburg, Germany)
<i>N,N</i> -Dimethylformamide ⁶	68-12-2	Iris Biotech (Marktredewitz, Germany)
Dimethyl sulfoxide ⁷	67-68-5	Sigma-Aldrich (Munich, Germany)
Ethanol absolute ⁵	64-17-5	VWR Int. (Darmstadt, Germany)
Ethyl acetate ⁸	141-78-6	Staub & Co. (Nürnberg, Germany)
n-Heptane ¹	142-82-5	Grüssing (Filsum, Germany)
n-Hexane ¹	110-54-3	Brenntag (Mülheim/Ruhr, Germany)
Methanol ⁵	67-56-1	Fisher Scientific (Schwerte, Germany)
Methanol-d ₄ ⁴	811-98-3	Euriso-Top (Saint-Aubin Cedex, France)
Methyl- <i>tert</i> -butyl ether ⁹	1634-04-4	Brenntag (Mülheim/Ruhr, Germany)
<i>N</i> -Methyl-2-pyrrolidone ⁶	872-50-4	Iris Biotech (Marktredewitz, Germany)
Tetrahydrofuran ⁵	109-99-9	Fisher Scientific (Schwerte, Germany)
Water ¹⁰	7732-18-5	In house purification

¹ purissimum; ² HPLC grade; ³ DAB grade, distilled before use; ⁴ NMR grade (> 99.9 %); ⁵ analytical grade; ⁶ peptide grade; ⁷ BioReagent grade (> 99.9 %); ⁸ purum, distilled before use; ⁹ synthesis grade, distilled before use; ¹⁰ purified, deionized; ^a 1,4-Dioxane was kindly provided by BASF as donation to the LMU.

Table 2.2 Reagents used for experimental procedures

Reagent	CAS-No.	Source
1,3-Diaminopropane · 2 HCl	10517-44-9	Sigma-Aldrich (Munich, Germany)
1,4-Diaminobutane · 2 HCl	333-93-7	Sigma-Aldrich (Munich, Germany)
1,5-Diaminopentane · 2 HCl	1476-39-7	Sigma-Aldrich (Munich, Germany)
1,6-Diaminohexane	124-09-4	Alfa Aesar (Karlsruhe, Germany)
1-Hydroxybenzotriazole hydrate	123333-53-9	Sigma-Aldrich (Munich, Germany)
2,2,2-Trifluoroethylamine · HCl	373-88-6	Alfa Aesar (Karlsruhe, Germany)
2-Chlorotriylchloride resin	42074-68-0	Iris Biotech (Marktredewitz, Germany)
4-[[[(2,4-diamino-6-pteridinyloxy)methyl]methylamino] benzoic acid	19741-14-1	Clauson-Kass A/S (Farum, Denmark)
Alexa Fluor® 488 NHS ester	-	Life Technologies (Darmstadt, Germany)
Ammoniumhydroxide solution	1336-21-6	Carl Roth (Karlsruhe, Germany)
Boc-L-Cys(Trt)-OH	21947-98-8	Iris Biotech (Marktredewitz, Germany)
Boric acid	10043-35-3	Sigma-Aldrich (Munich, Germany)
BPEI	25987-06-8	Sigma-Aldrich (Munich, Germany)
Bromophenol blue	115-39-9	Sigma-Aldrich (Munich, Germany)
Chloroacetic acid	79-11-8	Sigma-Aldrich (Munich, Germany)
Chloroquine diphosphate	50-63-5	Sigma-Aldrich (Munich, Germany)
D-(+)-Glucose monohydrate	14431-43-7	Merck Millipore (Darmstadt, Germany)
DBCO-PEG ₅ -NHS	-	Jena Bioscience (Jena, Germany)
DBU	6674-22-2	Sigma-Aldrich (Munich, Germany)
Dde-L-Lys(Fmoc)-OH	156648-40-7	Iris Biotech (Marktredewitz, Germany)
Diethylene triamine	111-40-0	Sigma-Aldrich (Munich, Germany)
EDTA disodium salt dihydrate	6381-92-6	Sigma-Aldrich (Munich, Germany)
Ethylene diamine	107-15-3	Sigma-Aldrich (Munich, Germany)
Fmoc-L-5ANV-OH	1097192-04-5	Sigma-Aldrich (Munich, Germany)
Fmoc-L-3PAL-OH	175453-07-3	Iris Biotech (Marktredewitz, Germany)
Fmoc-L-4PAL-OH	169555-95-7	Iris Biotech (Marktredewitz, Germany)
Fmoc-L-Ala Wang resin LL	-	Merck Millipore (Darmstadt, Germany)
Fmoc-L-Ala-OH	35661-39-3	Iris Biotech (Marktredewitz, Germany)
Fmoc-L-Arg(Pbf)-OH	154445-77-9	Iris Biotech (Marktredewitz, Germany)
Fmoc-L-Asp(OtBu)-OH	71989-14-5	Iris Biotech (Marktredewitz, Germany)
Fmoc-L-Cys(Trt)-OH	103213-32-7	Iris Biotech (Marktredewitz, Germany)
Fmoc-L-Glu-OtBu	84793-07-7	Merck Millipore (Darmstadt, Germany)
Fmoc-L-Gly-OH	29022-11-5	Iris Biotech (Marktredewitz, Germany)
Fmoc-L-His(Trt)-OH	109425-51-6	Iris Biotech (Marktredewitz, Germany)
Fmoc-L-Ile-OH	71989-23-6	Iris Biotech (Marktredewitz, Germany)
Fmoc-L-Leu-OH	35661-60-0	Iris Biotech (Marktredewitz, Germany)
Fmoc-L-Lys(Boc)-OH	71989-26-9	Iris Biotech (Marktredewitz, Germany)
Fmoc-L-Lys(Fmoc)-OH	78081-87-5	Iris Biotech (Marktredewitz, Germany)
Fmoc-L-Lys(ivDde)-OH	204777-78-6	Iris Biotech (Marktredewitz, Germany)
Fmoc-L-Phe-OH	35661-40-6	Iris Biotech (Marktredewitz, Germany)
Fmoc-L-Pro-OH monohydrate	71989-31-6	Iris Biotech (Marktredewitz, Germany)
Fmoc-L-Ser(tBu)-OH	71989-33-8	Iris Biotech (Marktredewitz, Germany)

Fmoc-L-Trp(Boc)-OH	43824-78-6	Iris Biotech (Marktredewitz, Germany)
Fmoc-L-Tyr(tBu)-OH	71989-38-3	Iris Biotech (Marktredewitz, Germany)
Fmoc-L-Val-OH	68858-20-8	Iris Biotech (Marktredewitz, Germany)
Fmoc- <i>N</i> -amido-dPEG ₂₄ -acid	756526-01-9	Quanta Biodesign (Powell, Ohio, USA)
Fmoc-OSu	82911-69-1	Iris Biotech (Marktredewitz, Germany)
GelRed	-	Biotium Inc. (Hayward, CA, USA)
HBTU	94790-37-1	Multisyntech (Witten, Germany)
HEPES	7365-45-9	Biomol (Hamburg, Germany)
Hydrazine monohydrate	7803-57-8	Sigma-Aldrich (Munich, Germany)
Hydrochloric acid solution (1 M)	7647-01-0	Sigma-Aldrich (Munich, Germany)
Iminodiacetic acid	142-73-4	Sigma-Aldrich (Munich, Germany)
LPEI	9002-98-6	In house synthesis [89]
Methylamine · HCl	593-51-1	Sigma-Aldrich (Munich, Germany)
Methyliminodiacetic acid	4408-64-4	Sigma-Aldrich (Munich, Germany)
MTT	298-93-1	Sigma-Aldrich (Munich, Germany)
<i>N,N'</i> -Dicyclohexylcarbodiimide	538-75-0	Sigma-Aldrich (Munich, Germany)
<i>N,N</i> -Diisopropylethylamine	7087-68-5	Iris Biotech (Marktredewitz, Germany)
<i>N</i> ¹⁰ -(Trifluoroacetyl)pteroic acid	37793-53-6	Clauson-Kass A/S (Farum, Denmark)
Ninhydrin	485-47-2	Sigma-Aldrich (Munich, Germany)
Pentaethylene hexamine	4067-16-7	Sigma-Aldrich (Munich, Germany)
Phenol	108-95-2	Sigma-Aldrich (Munich, Germany)
Piperidine	110-89-4	Iris Biotech (Marktredewitz, Germany)
Poly-L-arginine · HCl	26982-20-7	Sigma-Aldrich (Munich, Germany)
Poly-L-histidine	26062-48-6	Sigma-Aldrich (Munich, Germany)
Poly-L-lysine · HBr	25988-63-0	Sigma-Aldrich (Munich, Germany)
Potassium cyanide	151-50-8	Sigma-Aldrich (Munich, Germany)
Pybop [®]	128625-52-5	Multisyntech GmbH (Witten, Germany)
Pyridine	110-86-1	Sigma-Aldrich (Munich, Germany)
Sephadex [®] G-10	9050-68-4	GE Healthcare (Freiburg, Germany)
Sodium hydroxide (anhydrous)	1310-73-2	Sigma-Aldrich (Munich, Germany)
Sodium hydroxide solution (0.05 M)	1310-73-2	Sigma-Aldrich (Munich, Germany)
Superdex [®] 75 Prep Grade	-	GE Healthcare (Freiburg, Germany)
Tetraethylene pentamine · 5HCl	4961-41-5	Sigma-Aldrich (Munich, Germany)
Triethylamine	121-44-8	Sigma-Aldrich (Munich, Germany)
Triethylene tetramine	112-24-3	Sigma-Aldrich (Munich, Germany)
Trifluoroacetic acid	76-05-1	Iris Biotech (Marktredewitz, Germany)
Triisopropylsilane	6485-79-6	Sigma-Aldrich (Munich, Germany)
Triton [™] X-100	9002-93-1	Sigma-Aldrich (Munich, Germany)
Trizma [®] base	77-86-1	Sigma-Aldrich (Munich, Germany)

2.1.2 Buffers

Table 2.3 gives an overview over used buffers and their composition.

Table 2.3 Buffers used for experimental procedures

Buffer	Composition
Electrophoresis loading Buffer	6 mL glycerine, 1.2 mL 0.5 M EDTA solution (pH 8.0), 2.8 mL H ₂ O, 20 mg bromophenol blue
HBG	20 mM HEPES, 5 % glucose, pH 7.4
TBE buffer	89 mM Trizma [®] base, 89 mM boric acid, 2 mM EDTA-Na ₂

2.1.3 Equipment for solid-phase synthesis

Automated single peptide synthesis at room temperature (RT) was carried out using an ABI 431A peptide synthesizer (Applied Biosystems, Foster City, CA, USA). For the automated parallel synthesis or synthesis with microwave irradiation, a Biotage Syro Wave (Biotage AB, Uppsala, Sweden) peptide synthesizer was used. Disposable polypropylene (PP) syringe microreactors with the volume sizes 2 mL, 5 mL, and 10 mL were purchased from Multisyntech (Witten, Germany). Manual solid-phase synthesis was carried out on a laboratory vacuum manifold (Promega Corporation, Madison, WI, USA) using microreactors with polyethylene filters for vacuum filtration. The automated synthesis with the Biotage Syro Wave synthesizer was conducted with polytetrafluoroethylene (PTFE) filters. The size of the reactors was chosen according to the resin amount.

2.1.4 Proteins

Recombinant murine epidermal growth factor (mEGF) was purchased from PeproTech Germany (Hamburg, Germany).

2.1.5 Nucleic acids

The plasmid pCMVLuc (encoding for firefly luciferase under control of the CMV promoter) was purchased from Plasmid Factory (Bielefeld, Germany) for *in vivo* experiments. For *in vitro* experiments pCMVLuc was amplified in *E. coli* DH5 α and purified from the bacterial lysate using a Qiagen Plasmid Giga Kit (Qiagen, Hilden, Germany). Poly(I:C) sodium salt and poly(I) potassium salt were purchased from Sigma-Aldrich (Munich, Germany). The concentration of nucleic acid solutions was determined photometrically using an Eppendorf BioPhotometer (Eppendorf, Hamburg, Germany). Cy5-labeled nucleic acids were produced with a Cy5-labelling kit obtained from Mirus Bio (Madison, WI, USA).

2.1.6 Cell culture

Cell culture work was carried out by Dr. Petra Kos, Ana Krhac Levacic, Katharina Müller (Pharmaceutical Biotechnology, LMU) and Valentin Wittmann (graduate student, LMU). All cell culture media, antibiotics and fetal calf serum (FCS) were purchased from Invitrogen (Karlsruhe, Germany). The individual media used for the different cell cultures are summarized in Table 2.4. All media were supplemented with 10 % FCS, 4 mM stable glutamine, 100 U/mL penicillin and 100 μ g/mL streptomycin. Exponentially growing cells were detached from the culture flasks using trypsin-EDTA solution (Invitrogen, Karlsruhe, Germany) and cell suspensions were seeded at the desired density for each experiment. Luciferase cell culture lysis buffer and D-luciferin sodium salt were purchased from Promega (Mannheim, Germany).

Table 2.4 Overview over the used cell lines and culture media

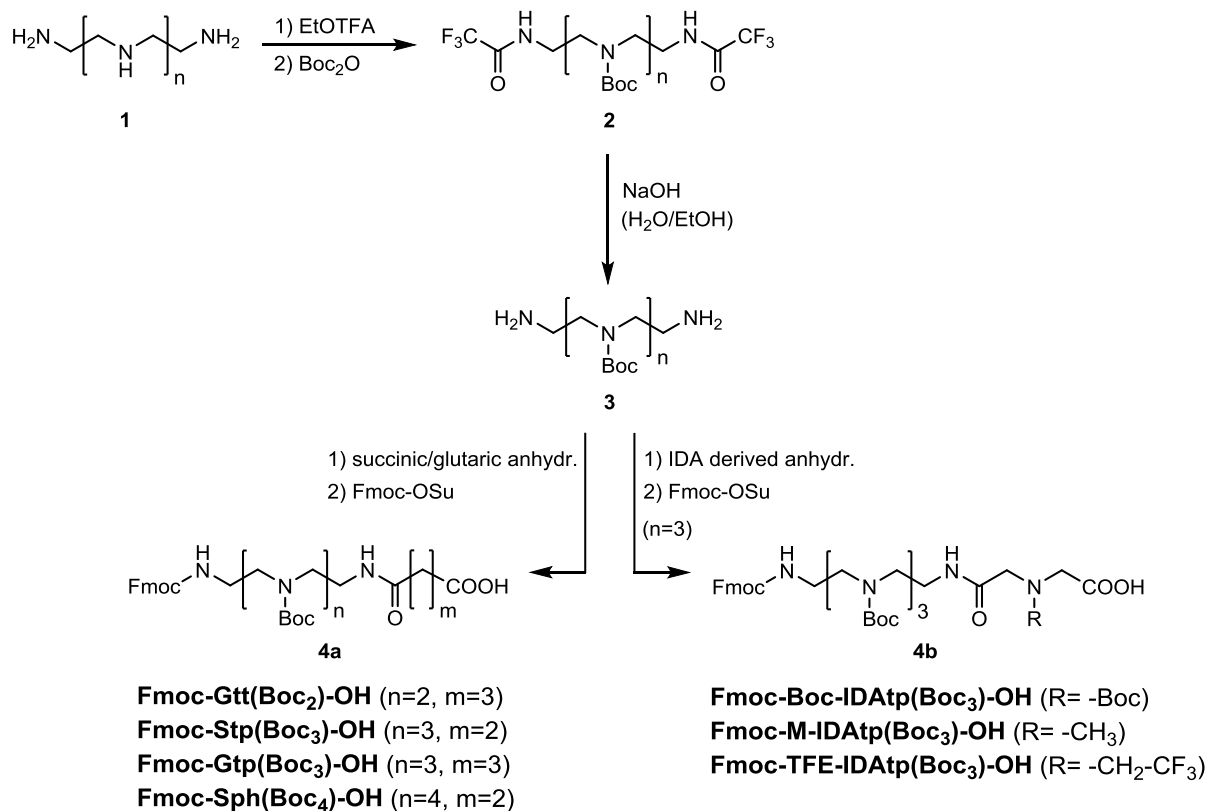
Cell line	Description	Medium
DU145	Human prostate cancer cells	RPMI-1640
Huh7	Human hepatocellular carcinoma cells	DMEM/Ham's F12 1:1
KB	Human cervix carcinoma cells	RPMI-1640, folate-free
Neuro2A	Mouse neuroblastoma cells	DMEM

2.2 Methods

2.2.1 Synthesis of polyamino acid building blocks

Scheme 2.1 illustrates the approach for the synthesis of the polyamino acid (PAA) building blocks. Fmoc-Gtt(Boc₂)-OH, Fmoc-Stp(Boc₃)-OH, Fmoc-Gtp(Boc₃)-OH and Fmoc-Sph(Boc₄)-OH were synthesized as described before [155, 169]. Briefly, the two primary amines of the polyamines 1 (TETA, TEPA or PEHA) were selectively protected with ethyl trifluoroacetate (EtOTFA). Subsequently the remaining secondary amines were Boc-protected by reaction with di-*tert*-butyl dicarbonate (Boc₂O) in a one-pot reaction. Work-up and recrystallization gave the compounds 2, bis-tfa-Tt(Boc₂), bis-tfa-Tp(Boc₃) or bis-tfa-Ph(Boc₄) respectively. The primary amines were deprotected by alkaline hydrolysis with aqueous NaOH containing 45 % EtOH to obtain the compounds 3, Tt(Boc₂), Tp(Boc₃) or Ph(Boc₄). In the final step, the two primary amines were asymmetrically substituted by reaction with a cyclic anhydride (succinic or glutaric anhydride) and Fmoc-OSu. Purification of the products 4a was carried out by dry column vacuum chromatography (DCVC) [171].

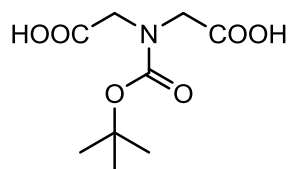
Scheme 2.1 Synthesis of Fmoc polyamino acid building blocks for SPS, adapted from [155, 169]



In case of the IDA derived building blocks 4b, TEPA (n=3) was used as the polyamine element. The first steps to obtain Tp(Boc₃) were carried out in the same manner as published for the other building blocks. In the last step, IDA derived anhydrides were used instead of succinic or glutaric anhydride, and the published synthesis protocol was adapted without additional modification.

2.2.1.1 Synthesis of Fmoc-Boc-IDAtp(Boc₃)-OH

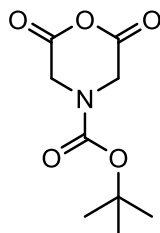
N-(tert-Butoxycarbonyl)iminodiacetic acid (Boc-IDA)



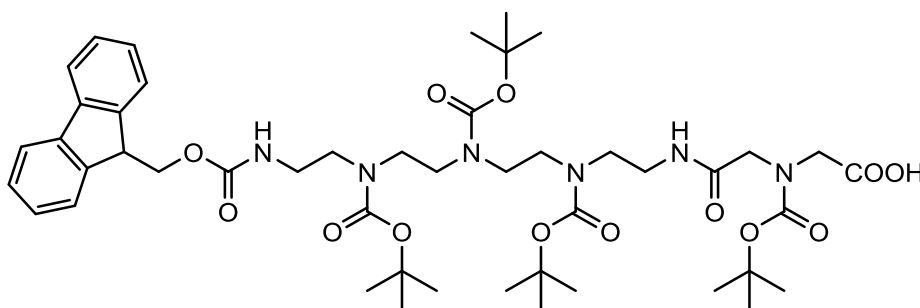
N-*tert*-Butoxycarbonyl protected iminodiacetic acid (Boc-IDA) was synthesized using the procedure reported elsewhere [172] with slight modification. Briefly 13.3 g iminodiacetic acid (0.1 mol) and 200 mL 1,4-dioxane were put into a 1 L round-bottom flask. 200 mL of 1 M sodium hydroxide solution were added and the mixture was stirred until a clear solution formed. 24.0 g of di-*tert*-butyl dicarbonate (0.11 mol, 1.1 eq) were dissolved in 50 mL 1,4-dioxane and added to the reaction mixture, which was stirred at RT for 72 h. The mixture was concentrated to approx. 200 mL under reduced pressure, washed twice with 150 mL diethyl ether. After acidification with 100 mL 10 % HCl, the reaction product was extracted with EtOAc (3 x 150 mL). The organic phases were combined and dried over anhydrous sodium sulfate. The EtOAc was evaporated after filtration, yielding 22.3 g of Boc-IDA (0.096 mol, 96 %) as white crystals.

¹H-NMR (400 MHz, methanol-d₄) δ = 1.44 (s, 9H, -CH₃), 3.99 (s, 2H, -CH₂-), 4.04 (s, 2H, -CH₂-).

ESI-MS: [M-H]⁻ calcd for C₉H₁₅NO₆ 232.0827; found 232.0826.

N-(tert-Butoxycarbonyl)iminodiacetic acid anhydride (Boc-IDA anhydride)

The cyclic anhydride of Boc-IDA was prepared by using dicyclohexylcarbodiimide (DCC) as dehydrating agent. 10.0 g of Boc-IDA (43 mmol) were put into a 500 mL round-bottom flask and 250 mL DCM were added. 8.9 g of DCC (43 mmol, 1 eq) were dissolved in 50 mL DCM and added into the round-bottom flask. The heterogeneous mixture was stirred at RT over night. The next day the mixture was concentrated to a volume of approx. 100 mL under reduced pressure and the insoluble dicyclohexyl urea was removed by filtration. The DCM was removed in the rotary evaporator and at high vacuum to yield 8.4 g of Boc-IDA anhydride (39 mmol, 91 %) as a solid.

Fmoc-Boc-IDAtp(Boc₃)-OH

Fmoc-Boc-IDAtp(Boc₃)-OH was prepared by adaption of the published protocol for the synthesis of Fmoc-Stp(Boc₃)-OH and Fmoc-Gtp(Boc₃)-OH [169] using Boc-IDA anhydride instead of succinic or glutaric anhydride. 13.5 g Tp(Boc₃) (27.6 mmol) were dissolved in 50 mL THF and cooled to -78 °C in a dry ice/acetone cooling bath. 7.4 g of Boc-IDA anhydride (34.4 mmol, 1.25 eq) were dissolved in 400 mL THF and added dropwise to the cooled solution over a period of 2 hours. After complete addition, the solution was stirred for 1 h at -78 °C and for 1 h at RT. 14.4 mL DIPEA (82.7 mmol, 3 eq) were added and the reaction mixture was cooled to 0 °C in an ice bath. 14.0 g

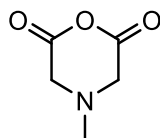
Fmoc-OSu (41.5 mmol, 1.5 eq) were dissolved in 60 mL MeCN and 30 mL THF and added dropwise to the cooled reaction mixture, which was stirred over night. The solution was concentrated to approx. 50 mL and 100 mL DCM were added. The solution was washed 5 times with 100 mL trisodium citrate buffer (0.1 M, pH 5.5) and dried over anhydrous sodium sulfate. The reaction product was purified by DCVC using a n-heptane/EtOAc gradient followed by an EtOAc/MeOH gradient yielding 6.9 g Fmoc-Boc-IDAtp(Boc₃)-OH (7.4 mmol, 27 %) as a white foamy solid.

¹H-NMR (400 MHz, chloroform-d) δ = 1.42 (s, 36H, -CH₃ Boc), 3.08-3.52 (m, 16H, -CH₂- TEPA), 3.89 (s, 4H, -CH₂- IDA), 4.18 (t, *J* = 7 Hz, 1H, Fmoc), 4.25-4.46 (m, 2H, Fmoc), 7.29 (d, *J* = 7.5 Hz, 2H, Ar-H Fmoc), 7.38 (t, *J* = 7.5 Hz, 2H, Ar-H Fmoc), 7.56 (d, *J* = 7.5 Hz, 2H, Ar-H Fmoc), 7.74 (d, *J* = 7.7 Hz, 2H, Ar-H Fmoc).

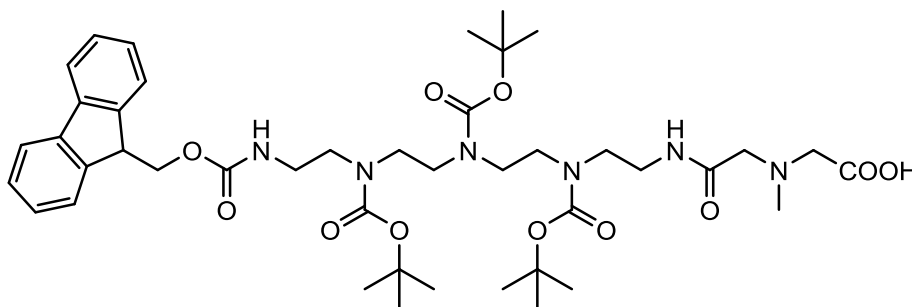
ESI-MS: [M-H]⁻ calcd for C₄₇H₇₀N₆O₁₃ 925.4928; found 925.4910.

2.2.1.2 Synthesis of Fmoc-M-IDAtp(Boc₃)-OH

Methyliminodiacetic acid anhydride (M-IDA anhydride)



The cyclic anhydride of methyliminodiacetic acid (M-IDA) was prepared analogously to Boc-IDA anhydride (cf. 2.2.1.1) by using DCC. 5.0 g of M-IDA (34 mmol) were put into a 250 mL round-bottom flask and 180 mL DCM were added. 7.0 g of DCC (34 mmol, 1 eq) were dissolved in 30 mL DCM and added into the round-bottom flask. The mixture was stirred at RT over night. The mixture was concentrated to a volume of approx. 80 mL under reduced pressure and the insoluble dicyclohexyl urea was removed by filtration. DCM was evaporated to yield 3.6 g of M-IDA anhydride (28 mmol, 82 %) as a solid.

Fmoc-M-IDAtp(Boc₃)-OH

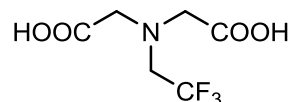
Fmoc-M-IDAtp(Boc₃)-OH was prepared analogously to Fmoc-Boc-IDAtp(Boc₃)-OH (cf. 2.2.1.1). 9.1 g Tp(Boc₃) (18.6 mmol) were dissolved in 30 mL THF and cooled to -78 °C in a dry ice/acetone cooling bath. 3.0 g of M-IDA anhydride (23.2 mmol, 1.25 eq) were dissolved in 250 mL THF and added dropwise to the cooled solution over a period of 2 hours. After complete addition, the solution was stirred for 1 h at -78 °C and for 1 h at RT. 9.7 mL DIPEA (55.8 mmol, 3 eq) were added and the reaction mixture was cooled to 0 °C in an ice bath. 9.4 g Fmoc-OSu (27.9 mmol, 1.5 eq) were dissolved in 40 mL MeCN and 20 mL THF and added dropwise to the cooled reaction mixture, which was stirred over night. The solution was concentrated to approx. 50 mL and 100 mL DCM were added. The solution was washed 5 times with 100 mL trisodium citrate buffer (0.1 M, pH 5.5) and dried over anhydrous sodium sulfate. The reaction product was purified by DCVC using a n-heptane/EtOAc gradient followed by an EtOAc/MeOH gradient yielding 4.4 g Fmoc-M-IDAtp(Boc₃)-OH (5.2 mmol, 28 %) as an amber foamy solid.

¹H-NMR (400 MHz, chloroform-d) δ = 1.42 (s, 27H, -CH₃ Boc), 2.29-2.41 (m, 3H, -CH₃ M-IDA), 2.97-3.55 (m, 20H, -CH₂- TEPA, -CH₂- M-IDA), 4.17 (t, *J* = 7.1 Hz, 1H, Fmoc), 4.25-4.46 (m, 2H, Fmoc), 7.28 (d, *J* = 7.7 Hz, 2H, Ar-H Fmoc), 7.37 (t, *J* = 7.5 Hz, 2H, Ar-H Fmoc), 7.56 (d, *J* = 7.8 Hz, 2H, Ar-H Fmoc), 7.74 (d, *J* = 7.5 Hz, 2H, Ar-H Fmoc).

ESI-MS: [M-H]⁻ calcd for C₄₃H₆₄N₆O₁₁ 839.4560; found 839.4548.

2.2.1.3 Synthesis of Fmoc-TFE-IDAtp(Boc₃)-OH

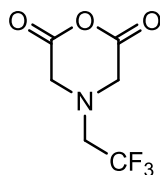
N-(Trifluoroethyl)iminodiacetic acid (TFE-IDA)



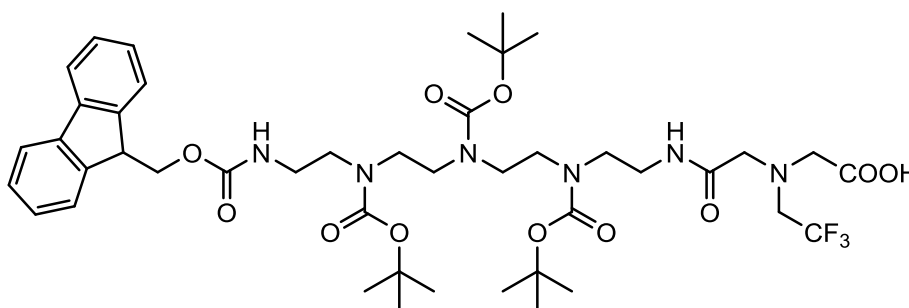
TFE-IDA was prepared by modification of a published protocol for the synthesis of methyliminodiacetic acid [173]. 27.9 g chloroacetic acid (295.2 mmol, 2 eq) were placed in a 500 mL round-bottom flask. 22 mL H₂O were added and the flask was cooled in an ice bath. A cold solution of 29.5 g NaOH (738 mmol, 5 eq) in 93 mL H₂O was added slowly under stirring. After the complete addition, the cooling bath was removed and a solution of 20.0 g trifluoroethylamine hydrochloride (147.6 mmol, 1 eq) in 65 mL H₂O was added dropwise. After complete addition, the solution was stirred overnight. 60 g BaCl₂ dihydrate in approx. 140 mL boiling H₂O were added and the mixture was heated for 1.5 hours. The solid was filtered off and dried in the drying cabinet over 2 days yielding 27.6 g of TFE-IDA barium salt (78.8 mmol). The dry TFE-IDA barium salt was placed in 500 mL RBF. 65 mL H₂O were added and heated to boiling. 31.5 mL of a 2.5 M H₂SO₄ solution (78.8 mmol) were added gradually over 1 hour under continuous heating to boiling. After cooling to RT, the mixture was centrifuged to remove the solid BaSO₄. The clear supernatant was freeze-dried yielding 16.1 g of TFE-IDA (74.8 mmol, 51 %) as colorless crystals.

¹H-NMR (400 MHz, deuterium oxide) δ = 3.42 (q, *J* = 9.6 Hz, 2H, -CH₂-CF₃), 3.65 (s, 4H, O=C-CH₂-).

ESI-MS: [M-H]⁻ calcd for C₆H₈F₃NO₄ 214.0333; found 214.0332.

N-(Trifluoroethyl)iminodiacetic acid anhydride (TFE-IDA anhydride)

The cyclic anhydride of TFE-IDA was prepared analogously to the anhydrides of Boc-IDA and M-IDA (cf. 2.2.1.1 and 2.2.1.2) by using DCC. 5.0 g TFE-IDA (23.2 mmol) were placed in a 250 mL round-bottom flask. 140 mL DCM were added. 4.8 g DCC (23.2 mmol, 1 eq) were dissolved in 30 mL DCM and added into the flask. The mixture was stirred at RT overnight. The mixture was concentrated to approx. 80 mL under reduced pressure and the insoluble dicyclohexyl urea was removed by filtration. The DCM was removed in the rotary evaporator and at high vacuum to yield 4.3 g TFE-IDA anhydride (21.8 mmol, 94 %) as a solid.

Fmoc-TFE-IDAtp(Boc₃)-OH

Fmoc-TFE-IDAtp(Boc₃)-OH was prepared analogously to Fmoc-Boc-IDAtp(Boc₃)-OH and Fmoc-M-IDAtp(Boc₃)-OH (cf. 2.2.1.1 and 2.2.1.2). 7.1 g Tp(Boc₃) (14.5 mmol) were dissolved in 30 mL THF and cooled to -78 °C in a dry ice/acetone cooling bath. 3.6 g of TFE-IDA anhydride (18.1 mmol, 1.25 eq) were dissolved in 200 mL THF and added dropwise to the cooled solution over a period of 2 hours. After complete addition, the solution was stirred for 1 h at -78 °C and for 1 h at RT. 7.6 mL DIPEA (43.6 mmol, 3 eq) were added and the reaction mixture was cooled to 0 °C in an ice bath. 7.4 g Fmoc-OSu (21.8 mmol, 1.5 eq) were dissolved in 40 mL MeCN and 20 mL THF and added dropwise to the cooled reaction mixture, which was stirred overnight. The solution was concentrated to approx. 50 mL and 100 mL DCM were

added. The solution was washed 5 times with 100 mL trisodium citrate buffer (0.1 M, pH 5.5) and dried over anhydrous sodium sulfate. The reaction product was purified by DCVC using a n-heptane/EtOAc gradient followed by an EtOAc/MeOH gradient yielding 3.4 g Fmoc-TFE-IDAtp(Boc₃)-OH (3.7 mmol, 26 %) as a yellow foamy solid.

¹H-NMR (400 MHz, chloroform-d) δ = 1.43 (s, 27H, -CH₃ Boc), 3.06-3.67 (m, 22H, -CH₂- TEPA, -CH₂- TFE-IDA), 4.18 (t, J = 7.0 Hz, 1H, Fmoc), 4.24-4.51 (m, 2H, Fmoc), 7.29 (d, J = 7.5 Hz, 2H, Ar-H Fmoc), 7.38 (t, J = 7.5 Hz, 2H, Ar-H Fmoc), 7.56 (d, J = 7.7 Hz, 2H, Ar-H Fmoc), 7.75 (d, J = 7.6 Hz, 2H, Ar-H Fmoc).

ESI-MS: [M-H]⁻ calcd for C₄₄H₆₃F₃N₆O₁₁ 907.4434; found 907.4430.

2.2.2 Resin loading

2.2.2.1 Loading of 2-chlorotrityl resin

The desired amount of 2-chlorotrityl chloride resin (chloride loading 1.6 mmol/g) was placed in a syringe reactor and preswelled in dry DCM (10 mL/g resin; dried over CaCl₂) for 30 min, the DCM was discarded subsequently. A solution containing 0.45 mmol Fmoc-amino acid and 0.9 mmol DIPEA (157 μ L) in dry DCM (10 mL) were added per gram resin and incubated for 1 h at RT. After disposal of the reaction mixture, the resin was incubated with a mixture of DCM/MeOH/DIPEA (10 mL/g resin; 80/15/5 v/v/v) for 30 min at RT to cap residual reactive chloride functions. The resin was washed 5 times with DCM (10 mL/g resin) and a resin sample was separated and dried under vacuum for the loading determination. The residual resin was washed twice with DMF (10 mL/g resin) and treated 5 times for 10 minutes with 20 % piperidine in DMF. Finally, the resin was washed 3 times with DMF, 3 times with DCM, 3 times with n-hexane and dried under vacuum. In general, by this procedure resin loadings between 0.28 and 0.35 mmol/g were achieved.

2.2.2.2 Loading of four-arm branching core on Fmoc-Ala-Wang resin

To avoid aggregation of the highly branched four-arm oligomers during chain assembly, a very low load of the four-arm branching core (AK(K)₂, AK(AK)₂ or AK(HK)₂) was prepared on Ala-Wang resins. The desired amount of Fmoc-L-Ala

wang resin (loading 0.35 mmol/g) was placed into a syringe reactor and preswelled with DCM (10 mL/g resin) for 30 min. The Fmoc protecting group was removed by treating the resin 5 times for 10 minutes with 20 % piperidine in DMF and subsequent washing 3 times with DMF, 3 times with DCM (10 mL/g resin). 0.07 mmol of Fmoc-Lys(Fmoc)-OH per gram resin (0.2 eq relative to resin amines) were dissolved together with equimolar amounts of HOBt, PyBop and twofold molar amount of DIPEA (0.4 eq, 24 μ L/g resin) in DCM/DMF 50/50 (10 mL/g resin). The coupling solution was incubated with the resin for 1 h and discarded subsequently. The resin was washed 3 times with DMF, 3 times with DCM (10 mL/g resin) and residual free amines were acetylated by a 10-fold excess (3.5 mmol/g resin) of acetic anhydride (Ac_2O) using a mixture of DCM/ Ac_2O /DIPEA (8450/330/1220 μ L/g resin). After incubation for 1 h, the reaction mixture was discarded and the resin was washed 3 times with DMF and 3 times with DCM (10 mL/g resin). The Fmoc protecting group was removed and the resin was washed as before. According to the individual oligomer sequence, 1.4 mmol of Fmoc-Lys(Fmoc)-OH, Fmoc-Ala-OH or Fmoc-His(Trt)-OH per gram resin (4 eq relative to initial resin loading) were dissolved together with equimolar amounts of HOBt, PyBop and twofold molar amount of DIPEA (8 eq, 488 μ L/g resin) in DCM/DMF 50/50 (10 mL/g resin). The coupling solution was added to the resin and incubated for 1 h. Subsequently the reaction mixture was discarded and the resin was washed 3 times with DMF and 3 times with DCM (10 mL/g resin). In case of the AK(AK)₂ and AK(HK)₂ cores, Fmoc was deprotected and the resin was washed before 1.4 mmol of Fmoc-Lys(Fmoc)-OH per gram resin (4 eq relative to initial resin loading), equimolar amounts of HOBt, PyBop and twofold molar amount of DIPEA (8 eq, 488 μ L/g resin) in DCM/DMF 50/50 (10 mL/g resin) were incubated with the resin for 1 h. The reaction mixture was discarded and the resin was washed 3 times with DMF and 3 times with DCM (10 mL/g resin). In all cases, after coupling of the second Fmoc-Lys(Fmoc)-OH and subsequent resin wash, resin samples were separated and dried under vacuum for the loading determination. The remaining resin was deprotected, washed and dried under vacuum for storage. In general, by this procedure resin loadings between 0.04 and 0.05 mmol/g related to the branched alanine lysine peptide were achieved, which corresponds to an amine content at the four N-termini between 0.16 and 0.2 mmol/g.

2.2.2.3 Loading determination

The resin loading was determined by the quantification of released fluorenyl derivative after piperidine deprotection. The vacuum-dried resin was weighed accurately (triplicates, in the range between 5 - 15 mg) into Eppendorf reaction tubes. 1 mL of 20 % piperidine was added to each sample, which was vortexed briefly and incubated for 1 h at RT under shaking. Subsequently the samples were vortexed again and the resin was allowed to settle for 1 min. 25 μ L of the supernatant were diluted with DMF to 1 mL. An analog dilution of 20 % piperidine in DMF served as blank solution. The absorption at 301 nm (A_{301}) against the blank solution was determined using a Genesys 10S UV-VIS spectrophotometer (Thermo Scientific, Dreieich, Germany), and the resin loading was calculated for each sample according to the following formula. The arithmetic mean of the triplicate values was used as the final result of resin loading.

$$L = \frac{1000 \cdot A_{301}}{m \cdot 7800 \cdot D}$$

L, resin loading [mmol/g]; A_{301} , extinction at 301 nm; m, resin mass [mg]; 7800, molar extinction coefficient under the specified conditions [$\text{L mol}^{-1} \text{cm}^{-1}$]; D, dilution factor (0.025).

2.2.3 Standard solid-phase synthesis conditions

2.2.3.1 General SPS algorithm

The sequential synthesis on solid-phase was carried out in defined steps of a synthesis cycle. Starting with a deprotected peptide resin, Table 2.5 summarizes the steps of a manual synthesis cycle and Table 2.6 the steps of an automated synthesis cycle. After the initial resin preswell (step 0), the steps 1 to 6 in case of the manual synthesis and steps 1 to 4 in case of the automated synthesis were continuously repeated according to the oligomer sequence. In the manual synthesis, the presence of free amines on the solid support was determined qualitatively by the Kaiser test (cf. 2.2.3.2) after each deprotection and coupling step. In case of an inadequate result (negative after deprotection or positive after coupling), the last deprotection or coupling step respectively was repeated. Since the automated synthesis does not offer the opportunity to separate resin samples for the Kaiser test, extended deprotection steps and double couplings were used in this case. In the coupling

steps, the resin was incubated with a 4-fold excess of the appropriate preactivated Fmoc amino acid (Fmoc-AA) specified by the oligomer sequence. Preactivation of the Fmoc-AA during manual synthesis was carried out with an equimolar amount of HOBt (1-Hydroxybenzotriazole), equimolar amount of PyBOP (benzotriazol-1-yl-oxytripyrrolidinophosphonium hexafluorophosphate) and a twofold molar amount of DIPEA. In case of the automated synthesis, HBTU (2-(1H-benzotriazole-1-yl)-1,1,3,3-tetramethyluronium hexafluorophosphate) was used instead of PyBOP. Incubation times during a coupling cycle were 60 min at RT or 10 min at 60 °C (microwave irradiation). Scheme 2.2 shows an illustration of the synthesis algorithms.

Table 2.5 General steps of a manual synthesis cycle

Step	Description	Solvent	V	Time
0 ^a	Resin preswell	DCM	10 mL/g resin	30 min
1	Coupling	DCM/DMF 50/50	5 mL/g resin ^c	60 min
2	Wash	DMF, DCM	10 mL/g resin	3 x 1 min DMF 3 x 1 min DCM
3 ^b	Kaiser test	-	-	-
4	Fmoc deprotection	20 % piperidine/DMF	10 mL/g resin	4 x 10 min
5	Wash	DMF, DCM	10 mL/g resin	3 x 1 min DMF 3 x 1 min DCM
6 ^b	Kaiser test	-	-	-
7 ^a	Cleavage	TFA/TIS/H ₂ O 95/2.5/2.5	10 mL/g resin	90 min

^a Initial resin preswell (step 0) and terminal cleavage (step 7) were only carried out once during a synthesis; steps 1-6 were repeated according to the oligomer sequence. ^b In case of an inadequate result of the Kaiser test, the previous coupling or deprotection step respectively was repeated. ^c The exact volume of coupling solution was dependent on the resin loading and solubility of the building blocks. In case of a high loading or poor solubility, the minimum volume (≥ 5 mL/g resin) for complete dissolution was used.

Table 2.6 General steps of an automated synthesis cycle using the Biotage Syro Wave synthesizer

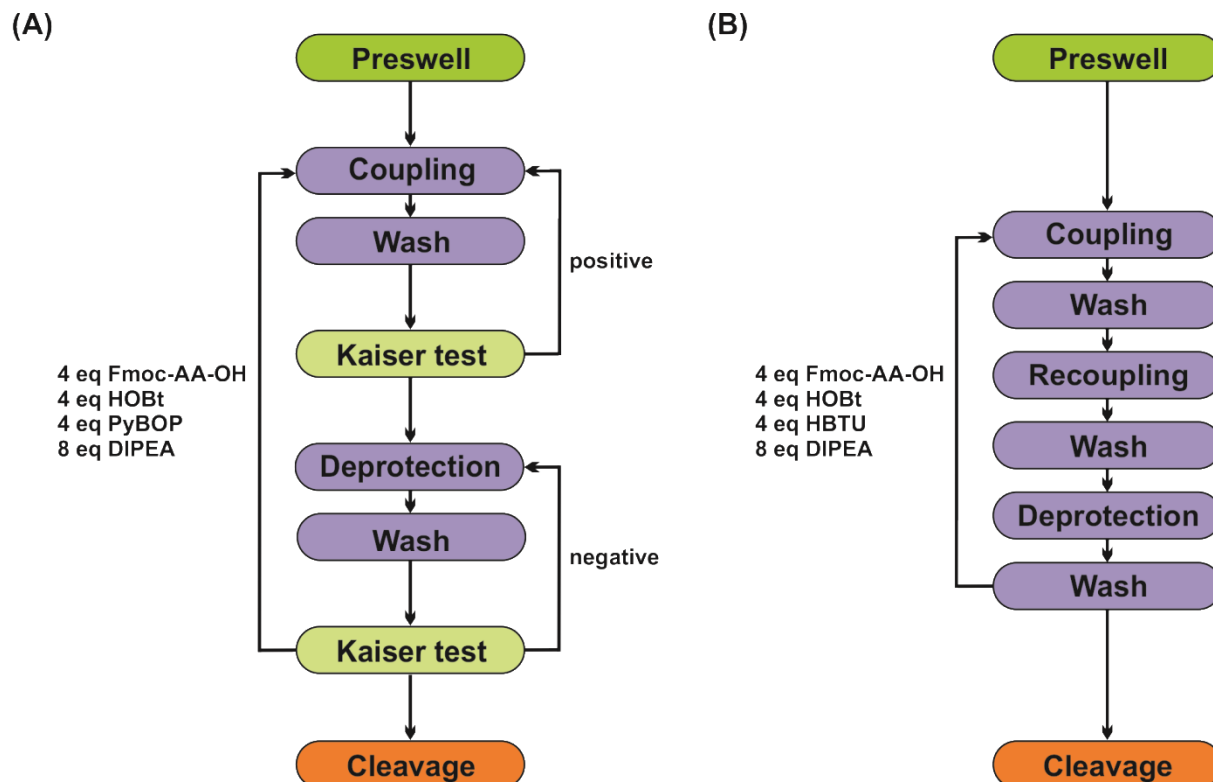
Step	Description	Solvent	V	Time
0 ^a	Resin preswell	DMF	10 mL/g resin	30 min
1	Coupling	NMP/DMF 60/40	7 mL/g resin	60 min at RT or 10 min at 60 °C ^b
	Double coupling			
	Wash	DMF	8 mL/g resin	1 x 1 min
	Recoupling	NMP/DMF 60/40	7 mL/g resin	60 min at RT or 10 min at 60 °C ^b
2	Wash	DMF	8 mL/g resin	5 x 1 min
3	Fmoc deprotection	20 % piperidine/DMF	7 mL/g resin	5 x 10 min
4	Wash	DMF	8 mL/g resin	5 x 1 min
5 ^a	Cleavage	TFA/TIS/H ₂ O 95/2.5/2.5	10 mL/g resin	90 min

^a Initial resin preswell (step 0) and terminal cleavage (step 7) were only carried out once in a synthesis; steps 1-4 were repeated according to the oligomer sequence. ^b Microwave irradiation.

2.2.3.2 Kaiser test

The presence of free amines on the resin was determined qualitatively by the Kaiser test [174]. A small sample of DCM washed resin was transferred into an Eppendorf reaction tube. Two drops of each 80 % phenol in EtOH (w/v), 5 % ninhydrin in EtOH (w/v) and 20 µM potassium cyanide (KCN) in pyridine (mixture of 1 mL aqueous 0.001 M KCN solution and 49 mL pyridine) were added. The tube was incubated at 99 °C for 4 min under shaking. The presence of free amines was indicated by a deep blue color.

Scheme 2.2 Illustration of the SPS algorithms during (A) manual oligomer synthesis and (B) automated oligomer synthesis using the Biotage Syro Wave synthesizer



2.2.3.3 Oligomer cleavage

After complete assembly of the sequence on solid phase and final Fmoc deprotection, cleavage was carried out using a mixture of TFA/TIS/H₂O (95/2.5/2.5 v/v/v). The cleavage mixture (10 mL/g resin) was added to the resin in a syringe reactor and incubated for 90 min under shaking. The solution was collected in a round-bottom flask and the resin was washed 3 times with TFA, 3 times with DCM (10 mL/g resin). The combined solutions were concentrated under reduced pressure to a final volume of approximately 1 mL and added dropwise to a cold mixture of MTBE/n-hexane (25/25 v/v) in a 50 mL centrifuge tube. After centrifugation for 20 min at 4000 RCF and 4 °C, the supernatant was discarded and the precipitate was dried under a nitrogen stream. The crude product was dissolved in 25 % acetonitrile in water, snap-frozen in liquid nitrogen and freeze-dried using a Christ Alpha 2-4 LDplus laboratory freeze-drier (Martin Christ Gefriertrocknungsanlagen GmbH, Osterode am Harz, Germany).

2.2.4 Oligomer synthesis

2.2.4.1 Synthesis of linear oligomers

(Oligomers **610-615**)

The linear topology oligomers were synthesized manually in 0.03 mmol scales under standard Fmoc SPS conditions (cf. 2.2.3) using 2-chlorotrityl resins preloaded with alanine or H-His(Trt)-OH. According to the individual sequences the polyamino acid building blocks Fmoc-Gtt(Boc₂)-OH, Fmoc-Stp(Boc₃)-OH or Fmoc-Sph(Boc₄)-OH were alternately coupled with Fmoc-Ala-OH or Fmoc-His(Trt)-OH. After complete assembly on solid-phase and final Fmoc deprotection, the oligomers were cleaved under standard conditions (cf. 2.2.3), purified by SEC and analyzed by ¹H-NMR, RP-HPLC and ESI-MS.

2.2.4.2 Synthesis of two-arm oligomers

(Oligomers **754-757, 811-817**)

The two-arm topology oligomers were synthesized automatically in 0.015 mmol scales using the parallel synthesis option of the Biotage Syro Wave synthesizer. The synthesis was carried out at RT under the standard SPS conditions (cf. 2.2.3) starting with 2-chlorotrityl resins preloaded with alanine. For the introduction of the symmetrical branching point, Fmoc-Lys(Fmoc)-OH was coupled. After Fmoc deprotection, the assembly was continued at both the α - and ϵ -amine of the branching lysine and therefore the scale size regarding resin bound amines was doubled. According to the individual oligomer sequences Fmoc-Gtt(Boc₂)-OH, Fmoc-Gtp(Boc₃)-OH, Fmoc-Stp(Boc₃)-OH, Fmoc-Boc-IDAtp(Boc₃)-OH, Fmoc-M-IDAtp(Boc₃)-OH, Fmoc-TFE-IDAtp(Boc₃)-OH, Fmoc-His(Trt)-OH, Fmoc-3PAL-OH, Fmoc-4PAL-OH and Boc-Cys(Trt)-OH were sequentially coupled. After the conjugation of N-terminal Boc-Cys(Trt)-OH in the last cycle, no Fmoc deprotection was required. The oligomers were cleaved under standard conditions (cf. 2.2.3), purified by SEC and analyzed by ¹H-NMR and RP-HPLC.

2.2.4.3 Synthesis of four-arm oligomers

(Oligomers **606-610**)

For the synthesis of four-arm topology oligomers, the standard SPS conditions were used with slight modification to avoid aggregation of the highly branched compounds during chain assembly (cf. [155]). Ala-Wang resins with a very low load (approx. 0.05 mmol/g) of four-arm branching core (AK(AK)₂ or AK(HK)₂) were prepared (cf. 2.2.2.2) and 1 % Triton X-100 was added to the solvents of the coupling and deprotection steps. Beyond that, the standard SPS and cleavage procedures were followed (cf. 2.2.3) using Fmoc-Ala-OH, Fmoc-His(Trt)-OH, Fmoc-Sph(Boc₄)-OH and Boc-Cys(Trt)-OH as building units. The oligomers were purified by SEC and analyzed by ¹H-NMR and RP-HPLC.

2.2.4.4 Synthesis of four-arm HK peptides

(Oligomers **582, 584**)

The four-arm HK peptides were synthesized by Wolfgang Rödl using the Biotage Syro Wave synthesizer. Ala-Wang resins with a very low load (approx. 0.05 mmol/g) of four-arm branching core (AK(K)₂) were prepared (cf. 2.2.2.2) and 1 % Triton X-100 was added to the solvents of the coupling and deprotection steps. Fmoc-Lys(Boc)-OH and Fmoc-His(Trt)-OH were used according to the individual sequences. Double-couplings were carried out under microwave irradiation (5 min, 75 °C) and Fmoc deprotection was accomplished by 3 times incubation for 20 min with a solution of 20 % piperidine and 2 % DBU in DMF. After complete assembly on solid-phase and final Fmoc deprotection, the oligomers were cleaved under standard conditions (cf. 2.2.3), purified by SEC and analyzed by ¹H-NMR and RP-HPLC.

2.2.4.5 Synthesis of PEGylated two-arm oligomers with C-terminal alanine

(Oligomers **188, 440, 616**)

The PEGylated two-arm oligomers with C-terminal alanine as substitute for a targeting ligand were synthesized manually in 0.02 – 0.05 mmol scales under standard Fmoc SPS conditions (cf. 2.2.3) using a 2-chlorotrityl resin preloaded with

alanine. Fmoc-N-amido-dPEG₂₄-acid, Fmoc-His(Trt)-OH, Fmoc-Lys(Fmoc)-OH, Fmoc-Stp(Boc₃)-OH and Boc-Cys(Trt)-OH were used as building units. In the first cycle, Fmoc-N-amido-dPEG₂₄-acid was coupled and the synthesis was continued according to the individual sequences of the oligomers. After the conjugation of N-terminal Boc-Cys(Trt)-OH in the last cycle, no Fmoc deprotection was required. The oligomers were cleaved under standard conditions (cf. 2.2.3), purified by SEC and analyzed by ¹H-NMR and RP-HPLC.

2.2.4.6 Synthesis of PEGylated two-arm oligomers with B6 ligand

(Oligomers **617, 618**)

The peptidic ligand B6 (GHKAKGPRK) [175] was synthesized on a 2-chlorotrityl resin preloaded with H-Lys(Boc)-OH in a 0.1 mmol scale using the Applied Biosystems 431A synthesizer with FastMoc™ protocols. Fmoc-Ala-OH, Fmoc-Arg(Pbf)-OH, Fmoc-Gly-OH, Fmoc-His(Trt)-OH and Fmoc-Pro-OH were used for the synthesis of the peptide sequence. After complete assembly on solid phase and terminal Fmoc deprotection, the resin was divided for subsequent oligomer syntheses. The syntheses of PEGylated two-arm oligomers with B6 ligand were continued manually in 0.02 mmol scales under standard Fmoc SPS conditions (cf. 2.2.3). Fmoc-N-amido-dPEG₂₄-acid, Fmoc-Ala-OH, Fmoc-His(Trt)-OH, Fmoc-Lys(Fmoc)-OH, Fmoc-Stp(Boc₃)-OH and Boc-Cys(Trt)-OH were used as building units according to the individual oligomer sequences. After the conjugation of N-terminal Boc-Cys(Trt)-OH in the last cycle, no Fmoc deprotection was required. The oligomers were cleaved under standard conditions (cf. 2.2.3), purified by SEC and analyzed by ¹H-NMR and RP-HPLC.

2.2.4.7 Synthesis of PEGylated two-arm oligomers with cMBP ligands

(Oligomers **442, 443, 694-700**)

Since the cMBP ligands were intended for N-terminal positions in the oligomers, an inverse synthesis approach was taken. A 2-chlorotrityl resin was preloaded with Fmoc-Lys(ivDde)-OH, which allows the assembly of asymmetric branches. After

Fmoc deprotection the peptides cMBP1 (YLFSVHWPPLKA) [176] and cMBP2 (KSLSRHDHIIHH) [177-179] were synthesized in 0.1 mmol scales using the Applied Biosystems 431A synthesizer with FastMoc™ protocols. The scrambled sequences cMBP2sc1 (LHHHDRKSSIIH), cMBP2sc2 (KSHHRDHIHLHS), cMBP2sc3 (HHSIHLRLHHKSD) and cMBP2sc4 (RKIHHHLHSHSD) were created randomly from the sequence of cMBP2 using an online sequence permutation generator (RANDOM.ORG). The scrambled peptides were synthesized in 0.02 mmol scales using the parallel synthesis option of the Biotage Syro Wave synthesizer and standard Fmoc SPS conditions at RT (cf. 2.2.3). Fmoc-Ala-OH, Fmoc-Arg(Pbf)-OH, Fmoc-Asp(OtBu)-OH, Fmoc-His(Trt)-OH, Fmoc-Ile-OH, Fmoc-Leu-OH, Fmoc-Lys(Boc)-OH, Fmoc-Phe-OH, Fmoc-Pro-OH, Fmoc-Ser(tBu)-OH, Fmoc-Trp(Boc)-OH, Fmoc-Tyr(tBu)-OH and Fmoc-Val-OH were used for the synthesis of the peptide sequences. After complete assembly on solid phase and final Fmoc deprotection, the N-terminal amines were protected by reaction with 10 eq Boc₂O (di-*tert*-butyl dicarbonate) and 20 eq DIPEA in DCM (10 ml/g resin). After 1 h reaction time, the resins were washed 3 times with DMF and 3 times with DCM (10 mL/g resin). The ivDde protecting group at the ε-amine of the C-terminal lysine was removed by repeated incubation with 2 % hydrazine monohydrate in DMF (v/v) [180, 181]. The deprotection solution was exchanged every 5 min until no absorbance at 290 nm was detectable. The syntheses of the PEGylated two-arm oligomers were continued at the deprotected ε-amine of the C-terminal lysine in the same manner as described for the oligomers with B6 ligand (cf. 2.2.4.6).

2.2.4.8 Synthesis of the PEGylated two-arm oligomer for SPAAC

(Oligomer **479**)

The azide containing oligomer **479** for a strain-promoted alkyne-azide cycloaddition (SPAAC) was synthesized manually in a 0.05 mmol scale under standard SPS conditions (cf. 2.2.3). A 2-chlorotrityl resin was preloaded with Fmoc-Lys(ivDde)-OH. After Fmoc deprotection, the protected oligomer backbone with the sequence (C->N) K(ivDde)-dPEG₂₄-K(Stp₄-C)₂ was assembled using Fmoc-N-amido-dPEG₂₄-acid, Fmoc-Lys(Fmoc)-OH, Fmoc-Stp(Boc₃)-OH and Boc-Cys(Trt)-OH as building units. After the conjugation of N-terminal Boc-Cys(Trt)-OH, the ivDde protecting group was

removed as described for the oligomers with cMBP ligands (cf. 2.2.4.7). After complete deprotection, Fmoc-L- δ -azidonorvaline-OH was coupled to the ϵ -amine of the C-terminal lysine. After final Fmoc deprotection, cleavage was carried out under standard conditions (cf. 2.2.3) and the oligomer **479** was purified by SEC and preparative RP-HPLC and analyzed by $^1\text{H-NMR}$ and analytical RP-HPLC.

2.2.4.9 Synthesis of mEGF conjugated PEGylated two-arm topology oligomer

5 mg of mEGF (0.83 μmol) were dissolved in 1400 μL of 20 mM HEPES pH 7.4 containing 30 % EtOH. 5.8 mg of DBCO-PEG₅-NHS (10 eq, 8.3 μmol) were dissolved in 100 μL DMSO and added to the protein solution. The reaction mixture was incubated for 3 h at RT. Free DBCO-linker was removed by 5 times ultrafiltration using an Amicon Ultra-4 centrifugal filter unit with a MWCO of 3 kDa (Merck Millipore, Darmstadt, Germany). Fresh 20 mM HEPES pH 7.4 containing 30 % EtOH was added to a final volume of 4 mL before each centrifugation step. In the last step, the protein solution was concentrated to a volume of 750 μL . 57.4 mg of oligomer **479** (TFA salt, 10 eq, 8.3 μmol) were dissolved in 3250 μL of 20 mM HEPES pH 7.4 (30 % EtOH), mixed with the protein solution and incubated for 3 h at RT. The reaction mixture was concentrated to a final volume of 2 mL by ultracentrifugation using the Amicon Ultra-4 centrifugal filter unit. Finally, the mEGF conjugate was purified by SEC using Superdex 75 as gel filtration medium and 20 mM HEPES pH 7.4 containing 30 % EtOH as eluent. The yield was 52 % (determined photometrically at 280 nm).

2.2.4.10 Synthesis of PEGylated two-arm oligomers with carbohydrates

(Oligomers **603-605, 651**)

The multivalent carbohydrate ligands were synthesized by Dr. Felix Wojcik (MPI of Colloids and Interfaces, Potsdam) and provided in a protected and resin bound form, ready for the subsequent solid-phase synthesis. The syntheses of the PEGylated two-arm oligomers were continued in 0.01 mmol scales under standard SPS conditions (cf. 2.2.3) using Fmoc-N-amido-dPEG₂₄-acid, Fmoc-Lys(Fmoc)-OH,

Fmoc-Stp(Boc₃)-OH and Boc-Cys(Trt)-OH as building units. Since the carbohydrate ligands were in a peracetylated form during the solid-phase synthesis, a deacetylation step by transesterification with 0.1 M sodium methoxide was introduced before cleavage (Zemplén deacetylation [182]). Cleavage of the oligomers was carried out with 50 % TFA and 5 % TIS in DCM to reduce the risk of acid catalyzed hydrolysis of glycosyl residues. The oligomers were analyzed by ¹H-NMR and analytical RP-HPLC.

2.2.4.11 Synthesis of PEGylated two-arm oligomers with FcIA ligands

(Oligomers **356**, **619**, **620**)

The folic acid containing oligomer **356** and the Alexa Fluor 488 labeled analog **583** were synthesized as described before [115]. The oligomers **619** and **620** were prepared in 0.02 mmol scales. For the syntheses, a 2-chlorotrityl resin was preloaded with Fmoc-Lys(ivDde)-OH and protected oligomer backbones with the sequences (C->N) K(ivDde)-AK[A-(Stp-A)₄-C]₂ and K(ivDde)-HK[H-(Stp-H)₄-C]₂ were assembled under standard SPS conditions (cf. 2.2.3) using Fmoc-Ala-OH, Fmoc-His(Trt)-OH, Fmoc-Lys(Fmoc)-OH, Fmoc-Stp(Boc₃)-OH and Boc-Cys(Trt)-OH as building units. The ivDde protecting group was removed as described for the oligomers with cMBP ligands (cf. 2.2.4.7). After complete deprotection, the two PEG₂₄ segments were attached to the ε-amine of the C-terminal lysine by coupling and deprotection of Fmoc-N-amido-dPEG₂₄-acid twice. Folic acid was assembled in two steps. First, Fmoc-Glu-OtBu was coupled to the N-terminus of the PEG amino acid and deprotected, second N¹⁰-(trifluoroacetyl)pteroic acid was attached. Both steps were carried out under the standard SPS conditions, however in case of the pteronic acid derivative, a mixture of NMP/DMF/DMSO (1/1/1 v/v/v) was used as solvent of the coupling solution. After washing of the resin 3 times with DMF and 3 times with DCM, the trifluoroacetyl protecting group was removed by incubation with a mixture of 25 % ammonium hydroxide solution and DMF (50/50 v/v, 10 ml/g resin) 4 times for 30 min. Cleavage was carried out under standard conditions (cf. 2.2.3) and the oligomers were purified by SEC and analyzed by ¹H-NMR and analytical RP-HPLC.

2.2.4.12 Synthesis of PEGylated two-arm oligomers with MTX ligands

(Oligomers **638-641**, **672**)

The oligomers containing MTX ligands were synthesized in 0.02 mmol scales. For the syntheses, a 2-chlorotrityl resin was preloaded with Fmoc-Lys(ivDde)-OH and protected oligomer backbones with the sequences (C->N) K(ivDde)-K(Stp₄-C)₂ and K(ivDde)-HK[H-(Stp-H)₄-C]₂ were assembled under standard SPS conditions (cf. 2.2.3) using Fmoc-His(Trt)-OH, Fmoc-Lys(Fmoc)-OH, Fmoc-Stp(Boc₃)-OH and Boc-Cys(Trt)-OH as building units. The ivDde protecting group was removed as described for the oligomers with cMBP ligands (cf. 2.2.4.7). After complete deprotection, the PEG segment was attached to the ε-amine of the C-terminal lysine; according to the individual sequences, Fmoc-N-amido-dPEG₂₄-acid was coupled once (**638-641**) or twice (**672**). MTX was assembled in two steps. First, Fmoc-Glu-OtBu was coupled and deprotected, second 4-[[[(2,4-Diamino-6-pteridiny)methyl]methyl-amino]benzoic acid was attached. Both steps were carried out under the standard SPS conditions, however in case of the pteric acid derivative, a mixture of NMP/DMF/DMSO (1/1/1 v/v/v) was used as solvent of the coupling solution. In case of the polyglutamylated oligomers **639-641** and **672**, additional glutamic acid residues in the sequence between PEG and MTX were integrated by repeated coupling and deprotection of Fmoc-Glu-OtBu. Cleavage was carried out under standard conditions (cf. 2.2.3) and the oligomers were purified by SEC and analyzed by ¹H-NMR and analytical RP-HPLC.

2.2.5 Oligomer purification

2.2.5.1 Size-exclusion chromatography

All oligomers were purified by size exclusion chromatography using the ÄKTApurifier 10 system (GE Healthcare Bio-Sciences AB, Uppsala, Sweden) equipped with a P-900 solvent pump module, a UV-900 UV/VIS multi-wavelength detector, a pH/C-900 conductivity module and a Frac-950 automated fraction collector. Sephadex G-10 (MWCO 700 Da) was used as the gel filtration medium and 10 mM hydrochloric acid solution/acetonitrile 7/3 as eluent. The absorption at 214, 260 and 280 nm was monitored and the fractions corresponding to the high-molecular weight oligomer

were pooled, snap-frozen and freeze-dried. The low molecular weight constituents with higher elution times, such as TIS, cleavage side-products and acetylated truncation products were discarded. In consequence of the used eluent, the final product was present as HCl salt after the purification.

2.2.5.2 Preparative RP-HPLC

If the purity of an oligomer determined by analytical RP-HPLC was considered to be unsatisfactory, additional purification was carried out by preparative RP-HPLC using a VWR LaPrep system (VWR International GmbH, Darmstadt, Germany) and a Waters SymmetryPrep C18 column (7µm, 19x150mm). A water/acetonitrile gradient containing 0.1 % TFA was adjusted to the individual compound. After collection of the product, the solution was snap-frozen and freeze-dried. In consequence of the used eluent, the final product was present as TFA salt after the purification.

2.2.6 Analytics

2.2.6.1 ¹H-NMR

¹H-NMR spectroscopy was carried out using a Jeol JNM-R-GX 400 (400 MHz) or JNM-R-GX 500 (500 MHz). Chloroform-d (CDCl₃), deuterium oxide (D₂O) and methanol-d₄ (CD₃OD) were used as solvents. Chemical shifts were calibrated to the residual proton signals of the solvent and are reported in ppm. Data is indicated with s = singlet, d = doublet, t = triplet, m = multiplet. Spectra were analyzed using MestReNova (Mestrelab Research).

2.2.6.2 Analytical RP-HPLC

The purity of the oligomers was analyzed by RP-HPLC using a Waters HPLC system equipped with a Waters 600E multisolvent delivery system, a Waters 996 PDA detector and a Waters 717plus autosampler. As indicated, the compounds were analyzed using a Waters Sunfire C18 or Xbridge C18 column (5 µm, 4.6 x 150 mm) and a water/acetonitrile gradient (95:5 – 0:100) containing 0.1 % TFA. For the detection the extinction at 214 nm was monitored.

2.2.6.3 ESI-MS

Electrospray ionization (ESI) mass spectrometry was carried out with a Thermo Scientific LTQ FT Ultra fourier transform ion cyclotron and an IonMax source. Water containing 1 % formic acid was used as solvent for oligomers. Building blocks were dissolved in water, ethyl acetate or chloroform.

2.2.6.4 SDS-PAGE

The samples were supplemented with Laemmli sample buffer (Biorad, Munich, Germany), denatured at 95 °C for 5 minutes and subsequently loaded on a 12 % polyacrylamide gel. Following electrophoresis, the gel was fixated with a solution containing 50 % methanol, 12 % acetic acid and 0.019 % formaldehyde for 1 hour. After treatment with a sodium thiosulfate solution (127 mg/L) for 1 min, the gel was incubated for 20 min with a silver nitrate solution (2 g/L) containing 0.019 % formaldehyde. The gel was developed by incubation with a solution containing sodium carbonate (60 g/L), sodium thiosulfate (2.5 mg/L) and 0.019 % formaldehyde. The reaction was stopped after 5 min by addition of a solution containing 50 % methanol and 12 % acetic acid.

2.2.7 Alkalimetric titrations

Automated titrations were carried out with a Metrohm Titrando 905 equipped with a Biotrode pH electrode (METROHM GmbH & Co. KG, Filderstadt, Germany). The sample amount corresponding to the indicated amount of protonatable amines was dissolved in 3.5 mL of 50 mM sodium chloride solution. The pH was adjusted below 2 with hydrochloric acid. Titrations were carried out with 50 mM sodium hydroxide solution until the endpoint of pH 11 was reached. To distinguish polymer and solvent effects, a control titration of 50 mM sodium chloride solution without polymer was performed. Volume differences (ΔV) between defined pH values were determined. The total endosomal buffer capacity C in the pH range between 5 and 7.4 was calculated according to formula (1), the relative protonation C' in endosomal sub-ranges pH_x to pH_y ($5 \leq pH_x < pH_y \leq 7.4$) was determined according to formula (2).

$$(1) \quad C_{pH5-7.4} = \frac{[\Delta V(\text{Sample})_{pH5-7.4} - \Delta V(\text{NaCl})_{pH5-7.4}] \cdot 50 \text{ mM}}{n} \cdot 100 \%$$

$$(2) \quad C'_{pH_x-pH_y} = \frac{\Delta V(\text{Sample})_{pH_x-pH_y} - \Delta V(\text{NaCl})_{pH_x-pH_y}}{\Delta V(\text{Sample})_{pH5-7.4} - \Delta V(\text{NaCl})_{pH5-7.4}} \cdot 100 \%$$

C, total buffer capacity between the indicated pH values [%]; C', relative protonation in the indicated pH subrange [%], total buffer capacity is set to 100 %; ΔV , volume difference between the indicated pH values [ml]; n, amount of protonatable amines [μmol].

2.2.8 Polyplex formation

2.2.8.1 pDNA polyplexes

For *in vitro* transfections 200 ng of pDNA and the corresponding amount of oligomer at indicated N/P ratio were diluted in separate tubes in HBG to a volume of 10 μL each. The oligomer solution was added to the pDNA solution and mixed by pipetting. The polyplex formation was accomplished after incubation at room temperature for 40 min. Polyplex solutions for DLS measurements, flow cytometry experiments and *in vivo* trials containing different amounts of pDNA were prepared similarly.

2.2.8.2 Poly(I:C) and poly(I) polyplexes

For *in vitro* transfections 1 μg of nucleic acid and the corresponding amount of oligomer at indicated N/P ratio were diluted in separate tubes in HBG to a volume of 10 μL each. The oligomer solution was added to the nucleic acid solution and mixed by pipetting. The polyplex formation was accomplished after incubation at room temperature for 40 min. Polyplex solutions for DLS measurements, electrophoretic mobility shift assays or flow cytometry experiments containing different amounts of nucleic acids were prepared similarly.

2.2.9 Ethidium bromide exclusion assay

A Cary Eclipse spectrophotometer (Varian, Germany) was used for the quantification of ethidium bromide (EtBr) fluorescence at the excitation wavelength $\lambda_{\text{ex}} = 510 \text{ nm}$ and emission wavelength $\lambda_{\text{em}} = 590 \text{ nm}$. 1 mL HBG buffer containing 0.4 μg EtBr was

used as blank. After addition of 10 µg pDNA the solution was incubated for 3 minutes and EtBr fluorescence was assigned to 100 %. Increasing amounts of oligomer corresponding to indicated N/P ratios were added, incubated for 30 seconds and the EtBr fluorescence was determined in relation to the 100 % value.

2.2.10 Electrophoretic mobility shift assay

A 1 % agarose gel was prepared by dissolution of agarose in TBE buffer under heating. After cooling to 50 °C, GelRed for the nucleic acid staining was added and the agarose solution was poured into the casting unit. Polyplexes containing 200 ng pDNA or 800 ng poly(I:C) and loading buffer were placed into the sample pockets. For pDNA polyplexes electrophoresis was carried out during 80 min using a voltage of 80 V, for poly(I:C) polyplexes a voltage of 85 V over a time of 90 min was used. For the investigation of serum stability, polyplexes containing 0.8 µg poly(I:C) and oligomer at N/P 20 were initially prepared at a 10-fold higher concentration than in the regular formulations. Subsequently the polyplex solutions were diluted 1:10 with FCS and incubated at room temperature for 15, 45 or 90 minutes before electrophoresis.

2.2.11 Particle size and zeta Potential

Particle size and zeta potential of polyplexes were determined by dynamic and electrophoretic light scattering using a Zetasizer Nano ZS with backscatter detection (Malvern Instruments, Worcestershire, UK). Polyplexes containing 10 µg nucleic acid and oligomer at indicated N/P ratio were prepared in 50 µL HBG as described before (cf. 2.2.8.1 and 2.2.8.2). After complete polyplex formation, the solution was diluted to a total volume of 800 µL with 20 mM HEPES (pH 7.4) and placed in a folded capillary cell (DTS1061). Measurements were carried out at 25 °C using a refractive index of 1.330 and a viscosity of 0.8872 cP as the defined parameters of the dispersion medium. The cumulants analysis method was used for the determination of the Z-average diameter and polydispersity index (PDI). Each sample was measured three times with 10 subruns of 10 s during particle size measurements and 10 to 30

subruns of 10 s during zeta potential measurements. Values are reported as arithmetic mean and standard deviation of the three measurements.

2.2.12 Luciferase reporter gene expression *in vitro*

pDNA transfections were carried out by Dr. Petra Kos and Ana Krhac Levacic (Pharmaceutical Biotechnology, LMU). Cells were seeded 24 h prior to the transfections in 96-well plates. In case of DU145, KB and Neuro2A cells, 10.000 cells were seeded per well. Huh7 cells were seeded using 8.000 cells per well. After 24 h, the culture medium was replaced by 80 μ L fresh medium containing 10 % FCS. Polyplexes containing 200 ng pCMVLuc, formed in 20 μ L HBG were added to each well and incubated on the cells for 24 h at 37 °C. For transfection experiments with targeted oligomers, the incubation time was shortened to 45 min, followed by incubation with fresh medium containing 100 μ M chloroquine (for control experiments without chloroquine, only fresh medium was added). After 4 h, the medium was again replaced by fresh medium and cells were further incubated for 20 h. LPEI at nontoxic optimum N/P 6 was used as positive control, HBG buffer was used as negative control. 24 h after the transfections, cells were treated with 100 μ L cell culture lysis reagent (Promega, Mannheim, Germany). Luciferase activity in the cell lysate was measured using the luciferase assay kit (Promega, Mannheim, Germany) and a Centro LB 960 plate reader luminometer (Berthold Technologies, Bad Wildbad, Germany). Experiments were performed in quintuplicates.

2.2.13 Luciferase reporter gene expression *in vivo*

Animal experiments were carried out by Annika Herrmann and Dr. Petra Kos (Pharmaceutical Biotechnology, LMU). Female Rj:NMRI-nu (nu/nu) mice (Janvier, Le Genest-St-Isle, France) were used for the *in vivo* trials. 5×10^6 N2A or Huh7 cells were inoculated subcutaneously into the left flank. 12 days after tumor cell injection, polyplexes were injected into the tumor or into the tail vein. In case of the intratumoral administration, polyplexes containing 50 μ g pCMVLuc at N/P 12 in a total volume of 60 μ L HBG were used and the mice were sacrificed after 24 h. For the systemic delivery, polyplexes at N/P 12 containing either 60 μ g pCMVLuc (N2A tumor model)

or 80 µg pCMVLuc (Huh7 tumor model) in a total volume of 200 µL HBG were injected into the tail vein and the animals were sacrificed after 48 h. Organs and/or tumors were dissected and homogenized in cell culture lysis reagent using a tissue and cell homogenizer (FastPrep®-24, MP Biomedicals, USA). Samples were centrifuged at 3000 g and 4 °C for 10 min to remove insoluble tissue components. Luciferase activity of the supernatant was determined using a Centro LB 960 luminometer (Berthold Technologies, Bad Wildbad, Germany). All animal procedures were approved and controlled by animal experiments ethical committee of Regierung von Oberbayern (District Government of Upper Bavaria, Germany) and carried out according to the guidelines of the German law of protection of animal life.

2.2.14 Flow cytometry

2.2.14.1 Cellular association of pDNA polyplexes

Flow cytometry experiments with pDNA polyplexes were carried out by Dr. Petra Kos (Pharmaceutical Biotechnology, LMU). Cells were seeded into 24-well plates coated with collagen at a density of 5×10^4 cells/well. After 24 h, the culture medium was replaced by 400 µL fresh growth medium. pDNA polyplexes containing 1 µg pDNA (20 % Cy5-labeled) and oligomer at N/P 12 in 100 µL HBG were added to each well and incubated on ice for 30 min. The cells were washed twice with 500 µL PBS subsequently. Cells were detached with trypsin/EDTA and collected in PBS containing 10 % FCS. Cy5 fluorescence was detected by excitation at 635 nm and emission at 665 nm. DAPI (4',6-diamidino-2-phenylindole) was used to discriminate between viable and dead cells. Data was recorded using a Cyan™ ADP flow Cytometer (Dako, Hamburg, Germany) and Summit™ acquisition software (Summit, Jamesville, NY, USA). Data evaluation was carried out using FlowJo® 7.6.5 flow cytometry data analysis software.

2.2.14.2 Cellular uptake of pDNA polyplexes

Flow cytometry experiments with pDNA polyplexes were carried out by Dr. Petra Kos (Pharmaceutical Biotechnology, LMU). Cells were seeded into 24-well plates coated with collagen at a density of 5×10^4 cells/well. After 24 h, culture medium was

replaced by 400 μL fresh growth medium. pDNA polyplexes containing 1 μg pDNA (20 % Cy5-labeled) and oligomer at indicated N/P in 100 μL HBG were added to each well and incubated for 30 min at 37 °C. Cells were then washed with PBS and incubated with 500 μL PBS containing 100 I.U. of heparin for 15 min to remove non-internalized polyplexes on the cell surface. Cells were detached with trypsin/EDTA and collected in PBS containing 10 % FCS. Cy5 fluorescence was detected by excitation at 635 nm and emission at 665 nm. DAPI was used to discriminate between viable and dead cells. Data was recorded using a Cyan™ ADP flow Cytometer (Dako, Hamburg, Germany) and Summit™ acquisition software (Summit, Jamesville, NY, USA). Data evaluation was carried out using FlowJo® 7.6.5 flow cytometry data analysis software.

2.2.14.3 Cellular uptake of poly(I:C) polyplexes

Flow cytometry experiments with poly(I:C) polyplexes were carried out by Valentin Wittmann (graduate student, LMU). Cells were seeded on collagen coated 24-well plates at a density of 5×10^4 cells/well one day before the experiment. After 24 h, culture medium was replaced by 450 μL fresh growth medium either folate-free or saturated with folic acid. Polyplexes containing 2.5 μg poly(I:C) (20 % Cy5-labeled) and oligomer at N/P 16 in 50 μL HBG were added to each well and incubated for 30 min at 37 °C. The medium was removed and cells were treated twice with PBS containing 100 I.U. Heparin/mL for 15 min to remove non-internalized polyplexes. Cells were detached with trypsin/EDTA and collected in PBS containing 10 % FCS. Cy5 fluorescence was detected by excitation at 635 nm and emission at 665 nm. DAPI was used to discriminate between viable and dead cells. Data were recorded using a Cyan™ ADP flow Cytometer (Dako, Hamburg, Germany) and Summit™ acquisition software (Summit, Jamesville, NY, USA). Data evaluation was carried out using FlowJo® 7.6.5 flow cytometry data analysis software. All experiments were performed in triplicates.

2.2.15 Metabolic activity assay (MTT)

2.2.15.1 Metabolic activity of pDNA transfected cells

MTT assays with pDNA transfected cells were carried out by Dr. Petra Kos and Ana Krhac Levacic (Pharmaceutical Biotechnology, LMU). Cells were transfected as described in 2.2.12. 24 h after the transfections, 10 μ L of a MTT solution (5 mg/mL) were added to the medium. After 2 h incubation, the supernatant was removed and cells were lysed by freezing at -80 °C and thawing at room temperature. The colored formazan product was dissolved in dimethyl sulfoxide (100 μ L/well) and quantified photometrically at 590 nm using a SpectraFluor™ Plus microplate reader (Tecan, Groedig, Austria). The relative metabolic activity was calculated by comparison with control cells treated with HBG. Experiments were performed in quintuplicates.

2.2.15.2 Metabolic activity of poly(I:C) transfected cells

MTT assays with poly(I:C) transfected cells were carried out by Valentin Wittmann (graduate student, LMU) and Katharina Müller (Pharmaceutical Biotechnology, LMU). KB cells were seeded into 96-well plates coated with collagen at a density of 4×10^3 cells/well in 100 μ L growth medium 24 h prior to the treatment. The medium was replaced by 80 μ L fresh medium and 20 μ L of polyplex solution in HBG. After 48 h incubation time (37 °C, 5 % CO₂), the medium was replaced by 100 μ L fresh growth medium. 10 μ L of MTT solution (5 mg/mL) were added to each well. After 2 h incubation, the supernatant was removed and cells were lysed by freezing at -80 °C and thawing at room temperature. The colored formazan product was dissolved in dimethyl sulfoxide (100 μ L/well) and quantified photometrically at 590 nm using a SpectraFluor™ Plus microplate reader (Tecan, Groedig, Austria). The relative metabolic activity was calculated by comparison with control cells treated with HBG. Experiments were performed in triplicates.

2.2.15.3 Metabolic activity of cells treated with oligomer and MTX solutions

MTT assays with cells treated with oligomer and MTX solutions were carried out by Valentin Wittmann (graduate student, LMU) and Katharina Müller (Pharmaceutical Biotechnology, LMU). KB cells were prepared as described in 2.2.15.2. 24 h after

seeding, the medium was replaced by 100 μL of oligomer or MTX solution (80 % medium, 20 % HBG) with defined concentration between 3 nM and 10 μM . After 48 h incubation time (37 $^{\circ}\text{C}$, 5 % CO_2), the medium was replaced by 100 μL fresh growth medium and 10 μL of MTT solution (5 mg/mL) were added. Subsequent steps were carried out in the same way as described in 2.2.15.2. The dose-response relationships were approximated by four-parameter logistic models and the values for the half maximal effective concentration (EC_{50}) and the maximal effect (E_{max}) were determined.

2.2.16 Dihydrofolate reductase activity assay

The enzymatic activity of DHFR in presence of MTX or MTX conjugates was determined by a dihydrofolate reductase assay kit (Sigma-Aldrich, Munich, Germany) based on the NADPH dependent reduction of dihydrofolic acid to tetrahydrofolic acid. The assay was conducted according to the manufacturer's protocol. MTX and all tested compounds were dissolved in the provided assay buffer and used at a final concentration of 100 nM in the reaction mixture. The reaction progress was monitored photometrically (Genesys 10S, Thermo Scientific, Dreieich, Germany) over a period of 5 min by measurement of NADPH absorption at 340 nm each 15 s. Control reactions in absence of inhibitors were carried out. Data points were fitted by linear regression and the gradient was determined. Relative enzyme activity was calculated as ratio between the gradient of the reaction with test compound to the gradient of the control reaction without inhibition according to formula (3). For each compound the assay was carried out in triplicates.

$$(3) \quad \text{DHFR Act. [\%]} = \frac{\frac{\Delta A}{\Delta t}(\text{Sample})}{\frac{\Delta A}{\Delta t}(\text{Control})} \cdot 100 \%$$

A, absorption at 340 nm; t, time [s].

2.2.17 Fluorescence microscopy

2.2.17.1 Calcein release assay

Calcein release assays were carried out by Dr. Frauke Mickler (Physical Chemistry, LMU). 10.000 DU145 cells per well were seeded on ibidi μ -slides (ibidi GmbH, Planegg/Martinsried, Germany) 48 h prior to particle addition. For the determination of calcein release by B6 targeted oligomers, 20 μ L of polyplexes (400 ng DNA, N/P 16) were coincubated with 0.5 mg/mL calcein in 200 μ L RPMI medium containing 10 % FCS for 3.5 hours on the cells. Afterwards cells were washed 4 times with PBS, and the medium was replaced with 300 μ L CO₂ independent medium (Gibco Life Technologies GmbH, Darmstadt, Germany) containing 10 % FCS. Z-slices of single cells were imaged by spinning disk confocal microscopy (Nikon TE2000E microscope with Yokogawa CSU10 spinning disk unit, an EM-CCD camera (iXon DV884, Andor) and a Nikon 1.49 NA 100x Plan Apo oil immersion objective) with 488 nm laser excitation. In case of the cMBP targeted oligomers, polyplexes at N/P 12 containing 400 ng pDNA were added to 200 μ L fresh RPMI medium on the cells. After 40 min incubation time, the cell medium was replaced by 300 μ L fresh RPMI medium containing 0.5 mg/ml calcein. Cells were imaged 20 h after particle addition. Calcein fluorescence in the cytosol was quantified by digital image analysis in ImageJ. Mean grey values of pixels from extracellular regions (background) and endosomal compartments (endosome fluorescence) were determined and two threshold values were set to exclude those regions from quantification. The integrated intensity of cytosolic pixels above the lower background threshold and below the upper endosomal threshold was then calculated (integrated intensity = number of selected pixels * mean grey value of selected pixels).

2.2.17.2 Live cell imaging

Live cell imaging experiments were carried out by Dr. Frauke Mickler (Physical Chemistry, LMU). Spinning disk confocal microscopy was performed with a Nikon TE2000E microscope equipped with a Yokogawa CSU10 spinning disk unit, an EM-CCD camera (iXon DV884, Andor) and a Nikon 1.49 NA 100x Plan Apo oil immersion objective. 640 nm laser light was used for the excitation of Cy5. Wide-field fluorescence microscopy was performed with a custom built Nikon Ti microscope

equipped with a Plan Apo 60x, 1.49 NA oil immersion objective and EM-CCD cameras (DU-897 iXon+, Andor). 633 nm laser light was used for the excitation of Cy5.

2.2.17.3 Intracellular distribution of poly(I:C) polyplexes

Fluorescence microscopy with poly(I:C) polyplexes was carried out by Katharina Müller and Miriam Höhn (Pharmaceutical Biotechnology, LMU). KB cells were seeded at a density of 2×10^4 cells/well in 300 μ L growth medium into a 8 well Labtek chamber slide coated with collagen 24 h prior to treatment. Polyplexes were formed as described using 1.5 μ g of a mixture of 80 % unlabeled and 20 % Cy5 labeled poly(I:C) and a mixture of the depicted oligomer at N/P 16 (80 %) and Alexa Fluor 488 labeled oligomer **583** at N/P 4 (20 %) in 60 μ L HBG. Medium was replaced with 240 μ L fresh growth medium and the polyplex solution was added. The chamber slide was incubated at 37 °C for 30 minutes. Cells were washed twice with 500 μ L PBS and cell nuclei were stained with Hoechst 33342 dye. A Leica TCS SP8 confocal microscope was used for image acquisition.

2.2.18 Statistical analysis

Unless otherwise stated, results are presented as arithmetic mean \pm standard deviation (SD) and the number of replicates. Statistical significance was determined in one-tailed t-tests. Significance levels are indicated with star symbols. *: $P \leq 0.05$; **: $P \leq 0.01$; ***: $P \leq 0.001$.

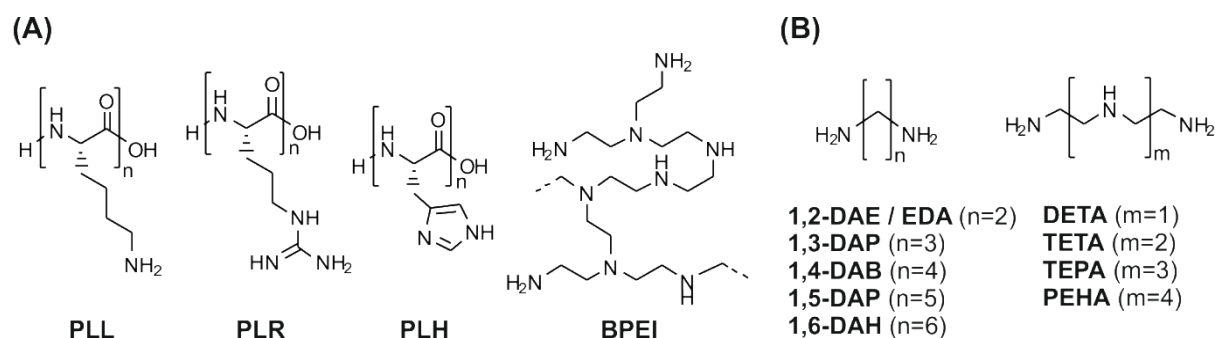
3 Results

3.1 The modulation of proton-sponge activity in oligo(ethanamino)amides

Basic polymers can facilitate nucleic acid delivery in several steps by means of their properties as protonatable bases. Protonated cationized groups account for the electrostatic nucleic acid binding and cellular uptake. Residual unprotonated functions can offer a buffer capacity to mediate polyplex escape from acidifying vesicles via the hypothesized proton-sponge effect. However, to serve these separate purposes, different basic strengths have to be combined and balanced. Therefore, not all basic polymers are suited as transfecting agents. Several basic polymers, despite a potent pDNA binding, do not mediate transgene expression. In general, the endosomal escape is regarded as one of the most critical barriers within the nucleic acid delivery pathway. This chapter describes different approaches, which were taken to modulate the endosomal buffering of oligo(ethanamino)amides and to identify requirements for an enhanced proton-sponge activity in pDNA polyplexes.

3.1.1 The protonation of basic polymers and polyamines

The characteristics of different basic compounds regarding the protonation and buffering in certain pH ranges were investigated by alkalimetric titrations. Poly-L-arginine (PLR), poly-L-lysine (PLL), poly-L-histidine (PLH) and branched polyethylenimine (BPEI) were chosen as a set of well-known basic polymers (Scheme 3.1 A). Figure 3.1 shows the titration curves with the highlighted endosomal range between pH 5 and 7.4. The titration curve of PLR did not show a big difference compared to the sodium chloride reference titration, since the highly stable guanidinium groups are not deprotonated to a notable extent in the investigated titration range below pH 11. PLL showed a similar course through the endosomal pH range like sodium chloride and PLR, but the gradient decreased in the range around pH 10.2, which represents the pK_a value of the primary ϵ -amines of lysine.

Scheme 3.1 Compounds investigated by alkalimetric titrations


(A) Selection of common basic polymers and (B) polyamines. PLL, poly-L-lysine; PLR, poly-L-arginine; PLH, poly-L-histidine; BPEI, branched polyethylenimine; 1,2-DAE, 1,2-diaminoethane; EDA, ethylene diamine; 1,3-DAP, 1,3-diaminopropane; 1,4-DAB, 1,4-diaminobutane; 1,5-DAP, 1,5-diaminopentane; 1,6-DAH, 1,6-diaminohexane; DETA, diethylene triamine; TETA, triethylene tetramine; TEPA, tetraethylene pentamine; PEHA, pentaethylene hexamine.

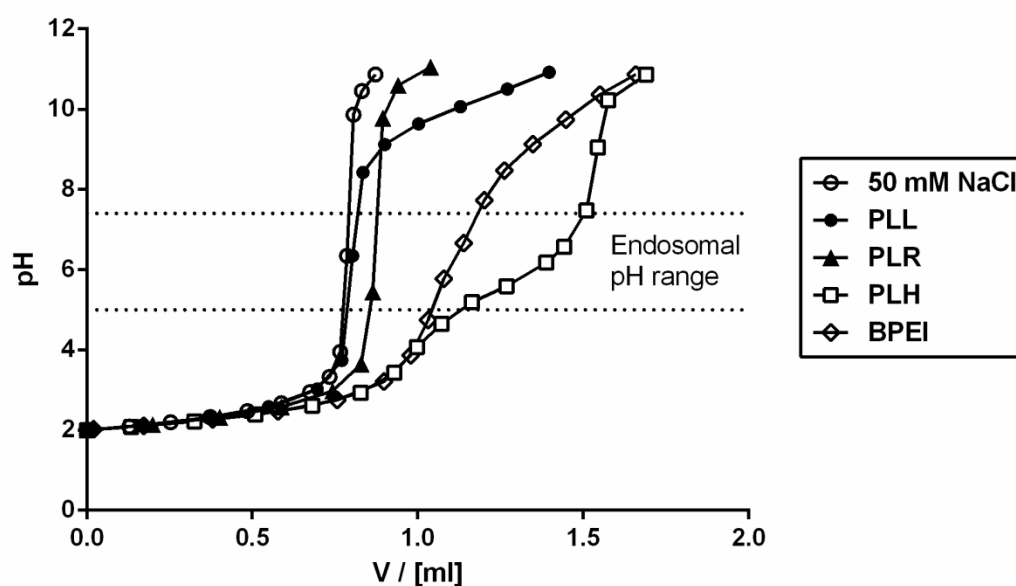


Figure 3.1 Titration curves between pH 2 and 11 of common basic polymers. Polymer solutions containing 30 μmol protonatable nitrogens were acidified with hydrochloric acid and backtitrated with 50 mM sodium hydroxide solution. Sodium chloride was used for a reference titration without buffering agent. PLL, poly-L-lysine; PLR, poly-L-arginine; PLH, poly-L-histidine; BPEI, branched polyethylenimine.

Within the whole set, the flattest slope between pH 5 and 7.4, indicating the highest endosomal buffer capacity, was observed in the titration curve of PLH. The gradient of the curve had its minimum around pH 6. However, above pH 7.4 the titration curve showed a similar course as sodium chloride or PLR, since the amount of

imidazolium groups available for deprotonation decreases exponentially with increasing pH. As a result of the definite pK_a values of arginine, histidine and lysine, the protonation (and deprotonation) of the peptidic homopolymers occurred in a rather narrow pH range. The exclusive protonation and buffering in a defined range of the pH scale explains the inability of the three basic polymers to mediate efficient gene transfer without additional modifications, since different pH ranges have to be covered for this purpose. In sharp contrast, BPEI exhibited a continuous buffering over a broad range, including the endosomal area and above, which provides sufficient protonation at neutral pH for pDNA binding but also a buffer capacity for proton-sponge activity in the endosomes. This can be explained by the proximity of the protonatable groups within the polymer. The protonation of the diaminoethane nitrogens in PEI affects the basicity of neighboring groups. With proceeding protonation the basicity of unprotonated groups decreases resulting in a continuous buffering. Thus the titration curve of BPEI is the result of a wide array of changing pK_a values, which depend on the pH and the protonation state of the polymer.

To investigate the sequential protonation of linear polyamines in more detail, two sets of compounds were arranged (Scheme 3.1 B). First, diamines with different length of the aliphatic spacer (C2 to C6) were used for alkalimetric back titrations to provide information about the influence of the distance between protonatable groups and the hindrance of protonation. Second, polyamines with different numbers of diaminoethane nitrogens (2N to 6N) were titrated. Figure 3.2 shows the titration curves of the different aliphatic diamines. Although all samples contained the same amount of primary amines, the curves deviated from each other as a result of the different hydrocarbon spacers. In all diamines the first protonation (second deprotonation) had its maximum at pH 10 or above. Since no big difference between the titration curves of 1,6-diaminohexane (1,6-DAH) and methylamine could be observed, the second protonation (first deprotonation) of 1,6-DAH seemed to be only marginally affected by the neighboring ammonium group. However, with decreasing length of the aliphatic spacer, the pK_a values for the second protonation decreased, which can be seen by the shifts of the flattened upper part of the curves toward lower pH values. In case of three or less separating methylene groups (1,3-DAP, 1,2-DAE), the proximity of a neighboring protonated amine decreased the pK_a for a second protonation to values below 9. Consequently, for the shortest compound 1,2-

diaminoethane (1,2-DAE) the lowest pK_a value of approx. 7.2, buffering also in the endosomal pH range, could be observed. These findings illustrate the utility of the diaminoethane motif to promote buffering in the biologically relevant pH ranges.

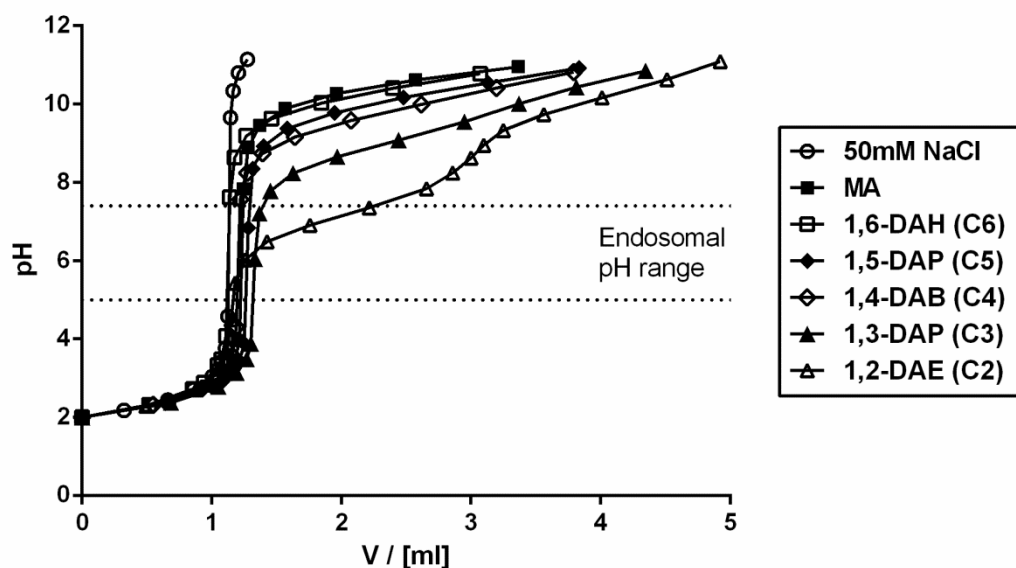


Figure 3.2 Titration curves between pH 2 and 11 of diamines with different aliphatic spacers. Polymer solutions containing 200 μmol protonatable nitrogens were acidified with hydrochloric acid and backtitrated with 50 mM sodium hydroxide solution. Sodium chloride was used for a reference titration without buffering agent, methylamine for a titration with unhindered protonation of primary amines. MA, methylamine; 1,6-DAH, 1,6-diaminohexane; 1,5-DAP, 1,5-diaminopentane; 1,4-DAB, 1,4-diaminobutane; 1,3-DAP, 1,3-diaminopropane; 1,2-DAE, 1,2-diaminoethane. C2 to C6 indicate the length of the aliphatic spacer.

The titration curves of larger polyamines, containing repeating diaminoethane units, revealed a remarkable pattern depending on an even or odd number of contained protonatable amines (Figure 3.3). The curves of diethylene triamine (DETA, 3N) and tetraethylene pentamine (TEPA, 5N) had a notably similar course. The same observation could be made for triethylene tetramine (TETA, 4N) and pentaethylene hexamine (PEHA, 6N). The compounds with even number of protonatable amines exhibited much higher buffering in the endosomal pH range than the odd numbered as a result of the location of their pK_a values.

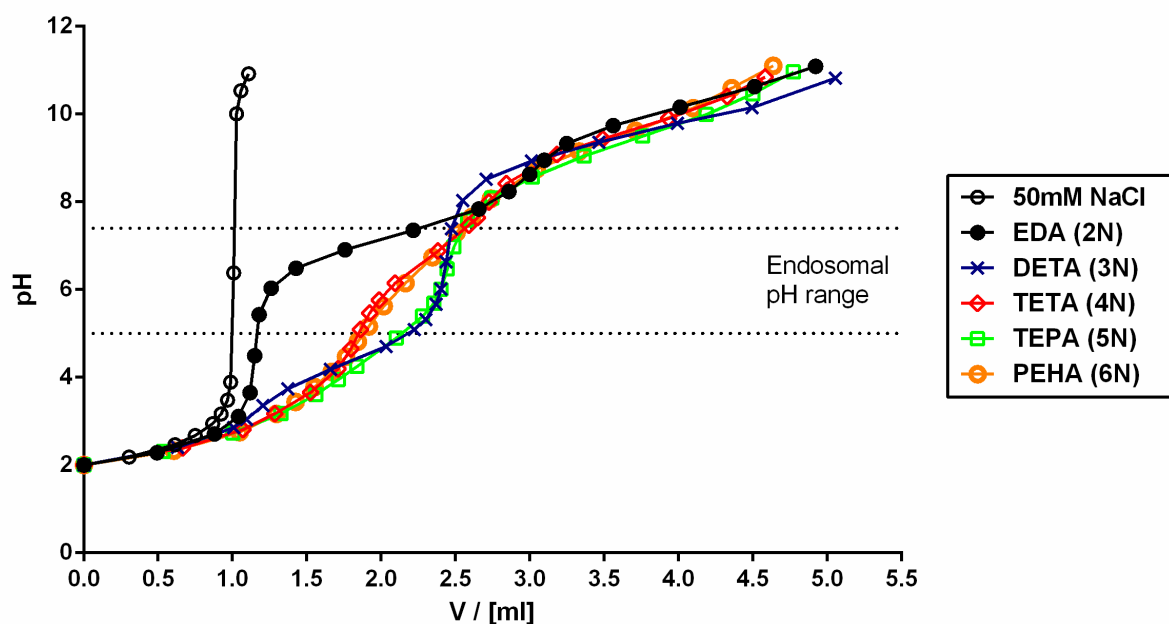


Figure 3.3 Titration curves between pH 2 and 11 of polyamines with different numbers of diaminoethane nitrogens. Polymer solutions containing 200 μmol protonatable nitrogens were acidified with hydrochloric acid and backtitrated with 50 mM sodium hydroxide solution. Sodium chloride was used for a reference titration without buffering agent. EDA, ethylene diamine; DETA, diethylene triamine; TETA, triethylene tetramine; TEPA, tetraethylene pentamine; PEHA, pentaethylene hexamine. N indicates the number of protonatable nitrogens per molecule.

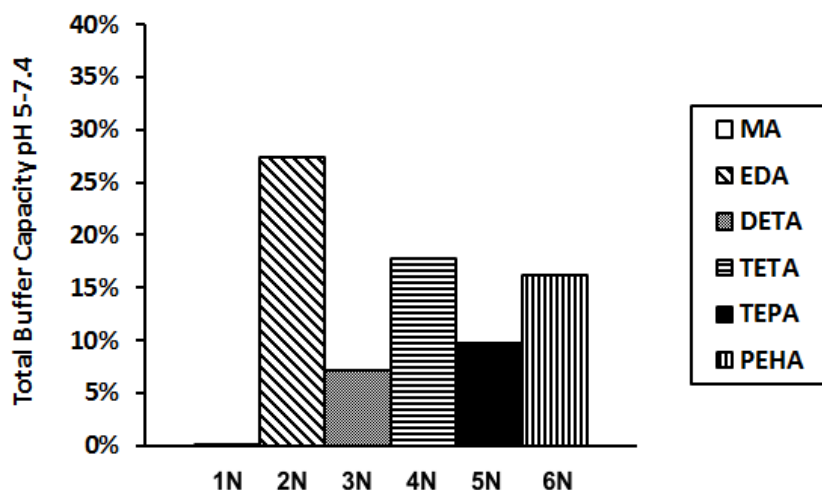


Figure 3.4 Total endosomal buffer capacity between pH 5 and 7.4 of linear polyamines as determined by alkalimetric titrations. Methylamine served as a reference compound with unhindered protonation of a primary amine. MA, methylamine; EDA, ethylene diamine; DETA, diethylene triamine; TETA, triethylene tetramine; TEPA, tetraethylene pentamine; PEHA, pentaethylene hexamine. N indicates the number of protonatable nitrogens per molecule.

Figure 3.4 illustrates the endosomal buffer capacity of the compounds, which measures the portion of basic groups getting protonated between pH 5 and 7.4. A clear even-odd correlation could be observed, since all polyamines with even number of diaminoethane nitrogens had higher buffer capacities than the members with odd number. The endosomal buffer capacities seemed to converge with increasing length of the polyamines. Obviously, the buffering over a broad pH range gets more homogeneous with increasing number of nitrogens (cf. Figure 3.1 BPEI). Therefore, the even-odd effect is most pronounced for short polyamines.

3.1.2 The proton-sponge activity of different polyamino acids and their combinations with histidine

This chapter has been adapted from:

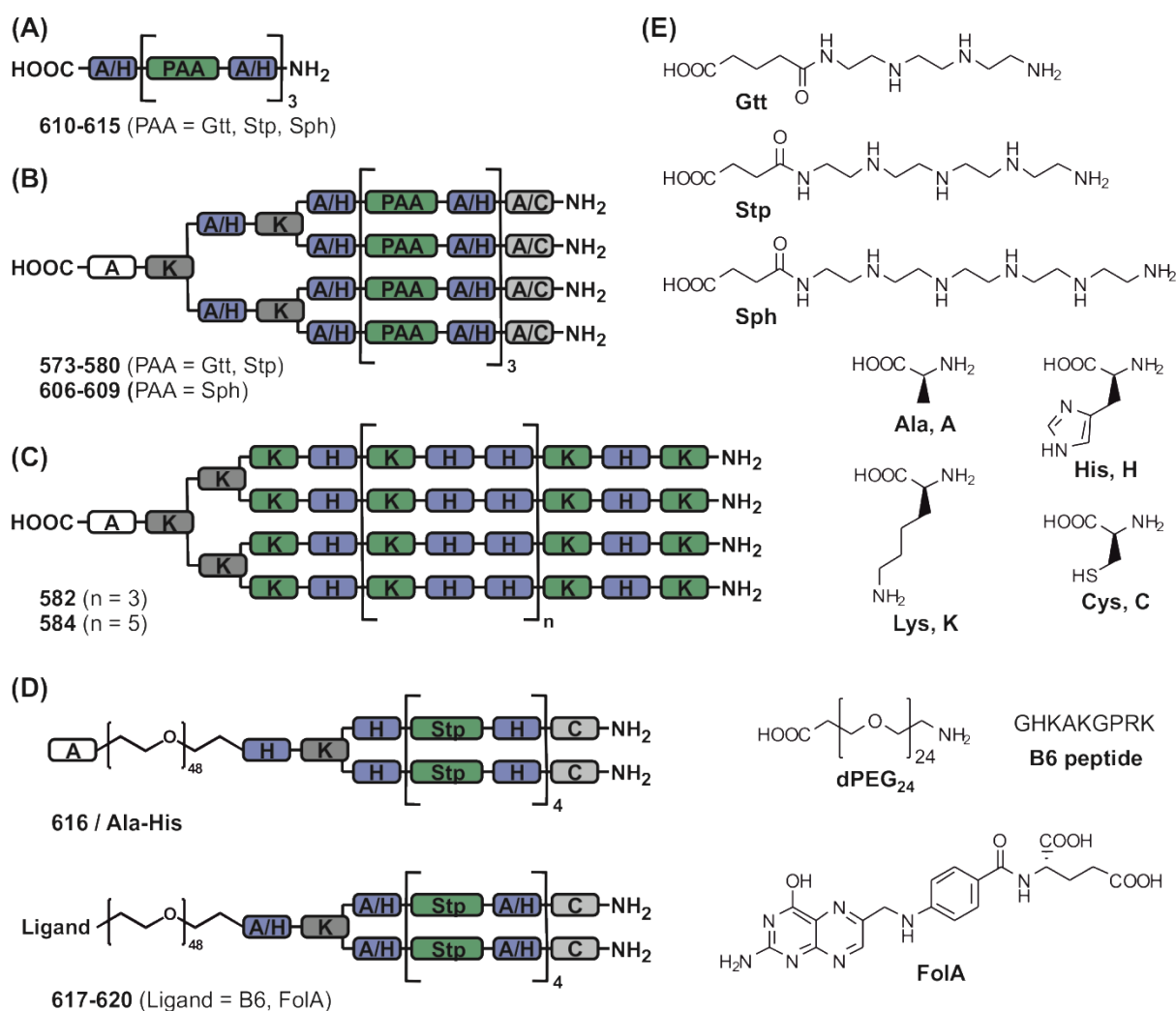
Lächelt U, Kos P, Mickler FM, Herrmann A, Salcher EE, Rödl W, Badgujar N, Bräuchle C and Wagner E, "Fine-tuning of proton sponges by precise diaminoethanes and histidines in pDNA polyplexes.", Nanomedicine NBM, 2014, 10(1):35-44.

Different polyamino acid (PAA) building blocks can be used for the synthesis of sequence-defined oligo(ethanamino)amides for pDNA delivery. Coupled at an internal position of the sequence, the polyamino acid glutaryl-triethylene tetramine (Gtt) offers two, succinyl-tetraethylene pentamine (Stp) three and succinyl-pentaethylene hexamine (Sph) four protonatable amines. Since polyamines with different numbers of diaminoethane units exhibit different characteristics, regarding protonation and endosomal buffering (cf. Figure 3.3 and 3.4), the individual properties of oligo(ethanamino)amides, based on the separate building blocks, were investigated. Within the set of natural amino acids, histidine with a pK_a of the imidazole group around 6 is ideal for a specific modulation of the endosomal buffer capacity. With this motivation, the additional effect of histidine on the endosomal buffering and proton-sponge activity of oligo(ethanamino)amides, based on the different PAA building blocks, was investigated.

3.1.2.1 Library design and synthesis

Solid-phase assisted synthesis was used for the assembly of oligomers comprising different PAA building blocks and histidines as DNA-binding and buffering units, optionally α,ϵ -amidated lysines as branching points, cysteines for a stabilizing disulfide formation and ligand-PEG as functional shielding and cell targeting domain. Alanines were used as non-functional substitutes for histidine, cysteine or the targeting ligand, respectively. The library can be classified into three topology groups with incremental complexity. Scheme 3.2 and Table 3.1 give an overview over the synthesized compounds.

Scheme 3.2 Illustration of the synthesized oligomers with different topologies



(A) Linear topology, (B) four-arm topology, (C) four-arm topology HK peptides, (D) PEGylated two-arm topology, (E) chemical structures of building blocks. Adapted from [183].

Table 3.1 Sequences, topologies and abbreviations of the investigated oligomers

ID	Sequence (C -> N)	Topology	Abbreviation
610	A-Gtt-A-Gtt-A-Gtt-A	linear	A-(Gtt-A) ₃
611	H-Gtt-H-Gtt-H-Gtt-H	linear	H-(Gtt-H) ₃
612	A-Stp-A-Stp-A-Stp-A	linear	A-(Stp-A) ₃
613	H-Stp-H-Stp-H-Stp-H	linear	H-(Stp-H) ₃
614	A-Sph-A-Sph-A-Sph-A	linear	A-(Sph-A) ₃
615	H-Sph-H-Sph-H-Sph-H	linear	H-(Sph-H) ₃
580	AK[AK(A-Gtt-A-Gtt-A-Gtt-AA) ₂] ₂	four-arm	Gtt-AA
578	AK[HK(H-Gtt-H-Gtt-H-Gtt-HA) ₂] ₂	four-arm	Gtt-HA
579	AK[AK(A-Gtt-A-Gtt-A-Gtt-AC) ₂] ₂	four-arm	Gtt-AC
577	AK[HK(H-Gtt-H-Gtt-H-Gtt-HC) ₂] ₂	four-arm	Gtt-HC
576	AK[AK(A-Stp-A-Stp-A-Stp-AA) ₂] ₂	four-arm	Stp-AA
574	AK[HK(H-Stp-H-Stp-H-Stp-HA) ₂] ₂	four-arm	Stp-HA
575	AK[AK(A-Stp-A-Stp-A-Stp-AC) ₂] ₂	four-arm	Stp-AC
573	AK[HK(H-Stp-H-Stp-H-Stp-HC) ₂] ₂	four-arm	Stp-HC
609	AK[AK(A-Sph-A-Sph-A-Sph-AA) ₂] ₂	four-arm	Sph-AA
607	AK[HK(H-Sph-H-Sph-H-Sph-HA) ₂] ₂	four-arm	Sph-HA
608	AK[AK(A-Sph-A-Sph-A-Sph-AC) ₂] ₂	four-arm	Sph-AC
606	AK[HK(H-Sph-H-Sph-H-Sph-HC) ₂] ₂	four-arm	Sph-HC
582	AK[K(KH-(KHH) ₃ -KHK) ₂] ₂	four-arm HK peptide	(KHH) ₃ -KHK
584	AK[K(KH-(KHH) ₅ -KHK) ₂] ₂	four-arm HK peptide	(KHH) ₅ -KHK
616	A-(dPEG ₂₄) ₂ -HK[H-(Stp-H) ₄ -C] ₂	PEGylated two-arm	Ala-His
617	KRPGKAKHG-(dPEG ₂₄) ₂ -AK[A-(Stp-A) ₄ -C] ₂	PEGylated two-arm	B6-Ala
618	KRPGKAKHG-(dPEG ₂₄) ₂ -HK[H-(Stp-H) ₄ -C] ₂	PEGylated two-arm	B6-His
619	K[(dPEG ₂₄) ₂ -FoIA]-AK[A-(Stp-A) ₄ -C] ₂	PEGylated two-arm	FoIA-Ala
620	K[(dPEG ₂₄) ₂ -FoIA]-HK[H-(Stp-H) ₄ -C] ₂	PEGylated two-arm	FoIA-His

Oligomers **573-580** were synthesized by Dr. Edith Salcher, oligomers **582** and **584** were synthesized by Wolfgang Rödl. Adapted from [183].

In a first step, linear structures (Scheme 3.2 A) based on the three PAA building blocks Gtt, Stp and Sph were alternately assembled with histidine or alanine. These linear oligomers served as simple model compounds for alkalimetric titrations and the determination of endosomal buffer characteristics.

In a second step, larger dendron-like four-arm topology oligomers (Scheme 3.2 B) for the formation of pDNA polyplexes were assembled. The oligomers were evaluated in pDNA complexation assays, size and zeta-potential measurements of the corresponding pDNA polyplexes and gene transfer experiments *in vitro* and *in vivo*. Four-arm histidine-/lysine (HK) peptides of different length (Scheme 3.2 C) were used as published benchmarks (cf. Leng & Mixson) [133] for the estimation of the transfection efficiency in direct comparison.

Finally, in order to investigate the effect of histidine incorporation on the endosomal escape under exclusion of a possible influence on the cellular uptake rate, PEGylated two-arm Stp oligomers with a peptidic ligand B6 (GHKAKGPRK) binding the transferrin receptor (TfR) [104, 175] or folic acid (FolA) for targeting the folate receptor (FR) were assembled (Scheme 3.2 D). Compounds with a comparable topology and the same targeting ligands, but no histidines, have been shown before to exhibit a rather low intrinsic endosomal escape performance [115, 126]. Therefore, this particular structure was chosen as an appropriate test system for enhancing effects on endosomal escape. The PEGylated two-arm compounds with alanine or histidine in the oligo(ethanamino)amide backbone were used for *in vitro* transfections and an endosomal calcein release assay by confocal microscopy.

The PAA building blocks were synthesized according to the published protocols [155, 169]. For the synthesis of the rather short linear topology oligomers, the standard Fmoc SPS conditions could be used. The synthesis of the more complex four-arm topology compounds required an optimized synthesis protocol, reported by Salcher et al., with the use of extremely low loaded peptide resins (loading ≤ 0.05 mmol amine/g) and DMF containing 1 % Triton X-100 to avoid aggregation of the highly branched structure [155]. The synthesis of PEGylated two-arm oligomers containing targeting ligands was accomplished under standard Fmoc SPS conditions within one continuous sequence. The PEGylation with a total of 48 ethylene oxide units was achieved by the twofold coupling of a discrete Fmoc-N-amido PEG carboxylic acid comprising an exact number of 24 ethylene oxide units. Folic acid was assembled at the exposed N-terminus of the PEG amino acid in two steps. First, coupling (and Fmoc deprotection) of Fmoc-Glu-OtBu, which ensures the site-specific attachment of folic acid via the γ -carboxy group, and second, coupling (and deprotection) of a pteronic acid derivative. All compounds were analyzed by $^1\text{H-NMR}$ and RP-HPLC. Figure 3.5 shows analytical RP-HPLC chromatograms of representative members of the library. More analytical data can be found in the appendix.

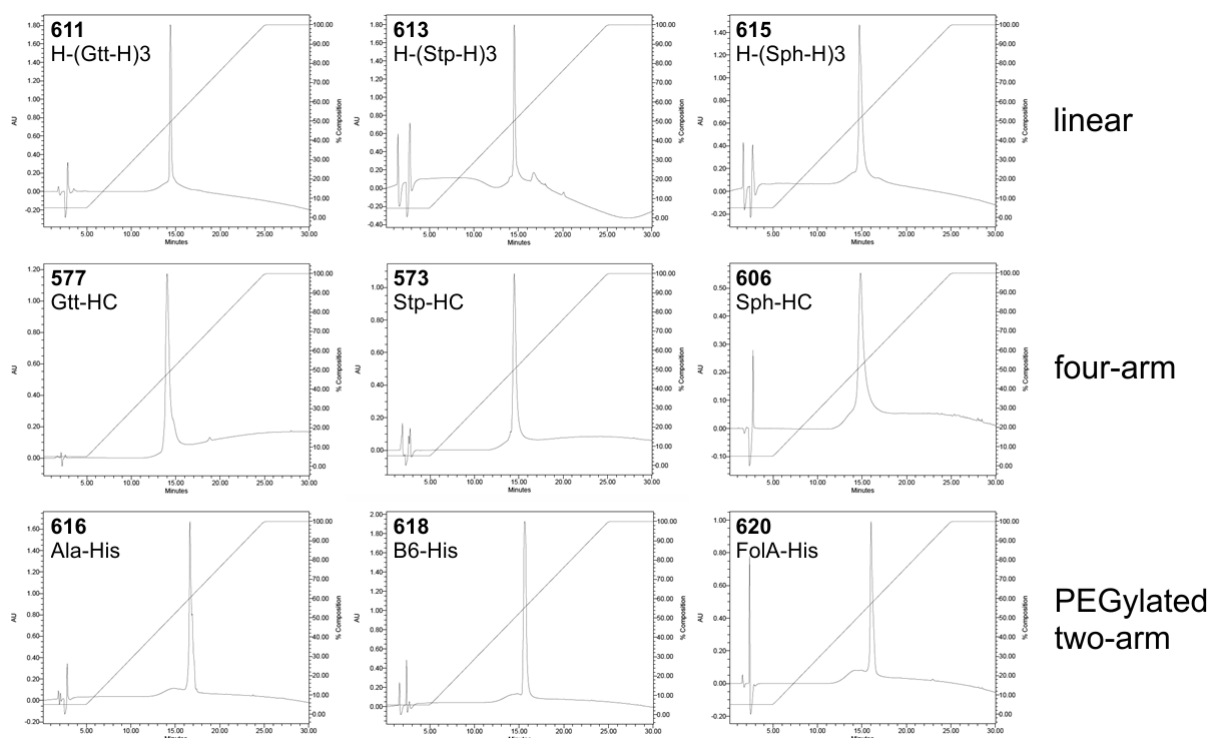


Figure 3.5 Analytical RP-HPLC chromatograms of representative library members. The analysis was carried out using a Waters Sunfire C18 column (5 μ m, 4.6 x 150mm) and a water/acetonitrile gradient (95:5 – 0:100 in 20 min) containing 0.1 % TFA. For the detection the extinction at 214 nm was monitored.

3.1.2.2 Protonation of linear oligomers

Alkalimetric back titrations of acidified sample solutions were carried out to determine the protonation characteristics and endosomal buffer capacity of the synthesized oligomers. As a result of the location of the building blocks at internal positions of the sequence, the polyamines exist in a diacylated form. Therefore, each Gtt unit offers two, each Stp unit three and each Sph unit four protonatable amines. To illustrate the protonation of the different polyamines, titrations of diacetyl-TETA, diacetyl-TEPA and diacetyl-PEHA as representative minimal motifs were carried out. The characteristic titration curves are shown in Figure 3.6. In accordance with the even/odd correlation of unmodified polyamines, the titration curve of diacetyl-TETA exhibited a reflection point and buffer maximum in the endosomal pH range, whereas diacetyl-TEPA showed a high gradient and rather low buffering in the endosomal pH range. Diacetyl-PEHA mediated homogeneous buffering over a broad range including the endosomal pH.

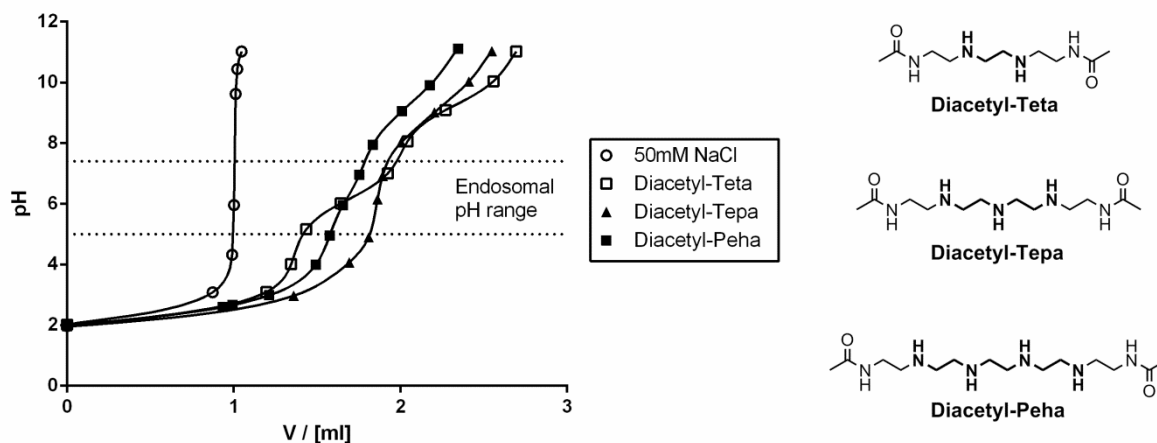


Figure 3.6 Titration curves between pH 2 and 11 of bis-acetylated polyamines. Solutions containing 100 μmol protonatable nitrogens were acidified with hydrochloric acid and backtitrated with 50 mM sodium hydroxide solution. Sodium chloride was used for a reference titration without buffering agent. Adapted from [183].

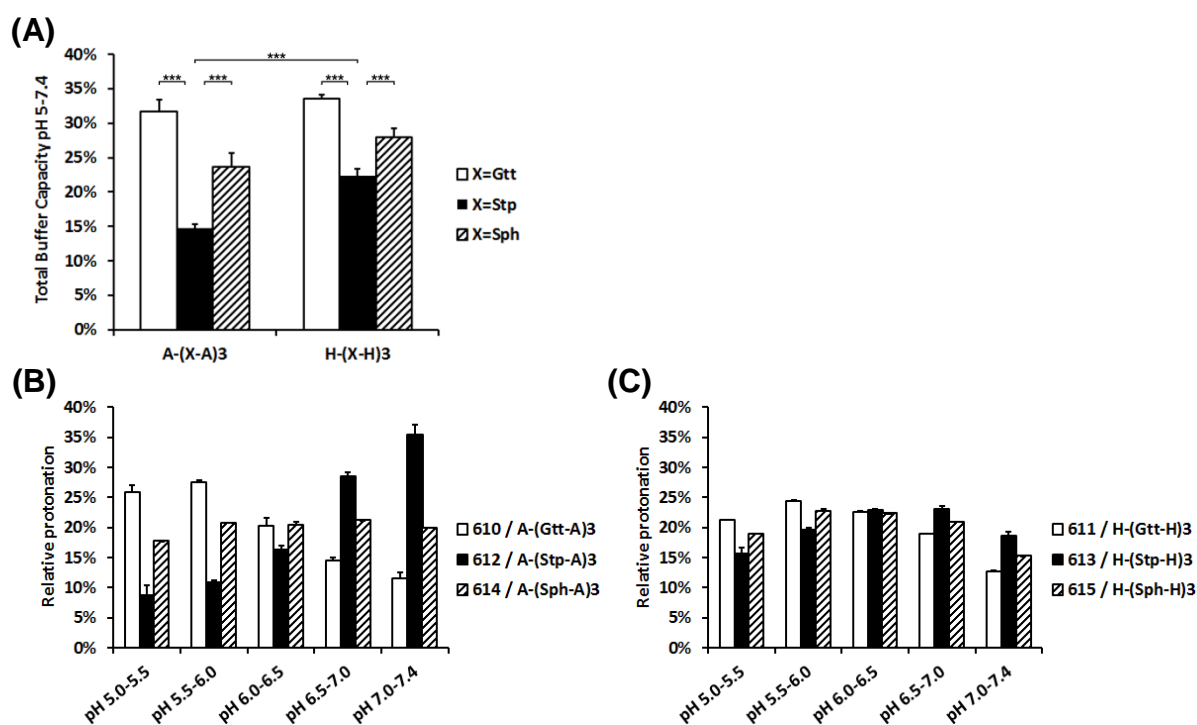


Figure 3.7 Buffer capacities of linear oligomers, determined by alkalimetric titrations. Sample solutions containing 15 μmol protonatable nitrogens were used for the titrations. $N=3$ for each compound. (A) Total endosomal buffer capacity (pH 5.0-7.4), (B) buffering profile of alanine analogs in the endosomal pH range, total endosomal buffer capacity was set to 100 %, (C) buffering profile of histidine analogs in the endosomal pH range, total endosomal buffer capacity was set to 100 %. Adapted from [183].

Consistent observations could be made by the quantitative evaluation of the titrations of the different linear oligo(ethanamino)amides (Figure 3.7). The oligomers comprising building blocks with even number of protonatable amines (Gtt, Sph) exhibited significantly higher total endosomal buffer capacities than structures with the odd number Stp block (Figure 3.7 A). Looking at the pH range between 5.0 and 7.4 in more detail (Figure 3.7 B), Gtt (**610/A-(Gtt-A)3**) predominantly mediated high buffering in the lowest sub-range and to a minor extent in higher sub-ranges. In contrast, Stp (**612/A-(Stp-A)3**) showed the opposite distribution with highest buffering in the highest pH range and lower buffering in the more acidic ranges. Sph (**614/A-(Sph-A)3**) with the longest continuous diaminoethane motif exhibited a rather homogeneous protonation distribution over the whole endosomal pH range.

Incorporation of histidine increased the total endosomal buffer capacity of all oligomers, with the effect being most pronounced for the Stp oligomer with an odd number of neighboring protonatable amines within the building blocks (Figure 3.7 A). For Gtt and Stp oligomers with strong even/odd correlation and contrasting protonation profiles, incorporation of histidine (**611/H-(Gtt-H)3**, **613/H-(Stp-H)3**) seems to serve as a compensating factor, mediating a more homogeneous buffering distribution between pH 5.0 and 7.4 (Figure 3.7 C). The already rather continuous relative protonation profile of Sph oligomers only changed slightly due to histidine incorporation (**615/H-(Sph-H)3**).

3.1.2.3 pDNA complexation of four-arm oligomers

The pDNA binding is expected to correlate with the basicity and the protonation of the oligomers at neutral pH. The exclusion of fluorescent ethidium bromide from pDNA during polyplex formation was used as a benchmark for the binding potency of the oligomers. The ethidium bromide fluorescence in absence of any pDNA complexing agent was set to 100 % and the decrease of intensity during the gradual addition of oligomer was monitored (Figure 3.8). Focusing on the oligo(ethanamino)amides without histidine modification, Sph four-arm oligomers (**609/Sph-AA**) exhibited the highest pDNA complexation capability, being followed by the Stp (**576/Stp-AA**) and Gtt (**580/Gtt-AA**) oligomers with the lowest pDNA complexation. In accordance with the influence of histidine on the relative protonation distribution (Figure 3.7 B/C), the incorporation of histidine slightly improved pDNA

condensation in case of Gtt four-arm oligomers (**580**/Gtt-AA versus **578**/Gtt-HA), but worsened complexation in case of Stp oligomers (**576**/Stp-AA versus **574**/Stp-HA), and did not change the complexation capability of Sph oligomers (**609**/Sph-AA versus **607**/Sph-HA). However, histidines only affected the pDNA binding to a minor extent, since the general complexation potency order of the building blocks (Sph > Stp > Gtt) was preserved.

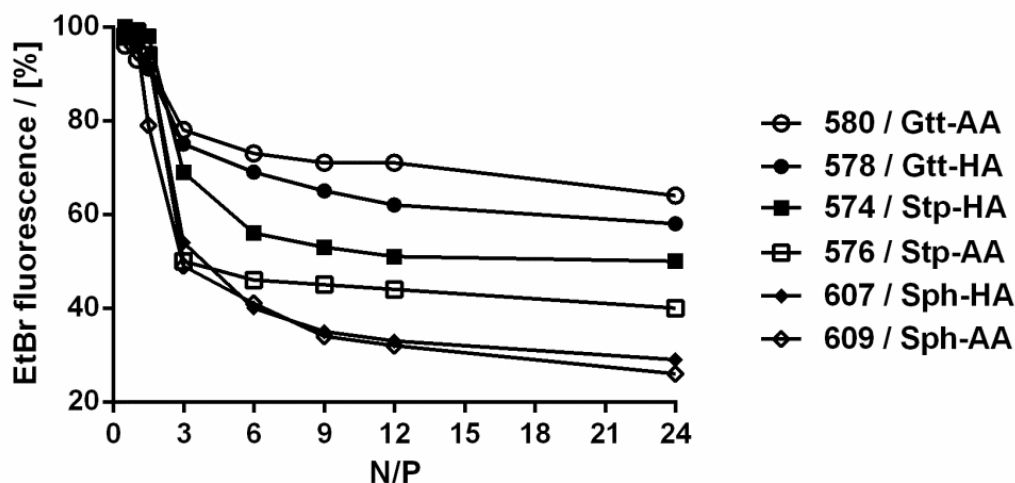


Figure 3.8 Ethidium bromide (EtBr) exclusion from pDNA by different four-arm oligomers. EtBr fluorescence without pDNA was used as blank, EtBr fluorescence in presence of pDNA and absence of oligomer was set to 100 %. Adapted from [183].

As reported by Schaffert et al. and Salcher et al., the incorporation of cysteines for the formation of disulfide-crosslinks has a highly positive effect on the polyplex stability beyond the electrostatic complexation [154, 155]. Since the ethidium bromide exclusion is based on the rapid interaction between pDNA and the basic oligomers, additional stabilization motifs, which need certain incubation times for the development of their potential, require other test systems. Therefore, agarose gel electrophoresis was used for electrophoretic mobility shift assays of pDNA polyplexes to investigate the stabilizing effect of disulfide-crosslinks (Figure 3.9). Free pDNA was used as a control with unhindered migration in the gel. A sharp band at the position of the sample pockets indicates a loss of electrophoretic mobility and the complete binding of pDNA. In all cases the integration of cysteines strongly improved the binding potency and the stability of the polyplexes. Especially for the Gtt oligomers with the lowest pDNA binding ability, the cysteine incorporation seemed to be essential to achieve a complete binding.

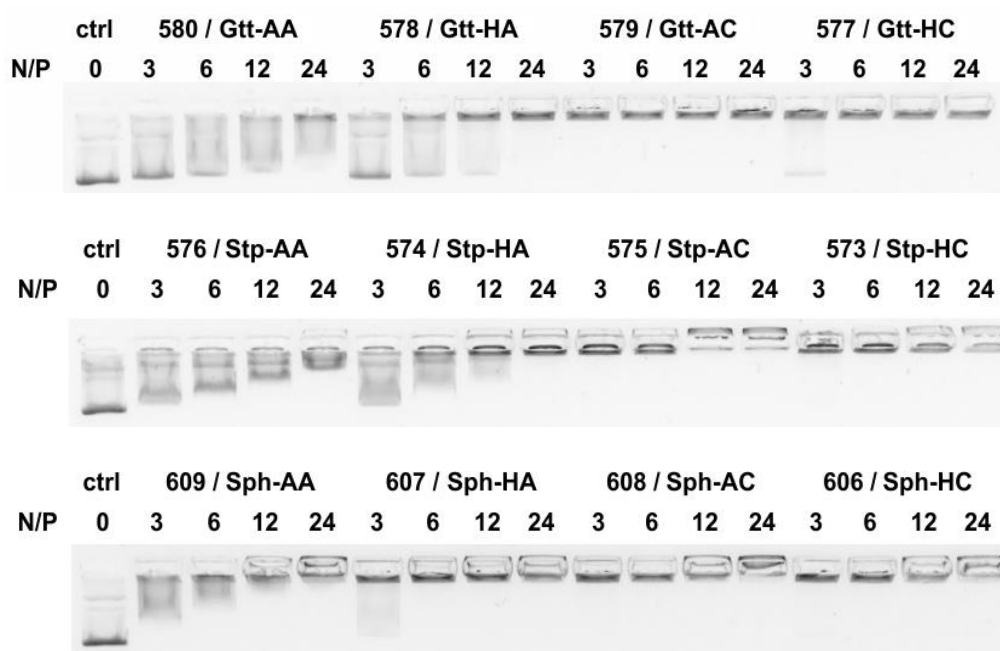


Figure 3.9 Electrophoretic mobility shift assays of different four-arm oligomers by agarose gel electrophoresis. All samples contained 200 ng pDNA and oligomer at indicated N/P ratio. Adapted from [183].

3.1.2.4 Size and zeta potential of pDNA polyplexes with four-arm oligomers

The hydrodynamic diameter and zeta-potential of pDNA polyplexes were determined by dynamic and electrophoretic light scattering (Table 3.2). All compounds formed detectable particles with pDNA in the range between 114.3 and 500.8 nm with PDI values of 0.084 to 0.346. Generally, the Gtt oligomers formed larger particles (230.8–500.8 nm) with lower zeta potential (12.7–16.4 mV) than Stp (114.3–127.8 nm, 24.4–27.6 mV) or Sph (119.2–244.2 nm, 14.6–28.0 mV). This is in accordance with the observed lower basicity of Gtt at neutral pH and the lower nucleic acid binding potency, since a lower degree of protonation implies a lower charge density, less pDNA condensation and more loose complexes. However, no clear effect of contained histidines on the physicochemical properties could be observed in the measurements. This finding is of particular importance, since a pronounced change of size or zeta potential could affect the cellular uptake of the polyplexes and therefore impact the transgene expression independently from the endosomal escape mechanism. The two four-arm HK peptides **582** and **584** exhibited by far the highest zeta potential values (> 35 mV), as a result of the multiple contained primary amines with high basicity.

Table 3.2 Hydrodynamic diameters and zeta potentials of pDNA polyplexes with different four-arm oligomers at N/P 12. N=3 for each compound.

ID	Abbr.	Z-Average / [nm]	PDI	ζ-Potential / [mV]
580	Gtt-AA	264.7 ± 30.5	0.212 ± 0.012	15.8 ± 0.3
578	Gtt-HA	230.8 ± 16.3	0.084 ± 0.041	15.0 ± 0.4
579	Gtt-AC	500.8 ± 77.1	0.346 ± 0.053	12.7 ± 0.5
577	Gtt-HC	255.8 ± 20.6	0.072 ± 0.005	16.4 ± 0.5
576	Stp-AA	127.8 ± 0.8	0.146 ± 0.028	27.6 ± 0.2
574	Stp-HA	119.3 ± 1.7	0.169 ± 0.034	25.4 ± 0.6
575	Stp-AC	114.3 ± 1.3	0.174 ± 0.017	24.4 ± 0.5
573	Stp-HC	124.8 ± 0.7	0.213 ± 0.012	26.7 ± 0.6
609	Sph-AA	129.5 ± 1.4	0.239 ± 0.005	14.6 ± 1.7
607	Sph-HA	119.2 ± 2.5	0.232 ± 0.025	28.0 ± 0.6
608	Sph-AC	244.2 ± 1.9	0.255 ± 0.006	26.3 ± 0.8
606	Sph-HC	191.2 ± 2.5	0.328 ± 0.026	25.9 ± 1.0
582	(KHH)3-KHK	128.5 ± 1.2	0.171 ± 0.003	35.2 ± 0.6
584	(KHH)5-KHK	157.0 ± 2.7	0.277 ± 0.004	35.4 ± 1.0

3.1.2.5 Gene transfer with four-arm oligomers in vitro

Plasmid DNA encoding for firefly luciferase was used for transfections of Neuro2A neuroblastoma cells to allow the quantification of transgene expression via bioluminescence (Figure 3.10). A significantly improved transgene expression by at least 10-fold was observed due to histidine modification of the four-arm structures based on Stp (**576**/Stp-AA versus **574**/Stp-HA) and Sph (**609**/Sph-AA versus **607**/Sph-HA) (Figure 3.10 A). The Stp oligomer containing histidine showed a strong N/P dependence with the highest gene expression values at the highest investigated N/P ratio, whereas for the Sph oligomer the N/P dependent variation was less. At the highest N/P ratio, the Stp-histidine oligomer achieved levels in the same range as the Sph-histidine oligomer at all investigated ratios, suggesting that Stp needs a higher N/P ratio to accumulate a critical endosomal buffer capacity and to achieve a vesicular escape, comparable to the Sph oligomer. For the Gtt oligomers (**580**/Gtt-AA versus **578**/Gtt-HA) without additional cysteines no significant improvement due to histidine incorporation could be observed. For benchmarking, the four-arm topology Sph structure containing histidines was compared to two four-arm topology lysine/histidine (HK) peptides (cf. Leng & Mixson [133]) of different lengths (Figure 3.10 B). The Sph based oligomer was significantly superior (20- to 80-fold) over both HK peptides at all investigated N/P values, showing the advantage of the artificial polyamino acids for gene delivery.

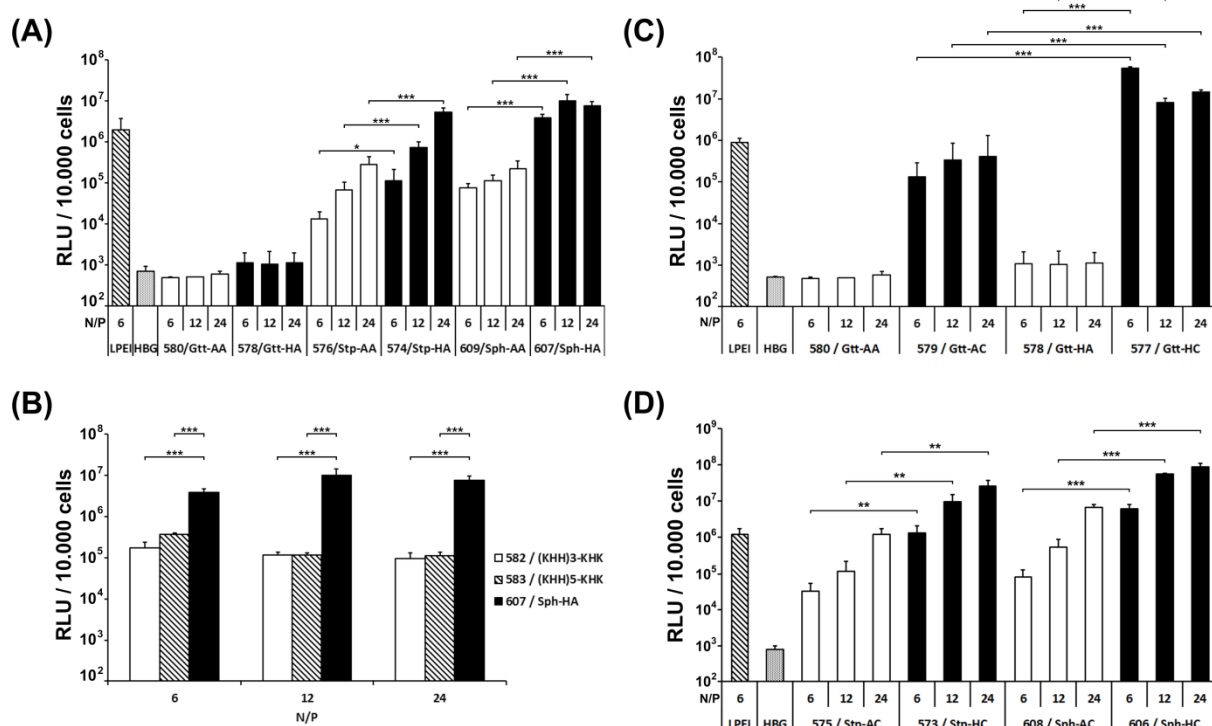


Figure 3.10 Luciferase pDNA transfections of Neuro2A neuroblastoma cells with four-arm oligomers at indicated N/P ratios. Bioluminescence levels are plotted as relative light units (RLU) per 10.000 cells. LPEI was used as a positive control agent, cells treated with HBG served as negative control cells. N=5 for each compound. (A) Comparison of Gtt, Stp and Sph based oligomers containing alanines or histidines, (B) comparison of histidine containing Sph based oligomer **607** with four-arm HK peptides **582** and **583** of different lengths, (C) comparison of Gtt based oligomers containing alanines, cysteines and /or histidines, (D) comparison of Stp and Sph based oligomers containing cysteines and alanines or histidines. Transfections were carried out by Dr. Petra Kos (Pharmaceutical Biotechnology, LMU). Adapted from [183].

The absence of an observable histidine effect on the pDNA transfections of Gtt oligomers without cysteine can be explained by the insufficient nucleic acid complexation. In accordance with the clear improvement of pDNA binding (cf. Figure 3.9), the integration of cysteines also mediated a highly positive effect on the transfection efficiency (Figure 3.10 C). In direct comparison both the histidine incorporation in the cysteine containing Gtt oligomer (**579/Gtt-AC** versus **577/Gtt-HC**, 20- to 400-fold) as well as cysteine incorporation into the histidine containing Gtt oligomer (**578/Gtt-HA** versus **577/Gtt-HC**, 7000- to 49000-fold) showed a highly significant improvement in transgene expression. The highest values were achieved when both elements, cysteine and histidine, were present in the structure. Since the 'histidylation' had no big influence on the total endosomal buffer capacity of the Gtt

oligomers but on the relative buffering profile, the specific rearrangement in endosomal sub-ranges seems to be the reason for the beneficial effect. Incorporation of cysteines in Stp and Sph oligomers also mediated an additional improvement (Figure 3.10 D), however not as dramatic as for the Gtt analogs, since both oligomer types exhibited rather potent nucleic acid complexation and transfection efficiency already without cysteines. Notably, all histidine and cysteine containing oligomers were superior to the positive control LPEI.

The cell viability of Neuro2A cells after transfections with the set of four-arm oligo(ethanamino)amides was evaluated by MTT assay (Figure 3.11). No member showed a significant impact on the metabolic activity indicating a good cellular tolerance toward the compound class.

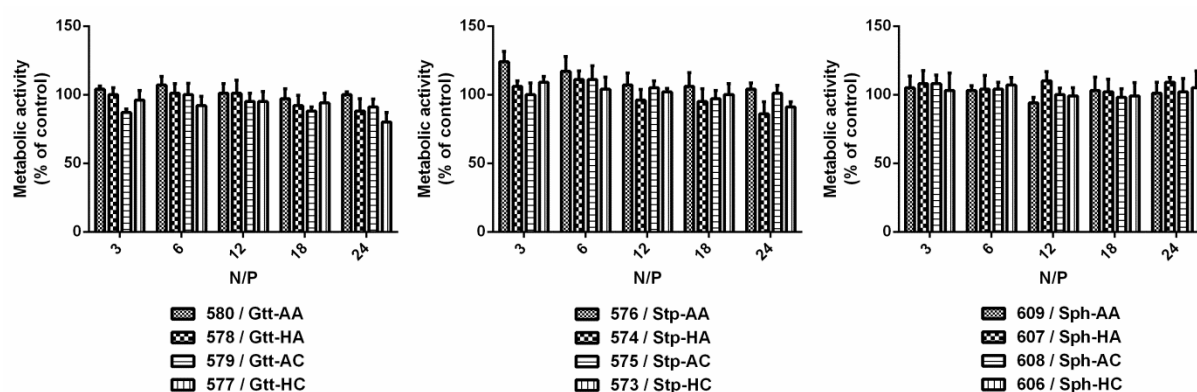


Figure 3.11 Metabolic activity of Neuro2A cells after pDNA transfections with different four-arm oligomers determined by MTT assay. The metabolic activity of control cells treated with HBG was set to 100 %. N=5 for each compound. MTT assays were carried out by Dr. Petra Kos (Pharmaceutical Biotechnology, LMU). Adapted from [183].

3.1.2.6 Gene transfer with four-arm oligomers *in vivo*

Based on the encouraging results of the *in vitro* transfections with four-arm topology oligomers, the effect of histidine was evaluated in a xenograft mouse model *in vivo*. The best performer of the library **606**/Sph-HC containing histidine and cysteine was compared to its histidine-free analog **608**/Sph-AC in Neuro2A tumor bearing mice. The mice treated by systemic tail vein injection of polyplexes did not display any noticeable signs of toxicity. The luciferase activity in homogenized tissue samples of tumor, lung, liver, spleen, kidney and heart was measured 48 hours after

administration of the polyplexes (Figure 3.12). Importantly, the histidine containing **606** polyplexes mediated the highest luciferase transgene expression in the tumor tissue (approx. 20000-fold above background). The tumor expression levels were over 32-fold improved over the histidine-free **608** polyplexes. Both formulations displayed significant transgene expression in the liver (approx. 3600- to 7500-fold above background), and low expression levels (approx. 600- to 800-fold above background) in lung and heart. In contrast to **608**, the histidine-containing **606** polyplexes also mediated considerable gene transfer (approx. 2300- to 2500-fold above background) in spleen and kidney. In sum, histidine containing **606** displayed 32-fold, 5-fold, 4-fold and 2-fold enhanced activity over histidine-free **608** in tumor, kidney, spleen and liver, respectively.

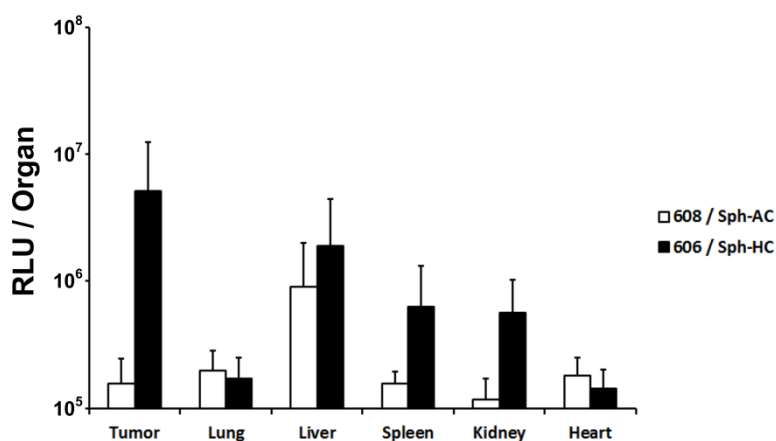


Figure 3.12 Luciferase reporter gene expression *in vivo*. Comparison of the four-arm Sph based oligomers containing cysteines and alanines (**608**/Sph-AC) or histidines (**606**/Sph-HC). Polyplexes containing pCMVLuc and oligomer at N/P 12 were injected intravenously in subcutaneous Neuro2A tumor bearing mice. Luciferase activity in homogenized tissue samples was measured 48 hours after administration. N=5 animals per group. Animal experiments were carried out by Annika Herrmann and Dr. Petra Kos (Pharmaceutical Biotechnology, LMU). Adapted from [183].

3.1.2.7 Receptor-targeted gene transfer with PEGylated two-arm oligomers

Since the advantageous effect of histidine on the pDNA transfections with oligo(ethanamino)amides could also be a result of a changed uptake rate of the polyplexes, PEGylated two-arm oligomers with attached targeting-ligands were synthesized (cf. Scheme 3.2 D). The shielding of the oligomer backbone charge was supposed to exclude any unspecific ionic interactions, while the targeting ligand

mediates a receptor-specific cellular uptake. Since the biggest effect of histidine modification on the total endosomal buffer capacity was observed for Stp based oligomers, this building block was chosen for the receptor-targeted pDNA delivery carriers. The peptidic ligand B6 binding to the transferrin receptor (TfR) and folic acid (FolA) targeting folate receptor (FR) were used for the ligand-equipped oligomers.

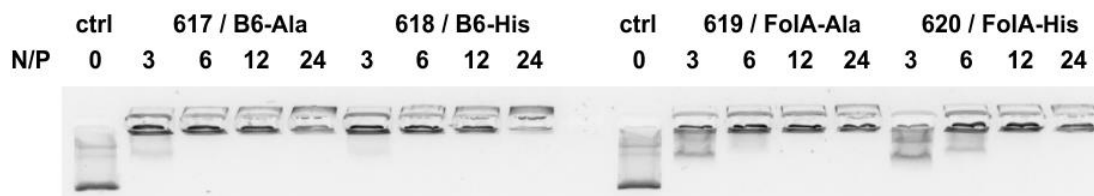


Figure 3.13 Electrophoretic mobility shift assay of PEGylated two-arm oligomers by agarose gel electrophoresis. All samples contained 200 ng pDNA and oligomer at indicated N/P ratio.

As illustrated by Figure 3.13 the oligomers with targeting ligand mediated complete pDNA binding at N/P 6 or higher and the hydrodynamic diameter of the PEGylated polyplexes is in the range between 336.3 and 493.2 nm (Table 3.3). The rather big size presumably is the result of a relatively loose condensation of pDNA into an elongated ‘spaghetti-like’ conformation, which has been reported for similar PEGylated compounds before [126]. Importantly, the PEGylation seems to achieve shielding of the oligo(ethanamino)amide backbone charge, since all polyplexes exhibited rather low zeta potentials.

Table 3.3 Hydrodynamic diameters and zeta potentials of pDNA polyplexes with PEGylated two-arm oligomers at N/P 12. N=3 for each compound.

ID	Abbr.	Z-Average / [nm]	PDI	Zeta-Potential / [mV]
616	Ala-His	356.3 ± 28.2	0.389 ± 0.103	-0.2 ± 0.4
617	B6-Ala	493.2 ± 200.4	0.469 ± 0.112	6.1 ± 2.1
618	B6-His	336.3 ± 111.4	0.436 ± 0.054	12.8 ± 1.5
619	FolA-Ala	398.4 ± 15.9	0.438 ± 0.027	9.5 ± 0.4
620	FolA-His	461.6 ± 43.2	0.794 ± 0.103	7.1 ± 0.2

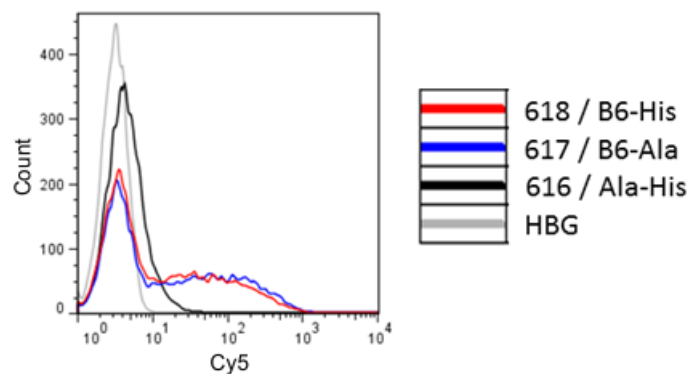


Figure 3.14 Cellular uptake of Cy5-pDNA polyplexes with PEGylated two-arm oligomers at N/P 12 in TfR expressing DU145 cells as determined by flow cytometry. Cells treated with HBG served as negative control. Flow cytometry was carried out by Dr. Petra Kos (Pharmaceutical Biotechnology, LMU). Adapted from [183].

As quantitated by flow cytometry (Figure 3.14), the pDNA polyplexes containing histidine but no targeting ligand (**616/Ala-His**) did not show an enhanced cellular uptake into TfR positive DU145 prostate cancer cells compared to the negative control. Furthermore both B6 containing structures (**617/B6-Ala** and **618/B6-His**) got internalized to the same extent, independent of alanine- or histidine in the backbone sequence.

Very consistent observations could be made in the luciferase gene expression assay (Figure 3.15), where the untargeted structure lacking B6 (**616/Ala-His**) did not mediate signals above background level, with or without addition of chloroquine as endosomolytic agent. In case of the targeted structures containing B6, plus or minus histidine, the two analogs (**618/B6-His**, **617/B6-Ala**) mediated comparable transfection levels when chloroquine was added in transfections to enforce the endosomal escape. This correlates with the comparable cellular uptake dominated by the presence of the receptor-targeting ligand. In the absence of chloroquine however, the histidine analog (**618/B6-His**) was 10- to 30-fold superior over the alanine analog (**617/B6-Ala**), indicating a far better intrinsic endosomal escape performance. In order to visualize effects on the endosomal release, the intracellular distribution of the fluorescent dye calcein, which was passively co-internalized into the cells during transfection, was monitored via spinning disk confocal microscopy (Figure 3.16). The transfection with the histidine-free analog **617** displayed primarily endosomal spotty calcein staining (Figure 3.16 A), whereas a clearly higher calcein release out of

endosomes was observable for the histidine containing oligomer **618** (Figure 3.16 B). The cytosolic calcein was quantified by digital image processing and a significant effect on the intracellular release could be found (Figure 3.16 C).

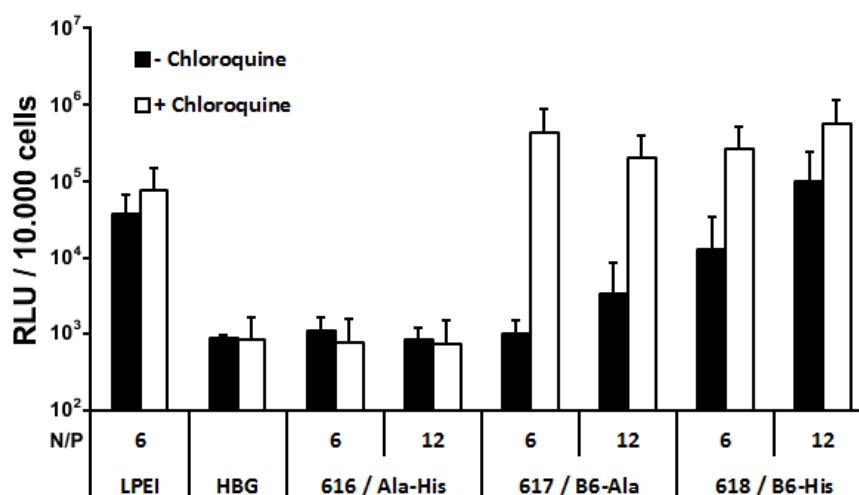


Figure 3.15 Luciferase pDNA transfections of TfR expressing DU145 prostate cancer cells with PEGylated two-arm oligomers. Comparison of oligomers containing histidine (**616**, **618**) or alanine (**617**) in the cationic core and as targeting ligand the TfR binding peptide B6 (**617**, **618**) or alanine as negative control ligand (**616**). Bioluminescence levels are plotted as relative light units (RLU) per 10.000 cells. Chloroquine was used as endosome disruptive agent in indicated transfections. N=5 for each compound. Transfections were carried out by Dr. Petra Kos (Pharmaceutical Biotechnology, LMU). Adapted from [183].

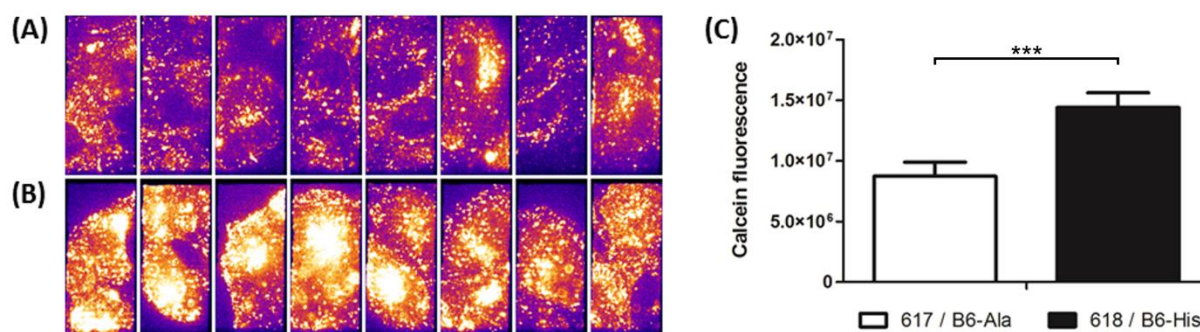


Figure 3.16 Calcein release assay in DU145 cells via spinning disk confocal microscopy. Images show representative cells transfected with pDNA polyplexes of oligomer (A) **617**/B6-Ala or (B) **618**/B6-His, in medium containing 0.5 mg/mL calcein. (C) Quantification of cytosolic calcein release by digital image processing (n=20 for **617**/B6-Ala, n=22 for **618**/B6-His). Experiments were carried out by Dr. Frauke Mickler (Physical Chemistry, LMU). Adapted from [183].

To confirm the positive effect of histidine modifications on pDNA transfections also in another cell model of receptor-mediated uptake, the analog oligomers containing Folate as targeting ligand and FR expressing KB cells were used (Figure 3.17). Also in the luciferase pDNA transfections of this cell line, the untargeted control lacking a targeting ligand (**616**/Ala-His), despite the presence of buffering histidine residues, did not mediate significant signals above background level with or without addition of chloroquine, indicating that the cellular uptake requires the presence of the receptor-targeting ligand. In case of the Folate targeted oligomers and in the absence of chloroquine, the histidine containing compound (**620**/Folate-His) mediated 30- to 100-fold higher transgene expression levels than the alanine analog (**619**/Folate-Ala). Thus also in this targeting-ligand and cell-line combination model the highly positive effect of histidines on endosomal escape and subsequently transgene expression could be shown.

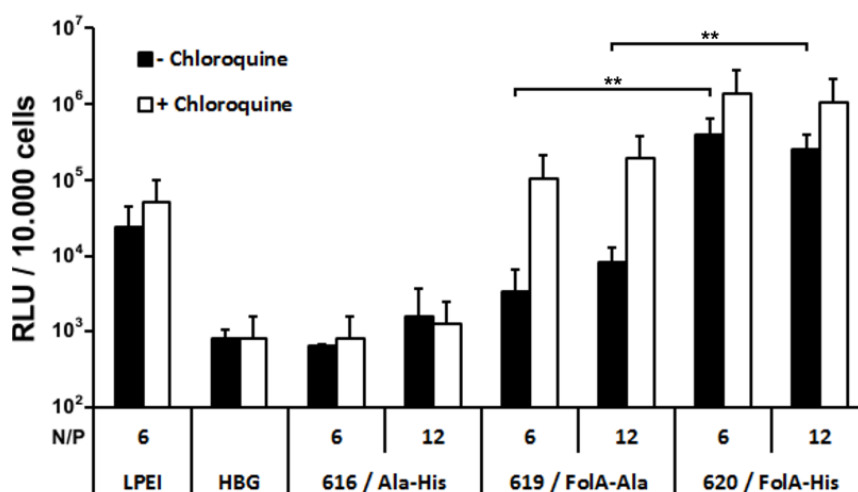


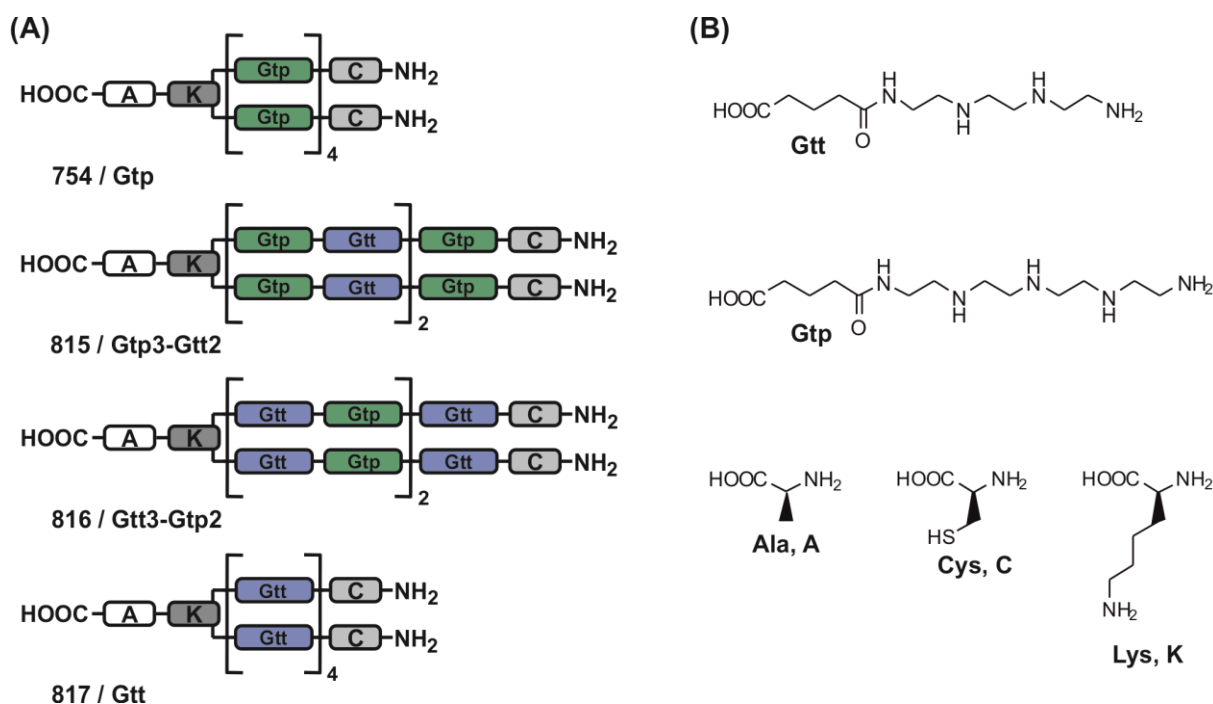
Figure 3.17 Luciferase pDNA transfections of FR expressing KB cells with PEGylated two-arm oligomers at indicated N/P ratios. Comparison of oligomers containing histidine (**616**, **620**) or alanine (**619**) in the cationic core, and folic acid as targeting ligand (**619**, **620**) or alanine as negative control ligand (**616**). Bioluminescence levels are plotted as relative light units (RLU) per 10.000 cells. Chloroquine was used as endosome disruptive agent in indicated transfections. N=5 for each compound. Transfections were carried out by Dr. Petra Kos (Pharmaceutical Biotechnology, LMU). Adapted from [183].

3.1.3 The combination of TETA and TEPA based polyamino acids

The diaminoethane building blocks Gtt, Stp and Sph based on polyamines of different lengths have shown to mediate individual protonation characteristics in oligo(ethanamino)amides with big impact on crucial stages of gene transfer, such as pDNA binding and endosomal escape. The two building blocks based on the polyamines triethylene tetramine (Gtt) and tetraethylene pentamine (Stp) exhibited big differences in the total endosomal buffer capacities and the relative protonation distribution. While Stp provided a rather low buffer capacity between pH 5 and 7.4 (approx. 15 % of amines) with the most frequent protonation between pH 7 and 7.4, the Gtt amines were protonated in the endosomal pH range to a much higher extent (> 30 % of amines) and predominantly in the lowest sub-ranges between pH 5 and 6. As a result of the opposing characteristics, both building blocks have their own drawbacks: Stp offers good pDNA binding but low endosomal buffering; Gtt exhibits a high buffer capacity, but poor binding. It has been shown that the integration of histidines modulates the endosomal protonation and affects pDNA delivery in a highly positive fashion. However, based on the made observations, it is also a consequent approach to combine the building blocks with opposing characteristics within one structure.

3.1.3.1 Library design and synthesis

Oligomers comprising different ratios of the two diaminoethane building blocks glutaryl-triethylene tetramine (Gtt) and glutaryl tetraethylene pentamine (Gtp) were assembled by solid-phase synthesis. Scheme 3.3 and Table 3.4 give an overview over the synthesized compounds. Coupled at an internal position of the sequence Gtt offers two and Gtp three protonatable amines, however in both building blocks glutaric acid serves as the molecular connector of the polyamine segments (Scheme 3.3 B). A topology comparable to the PEGylated two-arm oligomers (cf. Scheme 3.2 D) was chosen since these structures exhibit a rather poor intrinsic endosomal escape performance, which makes the clear observation of effects on endosomal escape possible.

Scheme 3.3 Illustration of the synthesized oligomers with combinations of Gtt and Gtp

(A) Schemes of oligomers with two-arm topology, (B) chemical structures of the used building blocks.

Table 3.4 Sequences, protonatable amines and abbreviations of the synthesized oligomers

ID	Sequence (C → N)	Proton. Amines			Abbreviation
		Gtp	Gtt	Total	
754	AK(Gtp ₄ -C) ₂	24	-	26	Gtp
815	AK[(Gtp-Gtt) ₂ -Gtp-C] ₂	18	8	28	Gtp3-Gtt2
816	AK[(Gtt-Gtp) ₂ -Gtt-C] ₂	12	12	26	Gtt3-Gtp2
817	AK(Gtt ₄ -C) ₂	-	16	18	Gtt

The number of protonatable amines, provided by the different building blocks, as well as the total number including N-terminal primary amines are indicated.

The polyamino acid Gtp was synthesized as reported previously [169]. For the synthesis of the oligo(ethanamino)amides, the same standard Fmoc SPS conditions were used as for the PEGylated two-arm oligomers before (cf. 3.1.2). All compounds were analyzed by ¹H-NMR and RP-HPLC. Figure 3.18 shows the analytical RP-HPLC chromatograms of the compounds. ¹H-NMR data can be found in the appendix.

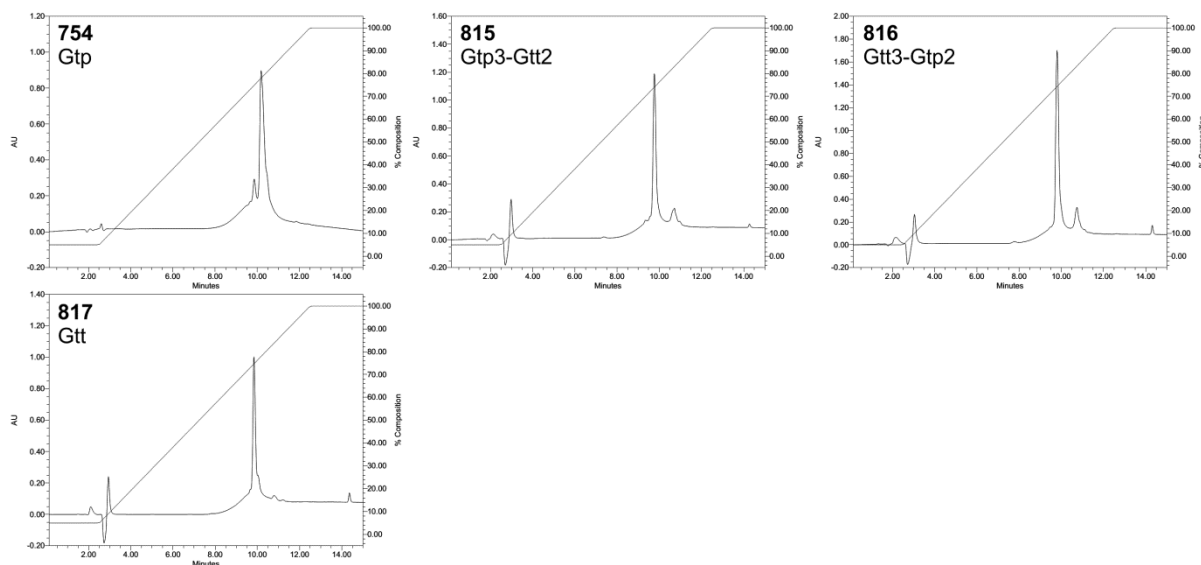


Figure 3.18 Analytical RP-HPLC chromatograms of two-arm oligomers with combinations of Gtt and Gtp. The analysis was carried out using a Xbridge C18 column (5 μ m, 4.6 x 150mm) and a water/acetonitrile gradient (95:5 – 0:100 in 10 min) containing 0.1 % TFA. For the detection the extinction at 214 nm was monitored.

3.1.3.2 Protonation of two-arm oligomers with combinations of Gtt and Gtp

Alkalimetric back titrations of acidified samples were carried out to determine the buffer capacity between pH 5 and 7.4 as well as the relative protonation in sub-ranges of the endosomal pH (Figure 3.19). Consistent with the previous observations, the oligomer **817**/Gtt mediated an over two-fold higher total buffer capacity than its analog **754** based on Gtp only (Figure 3.19 A). Moreover, the total buffer capacity of the Gtp oligomer was gradually increased with increasing content of Gtt. Looking at the protonation in the endosomal range in more detail, the previously observed opposing protonation characteristics of the oligomers containing Gtp (**754**) or Gtt (**817**) only could be reconfirmed (Figure 3.19 B). The protonation distributions of the mixed oligomers **815**/Gtp3-Gtt2 and **816**/Gtt3-Gtp2 represent hybrid forms of the contrary distributions of **754** and **817**. Since Gtp has its highest buffering in the highest pH sub-range and Gtt in the lowest, the increase of the total buffer capacity due to the integration of Gtt is based on a particularly enhanced buffering at low pH 5 to 6 and none of the compounds exhibited a maximal buffering in a medium sub-range. This is in sharp contrast to the effect of histidine integration, since the pK_a of the imidazole group particularly mediates buffering around 6 and therefore causes a more homogeneous protonation distribution in the whole endosomal pH range.

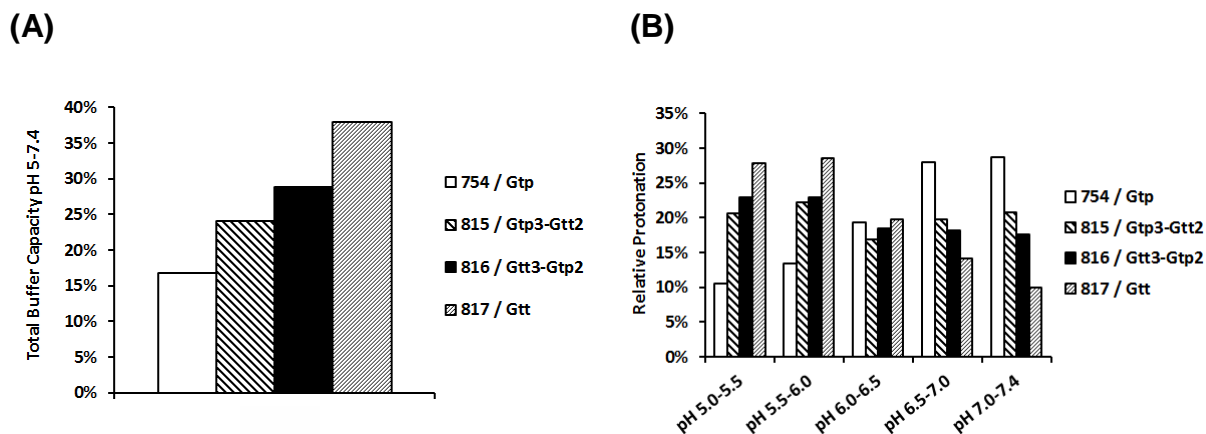


Figure 3.19 Buffer capacities of two-arm oligo(ethanamino)amides with combinations of Gtt and Gtp determined by alkalimetric titrations. Oligomer amounts containing 15 μ moles of protonatable amines were used for the titrations. (A) Total endosomal buffer capacity (pH 5.0-7.4), (B) buffering profile in the endosomal pH range, total endosomal buffer capacity was set to 100 %.

3.1.3.3 pDNA complexation of two-arm oligomers with combinations of Gtt and Gtp

In Figure 3.20 the ethidium bromide exclusion from pDNA due to ionic complexation by the oligomers is shown. Within the set **817/Gtt**, **816/Gtt3-Gtp2** and **754/Gtp**, the decreased basicity at neutral pH due to an increased content of Gtt building block can be recognized. However, the differences are not as pronounced as in case of the four-arm oligomers (cf. 3.1.2). The compound **815/Gtp3-Gtt2** exhibited the highest pDNA complexation potency, which cannot be explained by the basicity of the single building blocks only, since a portion of the protonatable amines in this mixed oligomer is provided by the less basic Gtt. One simple explanation could be that **815** represents the member with the highest total number of protonatable amines (cf. Table 3.4). Looking at the electrophoretic mobility shift assay (Figure 3.21), all oligomers containing the Gtp building block (**754**, **815** and **816**), exhibited comparable efficient pDNA complexation. The analog **817** containing Gtt only clearly showed lower binding, since complete shift of the pDNA band could first be observed at a higher N/P of 12.

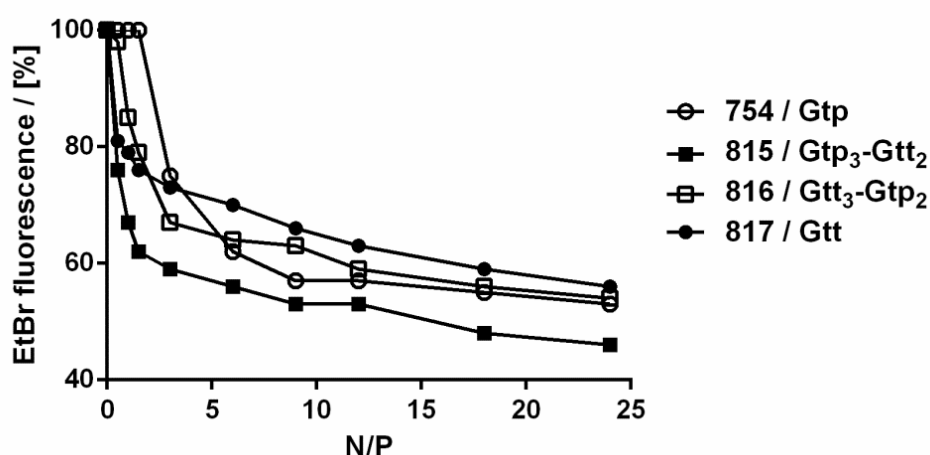


Figure 3.20 Ethidium bromide (EtBr) exclusion from pDNA by two-arm oligomers with combinations of Gtt and Gtp. EtBr fluorescence without pDNA was used as blank, EtBr fluorescence in presence of pDNA and absence of oligomer was set to 100 %.

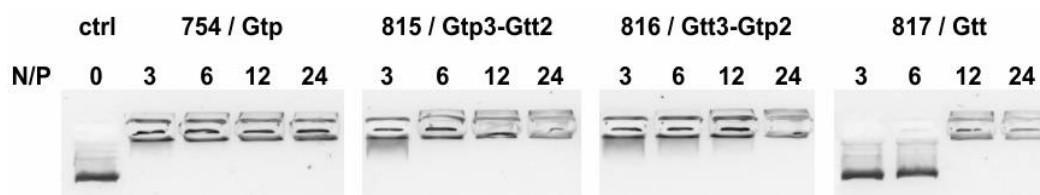


Figure 3.21 Electrophoretic mobility shift assay of two-arm oligomers with combinations of Gtt and Gtp by agarose gel electrophoresis. All samples contained 200 ng pDNA and oligomer at indicated N/P ratio.

3.1.3.4 Size and zeta potential of pDNA polyplexes with two-arm oligomers containing combinations of Gtt and Gtp

In Figure 3.22 the different z-average diameters of the pDNA polyplexes as determined by DLS are illustrated. Consistent with the lower degree of protonation at neutral pH, an increasing content of Gtt increases the particle size, since the pDNA gets less compacted by oligomers with lower charge density. In case of the Gtt oligomer **817** huge aggregates and particles with high polydispersity were observed. Therefore, no reliable size or zeta potential determinations were possible. For reasons of completeness and to note the destructive effect of Gtt, the recorded values are also depicted in the graph.

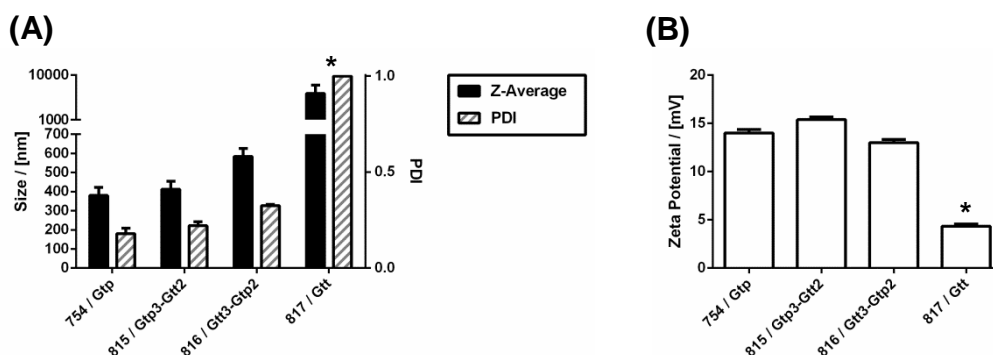


Figure 3.22 Hydrodynamic diameter and zeta potential of pDNA polyplexes at N/P 12 of two-arm oligomer with combinations of Gtt and Gtp. N=3 for each compound. (A) Z-average in nm (left axis, black bars) and PDI (right axis, shaded bars), (B) zeta potential in mV. * Oligomer **817** did not form appropriate particles meeting the criteria for reliable determinations.

3.1.3.5 pDNA transfections with two-arm oligomers containing combinations of Gtt and Gtp

Neuro2A cells were transfected with pCMVLuc and the set of two-arm oligomers. As shown in Figure 3.23 the Gtp oligomer **754** mediated remarkable transgene expression levels superior to LPEI with the addition of chloroquine as endosome disruptive agent. However, in the absence of chloroquine, no transgene expression above background level could be observed. This clearly shows the potential and requirement for strategies to enhance the endosomal escape. Unfortunately, despite the gradually increased endosomal buffer capacities, none of the two-arm oligomers with combinations of Gtp and Gtt mediated transgene expression. Since all compounds containing Gtp showed sufficient pDNA binding as well as comparable particle formation and zeta potentials, obviously the integration of Gtt is not suitable to enhance the endosomal escape. As determined by the alkalimetric titrations, the increase of total endosomal buffer capacity results from a modulation in the low range between pH 5 and 6. In contrast, histidine increases buffering in the higher less acidic ranges of endosomal pH. Obviously the buffer maximum of Gtt alone is not appropriate to promote proton-sponge activity of polyplexes and to enhance transgene expression. This explanation is consistent with the observation that Gtt based four-arm oligomers also showed a great benefit due to histidine incorporation, although the total buffer capacity of the Gtt four-arm oligomers was not greatly

enhanced. However, the histidines caused a rearrangement of the protonation distribution of Gtt oligomers and a higher buffering in higher pH sub-ranges.

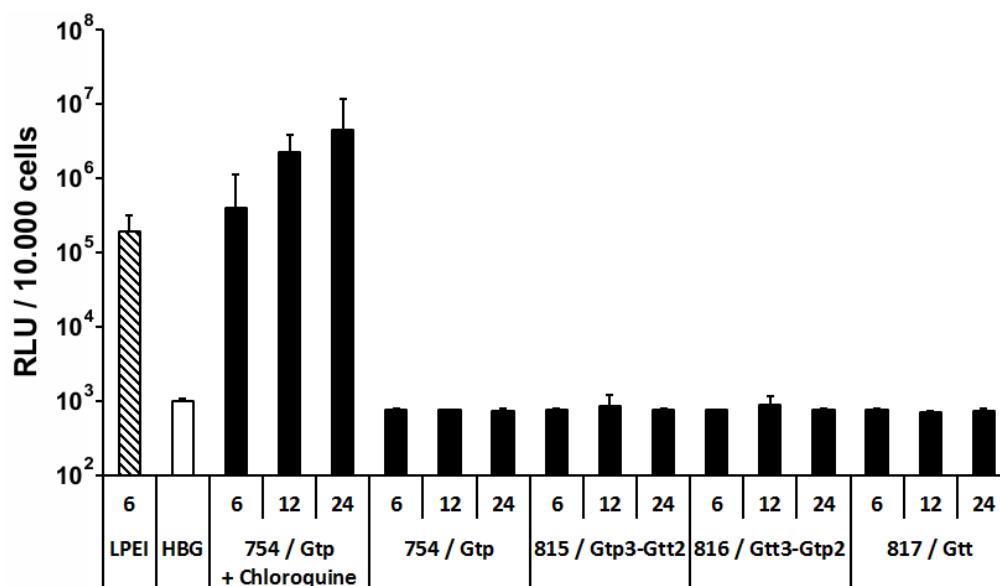


Figure 3.23 Luciferase pDNA transfections of Neuro2A neuroblastoma cells with two-arm oligomers at indicated N/P ratios. Bioluminescence levels are plotted as relative light units (RLU) per 10.000 cells. N=5 for each compound. Chloroquine was added in indicated transfections with **754** to illustrate the effect of an enhanced endosomal escape. Transfections were carried out by Ana Krhac Levacic (Pharmaceutical Biotechnology, LMU).

3.1.4 The influence of pyridyl amino acids on the proton-sponge activity

The integration of histidines in oligo(ethanamino)amides has shown an enhancement of the buffer capacity with great improvement of endosomal escape and the final transgene expression. Within the set of proteinogenic amino acids, histidine with a pK_a of the imidazole group around 6 offers the most appropriate properties for this purpose. However, the oligo(ethanamino)amide synthesis platform is not limited to natural α -amino acids. Therefore, it is unclear whether other protonatable building blocks or artificial amino acids with slightly different pK_a values could offer even more suitable buffering properties for a higher boost of proton-sponge activity and gene transfer efficiency. Pyridine is a basic heterocyclic compound with a lower pK_a (approx. 5.2) than imidazole. The pK_a values of alkylated pyridines depend on the exact position at the pyridine ring. The methylpyridine derivatives 3-picoline and 4-picoline for instance exhibit pK_a values of approx. 5.6 or 6.0 respectively (Figure

3.24) [184]. To investigate the effect of pyridines with gradual lower basicities compared to histidine, 3-(3-pyridyl)-alanine and 3-(4-pyridyl)-alanine, abbreviated 3PAL or 4PAL below, were integrated in Stp based oligo(ethanamino)amides to investigate the effect on the endosomal buffering and endosomal escape.

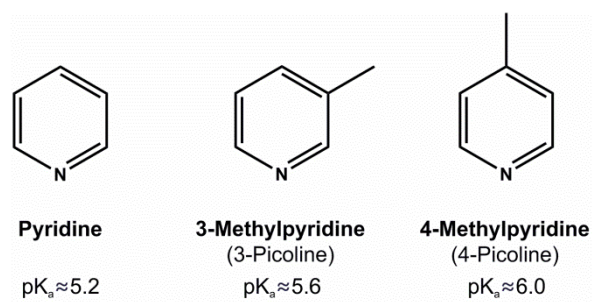
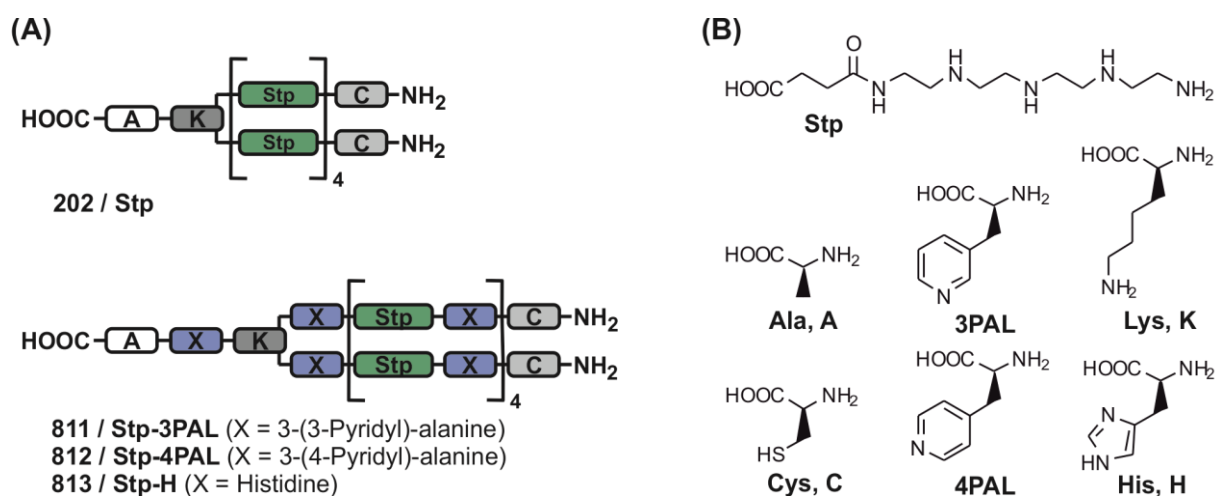


Figure 3.24 Chemical structures and pK_a values of pyridine derivatives [184].

3.1.4.1 Library design and synthesis

Commercially available $N\alpha$ -Fmoc derivatives of 3PAL and 4PAL were used in the solid-phase assisted synthesis of two-arm oligomers. Scheme 3.4 and Table 3.5 give an overview over the set of compounds. Three members contained either 3PAL (**811**/Stp-3PAL), 4PAL (**812**/Stp-4PAL) or histidine (**813**/Stp-H) alternatingly coupled with Stp in the backbone. Compound **202**/Stp represents the control oligomer without additional buffering units beside Stp.

Scheme 3.4 Illustration of the synthesized oligomers with additional pyridylalanines or histidine



(A) Schemes of oligomers with two-arm topology, (B) chemical structures of the used building blocks.

Table 3.5 Sequences, protonatable nitrogens and abbreviations of the synthesized oligomers

ID	Sequence (C -> N)	Proton. Nitrogens	Abbreviation
202	AK(Stp ₄ -C) ₂	26	Stp
811	A-3PAL-K[(3PAL-Stp) ₄ -3Pal-C] ₂	37	Stp-3PAL
812	A-4PAL-K[(4PAL-Stp) ₄ -4Pal-C] ₂	37	Stp-4PAL
813	AHK[(H-Stp) ₄ -HC] ₂	37	Stp-H

Oligomer **202** was synthesized by Dr. Irene Martin (visiting scientist, IRB Barcelona, Spain). 3PAL, 3-(3-Pyridyl)-alanine; 4PAL, 3-(4-Pyridyl)-alanine.

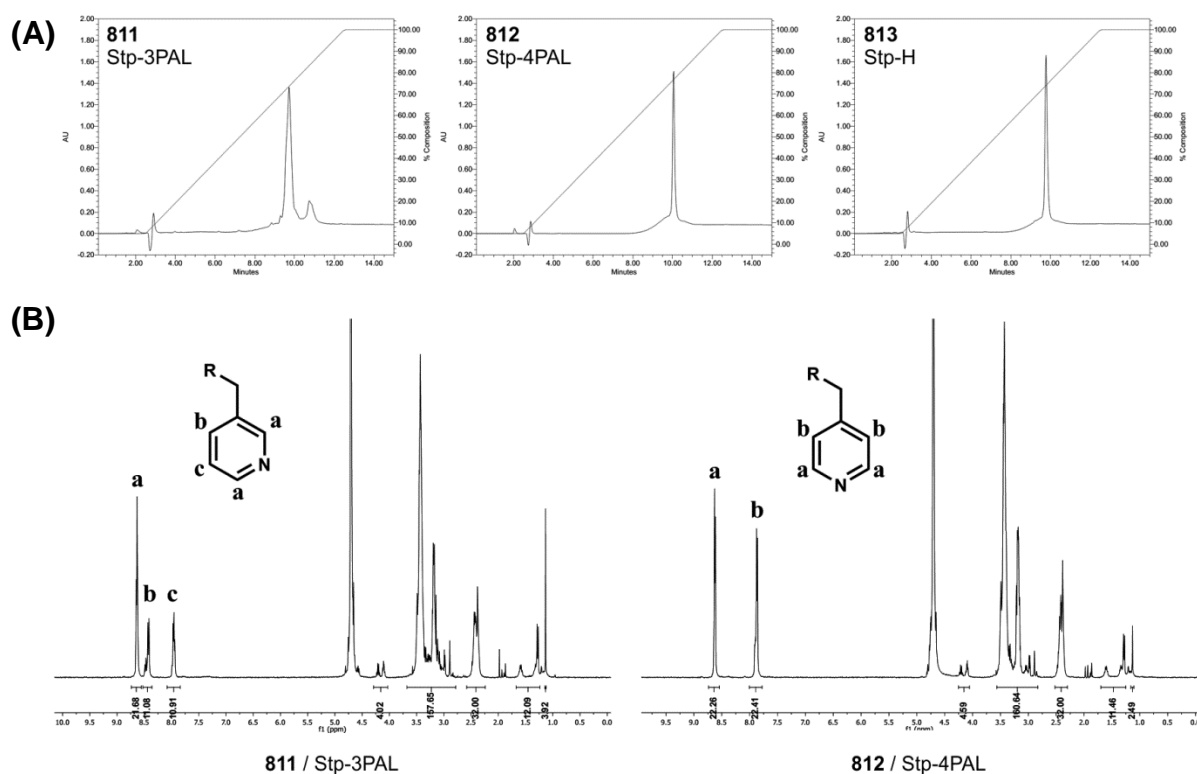


Figure 3.25 Analytical data of two-arm oligomers with pyridylalanines or histidine. (A) Analytical RP-HPLC chromatograms. The analysis was carried out using a Xbridge C18 column (5 μ m, 4.6 x 150mm) and a water/acetonitrile gradient (95:5 – 0:100 in 10 min) containing 0.1 % TFA. For the detection the extinction at 214 nm was monitored. (B) ¹H-NMR spectra of oligomers containing pyridylalanines.

The standard Fmoc SPS conditions were used. All compounds were analyzed by ¹H-NMR and RP-HPLC. Figure 3.25 shows the analytical RP-HPLC chromatograms of the compounds and ¹H-NMR spectra of the pyridylalanine containing compounds **811** and **812**. More analytical data can be found in the appendix. Importantly, both pyridylalanine building blocks seemed to be compatible with the used solid-phase synthesis chemistry. Since pyridine derivatives can undergo N-acylation reactions

with activated carboxylic acids (e.g. anhydrides), which might decrease coupling efficiency or produce side-products due to a subsequent acyl transfer, the suitability of the chosen conditions is not trivial. However, no indication for interference with the synthesis procedure could be observed.

3.1.4.2 Protonation of two-arm oligomers with pyridylalanines or histidines

Figure 3.26 shows the total buffer capacity between pH 5 and 7.4 and the relative protonation in the accordant sub-ranges as determined by alkalimetric back titrations. Both pyridylalanine derivatives slightly increased the total buffer capacity of the corresponding oligo(ethanamino)amides (**811**, 19.3 %; **812**, 22.4 %) compared to the bare Stp oligomer (**202**, 16.6 %). However, the effect of histidine (**813**, 35.8 %) could not be approached. Looking at the relative protonation (Figure 3.26 B), the oligomer **202** exhibited the characteristic distribution of Stp as observed before. In case of **811** and **812** the relative protonation is most influenced in the lowest pH range, indicating the lower pK_a values of the pyridine derivatives. Consistent with the inductive effect depending on the position at the pyridine ring, 4PAL exhibited higher basicity. However, for both pyridylalanines a significant ratio of buffer capacity lies below pH 5 and presumably is not biologically active. In the comparison of the pyridylalanines and histidines, a higher endosomal buffer capacity does not equal lower protonation at neutral pH, in consequence of the pK_a location on the pH scale. **813**/Stp-H exhibits much higher buffer capacity than **811**/Stp-3PAL or **812**/Stp-4PAL; but since the pK_a of the imidazole group is closer to 7.4 it also exhibits a higher degree of protonation at neutrality.

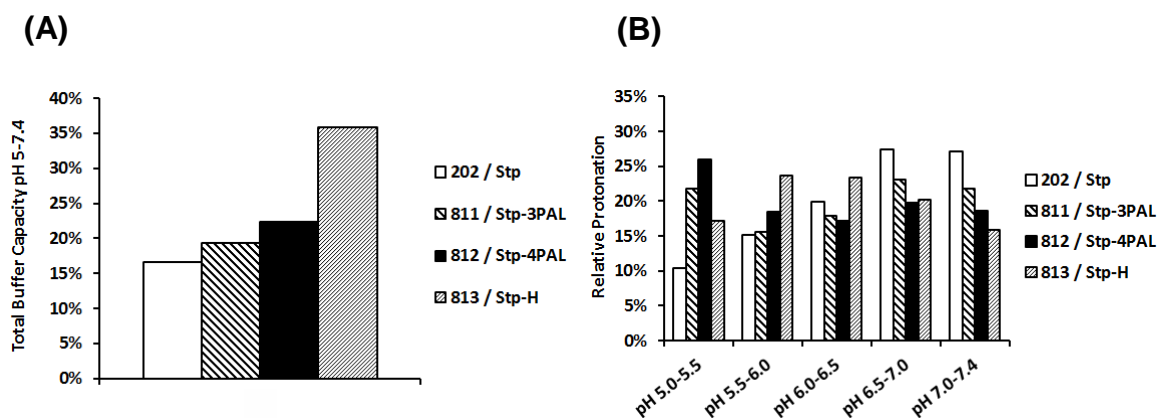


Figure 3.26 Buffer capacities of two-arm oligomers with additional pyridylalanines or histidine determined by alkalimetric titrations. Oligomer amounts containing 15 μ moles of protonatable nitrogens were used for the titrations. (A) Total endosomal buffer capacity (pH 5.0-7.4), (B) buffering profile in the endosomal pH range, total endosomal buffer capacity was set to 100 %.

3.1.4.3 pDNA complexation of two-arm oligomers with pyridylalanines or histidine

The degree of protonation at neutral pH ($811/\text{Stp-3PAL} < 812/\text{Stp-4PAL} < 813/\text{Stp-H} < 202/\text{Stp}$) correlates with the pDNA binding potencies as determined by the electrophoretic mobility shift (Figure 3.27) and ethidium bromide exclusion assays (Figure 3.28). In both assays, the Stp oligomer **202** exhibited the highest binding ability, followed by the histidine analog **813** and finally the two compounds containing pyridylalanines with the lowest potency.

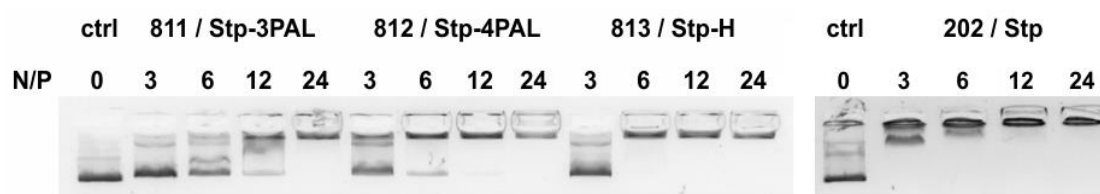


Figure 3.27 Electrophoretic mobility shift assay of two-arm oligomers with additional pyridylalanines or histidine by agarose gel electrophoresis. All samples contained 200 ng pDNA and oligomer at indicated N/P ratios.

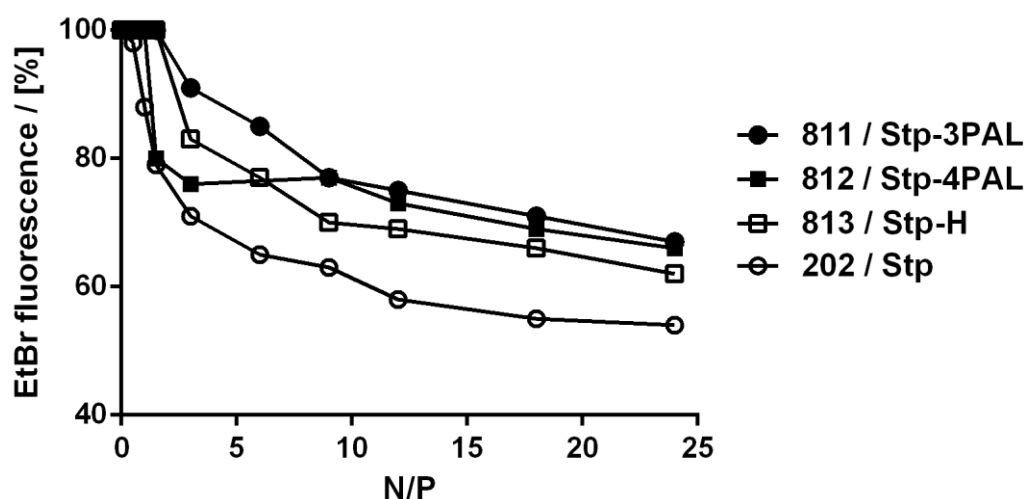


Figure 3.28 Ethidium bromide (EtBr) exclusion from pDNA by two-arm oligomers with additional pyridylalanines or histidine. EtBr fluorescence without pDNA was used as blank, EtBr fluorescence in presence of pDNA and absence of oligomer was set to 100 %.

3.1.4.4 Size and zeta potential of pDNA polyplexes with two-arm oligomers containing pyridylalanines or histidine

All oligomers formed pDNA polyplexes with a hydrodynamic diameter in the range between 239.3 and 365.3 nm (Figure 3.29 A). A slight tendency of the physicochemical properties of the polyplexes, in accordance with the correlation between basicity and pDNA binding, could be recognized. With increasing degree of protonation at neutral pH, the size of the polyplexes decreases. The results of the zeta potential measurements suggest a similar effect (higher protonation, higher zeta potential), however here the differences are even less pronounced and rather negligible (Figure 3.29 B).

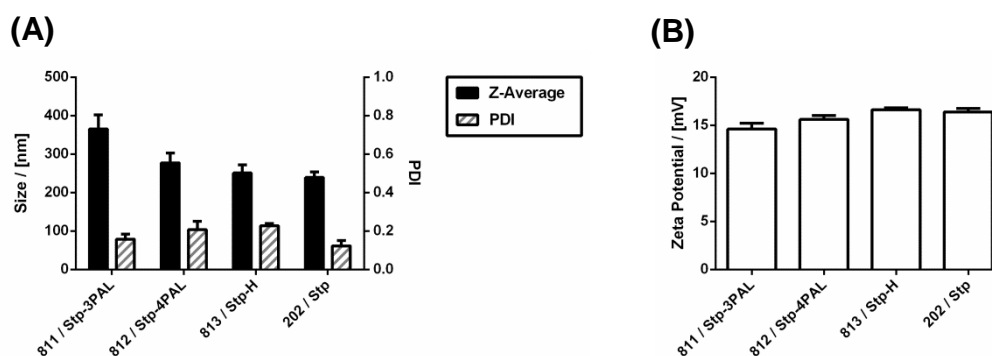


Figure 3.29 Hydrodynamic diameter and zeta potential of pDNA polyplexes with two-arm oligomers containing additional pyridylalanines or histidine. Polyplexes were formed at N/P 12. N=3 for each compound. (A) Z-average in nm (left axis, black bars) and PDI (right axis, shaded bars), (B) zeta potential in mV.

3.1.4.5 *pDNA transfections with two-arm oligomers containing pyridylalanines or histidine*

In pCMVLuc transfections of Neuro2A cells, the histidine containing oligomer **813** was the only compound mediating notably high transgene expression (Figure 3.30 A). At the highest N/P of 24, LPEI was even outperformed by this rather simple conjugate. In contrast, no significant indication of gene transfer was observed in case of transfections with the pyridylalanine analogs **811** or **812**. Since no effect on the cell viability after transfection was found in any case (Figure 3.30 B), an increase of cytotoxicity due to incorporation of pyridylalanines is excluded as reason for the absence of transgene expression. Both pyridylalanine derivatives seem to be inappropriate for an enhancement of the endosomal escape of pDNA polyplexes. An obvious explanation is the only marginal effect on the total buffer capacity (cf. Figure 3.26). In addition, the most pronounced effect on the endosomal protonation is located in the lowest sub-range between pH 5 and 5.5. As observed for the combinations of Gtt and Gtp before, the total buffer capacity between pH 5 and 7.4 alone is no good predictor for proton-sponge activity (cf. Figure 3.19 and Figure 3.23). The exact location of buffering in the endosomal pH range obviously is a critical parameter, which seems to be met by histidine in an ideal fashion.

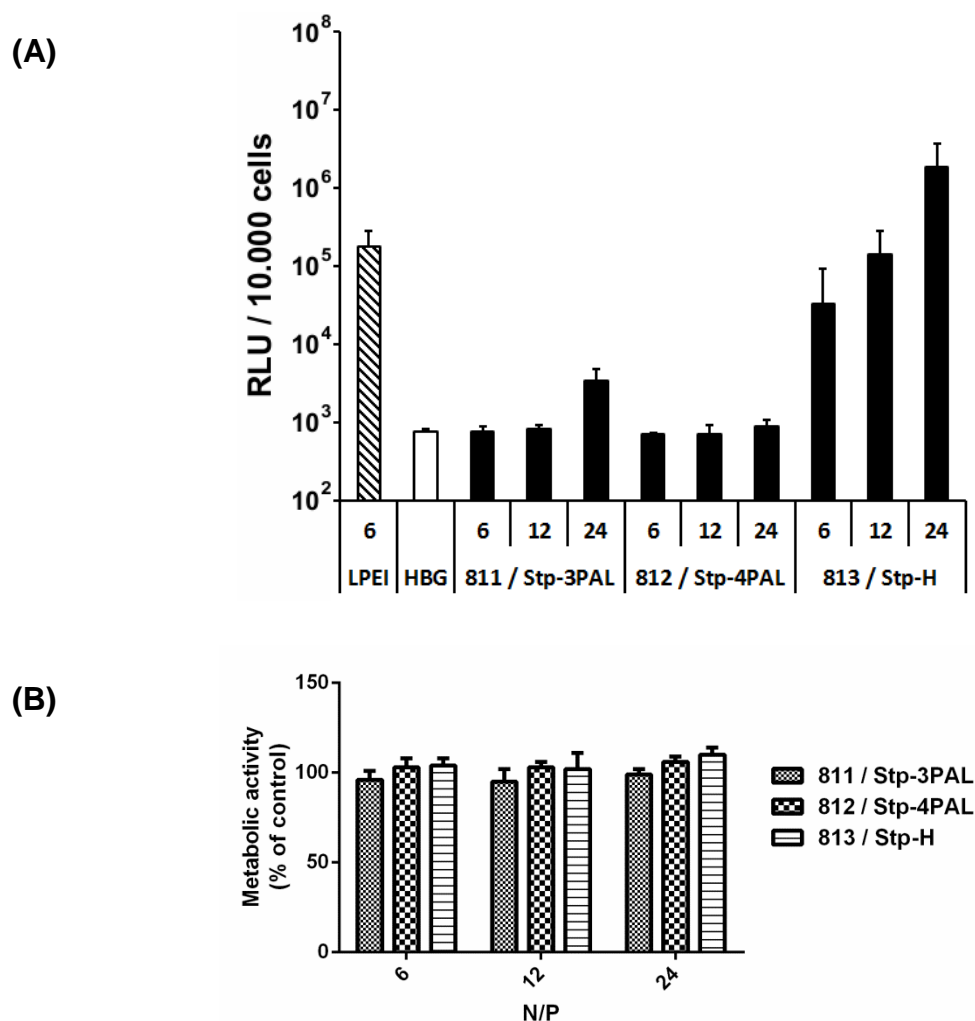


Figure 3.30 Luciferase pDNA transfections of Neuro2A neuroblastoma cells with two-arm oligomers at indicated N/P ratios. N=5 for each compound. (A) Bioluminescence levels are plotted as relative light units (RLU) per 10.000 cells. (B) Metabolic activity of transfected cells was determined by MTT assay, levels of control cells treated with HBG were set to 100 %. Experiments were carried out by Ana Krhac Levacic (Pharmaceutical Biotechnology, LMU).

3.1.5 Iminodiacetic acid derived polyamino acids

The combination of Stp and histidine showed remarkable potency and enhancement of transgene expression in several examples. Here, the polyamino acid building block Stp, with the lowest endosomal buffer capacity, predominantly served as pDNA binding unit, whereas histidine offered the required buffer capacity to promote endosomal escape. However, the integration of separate domains for both tasks within one building block would be an attractive approach to simplify the solid-phase synthesis process. The established building blocks (Gtt, Stp, Gtp, etc.) contain

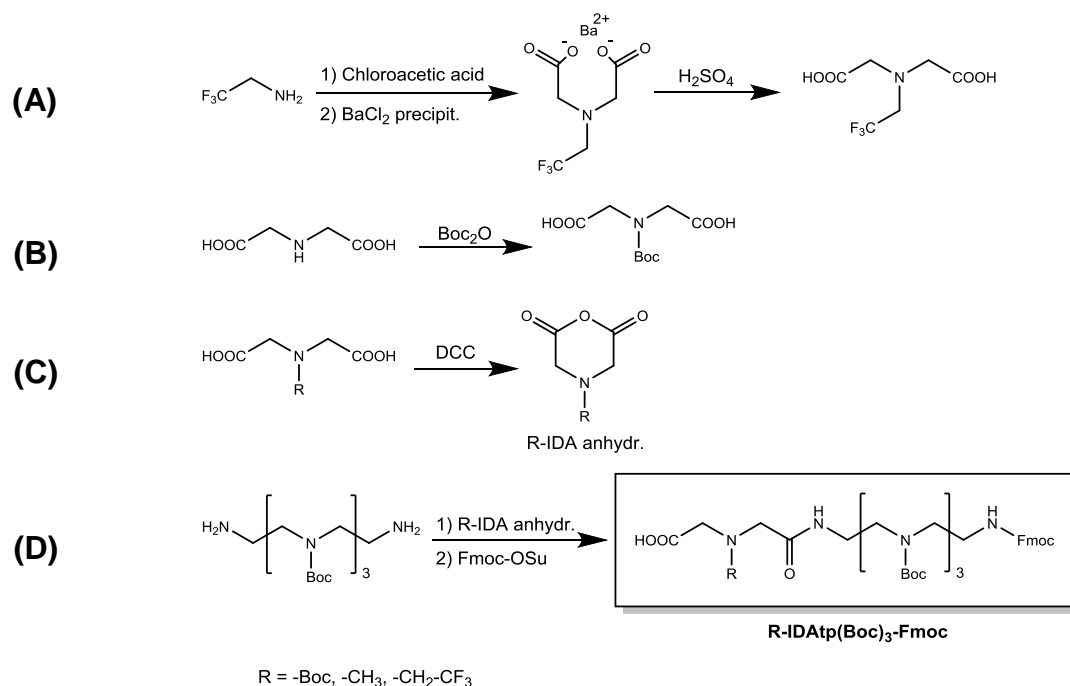
dicarboxylic acids, which serve as molecular adapter for the linkage of the polyamine segments by amide formation. By using iminodiacetic acid (IDA) derivatives (Figure 3.31) as the dicarboxylic acid part, an additional nitrogen can be introduced, giving the diacid part a new function beyond the simple chemical linkage. IDA and the two derivatives methyl-IDA (M-IDA) and trifluoroethyl-IDA (TFE-IDA) were used for the synthesis of TEPA based building blocks with gradually decreased basicity and compared to the structural analog Gtp.



Figure 3.31 Chemical structures of different dicarboxylic acids.

3.1.5.1 Building block synthesis

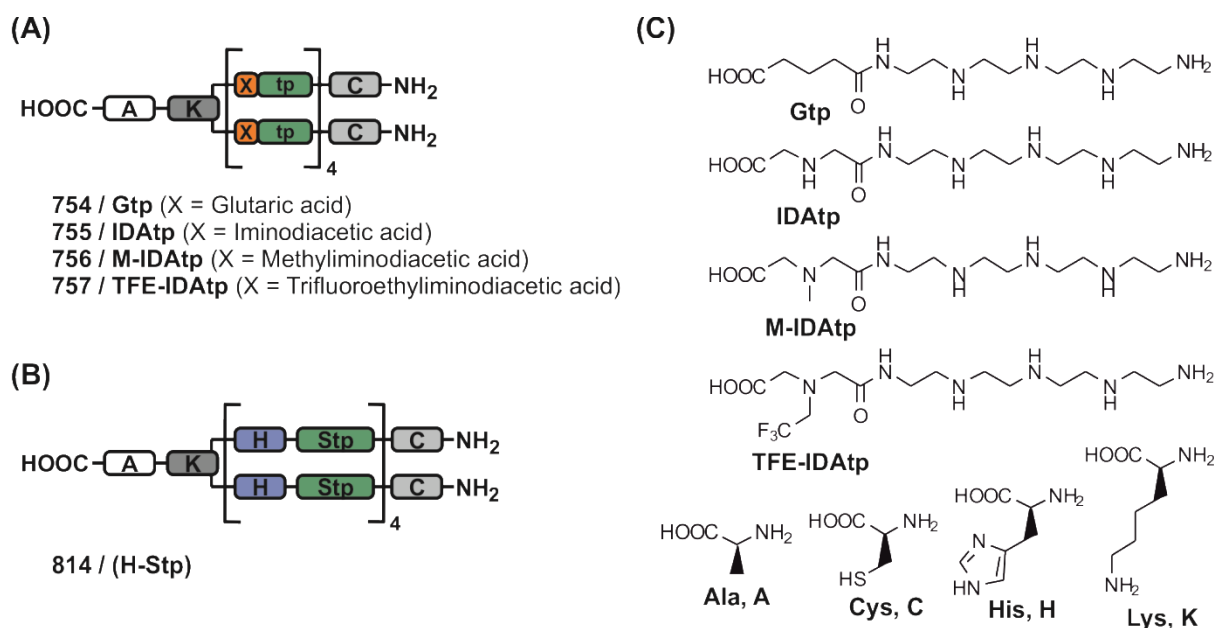
IDA and M-IDA are commercially available organic compounds. TFE-IDA was synthesized as summarized in Scheme 3.5 A. Briefly, 2,2,2-trifluoroethylamine was reacted with two equivalents of chloroacetic acid in an aqueous alkaline solution. Since IDA derivatives can act as strong chelating agents, the disubstituted product could be precipitated selectively by addition of barium chloride solution. Finally, TFE-IDA was obtained by heating with sulfuric acid and removal of the barium sulfate. For the intended use as building block during solid-phase synthesis, the secondary amine of IDA was protected with a *tert*-butoxycarbonyl (Boc) group (Scheme 3.5 B). Cyclic anhydrides of the derivatives Boc-IDA, M-IDA and TFE-IDA were prepared by dehydration with dicyclohexylcarbodiimide (DCC) in dichloromethane (Scheme 3.5 C). The subsequent steps were carried out according to the published Gtp synthesis protocol but with substitution of glutaric anhydride against the IDA anhydrides (Scheme 3.5 D). ¹H-NMR data and mass spectrums of intermediate products and building blocks can be found in the appendix.

Scheme 3.5 Synthesis of iminodiacetic acid (IDA) derived polyamino acid building blocks

Boc₂O, di-*tert*-butyl dicarbonate (Boc anhydride); DCC, dicyclohexylcarbodiimide; Fmoc-OSu, Fmoc N-hydroxysuccinimide ester.

3.1.5.2 Library design and synthesis

The two-arm topology, which was used before for the investigation of effects on endosomal escape, was chosen for the incorporation of the new IDA derived building blocks (**755**/IDAtp, **756**/M-IDAtp, **757**/TFE-IDAtp). The Gtp analog **754** and a new oligomer **814**, with a repetitive (H-Stp) motif and the same number of protonatable nitrogens as the IDAtp based compounds, served as references. Scheme 3.6 and Table 3.6 give an overview over the set of compounds. For the syntheses, the standard Fmoc SPS conditions were used. Figure 3.32 shows the analytical RP-HPLC chromatograms of the compounds. ¹H-NMR data can be found in the appendix.

Scheme 3.6 Illustration of the synthesized oligomers with new IDA derived building blocks

(A) IDA and Gtp oligomers, (B) control oligomer with (histidine-Stp) repeating unit, (C) chemical structures of building units.

Table 3.6 Sequences, protonatable nitrogens and abbreviations of the synthesized oligomers

ID	Sequence (C -> N)	Proton. Nitrogens	Abbreviation
754	AK(Gtp ₄ -C) ₂	26	Gtp
755	AK(IDAtp ₄ -C) ₂	34	IDAtp
756	AK[(M-IDAtp) ₄ -C] ₂	34	M-IDAtp
757	AK[(TFE-IDAtp) ₄ -C] ₂	34	TFE-IDAtp
814	AK[(H-Stp) ₄ -C] ₂	34	(H-Stp)

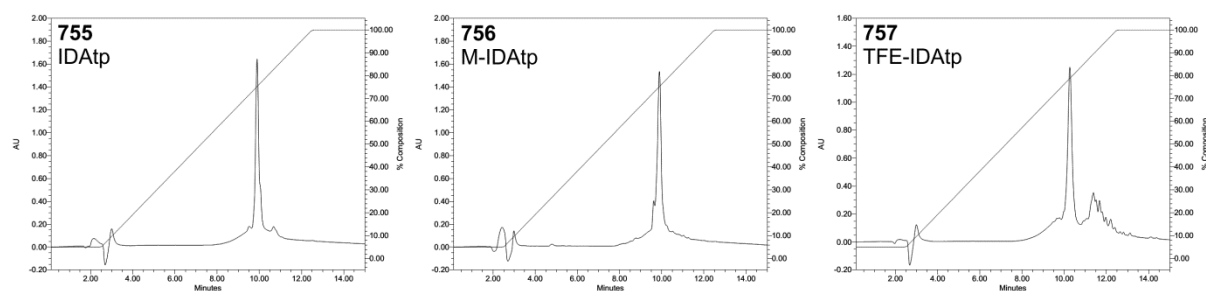


Figure 3.32 Analytical RP-HPLC chromatograms of IDA based two-arm oligomers. The analysis was carried out using a Xbridge C18 column (5 μ m, 4.6 x 150mm) and a water/acetonitrile gradient (95:5 – 0:100 in 10 min) containing 0.1 % TFA. For the detection the extinction at 214 nm was monitored.

3.1.5.3 Protonation of two-arm oligomers with IDA derived building blocks

As illustrated by Figure 3.33 A, only oligomer **755** with the IDAtp building block exhibited a slightly increased total endosomal buffer capacity compared to the Gtp analog **754**. Both M-IDAtp and TFE-IDAtp decreased the buffer capacity of the related compounds. The reason for this can be found by looking at the relative protonation (Figure 3.33 B). The secondary amine of IDA has a low basicity, which only affects protonation in the lower sub-ranges between pH 5 and 6. Like expected the basicity of the tertiary amine in M-IDA is lower, since only a slight effect on the lower pH ranges can be observed. In case of TFE-IDA no big difference compared to Gtp is observable, since the pK_a lies far below pH 5 and therefore does not affect the protonation in the endosomal pH range at all. Since the M-IDA and TFE-IDA nitrogen almost had no effect on the endosomal pH range, but were considered in the calculation of the sample amounts for titrations, the determined total buffer capacity of **756** and **757** even decreased compared to **754**.

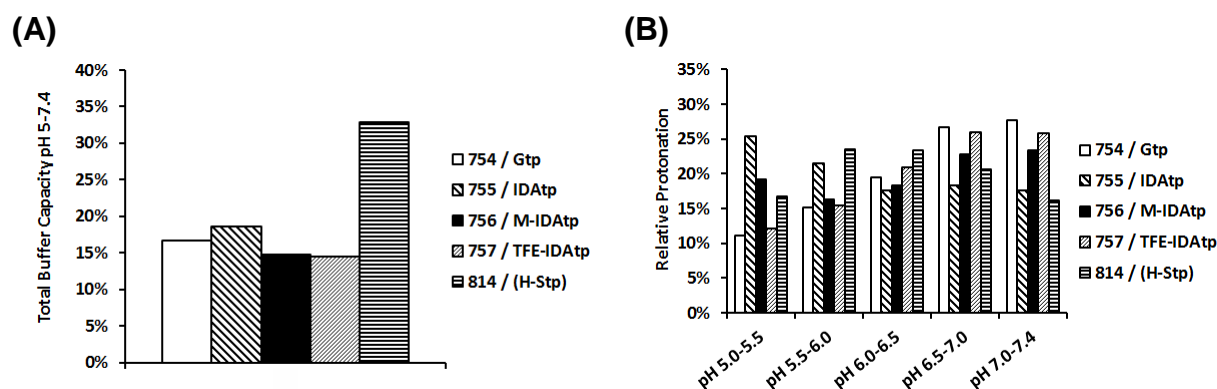


Figure 3.33 Buffer capacities of two-arm oligomers with IDA derived building blocks. Oligomer amounts containing 15 μ moles of protonatable nitrogens were used for the titrations. (A) Total endosomal buffer capacity (pH 5.0-7.4), (B) buffering profile in the endosomal pH range, total endosomal buffer capacity was set to 100 %.

3.1.5.4 pDNA complexation of two-arm oligomers with IDA derived building blocks

All compounds mediated comparable ethidium bromide exclusion from pDNA. This result was expected, since the building blocks were designed to keep the pDNA binding motif TEPA unmodified.

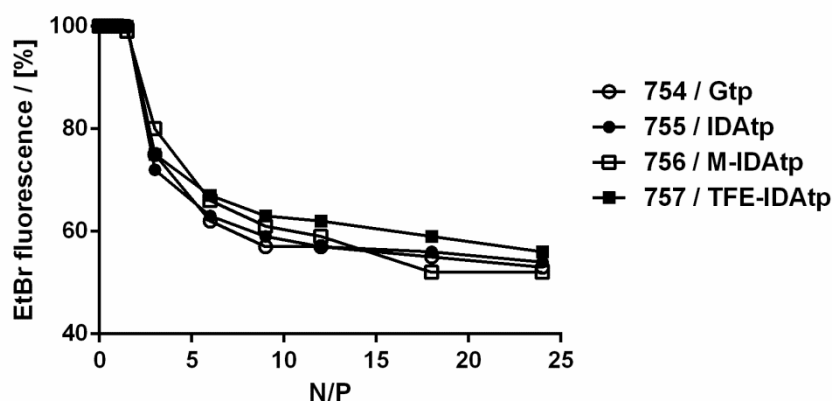


Figure 3.34 Ethidium bromide (EtBr) exclusion from pDNA by two-arm oligomers with IDA derived building blocks. EtBr fluorescence without pDNA was used as blank, EtBr fluorescence in presence of pDNA and absence of oligomer was set to 100 %.

3.1.5.5 pDNA transfections with two-arm oligomers containing IDA derived building blocks

In pCMVLuc transfections of Neuro2A cells no enhancing effect of the IDA building blocks on endosomal escape or transgene expression could be observed (Figure 3.35 A). In contrast, the control oligomer **814** with the same number of TEPA units and protonatable nitrogens, but histidine instead of IDA derivatives, mediated distinct transgene expression. The basicity of the IDA nitrogens obviously is too low to affect the endosomal buffering in a proper way. Fortunately, no obvious sign of an increased cytotoxicity of the oligomers containing IDA derivatives could be found (Figure 3.35 B). Although the new building blocks did not serve the intended purpose, the described synthesis approach represents a possibility for the integration of new functionalities, giving the dicarboxylic acid part a new function without modifying the pDNA binding polyamine motif.

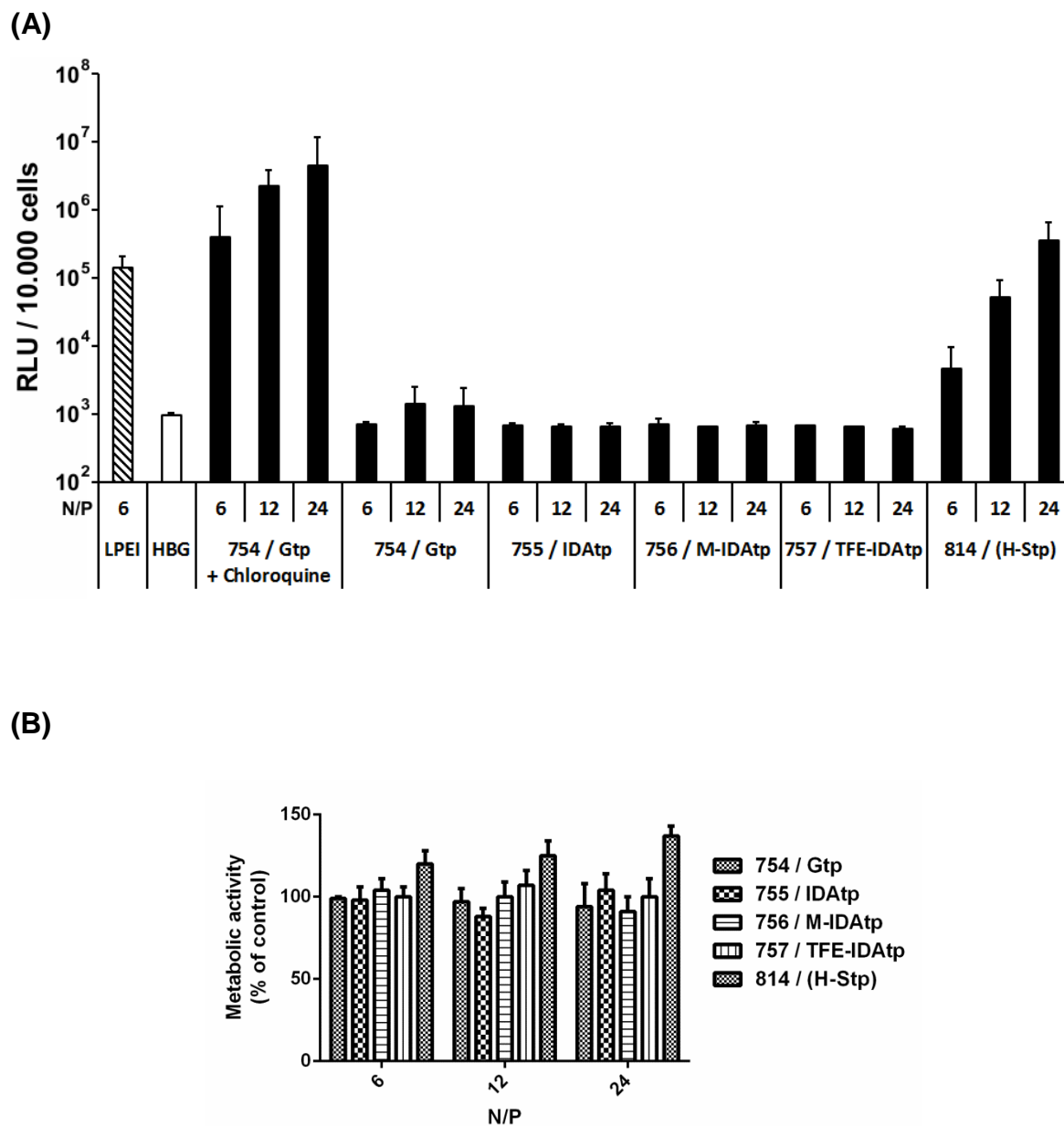
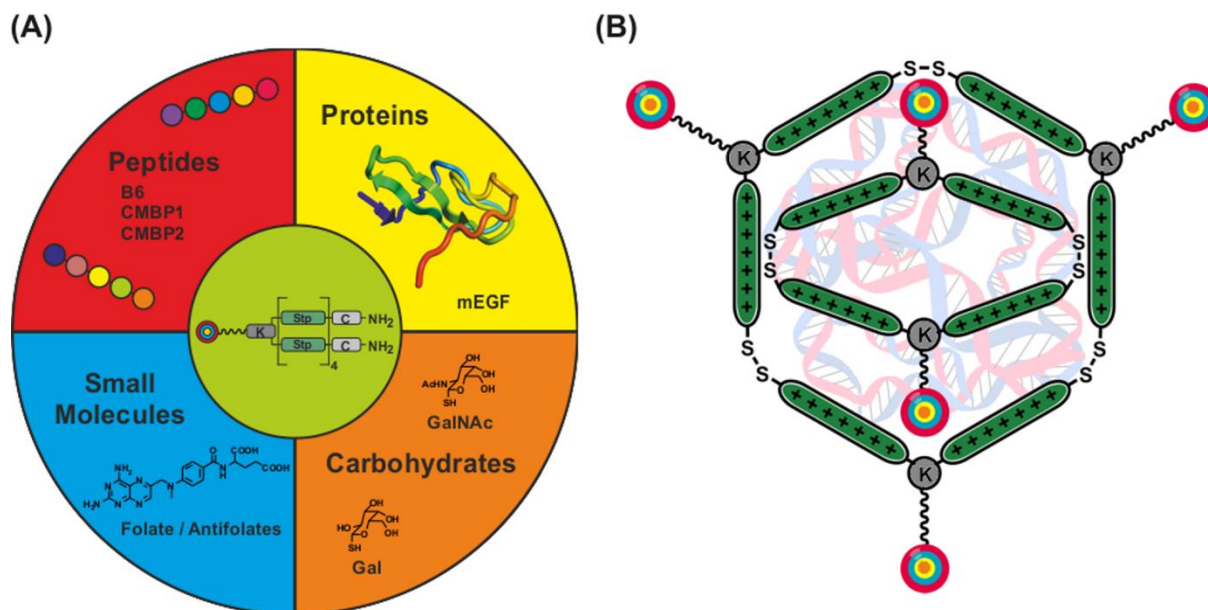


Figure 3.35 Luciferase pDNA transfections of Neuro2A neuroblastoma cells with two-arm oligomers at indicated N/P ratios. N=5 for each compound. (A) Bioluminescence levels are plotted as relative light units (RLU) per 10.000 cells. (B) Metabolic activity of transfected cells was determined by MTT assay, levels of control cells treated with HBG were set to 100 %. Experiments were carried out by Ana Krhac Levacic (Pharmaceutical Biotechnology, LMU).

3.2 Targeted and shielded oligo(ethanamino)amides for receptor-specific nucleic acid delivery

Bare basic polymers, which form nanosized polyplexes with pDNA, are subjected to a biodistribution after systemic administration, which depends on the individual physicochemical properties. Particle size and surface charge are key parameters determining the circulation time, tissue accumulation and clearance of nanoparticles. Shielding of the surface charge is a common approach to evade unspecific ionic interactions, opsonization and clearance by the mononuclear phagocyte system. The increased circulation time of shielded particles can result in a certain tissue specific accumulation, e.g. due to the enhanced-permeability and retention effect, also called 'passive targeting'. However, additional mechanisms are required to achieve a cell-type specificity beyond the tissue accumulation. Moreover, since the cellular uptake of polycationic complexes is based on the positive surface charge, shielding not only suppresses unintended interactions but also the attachment to target cells. Targeting-ligands, which bind to surface-markers of the target cells, can restore cellular uptake in a specific fashion after the unspecific interactions have been eliminated by surface shielding. The numerous ligands, which have been used for the general purpose of drug targeting, exhibit a great diversity of chemical nature. Examples of compound classes of targeting ligands are peptides, proteins (including antibodies), carbohydrates and small (organic) molecules. Here the compatibility and feasibility of the solid-phase synthesis approach for the assembly of targeted and shielded oligo(ethanamino)amides with ligands of different chemical nature was investigated. The PEGylated two-arm topology was used as platform for the nucleic acid carriers with different heterogeneous ligands (Scheme 3.7). This particular structure consists of a branched Stp sequence as charged nucleic acid binding core. Terminal cysteines are integrated for the formation of disulfide crosslinks, which increase the extracellular polyplex stability, but get disassembled in the reductive environment of the cytosol. A discrete PEG segment of defined length is located at the central position of the branching backbone lysine and coupled to the targeting ligand at the exposed terminus. Peptides (cMBP1, cMBP2), a protein (mEGF), carbohydrates (S-glycoside mimetics of galactose and N-acetylgalactosamine) and small molecules (folic acid, MTX derivatives) were used as ligands.

Scheme 3.7 Illustration of the PEGylated two-arm topology with different ligands as flexible platform for targeted nucleic acid carriers



(A) Overview over the used targeting ligands classified by their chemical nature, (B) concept of nucleic acid encaging by the targeted PEGylated two-arm oligomers based on ionic interaction of the Stp sequence and bio-reducible disulfide links formed by cysteines. The structure of mEGF has been derived from the Protein Data Bank Japan: PDBj (dataset 1EGF).

Two phage display derived c-Met binding peptides (cMBP1 and cMBP2) were reported in the literature as diagnostic agents for the purpose of *in vivo* tumor imaging [176-179]. Here active c-Met receptor-targeting was used for the first time in context of non-viral gene delivery (Chapter 3.2.1).

In contrast to the integration of peptides, which can easily be integrated into the sequence during solid-phase synthesis, the conjugation of proteins requires a different strategy. Here a strain-promoted alkyne-azide cycloaddition (SPAAC) under mild aqueous conditions was used for the site-specific attachment of murine epidermal growth factor (mEGF) to a PEGylated two-arm oligo(ethanamino)amide, which has been synthesized by SPS before (Chapter 3.2.2). Although mEGF (approx. 6 kDa) is still a rather small member of the protein class, the conjugation represents a step forward toward larger macromolecular targeting ligands. Moreover, the chosen conjugation strategy was supposed to demonstrate the feasibility of the platform to be compatible also with ligands which cannot be coupled on solid-phase.

Beyond peptides and proteins, another particularly interesting class of biopolymers is represented by carbohydrates. The great importance of these compounds in molecular recognition processes such as intercellular contact and communication or antigen binding also account for their great potential as targeting ligands. In general, multivalent interactions are responsible for the selective binding of saccharides to their recognition partners. In collaboration with Prof. Dr. Laura Hartmann (University Düsseldorf; former MPI of Colloids and Interfaces, Potsdam) and Dr. Felix Wojcik (MPI of Colloids and Interfaces, Potsdam) several multivalent glycoligands were used in combination with the PEGylated two-arm oligo(ethanamino)amides and screened for their activity to mediate asialoglycoprotein receptor (ASGPR) targeted gene delivery (Chapter 3.2.3).

As an example of small molecule ligands with additional function beyond receptor-targeting, the antifolate methotrexate and a set of variants were used as drug conjugates with the nucleic acid carriers. The potency as targeting ligands, in comparison to folic acid, as well as the additional effect in cytotoxic poly(I:C) delivery were investigated (Chapter 3.2.4).

3.2.1 c-Met binding peptides for receptor-specific gene transfer by oligo(ethanamino)amides *in vitro* and *in vivo*

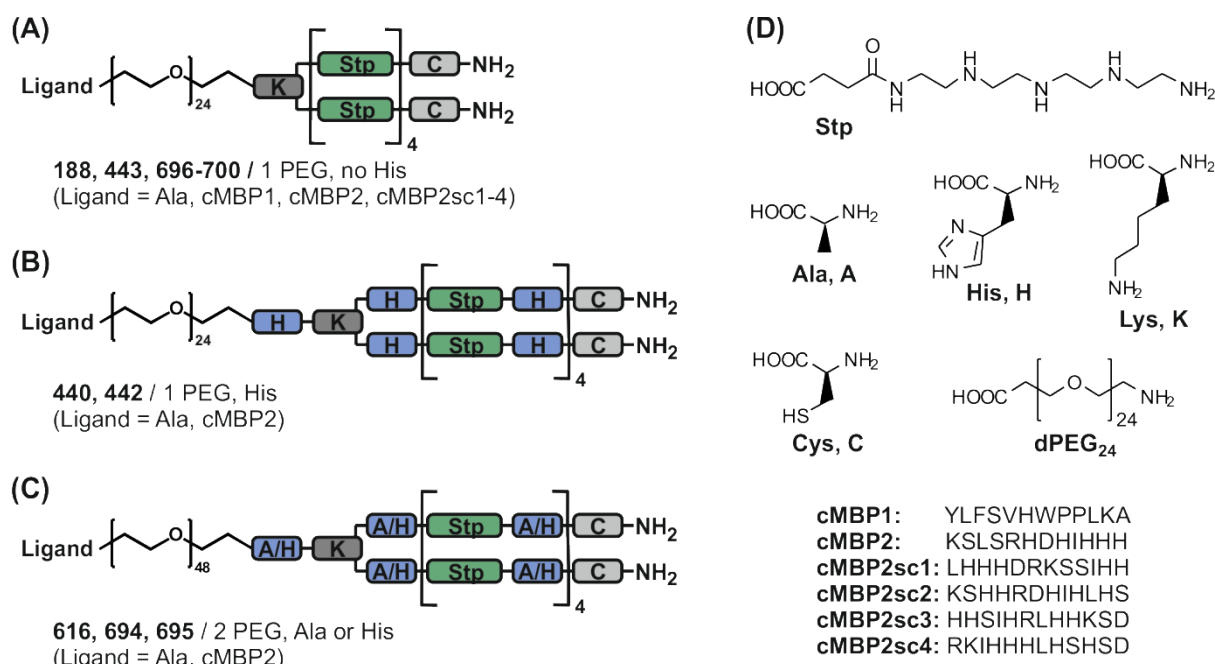
The receptor tyrosine kinase c-Met (hepatocyte growth factor receptor, HGFR) triggers several cellular processes, such as mitogenesis, motogenesis and morphogenesis, after binding of its native ligand HGF [185]. For this reason c-Met plays an important role in physiological tissue development, homeostasis and regeneration. However, it can also promote malignant transformation, tumor progression and invasive growth [186]. Several studies indicated the overexpression of c-Met and dysregulation of its pathway to be a poor prognostic factor for therapeutic outcome and survival in a variety of different types of cancer [187-189]. Therefore, targeting the c-Met signaling pathway is considered as promising therapeutic approach and has attracted much attention in drug development and research. Most approaches focus on the inhibition of HGF binding or interference with the c-Met signaling pathway, e.g. by inhibition of the tyrosine kinase activity. Moreover, anti-c-Met antibodies have been used for immunotherapy and imaging purposes [190-192]. However, only a few published works demonstrate the potency of c-Met targeting in terms of drug delivery. Chen et al. reported c-Met dependent cytotoxicity and reduced side-effects of a doxorubicin conjugate with an anti-c-Met Fab fragment [193]. Nguyen et al. developed retroviral vectors with insertion of single-chain variable-fragments (scFv) against c-Met in the viral envelope protein [194]. By this means a higher selectivity of gene transfer to human hepatoma cells could be achieved. Beyond that, c-Met targeting has not been used for the purpose of non-viral gene delivery before.

Here two published c-Met binding peptide sequences (cMBP1 and cMBP2, [176, 177]) identified by phage display were integrated into PEGylated two-arm oligo(ethanamino)amides. The aim was the identification of the more potent ligand and a stepwise optimization process of the nucleic acid carrier for the final purpose of a targeted *in vivo* gene transfer.

3.2.1.1 *Library design and synthesis*

The polyamino acid Stp was used for the assembly of the two-arm topology oligomers with PEGylation and cMBP ligands. Peptidic ligands are perfectly compatible with the used SPS approach and can readily be integrated in the sequences of the oligo(ethanamino)amide based compounds. Three different carrier variants were used for the structure-activity relationship studies and represent different stages of a gradual optimization process. Scheme 3.8 and Table 3.7 give an overview over the set of compounds. The first variant class (Scheme 3.8 A, 1 PEG, no His) consisted of the branched two-arm structure with a continuous Stp sequence and terminal cysteines as nucleic acid encaging core without additional backbone modifications. A monodisperse PEG₂₄ was placed at the central position of the branching lysine. Both ligands, cMBP1 and cMBP2, as well as four scrambled sequences of cMBP2 (cMBP2sc1-4) and alanine as untargeted control were attached at the exposed part of the PEG segment in separate structures. With these first compounds, the potencies of the two cMBP ligands were compared and the sequence specificity of cMBP2 was investigated. The second carrier variant (Scheme 3.8 B, 1 PEG, His) contained additional histidines in the backbone sequence and either cMBP2 as a ligand or alanine as control. In the last carrier class (Scheme 3.8 C, 2 PEG, Ala or His) the influence of an extended PEG chain was investigated, as well as backbone histidine compared to backbone alanine without buffering effect.

For the synthesis of the oligo(ethanamino)amides, the standard Fmoc SPS conditions were used. All compounds were analyzed by ¹H-NMR and RP-HPLC. Figure 3.36 shows the analytical RP-HPLC chromatograms of representative members of the set and each variant class. ¹H-NMR data can be found in the appendix.

Scheme 3.8 Illustration of the synthesized oligomers with different ligands and structure variants

(A) 1 PEG₂₄, no backbone histidines, (B) 1 PEG₂₄, additional backbone histidines, (C) 2 PEG₂₄, additional backbone alanines or histidines, (D) chemical structures of sequence components and peptide ligand sequences. cMBP, c-Met binding peptide; cMBP2sc, scrambled sequence of cMBP2.

Table 3.7 Sequences, structure variants and abbreviations of the synthesized oligomers

ID	Sequence (C -> N)	Variant	Abbreviation
188	A-dPEG ₂₄ -K(Stp ₄ -C) ₂	1 PEG, no His	Ala
696	K[dPEG ₂₄ -K(Stp ₄ -C) ₂]-cMBP1	1 PEG, no His	cMBP1
443	K[dPEG ₂₄ -K(Stp ₄ -C) ₂]-cMBP2	1 PEG, no His	cMBP2
697	K[dPEG ₂₄ -K(Stp ₄ -C) ₂]-cMBP2sc1	1 PEG, no His	cMBP2sc1
698	K[dPEG ₂₄ -K(Stp ₄ -C) ₂]-cMBP2sc2	1 PEG, no His	cMBP2sc2
699	K[dPEG ₂₄ -K(Stp ₄ -C) ₂]-cMBP2sc3	1 PEG, no His	cMBP2sc3
700	K[dPEG ₂₄ -K(Stp ₄ -C) ₂]-cMBP2sc4	1 PEG, no His	cMBP2sc4
440	A-dPEG ₂₄ -HK[H-(Stp-H) ₄ -C] ₂	1 PEG, His	Ala-His
442	K[dPEG ₂₄ -HK(H-(Stp-H) ₄ -C) ₂]-cMBP2	1 PEG, His	cMBP2-His
616	A-(dPEG ₂₄) ₂ -HK[H-(Stp-H) ₄ -C] ₂	2 PEG, His	Ala-2PEG-His
694	K[(dPEG ₂₄) ₂ -HK(H-(Stp-H) ₄ -C) ₂]-cMBP2	2 PEG, His	cMBP2-2PEG-His
695	K[(dPEG ₂₄) ₂ -AK(A-(Stp-A) ₄ -C) ₂]-cMBP2	2 PEG, Ala	cMBP2-2PEG-Ala
689*	C-(H-Stp) ₃ -HK[H-(Stp-H) ₃ -C] ₂	three-arm	-

* Oligomer **689** was synthesized by Dongsheng He (Pharmaceutical Biotechnology, LMU) and was used as a co-formulation oligomer for *in vivo* trials.

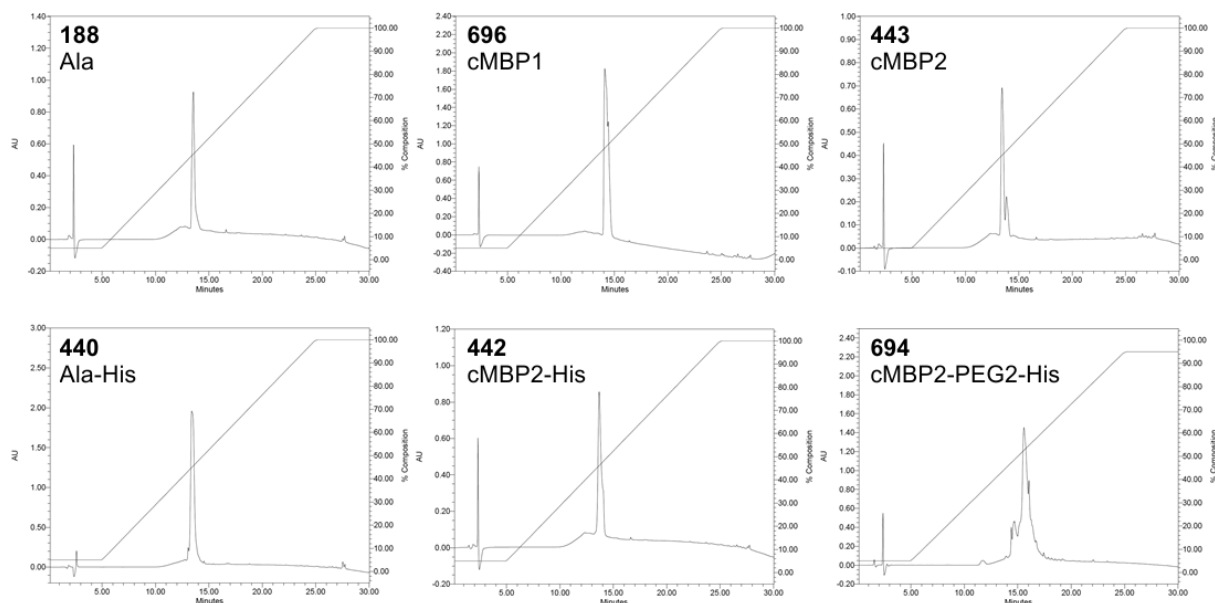


Figure 3.36 Analytical RP-HPLC chromatograms of representative library members. The analysis was carried out using a Waters Sunfire C18 column (5 μ m, 4.6 x 150mm) and a water/acetonitrile gradient (95:5 – 0:100 in 20 min) containing 0.1 % TFA. For the detection the extinction at 214 nm was monitored.

3.2.1.2 Targeting ligand evaluation

The first variant class (1 PEG, no His) was used for the evaluation of the two peptide ligands. For this purpose the cellular association of pDNA polyplexes with hepatocarcinoma Huh7 cells, which display high c-Met expression (PhD thesis Dr. Petra Kos, Pharmaceutical Biotechnology, LMU), was determined by flow cytometry (Figure 3.37 A). Both peptide sequences cMBP1 (**696**) and cMBP2 (**443**) mediated a greatly enhanced cellular association of the corresponding polyplexes (> 90 % positive cells) compared to the untargeted alanine control (**188**). In direct comparison of the two ligands, cMBP2 showed the higher potency and mediated higher cellular binding of the corresponding polyplexes, since a slightly higher number of Cy5 positive cells was found. The sequence-specificity of cMBP2 was investigated by the use of scrambled sequences in analog carriers (**697-700**) and the same experimental set up (Figure 3.37 B). None of the four scrambled sequences cMBP2sc1-4 was able to mediate significant cellular association of the corresponding pDNA polyplexes, which indicates the cMBP2-mediated cell-binding to be a sequence-specific effect.

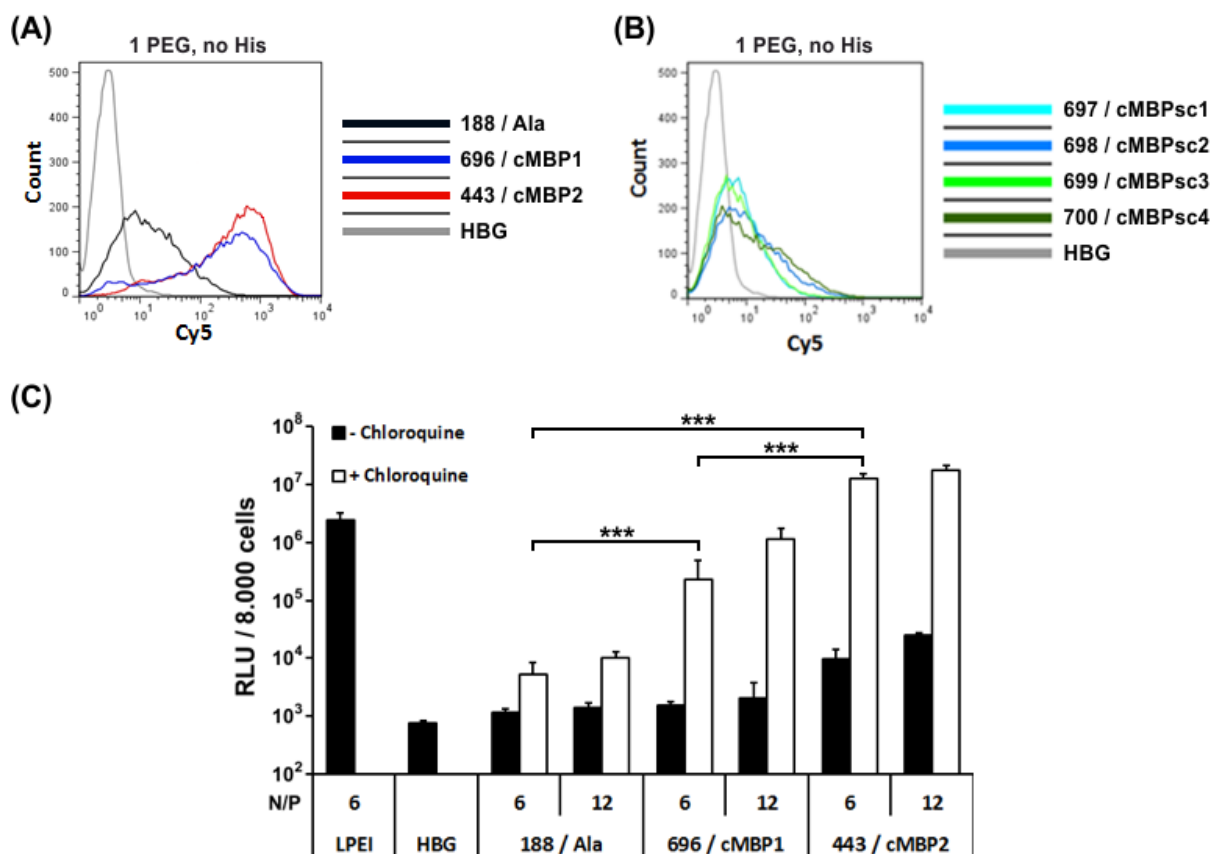


Figure 3.37 Cellular association of Cy5-pDNA polyplexes (1 PEG, no His) and luciferase reporter gene expression in Huh7 cells. Comparison of (A) cell binding of cMBP1 (**696**) or cMBP2 (**443**) targeted and untargeted Ala (**188**) polyplexes at N/P 12, (B) cell binding of polyplexes at N/P 12 with scrambled cMBP2 sequences (**697-700**) and (C) transgene expression after transfections with cMBP1 (**696**), cMBP2 (**443**) targeted and untargeted Ala (**188**) polyplexes. Bioluminescence levels in (C) are plotted as relative light units (RLU) per 8,000 cells. Cells treated with HBG served as negative control. N=1 for each compound in the cellular association assays, N=5 for each compound in the transfection experiments. Experiments were carried out by Dr. Petra Kos (Pharmaceutical Biotechnology, LMU).

The ability of the carriers to mediate gene transfer was evaluated by pCMVLuc transfections of Huh7 cells and subsequent bioluminescence quantification (Figure 3.37 C). With the addition of chloroquine as endosome disruptive agent, both ligands significantly enhanced transgene expression compared to the untargeted control **188/Ala**. Consistent with the higher cellular association, the cMBP2 polyplexes also mediated significant higher luciferase activity than the cMBP1 analog and even outperformed LPEI, however only when chloroquine was added. Without chloroquine, the cMBP1 targeted oligomer did not mediate transgene expression above background level. Interestingly, the cMBP2 oligomers mediated increased luciferase activity compared to the untransfected (HBG) or **188** transfected cells even without

chloroquine. A reason for this presumably is the presence of several histidines in the cMBP2 sequence. Nevertheless, also for cMBP2 the effect on the transgene expression without addition of chloroquine is poor, indicating the need for an improved endosomal escape performance of the nucleic acid carriers.

3.2.1.3 Carrier optimization

Based on the gained experience with the modulation of endosomal buffer capacity and the correlation with endosomal escape, histidines were integrated in the oligo(ethanamino)amide backbone of the carriers (cf. Scheme 3.8 B). Additionally the PEG chain was extended to the two-fold length and backbone histidines substituted by alanines without buffering properties (cf. Scheme 3.8 C). The effect of the additional backbone histidines in the structure variants with one PEG₂₄ on the cellular association of the related pDNA polyplexes as well as the difference between backbone alanines and histidines in the variants with two PEG₂₄ were investigated by flow cytometry like before (Figure 3.38 A). No influence of the backbone histidines on the cellular association of the cMBP2 targeted or untargeted alanine polyplexes with one PEG could be observed. Likewise, backbone alanines or histidines did not alter the cellular association of the polyplexes with doubled PEG length. However, a clear effect of backbone histidines on the endosomal escape could be observed in an intracellular calcein release assay (Figure 3.38 B). Images of the intracellular distribution of fluorescent calcein, which was passively co-internalized with the polyplexes during the transfections, were acquired by spinning disk confocal microscopy. In case of the cMBP2 polyplexes with backbone histidines, a bright and homogeneously distributed cytosolic calcein fluorescence could be observed, whereas the analog with backbone alanines only caused a spotty calcein distribution, indicating a vesicular entrapment of the dye.

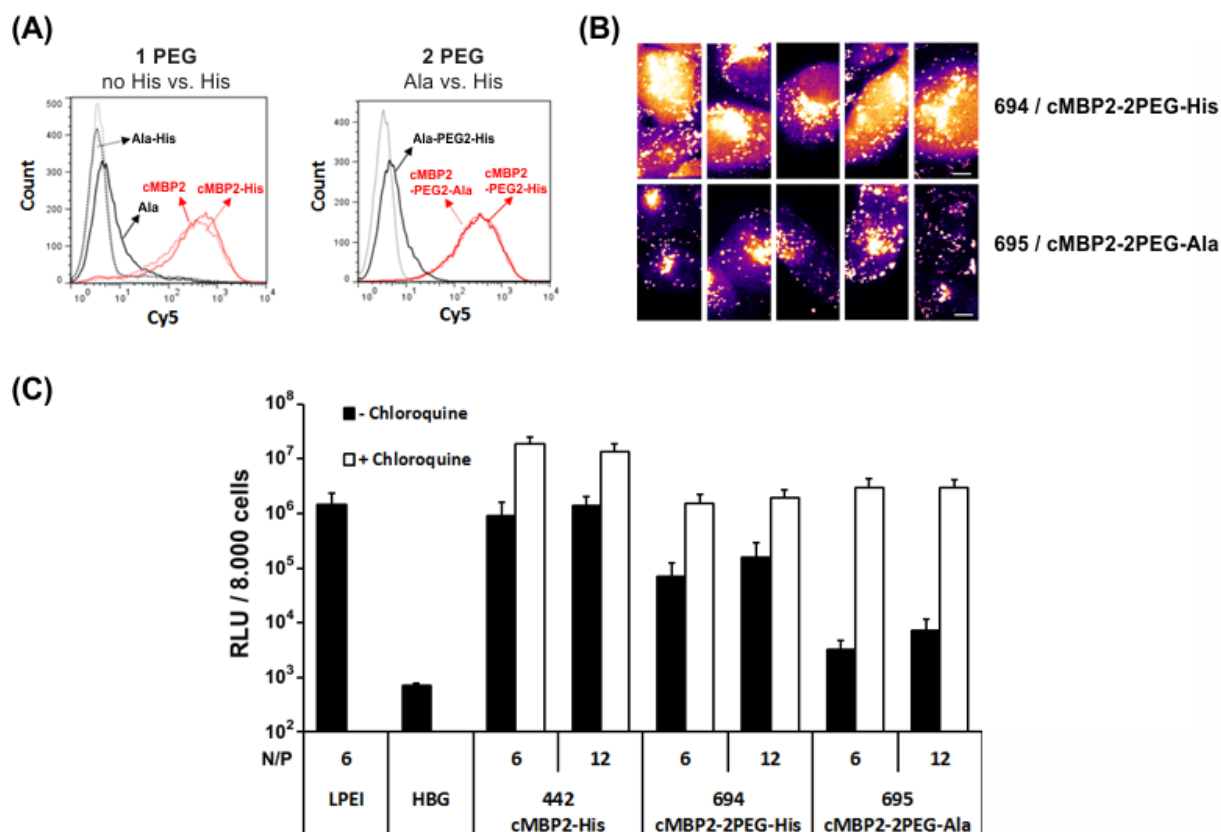


Figure 3.38 Cellular association of Cy5-pDNA polyplexes, endosomal escape performance and luciferase reporter gene expression after transfections of Huh7 cells. (A) Influence of backbone histidines on the cellular association of polyplexes at N/P 12 containing 1 or 2 PEG₂₄, (B) influence of backbone histidines on the endosomal escape investigated by intracellular calcein release (cf. Fig. 3.16) and (C) influence of backbone histidines and PEG chain length on transgene expression levels. Bioluminescence levels in (C) are plotted as relative light units (RLU) per 8,000 cells. Cells treated with HBG served as negative control in (A) and (C). N=1 for each compound in the cellular association assays, N=5 for each compound in the transfection experiments. Cellular association and transgene expression experiments were carried out by Dr. Petra Kos (Pharmaceutical Biotechnology, LMU). Calcein release experiments were carried out by Dr. Frauke Mickler (Physical Chemistry, LMU).

The introduction of backbone histidines also had great impact on the transgene expression without addition of chloroquine (Figure 3.38 C). Greatly enhanced luciferase activity could be observed in case of the histidine containing oligomers. Importantly, the cMBP targeted polyplexes with two PEG₂₄ segments mediated lower expression levels than the analog with one PEG₂₄, both with or without addition of chloroquine. Therefore, the structure variant containing one PEG₂₄ element and backbone histidines was identified as the most potent and considered for the *in vivo* trials.

3.2.1.4 Gene transfer *in vivo*

After the encouraging *in vitro* results with the most promising carrier, containing the cMBP2 ligand, one PEG₂₄ element and backbone histidines, *in vivo* experiments with Huh7 tumor bearing mice were carried out (Figure 3.39). The oligomer **442**/cMBP2-His and its untargeted control **440**/Ala-His were compared in their *in vivo* gene transfer efficiency after local intratumoral (IT) and intravenous (IV) injection of pDNA polyplexes at N/P 12 (Figure 3.39 A). A significant (approx. 15-fold) higher transgene expression, mediated by the cMBP2 targeted polyplexes compared to the alanine control, was observed after intratumoral injection.

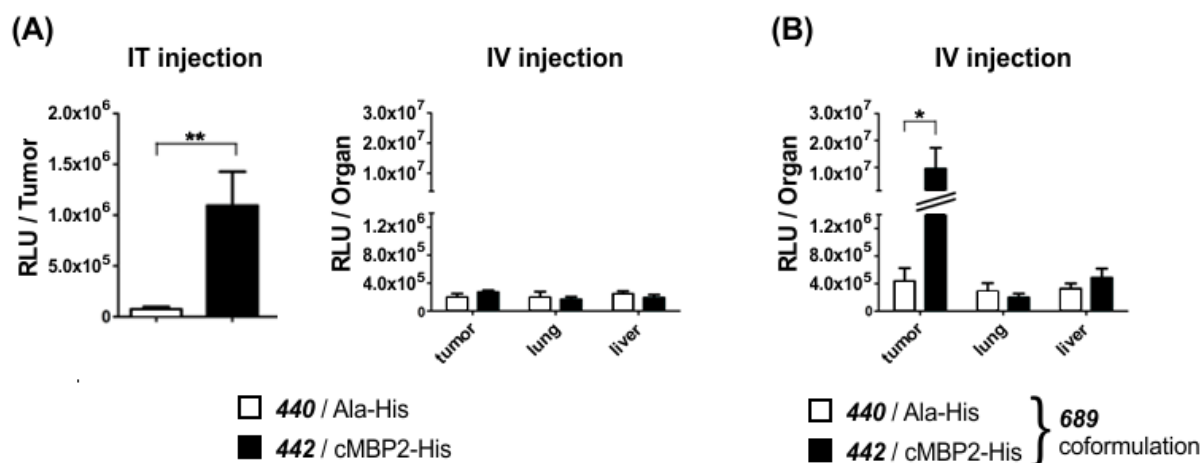


Figure 3.39 Luciferase reporter gene expression *in vivo* after local and systemic administration of single-oligomer or oligomer-blend polyplex formulations (1 PEG, His). Luciferase activity after (A) injection of cMBP2 targeted (**442**) or untargeted (**440**) pDNA polyplexes locally (IT) or systemically (IV), (B) intravenous injection of mixed **442/689** or **440/689** pDNA polyplexes with an untargeted three-arm Stp/histidine oligomer **689**. Polyplexes containing pCMVLuc and oligomer at N/P 12 were injected into Huh7 tumor bearing mice. Luciferase activity in homogenized tissue samples was measured 48 hours after administration. N=5 animals per group. Animal experiments were carried out by Annika Herrmann and Dr. Petra Kos, oligomer **689** was synthesized by Dongsheng He (Pharmaceutical Biotechnology, LMU).

However, no difference between cMBP2 targeted and untargeted polyplexes could be found after the systemic administration; no effect of the homing ligand on the transgene expression in tumor, lung or liver could be observed. It has been shown by transmission electron microscopy before that similar PEGylated oligomers form loose 'spaghetti-like' complexes with pDNA. Obviously the PEG chain hinders pDNA condensation, despite a potent pDNA binding of the basic oligomer backbone. Since

the spatial arrangement and tightness of the pDNA polyplexes can affect their biodistribution, an alternative approach with an untargeted Stp/histidine co-formulation oligomer **689** was taken. The co-formulation oligomer has a three-arm topology with an alternating Stp/histidine sequence and three terminal cysteines. For the polyplex formation, a blend of the PEGylated oligomer (**442**/cMBP2-His or **440**/Ala-His) with the co-formulation oligomer **689** in an amine ratio of 70:30 (30 % of N/P ratio is covered by **689**) was prepared before addition of the pDNA. It was shown by transmission electron microscopy and ethidium bromide exclusion assays that the co-formulation with **689** caused a great increase of pDNA compaction and a different spatial arrangement of the resulting polyplexes (PhD thesis Dr. Petra Kos, Pharmaceutical Biotechnology, LMU). With the alternative co-formulation approach, a greatly enhanced gene transfer in the tumor was observed after intravenous injection of the cMBP2 targeted polyplexes (Figure 3.39 B). The **442/689** polyplexes mediated approximately 22-fold higher transgene expression in the tumor tissue than the untargeted co-formulation **440/689** polyplexes, whereas no differences were observed in lung or liver tissue. In sum, these results show the tumor homing potential of the cMBP2 ligand as well as the suitability of the used nucleic acid carrier class to mediate targeted gene transfer *in vivo*. Moreover, the results indicate the importance of the pDNA condensation state and optimized polyplex formulations for a proper biodistribution and successful delivery to the target site.

3.2.2 EGF receptor directed cellular uptake of pDNA polyplexes mediated by mEGF-oligo(ethanamino)amide conjugates

The epidermal growth factor receptor (EGFR) is a member of the ERBB receptor tyrosine kinases, which play an important role in human cancer [195]. Binding of epidermal growth factor (EGF) triggers the receptor dimerization, phosphorylation and activation of downstream signaling pathways, which contribute to tumor cell proliferation, evasion of apoptosis, angiogenesis and metastasis [196]. An overexpression of EGFR has been observed in cancers of head and neck, ovary, cervix, bladder, oesophagus, stomach, brain, breast, endometrium, colon and lung [197]. Because of the significant role in neoplastic transformation and tumor progression, several drugs have been developed, which interfere with the activation

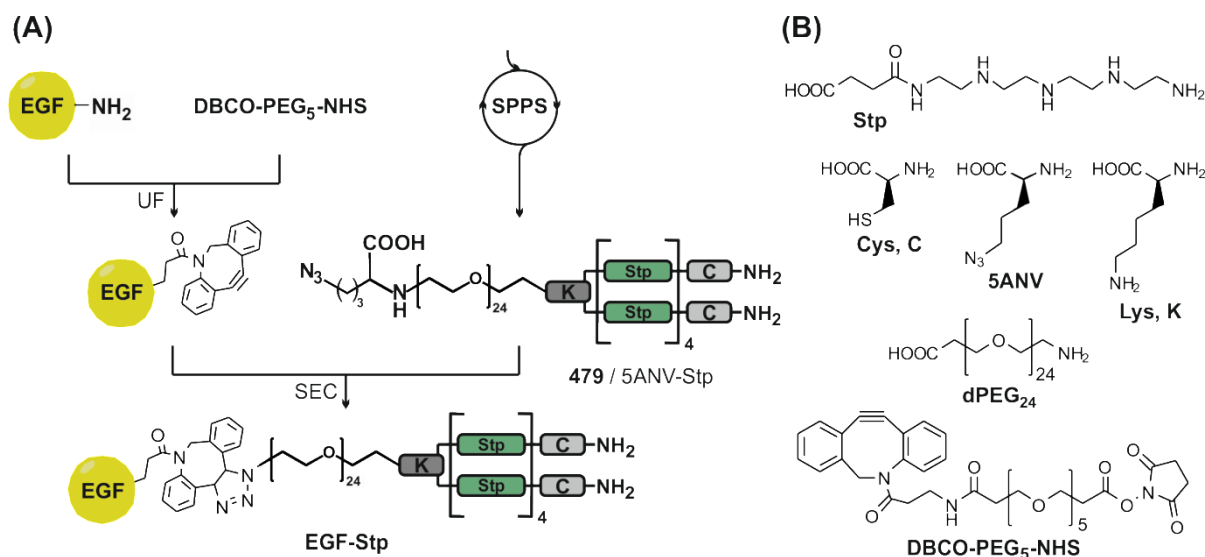
or signaling of EGFR, such as anti-EGFR antibodies or tyrosine kinase inhibitors. However, the high abundance of EGFR in a wide variety of human carcinomas makes it also an attractive target for the tumor homing purpose in drug delivery. Several antibody-drug conjugates, targeting members of the EGFR family, have been developed and reported [198-200]. The conjugate of trastuzumab with the antimicrotubule agent mertansine (trastuzumab emtansine) recently got approval by the FDA and EMA for the treatment of HER2-positive metastatic breast cancer. This makes clear that EGFR is also an interesting target for receptor-directed cancer gene therapy. Beside anti-EGFR antibodies, also artificial peptides, such as GE11, or the native ligand EGF can be used for targeting purposes [89, 201]. The investigation of the cellular uptake kinetic of EGF targeted pDNA/PEI polyplexes revealed a highly accelerated endocytosis compared to the GE11 targeted analogs [98]. In addition, with a rather small size, EGF is an ideal model protein to extend the compound space of compatible targeting ligands and to establish the required strategy for the conjugation with oligo(ethanamino)amides.

3.2.2.1 Conjugate design and synthesis

Since the PEGylated two-arm molecules contain multiple amino groups and cysteines which are indispensable for the functionality of the nucleic acid carriers, an orthogonal conjugation chemistry had to be chosen. Scheme 3.9 illustrates the used synthetic approach. The strain-promoted alkyne-azide cycloaddition (SPAAC) between dibenzocyclooctyne (DBCO) and azides was used for the site-specific attachment of EGF to the exposed part of the PEG segment. For this purpose, a PEGylated two-arm oligomer, containing the artificial α -amino acid 5-azido-L-norvaline (5ANV), was prepared under standard conditions on solid-phase. Murine EGF (mEGF) exhibits high homology with the human variant (hEGF), and it is able to bind the human EGFR [89, 202]. However, in contrast to hEGF, the sequence of mEGF contains no lysines and therefore allows the site-specific modification of the N-terminus with amine reactive groups. For this reason, mEGF was chosen to be functionalized with an excess of dibenzocyclooctyne-PEG₅-NHS ester in solution. Remaining unreacted DBCO reagent was removed by ultrafiltration (UF). Subsequently the DBCO functionalized EGF was conjugated to the azide containing oligomer **479**/5ANV-Stp by SPAAC in solution. The final reaction product EGF-Stp

(MW \approx 10 kDa, free base) was purified and separated from the excess of free **479** (MW \approx 4 kDa, free base) or unreacted EGF (MW \approx 6 kDa) by size-exclusion chromatography (SEC).

Scheme 3.9 Illustration of the synthetic approach for the assembly of EGF-Stp



Oligomer **479** was derived from SPS with the use of the artificial amino acid 5-azido-L-norvaline (5ANV). The conjugation of dibenzocyclooctyne (DBCO)-PEG₅-NHS ester to murine EGF and subsequent alkyne-azide cycloaddition with **479** was carried out in solution. Free DBCO-linker was removed by ultrafiltration (UF) after the first coupling step. Purification of the final product was carried out by size-exclusion chromatography (SEC).

¹H-NMR data of **479** can be found in the appendix. The conjugation product EGF-Stp was analyzed by RP-HPLC and compared to the starting compound **479** and mEGF (Figure 3.40). Under the used HPLC conditions, the compounds eluted at retention times of 17.101 min (mEGF), 15.289 min (**479**) and 16.783 min (EGF-Stp). An additional smaller peak at 15.724 min with an integral of approximately 14 % at 214 nm was observed in the chromatogram of EGF-Stp, which presumably represents remaining uncoupled **479** oligomer. Importantly, no free mEGF could be identified in the chromatogram of the final conjugation product. This could also be confirmed by SDS-PAGE (Figure 3.41 A). The EGF-Stp exhibited a complete shift of the protein band toward higher molecular weight (lane 3) compared to the control with free mEGF (lane 2). Unconjugated **479**/5ANV-Stp could not be visualized. A suggested explanation is that the highly basic Stp oligomers are not compatible with the chosen SDS-PAGE conditions, which enforce a negative netto charge of the analytes and

the migration toward the anode. An acetic acid-urea PAGE, which is frequently used for basic proteins, might be more suitable for oligo(ethan amino)amides. However, since the main focus was the identification of free and conjugated mEGF, SDS-PAGE was the method of choice.

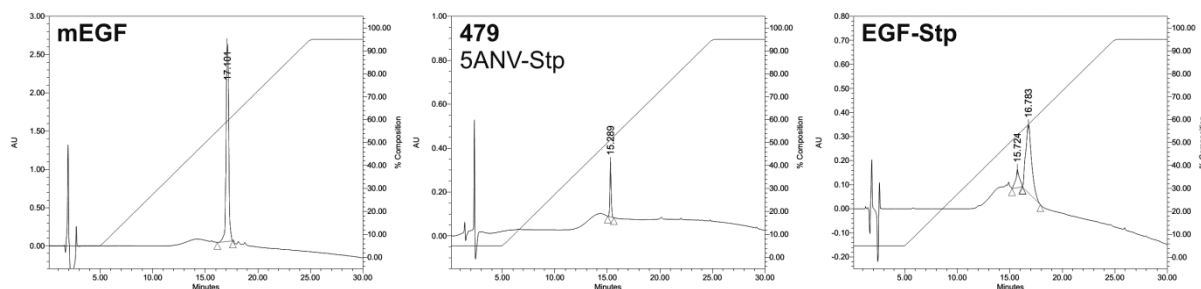


Figure 3.40 Analytical RP-HPLC chromatograms. The analysis was carried out using a Waters Sunfire C18 column (5 μ m, 4.6 x 150mm) and a water/acetonitrile gradient (95:5 – 0:100 in 20 min) containing 0.1 % TFA. For the detection the extinction at 214 nm was monitored.

The ability of EGF-Stp to complex pDNA was investigated by an electrophoretic mobility shift assay (Figure 3.41 B). The protein conjugate mediated an almost complete binding at N/P 6 and no free pDNA could be observed at higher N/P values. This result is comparable to the potency of related PEGylated two-arm oligomers with smaller targeting ligands (cf. Chapter 3.1.2, Figure 3.13). Since with increasing size of the ligand an increasing sterical hindrance of nucleic acid complexation is expected, the result is considered as an important finding. Despite the rather small size for a protein, mEGF represents the largest targeting ligand used with the oligo(ethan amino)amides so far and for the first time the molecular weight of the ligand exceeded the molecular weight of the carrier molecule.

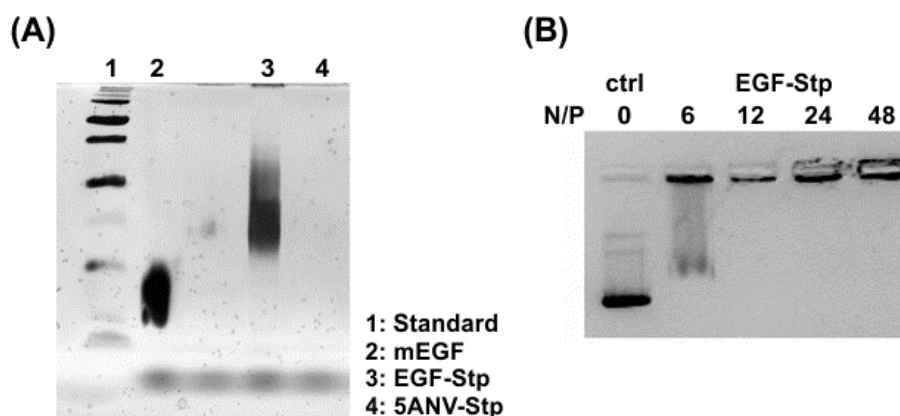


Figure 3.41 (A) SDS-PAGE with silver staining of the conjugation product EGF-Stp and the reaction partners mEGF and oligomer **479**/5ANV-Stp before conjugation, (B) electrophoretic mobility shift assay of the EGF-Stp conjugate by agarose gel electrophoresis; all samples contained 200 ng pDNA and oligomer at indicated N/P ratios.

3.2.2.2 Cellular uptake and gene transfer *in vitro*

The potency of the EGF conjugate to mediate cellular uptake of pDNA polyplexes into EGFR expressing Huh7 cells was investigated by flow cytometry and live cell imaging studies (Figure 3.42). The quantitative determination of the cells positive for Cy5 fluorescence (Figure 3.42 A) reveals a greatly enhanced uptake of EGF-targeted polyplexes compared to the control polyplexes with an alanine attached to the PEG instead of a targeting ligand (oligomer **188**, cf. Chapter 3.2.1). At both investigated N/P values 6 and 12, the alanine control failed to mediate notable cellular uptake of Cy5-pDNA polyplexes, confirming the good shielding and absence of an unspecific cellular interaction. In contrast, with the EGF targeted polyplexes at both N/P ratios a distinct majority of the cells were found to be Cy5 positive. Considering that the cellular uptake was determined after a short incubation time of 30 minutes, the cellular uptake mediated by EGF seems to be considerably fast and efficient. The uptake kinetic of the EGF targeted polyplexes was investigated more in detail within live cell imaging experiments. Images of the Cy5-pDNA polyplexes were continuously acquired by confocal microscopy, which allows the identification of internalized particles by their characteristic intracellular motion [98, 203]. Figure 3.42 B shows images of representative cells at two time points. By this means, the rapid uptake kinetic of the mEGF targeted polyplexes could be confirmed. Already after 21 minutes, intracellular polyplexes could be identified, and their number considerably

increased within the following 21 minutes. Importantly, the number of internalized polyplexes after two hours incubation time could be clearly reduced by competition with free EGF (Figure 3.42 C), which confirms the EGF specific cellular uptake via EGFR.

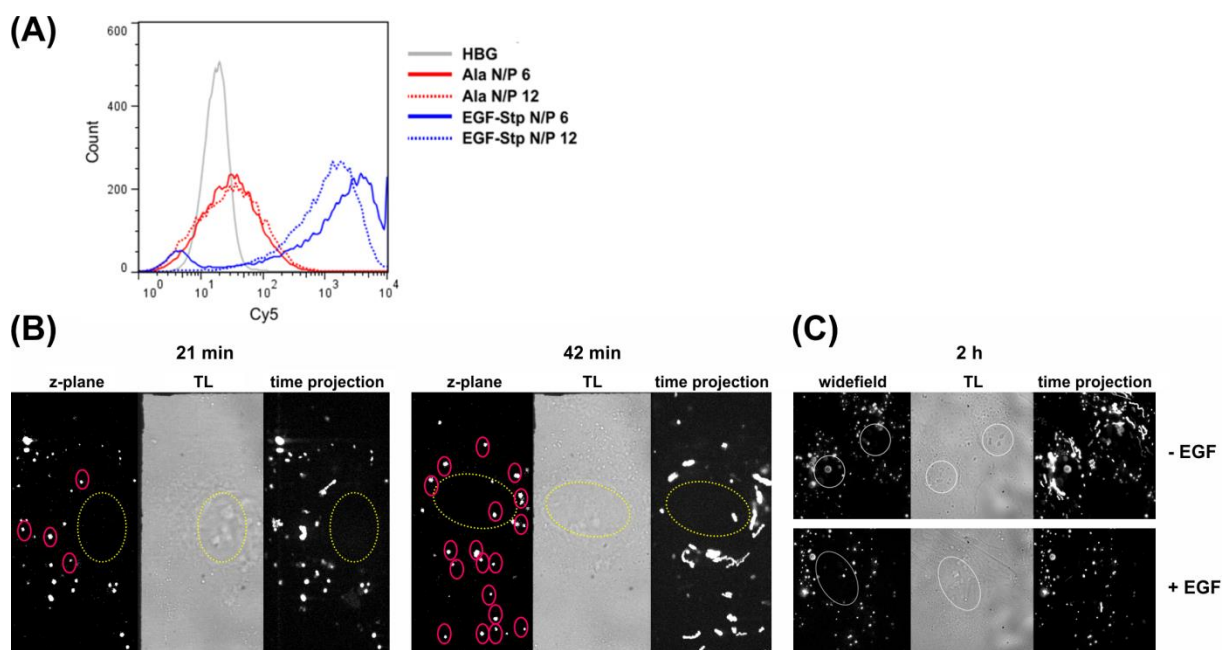


Figure 3.42 Cellular uptake of Cy5-pDNA polyplexes in Huh7 cells as determined by flow cytometry (A) and live cell imaging (B and C). (A) Comparison of the cellular uptake of mEGF targeted or untargeted Ala polyplexes at indicated N/P ratios after 30 min incubation time. (B) Internalized EGF-Stp polyplexes (N/P 12) at two time points (21 min, 42 min), identified by the characteristic intracellular motion during live cell imaging. Confocal z-planes of representative cells are shown together with the transmission light image (TL) and the time projection (100 frames, framerate 330 ms, equivalent to 33 s time interval). Nucleus is highlighted yellow, identified intracellular polyplexes are marked red. (C) Internalized EGF-Stp polyplexes (N/P 12) after 2 h incubation time and under EGF competition (+ EGF) or normal (- EGF) conditions. Flow cytometry was carried out by Dr. Petra Kos (Pharmaceutical Biotechnology, LMU). Microscopy experiments were carried out by Dr. Frauke Mickler (Physical Chemistry, LMU).

The efficient cellular uptake of EGF targeted polyplexes also correlated with the luciferase reporter gene expression after transfections of Huh7 cells (Figure 3.43). As before, the untargeted alanine control **188** did not exhibit notable gene transfer efficiency. In contrast, EGF-Stp mediated over 1000-fold increased bioluminescence above background level, also exceeding the levels of LPEI, in transfections with the addition of chloroquine.

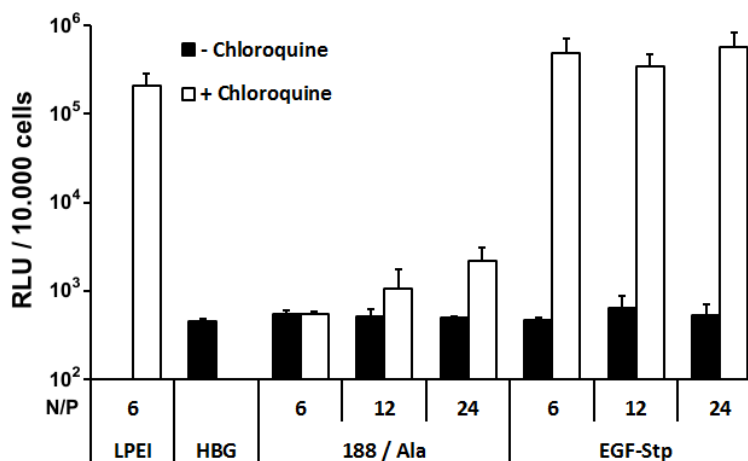


Figure 3.43 Luciferase pDNA transfections of Huh7 cells with EGF-Stp or untargeted Ala oligomers at indicated N/P ratios. Bioluminescence levels are plotted as relative light units (RLU) per 10.000 cells. N=5 for each compound. Transfections were carried out by Dr. Petra Kos (Pharmaceutical Biotechnology, LMU).

However, as observed before, the used PEGylated two-arm oligomer with continuous Stp sequence and terminal cysteines exhibits a very poor intrinsic endosomal escape performance. Without addition of chloroquine, no transgene expression could be observed. Nevertheless, the well shielded structure allows the evaluation of the potency and suitability of different targeting ligands in a clear-cut fashion *in vitro*. By this means, mEGF has shown to be a very potent ligand, which is compatible with the nucleic acid carrier class. Therefore, the rational next step in the modular optimization process would be the combination of mEGF with improved carriers, which have demonstrated a better endosomal escape performance.

3.2.3 Multivalent carbohydrate ligands for asialoglycoprotein receptor directed gene transfer by oligo(ethanamino)amides

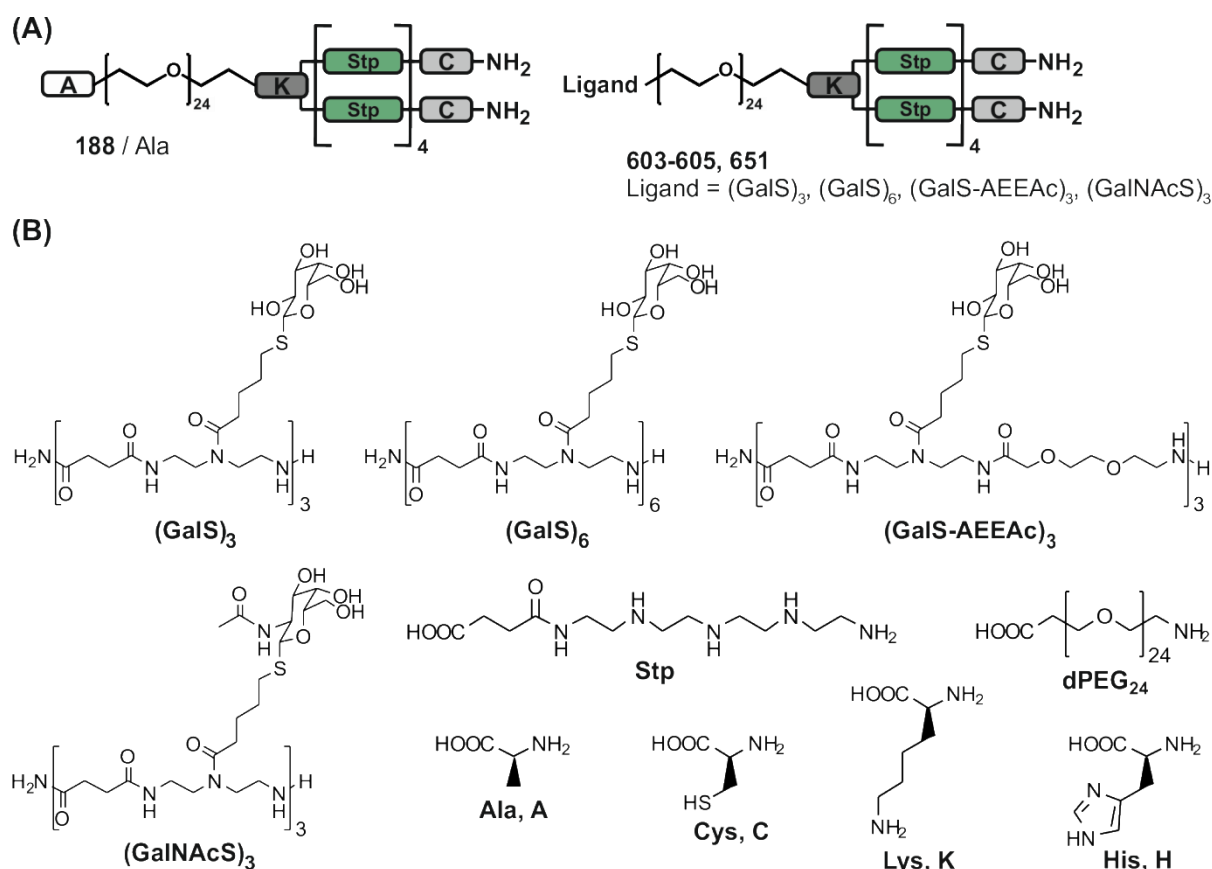
The asialoglycoprotein receptor (ASGPR) is a membrane bound lectin expressed on hepatocytes, which binds and internalizes glycoproteins with terminal galactose (Gal) or N-acetylgalactosamine (GalNAc) residues for a subsequent lysosomal processing. Therefore, the enzymatic removal of terminal sialic acids from protein glycosylation, which in consequence exposes subterminal galactose or N-acetylgalactosamine residues, represents a recognition feature for an upcoming clearance from the systemic circulation [204, 205]. The highly specific recognition, efficient cellular

uptake and exclusive expression make the ASGPR an attractive target for receptor-specific delivery of nucleic acid therapeutics to hepatocytes [95, 206-208]. However, the use of simple monosaccharides results in a rather weak binding toward the receptor. In general, the complex branched architectures of glycan ligands offer multiple sites for interactions with carbohydrate recognition domains, which are responsible for the specific binding with high affinity [209]. Therefore, multivalent carbohydrate ligands with precise distance and spatial orientation are required for high affinity binding.

Dr. Felix Wojcik from the former lab of Prof. Laura Hartmann at the MPI of Colloids and Interfaces (Potsdam, Germany) developed a synthesis procedure for the assembly of S-glycoside functionalized diethylene triamine building blocks, which can be used for a subsequent solid-phase synthesis [210, 211]. The taken approach allows the precise control over the number of exposed sugar moieties as well as their distance and spatial orientation. By this means a set of four different ligands was provided by Dr. Felix Wojcik for the use in the solid-phase synthesis of carbohydrate targeted nucleic acid carriers.

3.2.3.1 Library design and synthesis

The set of oligomers used for the study consisted of five members, which were all based on the same PEGylated oligo(ethanamino)amide backbone with continuous Stp sequence and terminal cysteines, but differed in the conjugated targeting ligand. Scheme 3.10 and Table 3.8 give an overview over the set of compounds.

Scheme 3.10 Illustration of the synthesized oligomers with multivalent carbohydrate ligands

(A) Schematic structures of the carriers. Multivalent ligands vary in the number of the repetitive ligand motif (3 or 6 β -D-thiogalactose units, GalS), the spacer length (additional monoethylene glycol derivative) and the type of integrated S-glycoside (GalS, GalNAcS), (B) chemical structures of the multivalent glyco-ligands and sequence components. The carbohydrate ligands were synthesized by Dr. Felix Wojcik (MPI of Colloids and Interfaces, Potsdam).

Table 3.8 Sequences, structure variants and abbreviations of the synthesized oligomers

ID	Sequence (C -> N)	Variant	Abbreviation
188	A-dPEG ₂₄ -K(Stp ₄ -C) ₂	neg. control targeting	Ala
603	(GalS) ₃ -dPEG ₂₄ -K(Stp ₄ -C) ₂	trivalent GalS	(GalS)3-Stp
604	(GalS) ₆ -dPEG ₂₄ -K(Stp ₄ -C) ₂	hexavalent GalS	(GalS)6-Stp
605	(GalS-AEEAc) ₃ -K(Stp ₄ -C) ₂	trivalent GalS, MEG spacer	(Gal-MEG)3-Stp
651	(GalNAcS) ₃ -dPEG ₂₄ -K(Stp ₄ -C) ₂	trivalent GalNAcS	(GalNAcS)3-Stp

The alanine analog **188** was used as untargeted control as before. Three oligomers contained β -D-thiogalactose residues (**603-605**) in different numbers (**603**, trivalent GalS; **604**, hexavalent GalS) and optionally an additional monoethylene glycol derivative for increased distance of the sugar moieties (**605**, trivalent GalS, MEG).

Oligomer **651** is the structural analog of the trivalent ligand **603** with GalNAcS instead of GalS. The ligands were synthesized by Dr. Felix Wojcik and provided in a protected and resin bound form ready for the subsequent solid-phase synthesis of the PEGylated oligo(ethanamino)amide core. With the resin bound ligands, SPS was conducted according to the sequences listed in Table 3.8 under the standard synthesis conditions. However, since the carbohydrate ligands were in a peracetylated form during the solid-phase synthesis, a deacetylation step by transesterification with sodium methoxide was introduced [182]. The deacetylation was carried out before cleavage and deprotection of the resin bound oligomers, since an acetyl transfer to the multiple amines would be possible under the chosen conditions. In addition, milder cleavage conditions, without use of water as a scavenger, were chosen to reduce any risk of acid catalyzed hydrolysis of glycosyl residues. All compounds were analyzed by $^1\text{H-NMR}$ and RP-HPLC. Figure 3.44 shows the analytical RP-HPLC chromatograms of the carbohydrate containing compounds. $^1\text{H-NMR}$ data can be found in the appendix.

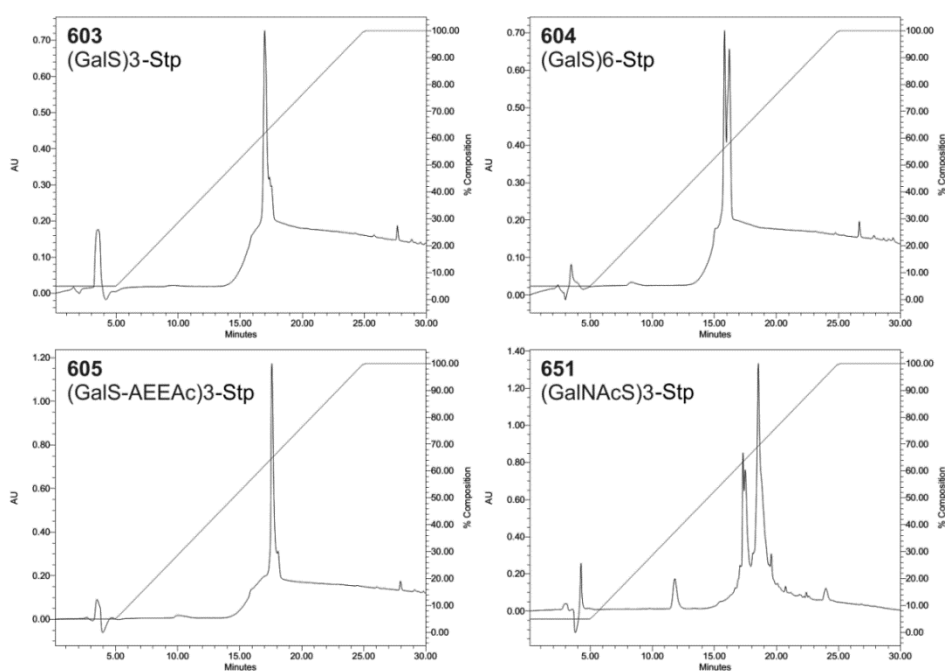


Figure 3.44 Analytical RP-HPLC chromatograms. The analysis was carried out using a Waters Sunfire C18 column (5 μm , 4.6 x 150mm) and a water/acetonitrile gradient (95:5 – 0:100 in 20 min) containing 0.1 % TFA. For the detection the extinction at 214 nm was monitored.

3.2.3.2 Cellular association and gene transfer *in vitro*

Hepatocellular Huh7 cells and prostate carcinoma DU145 cells were used for the investigation of the cellular association of GalS targeted pDNA polyplexes by flow cytometry (Figure 3.45). As before, the alanine control (**188**) did not mediate a significant cell binding to any of the chosen cell lines, indicating the efficient shielding and low unspecific interaction of the used carrier system (Figure 3.45 B). In contrast, the GalS targeted polyplexes exhibited a ligand dependent cellular association to Huh7 cells and to a considerable lower extent to the control cell line DU145, with low ASGPR expression (Figure 3.45 A). The highest binding to Huh7 cells was mediated by the two compounds **603** and **605** with trivalent GalS ligands. The additional monoethylene glycol spacer in **605** did not seem to change the affinity of the pDNA polyplexes. Surprisingly, the increase of ligand valency in the polyplexes with oligomer **604** did not enhance but rather slightly diminish the cell binding potency. It has to be noted that as a result of the rather small size of this carrier class compared to other polymers used for gene delivery, several ligand equipped oligo(ethan amino)amide molecules are integrated into the polyplexes, which already causes a kind of multivalency, even if only monovalent ligands were used during synthesis. Taken into consideration that the ASGPR can bind tri- or tetra-antennary glycans [212], this might be an explanation, why the affinity is not enhanced by an additional increase of ligand density on the surface of the polyplexes. Moreover, there are examples for nanoparticles with optimal ligand densities on the surface, which must not be under- or overrun, for a most efficient receptor-targeting [213]. However, a great improvement of cellular binding to Huh7 cells was achieved by the exchange of GalS for GalNAcS (Figure 3.46 A). In direct comparison of the two analogs **603** and **651**, an increase from 24.2 to 78.6 % Cy5 positive cells due to the substitution of the sugar moiety could be observed. This is consistent with the severalfold higher binding affinity of ASGPR for terminal GalNAc than Gal residues in comparable structures [209]. In pCMVLuc transfections of Huh7 cells the potential of the trivalent GalNAcS ligand to mediate cellular uptake of pDNA polyplexes was confirmed (Figure 3.46 B). With the addition of chloroquine as endosome disruptive agent, luciferase activity levels of up to 800-fold above background were observed. At N/P 12 and higher, expression levels in the same magnitude as mediated by LPEI were achieved.

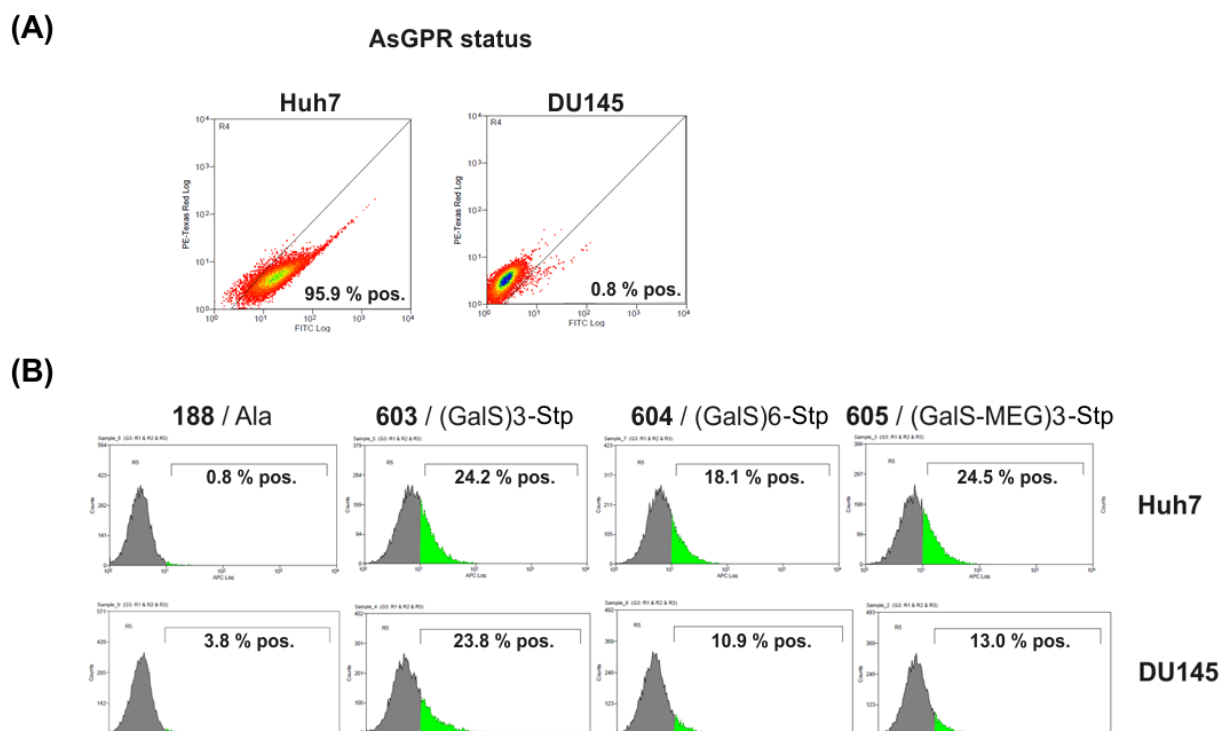


Figure 3.45 Receptor status and cellular association of Cy5-pDNA polyplexes at N/P 12 as determined by flow cytometry. (A) AsGPR expression in Huh7 and negative control DU145 cells. (B) The cellular association levels of pDNA polyplexes show a low but ligand dependent and cell-specific binding of GalS targeted polyplexes (**603-605**) to Huh7 cells. Flow cytometry was carried out by Dr. Petra Kos (Pharmaceutical Biotechnology, LMU).

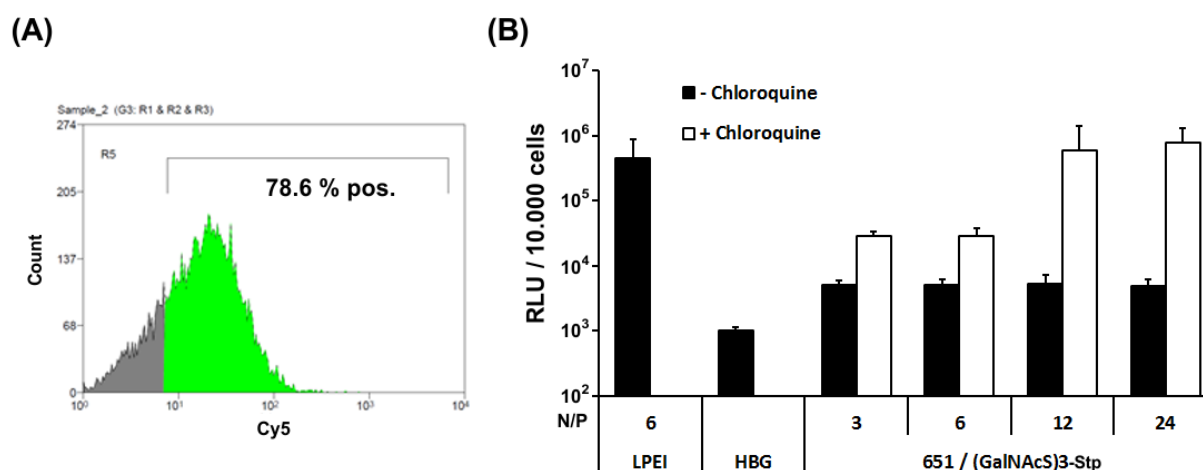


Figure 3.46 Cellular association of GalNAcS targeted polyplexes at N/P 12 to Huh7 cells and luciferase reporter gene expression after transfections. (A) The cellular association of pDNA polyplexes to Huh7 cells shows an enhancement by the trivalent GalNAcS based ligand, (B) transfection with GalNAcS containing **651** polyplexes and chloroquine addition greatly increased transgene expression levels. Bioluminescence levels are plotted as relative light units (RLU) per 10.000 cells. N=5 for each compound in the transfection experiment. Experiments were carried out by Dr. Petra Kos (Pharmaceutical Biotechnology, LMU).

In sum, the results demonstrate the feasibility to combine the carbohydrate building blocks of the collaboration partner with the nucleic acid carrier platform in one sequential solid-phase synthesis of glyco-functionalized conjugates for gene delivery. Moreover, the potential of the used carrier system to be used for the screening and comparison of related targeting ligands has been confirmed. By this means, the most potent ligand has been identified and can be used with the next generation nucleic acid carriers for hepatic gene delivery.

3.2.4 Methotrexate polyglutamates as dual-functional ligands in oligo(ethanamino)amides for cytotoxic poly(I:C) delivery

This chapter has been adapted from:

Lächelt U, Wittmann V, Müller K, Edinger D, Kos P, Höhn M and Wagner E, "Synthetic polyglutamylation of dual-functional MTX Ligands for enhanced combined cytotoxicity of poly(I:C) nanoplexes.", Mol Pharm, 2014, 11(8):2631-9.

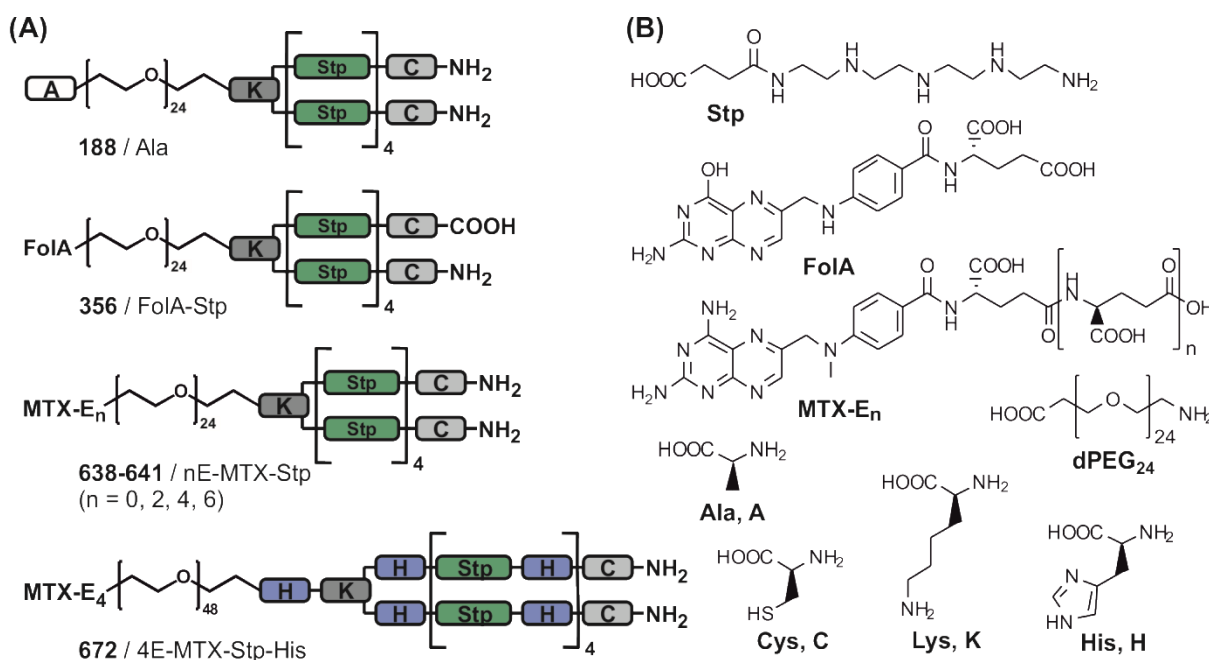
Folic acid (FolA, vitamin B₉) and the related folate derivatives play important roles as single-carbon donors in several biosynthetic cellular pathways, such as the syntheses of purine bases, of the pyrimidine nucleotide dTMP from dUMP as well as the conversion of homocysteine to methionine. Therefore, folate is required for the maintenance of several cellular processes, especially in cells with high metabolic and proliferative activity. For this reason certain types of malignant cells and activated macrophages exhibit elevated expression levels of the folate receptor (FR). Methotrexate (MTX) and other antifolate drugs are widely used medications against different types of cancer and autoimmune diseases, such as rheumatoid arthritis. The discovery of dihydrofolate reductase (DHFR) as a key target of MTX and the elucidation of the detailed mode of action made an important contribution to the current understanding of molecular tumor pharmacology and the development of chemoresistance. Low molecular weight MTX is transported into cells via the reduced folate carrier (RFC) and undergoes an intracellular conversion to poly- γ -glutamyl derivatives due to acceptance as substrate of the enzyme folylpolyglutamyl

synthetase (FPGS). Polyglutamylation is a key step in the molecular mechanism of MTX and affects the drug's activity in several ways, e.g. by evasion of efflux transport mechanisms and increased affinity toward DHFR and other target enzymes.

Since it has already been shown that folic acid is compatible with the solid-phase synthesis platform and can easily be introduced in oligo(ethanamino)amides, the chemically closely related MTX could be a promising alternative with additional therapeutic effect. MTX could serve as a dual-functional ligand in antitumoral drug delivery, inducing both FR mediated cellular uptake and intrinsic cytotoxic action. However, the bioactivity of MTX changes by conjugation, since the activity is affected by the hampered intracellular conversion to the more potent poly- γ -glutamyl derivatives. In a cancer combination therapy approach for the co-delivery of cytotoxic dsRNA polyinosinic-polycytidylic acid poly(I:C), a set of molecularly precise oligo(ethanamino)amides was synthesized, comprising polyethylene glycol conjugated MTX-ligands. The conjugates differed in the number of additional glutamic acid residues to investigate the effect of different degrees of synthetic 'a priori' polyglutamylation. In structure-activity relationship studies the bioactivity of these compounds concerning dihydrofolate reductase (DHFR) inhibition, cytotoxicity, nucleic acid binding potency, cellular uptake of poly(I:C) polyplexes and combined antifolate/poly(I:C) toxicity was investigated and correlated with the glutamylation degree.

3.2.4.1 Library design and synthesis

The polyamino acid Stp was used in combination with commercially available building blocks and α -amino acids for the solid-phase assisted assembly of the two-arm topology oligomers with PEGylation and dual-functional MTX ligands or control substitutes. Scheme 3.11 and Table 3.9 give an overview over the set of compounds used for the study. For the syntheses, the same standard Fmoc SPS conditions were used as for the PEGylated two-arm topology oligomers before.

Scheme 3.11 Illustration of the synthesized two-arm oligomers with (anti)folate ligands

(A) Schematic structures of MTX carriers with different glutamylation degrees (**639-641**), additional histidines in the backbone (**672**) and control carriers (**188**, **356**), (B) chemical structures of the sequence components.

Table 3.9 Sequences, structure variants and abbreviations of the synthesized oligomers

ID	Sequence (C → N)	Variant	Abbreviation
188	A-dPEG ₂₄ -K(Stp ₄ -C) ₂	neg. control targeting	Ala
356	C-Stp ₄ -K(Stp ₄ -C)-dPEG ₂₄ -Fola	neg. control MTX-tox.	Fola-Stp
638	K(dPEG ₂₄ -MTX)-K(Stp ₄ -C) ₂	-	MTX-Stp
639	K(dPEG ₂₄ -E ₂ -MTX)-K(Stp ₄ -C) ₂	polyglutam.	2E-MTX-Stp
640	K(dPEG ₂₄ -E ₄ -MTX)-K(Stp ₄ -C) ₂	polyglutam.	4E-MTX-Stp
641	K(dPEG ₂₄ -E ₆ -MTX)-K(Stp ₄ -C) ₂	polyglutam.	6E-MTX-Stp
672	K[(dPEG ₂₄) ₂ -E ₄ -MTX]-HK[H-(Stp-H) ₄ -C] ₂	polyglutam., His	4E-MTX-Stp-His
583	C-Stp ₄ -K(Stp ₄ -C)-dPEG ₂₄ -AlexaFluor488	fluoresc. label	AF488-Stp

MTX was attached to the exposed N-terminal part of the PEG segment in two steps: conjugation of (1) glutamic acid and (2) the pteric acid derivative. The other MTX-based ligands were varied in the number of glutamic acids incorporated additionally between PEG and MTX in the sequence. The rather untypical γ -peptide linkage (Scheme 3.11 B) of naturally occurring polyglutamates was assimilated in the oligomers by use of the proper Fmoc glutamic acid *tert*-butyl ester isomer with protected α -carboxy group. Folic acid was used as a nontoxic mono-functional targeting ligand (neg. control MTX-tox.) and alanine as a nonfunctional ligand

substitute (negative control targeting). In order to improve the efficiency of the carrier system, endosomal buffering histidines were incorporated in the basic core of a tetraglutamylated MTX conjugate to enhance endosomal release. In addition, a fluorescently labeled conjugate, carrying an Alexa Fluor 488 dye attached to the PEG segment in place of a folate ligand, was synthesized for fluorescence microscopy experiments.

All compounds were analyzed by $^1\text{H-NMR}$ and RP-HPLC. Figure 3.47 shows the analytical RP-HPLC chromatograms of the polyglutamylated MTX representatives. $^1\text{H-NMR}$ data can be found in the appendix.

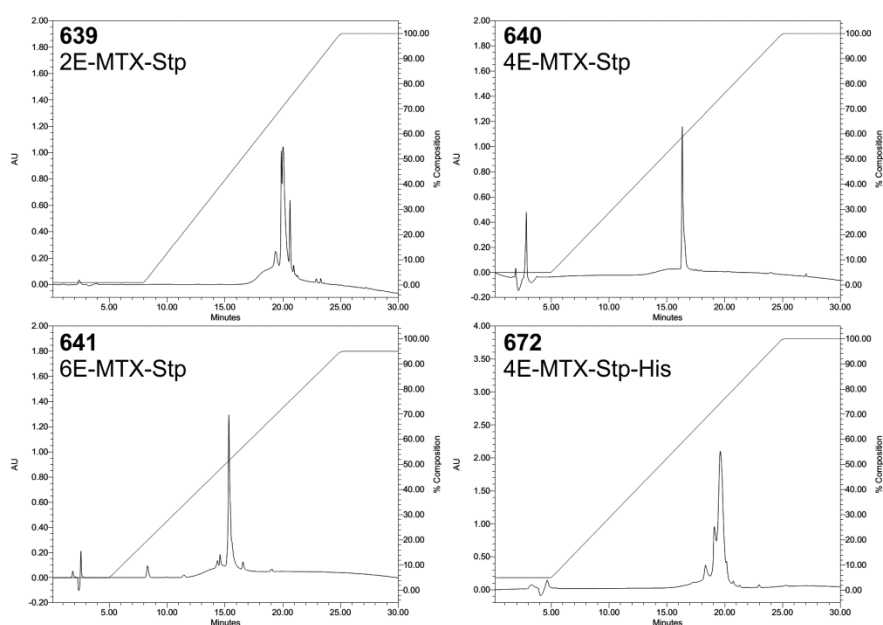


Figure 3.47 Analytical RP-HPLC chromatograms of oligomers with polyglutamylated MTX ligands. The analysis was carried out using a Waters Sunfire C18 column (5 μm , 4.6 x 150mm) and a water/acetonitrile gradient (95:5 – 0:100 in 20 min) containing 0.1 % TFA. For the detection the extinction at 214 nm was monitored.

3.2.4.2 DHFR inhibition

The inhibitory effect of MTX conjugates on human DHFR was investigated by determination of the relative DHFR activity in 100 nM solutions of the test compounds (Figure 3.48). Free MTX clearly showed stronger inhibitory effect than the corresponding conjugate **638** (MTX-Stp) without additional glutamic acid residues (95 vs. 86 % inhibition). However, the inhibitory potency of the conjugates increased significantly with increasing degree of polyglutamylation between **638** and **641** (86 vs.

89 vs. 93 vs. 98 % inhibition). The tetraglutamylated member **640/4E-MTX-Stp** showed an inhibitory effect comparable to free MTX, whereas the hexaglutamylated analog **641/6E-MTX-Stp** even outperformed the effect of free MTX. These data indicate that even in conjugated form the inhibitory potency of MTX can be enhanced by polyglutamylation.

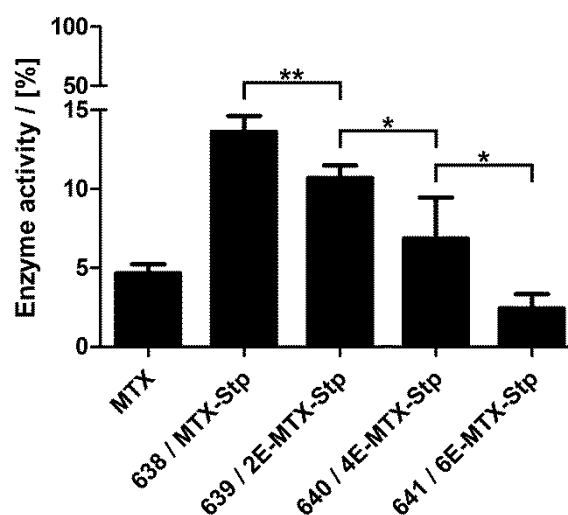


Figure 3.48 Effect of polyglutamylation on dihydrofolate reductase (DHFR) inhibition. Relative DHFR activity in 100 nM oligomer solutions was determined. A solution with 100 nM free MTX served as reference. N = 3 for each compound. Adapted from [214].

3.2.4.3 Oligomer toxicity

The toxic effect of MTX and MTX-conjugates on human cervix carcinoma KB cells was determined by MTT assay over a concentration range between 3 and 10000 nM (Figure 3.49). Based on dose-response curve fittings the half maximal effective concentration (EC_{50} , Figure 3.49 B, left scale black bars) and maximal efficacy (E_{max} = 100 % - cell viability [%], Figure 3.49 B, right scale white bars) were determined. Since the folic acid substituted control conjugate **356/FoIA-Stp** showed no notable reduction in cell viability, there is no evidence for unspecific oligomer toxicity in the investigated concentration range (Figure 3.49 A). Thus the folate conjugate seems to be an appropriate control with mono-functional ligand, serving for the purpose of targeting without intrinsic cytotoxicity (neg. control MTX-tox.). Looking at EC_{50} values, free MTX showed the highest potency in respect of the lowest EC_{50} value (5 nM). In case of the MTX conjugates, the potency seems to increase (EC_{50} values decrease)

with an increasing number of additional glutamates (EC_{50} of 195 vs. 86 vs. 82 vs. 15 nM). Most importantly, all conjugates mediated higher maximal cell killing (Figure 3.49 A and B) in the investigated concentration range than free MTX, indicating higher efficacy in the KB tumor cell line. Within the set of MTX conjugates, the hexaglutamylated variant **641** exhibited the best performance, almost reaching EC_{50} levels of free MTX.

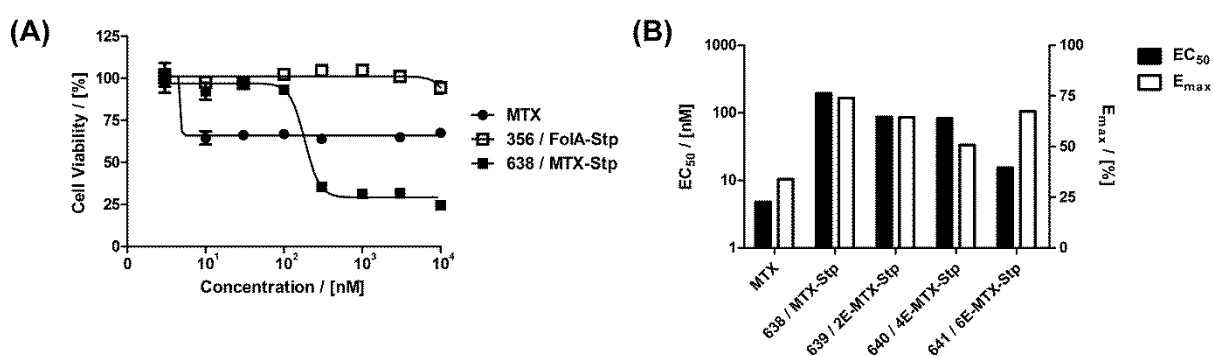


Figure 3.49 Cytotoxicity of MTX-oligomers with different polyglutamylation degree on KB cells determined by MTT assay. N=3 for each compound. (A) Dose-response curves of free MTX and conjugates **356**/FolA-Stp and **638**/MTX-Stp, (B) cytotoxicity parameters half maximal effective concentration (EC_{50} , left scale, black bars) and maximal efficacy (E_{max} = 100 % - cell viability [%], right scale, white bars) of free MTX and MTX-conjugates were calculated by approximation of the dose-response curves with four-parameter logistic models. MTT assays were carried out by Valentin Wittmann (graduate student, LMU). Adapted from [214].

3.2.4.4 Physicochemical characterization of poly(I:C) polyplexes

Poly(I:C) binding potency of the synthesized MTX conjugates at different nitrogen to phosphate (N/P) ratios was investigated in electrophoretic mobility shift assays (Figure 3.50 A). The conjugates **638-641** showed comparable binding potency with complete binding and shift of the nucleic acid band at N/P 6 and higher. Moreover, all conjugates also showed high serum stability (Figure 3.50 B). After incubation in 90 % FCS for up to 90 minutes, the majority of nucleic acid was retained within the complexes and no time-dependent destabilization at different time points could be observed. Importantly, the polyglutamylation of the MTX ligands did not affect nucleic acid binding potency of the cationic oligomer core, although additional negative charges were introduced into the structures.

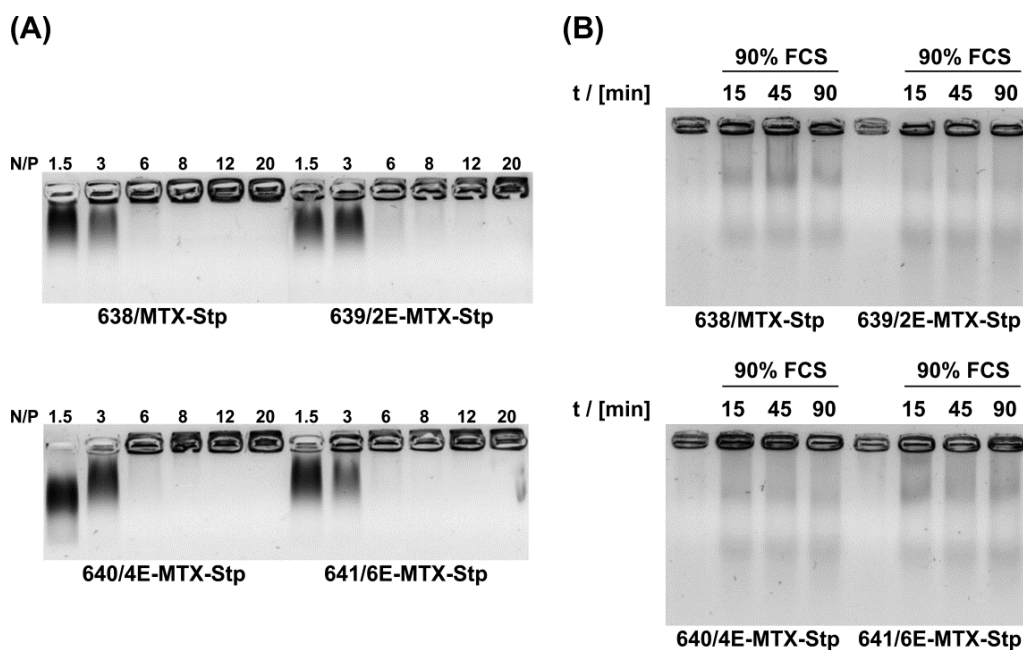


Figure 3.50 Electrophoretic mobility shift assay of poly(I:C) polyplexes with MTX-oligo(ethanamino)amide conjugates. All samples contained 800 ng poly(I:C). (A) Poly(I:C) polyplexes at different N/P ratios, (B) poly(I:C) polyplexes at N/P 20 incubated in fetal calf serum (FCS) for indicated times. Adapted from [214].

The hydrodynamic diameter and zeta potential of poly(I:C) and poly(I) polyplexes were determined by dynamic and electrophoretic light scattering (Figure 3.51). The MTX oligomers formed poly(I:C) polyplexes with Z-average diameters between 439.2 nm (**640/4E-MTX-Stp**) and 640.3 nm (**641/6E-MTX-Stp**) (Figure 3.51 A) and zeta potentials between 6.0 mV (**640/4E-MTX-Stp**) and 8.7 mV (**641/6E-MTX-Stp**). With poly(I), polyplexes in the range of 525.9 (**638/MTX-Stp**) to 688.3 nm (**640/4E-MTX-Stp**) and with zeta potentials between 5.2 (**640/4E-MTX-Stp**) and 9.2 mV (**638/MTX-Stp**) (Figure 3.51 B) were formed. However, in all cases the variation of the hydrodynamic diameters and zeta potentials was rather low. Therefore, neither the degree of polyglutamylation nor the type of nucleic acid used for polyplex formation showed a notable impact on the physicochemical parameters. These findings are of particular importance, since in subsequent cell culture experiments the influence of different glutamylation degrees as well as the effect of cytotoxic poly(I:C) and the nontoxic poly(I) control were compared.

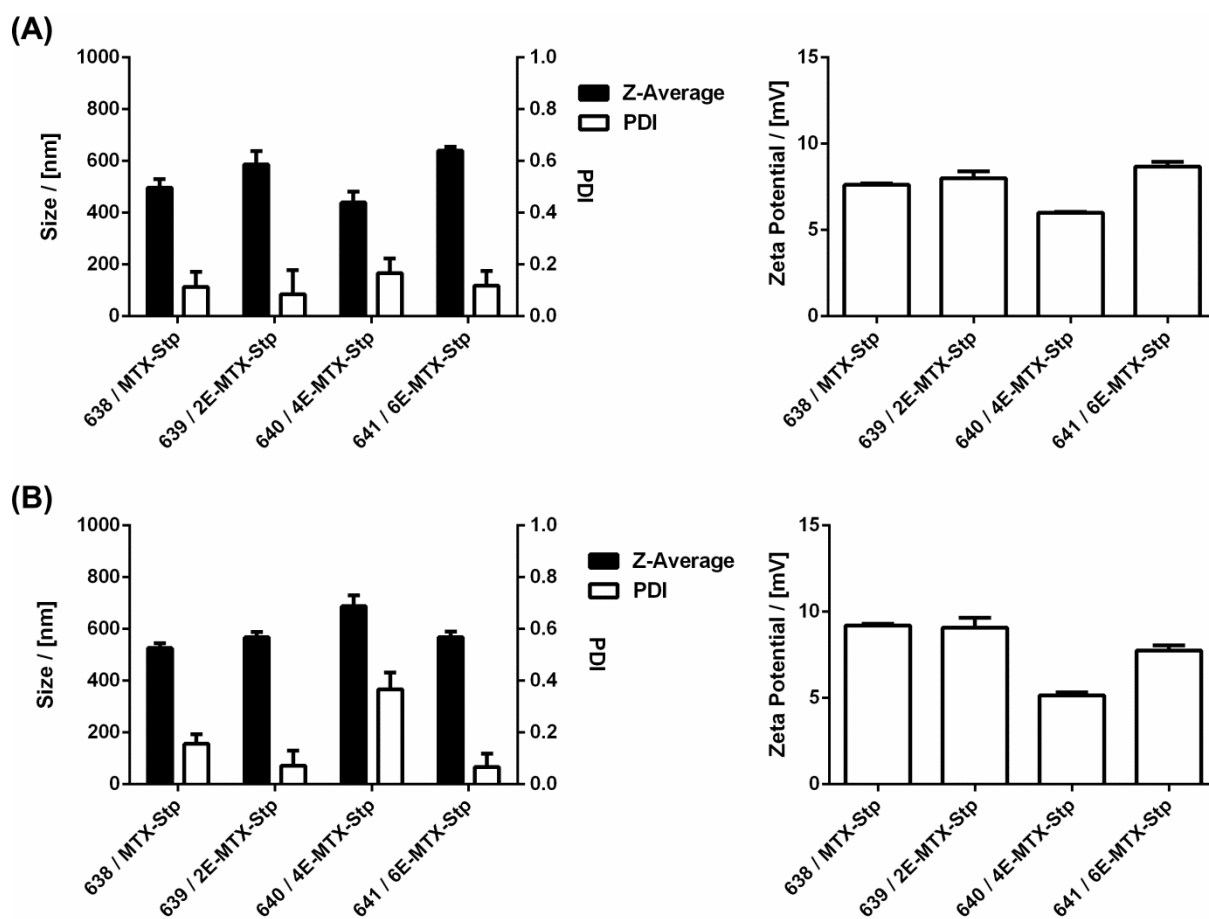


Figure 3.51 Size parameters and Zeta potentials of polyplexes as determined by dynamic and electrophoretic light scattering. (A) Z-averages, PDI values and zeta potentials of poly(l:C) polyplexes at N/P 10, (B) Z-averages, PDI values and zeta potentials of poly(l) polyplexes at N/P 10. Polyplexes contained 10 μ g of nucleic acids. N=3 for each compound.

3.2.4.5 Cellular uptake of poly(l:C) polyplexes

Cellular uptake of poly(l:C) polyplexes in folic acid receptor (FR) expressing KB cells was investigated by flow cytometry (Figure 3.52 A and B) and confocal microscopy (Figure 3.52 C). The alanine substituted control **188**/Ala did not mediate strong cellular uptake (< 4 % pos. cells), indicating good nanoparticle shielding by the incorporated PEG segment and absence of unspecific cellular interactions also in case of poly(l:C) polyplexes. In contrast, the analog folic acid **356** polyplexes exhibited remarkable high levels of cellular uptake (> 90 %) confirming the high potency of folate as a targeting ligand. In case of the MTX conjugate **638**/MTX-Stp the majority of cells (approx. 60 %) was Cy5 fluorescence positive, however the high level of **356** was not reached. Looking at the MTX conjugates side-by-side,

polyglutamylation seems to enhance cellular uptake, with the tetraglutamylated analog **640**/4E-MTX-Stp being the most potent candidate. Since the folic acid analog **356** and the tetraglutamyl-MTX conjugate **640** exhibited highest potency of cellular uptake induction, both were challenged under folic acid competition conditions (Figure 3.52 B). In folic acid saturated medium the cellular uptake of the tetraglutamylated MTX conjugate **640** was suppressed to a value below 6 %, whereas cellular uptake of the folic acid analog **356** still reached levels of over 20 % positive cells.

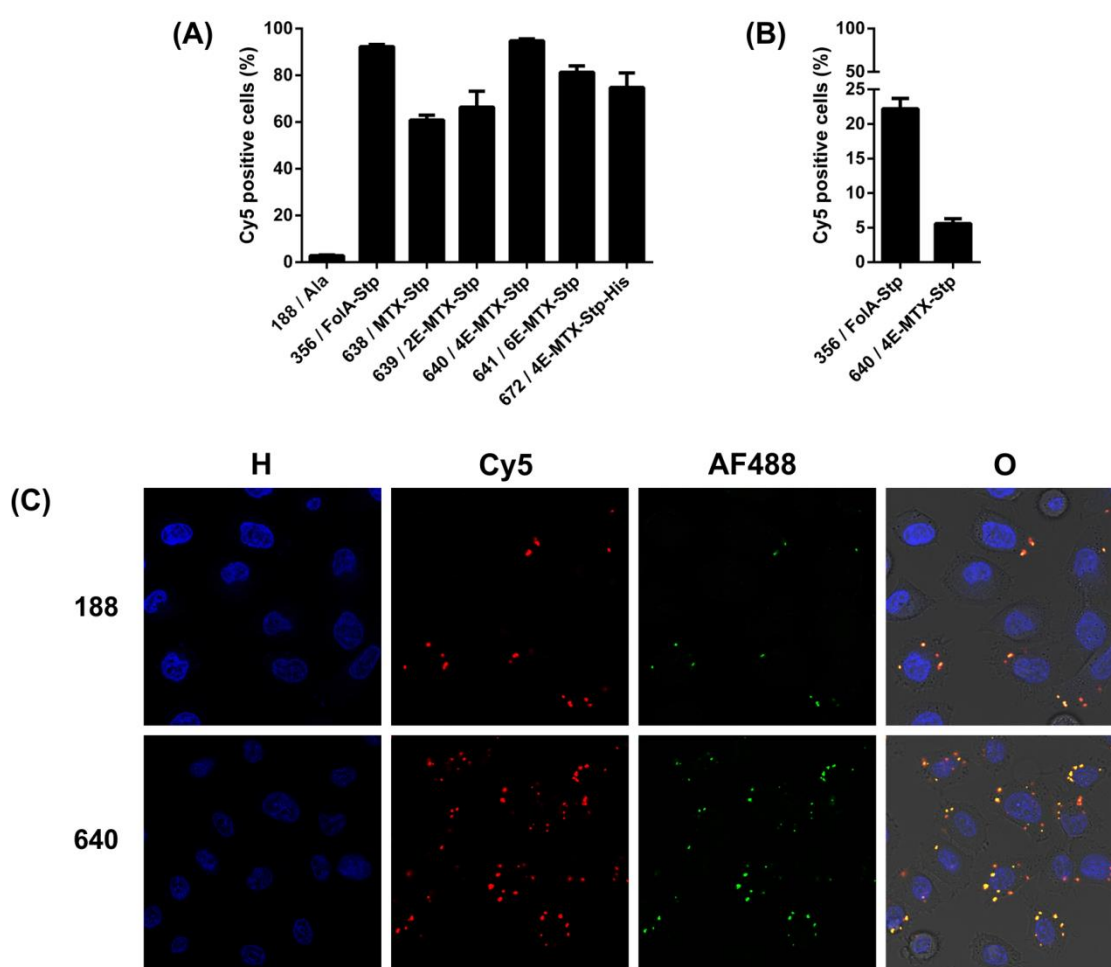


Figure 3.52 Cellular uptake of Cy5-poly(I:C) polyplexes in KB cells as determined by flow cytometry (A and B) and visualized by confocal microscopy (C). (A) Cellular uptake levels in folate free culture medium and (B) folic acid saturated culture medium. (C) Intracellular distribution of poly(I:C) polyplexes acquired by confocal laser scanning microscopy. Nuclei were stained with Hoechst 33342 (H). Poly(I:C) was spiked with 20 % Cy5 labeled poly(I:C). Polyplexes of oligomers **188** (Ala) and **640** (4E-MTX-Stp) were spiked with 20 % Alexa Fluor 488 (AF488) labeled oligomer **583**. Flow cytometry experiments were carried out by Valentin Wittmann (graduate student, LMU), microscopy experiments were carried out by Katharina Müller and Miriam Höhn (Pharmaceutical Biotechnology, LMU). Adapted from [214].

This finding is consistent with the reported higher affinity of folic acid to FR compared to MTX. However, the uptake of MTX targeted polyplexes seems to be tunable by polyglutamylation. The intracellular distribution of internalized poly(I:C) polyplexes of conjugate **180** and **640** was investigated by confocal laser scanning microscopy (Figure 3.52 C). Both the nucleic acids and conjugates were spiked with fluorescently labeled analogs to investigate the colocalization of the oligomers and the nucleic acids. The acquired images confirm the higher cellular uptake of the MTX-targeted polyplexes and the assumed colocalization of both therapeutic entities, conjugates and poly(I:C), in the combination therapy approach.

3.2.4.6 Poly(I:C) transfections

The combined cytotoxicity of MTX ligands and co-delivered poly(I:C) was investigated in transfections of KB cells and subsequent MTT assays (Figure 3.53). Poly(I) served as a nontoxic control nucleic acid for the differentiation between MTX and combined MTX/poly(I:C) mediated toxicity. The untargeted alanine control **188/Ala** showed neither oligomer or ligand mediated nor poly(I:C) triggered reduction of cell viability, in accordance with the previously shown extremely low cellular uptake of the untargeted polyplexes (cf. Figure 3.52 A) and the absence of unspecific oligomer cytotoxicity in the investigated concentration range. Although the folic acid conjugate **356** mediated the highest uptake levels of poly(I:C) polyplexes, within the transfections only a slight poly(I:C) mediated toxic effect could be observed at the highest N/P value. Moreover, the addition of free MTX in equimolar amounts compared to **356** only had a moderate additional effect on the poly(I:C) independent toxicity. In contrast, all MTX conjugates showed both more effective ligand and poly(I:C) mediated cell killing. The degree of glutamylation only marginally affected cell viability within poly(I) transfections, indicating that polyglutamylation does not seem to have a big impact on the exclusive ligand-toxicity of the polyplexes. However, in poly(I:C) transfections, a pronounced effect of polyglutamylation could be observed. The combined MTX/poly(I:C) mediated cell killing clearly increased with increasing glutamylation. Especially at lower N/P ratios, the additional poly(I:C) effects in transfections with polyglutamylated isoforms became apparent. Conjugate **672/4E-MTX-Stp-His** with additional histidine modifications in the cationic core showed both most effective ligand and combined ligand/poly(I:C) mediated

cytotoxicity (> 95 % killing). Obviously, an enhanced buffering in the endosomal pH range is also beneficial in context of poly(I:C) polyplexes and causes an additional boost of the combined antitumor activity, as both MTX and poly(I:C) pharmacologically act in the cytoplasm.

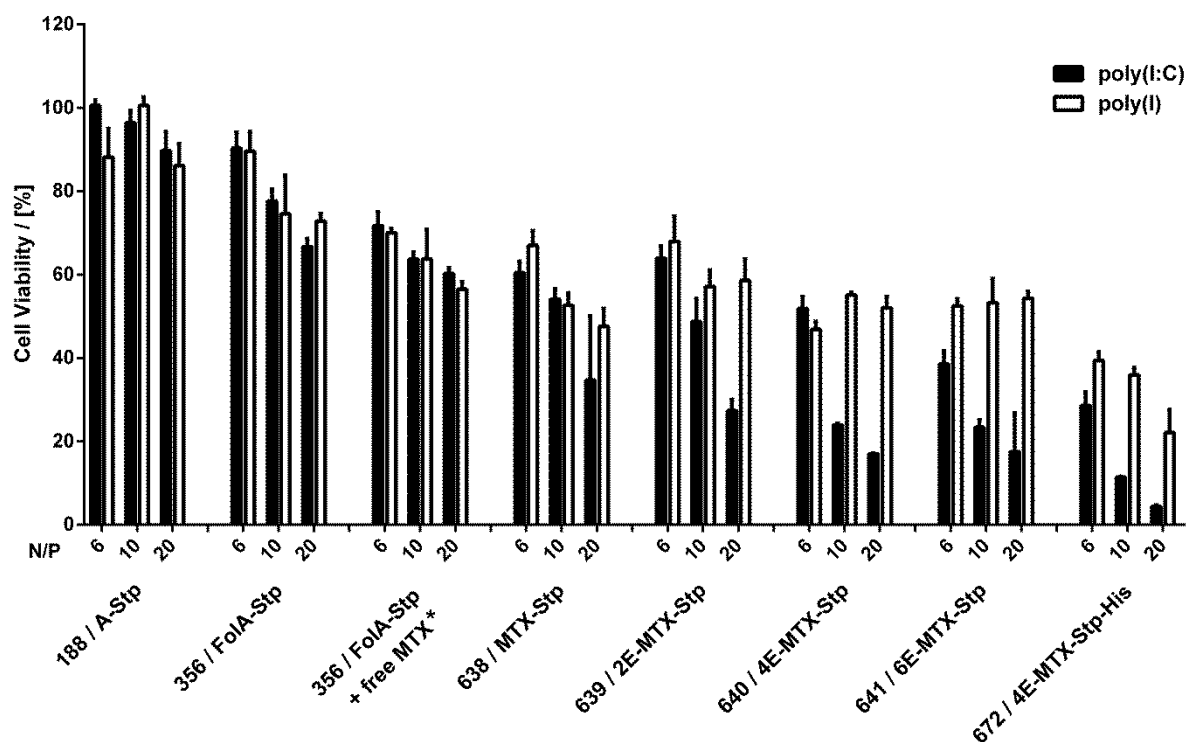


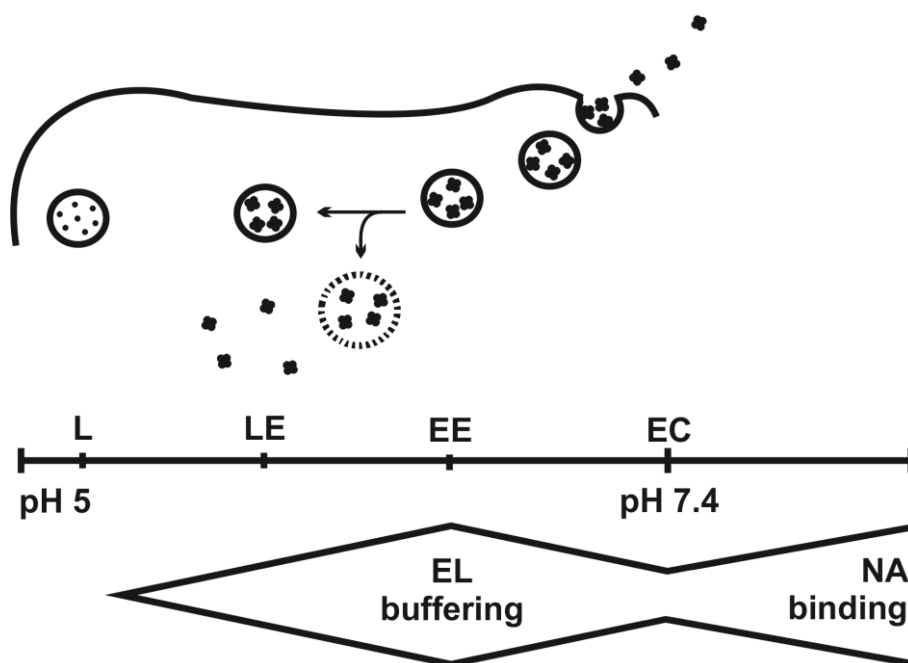
Figure 3.53 Cell viability of KB cells after transfections with poly(I:C) polyplexes at indicated N/P ratios determined by MTT assay. N=3 for each compound. *Free MTX was added in equimolar concentrations compared to **356** at the indicated N/P values. Transfections were carried out by Valentin Wittmann (graduate student, LMU) and Katharina Müller (Pharmaceutical Biotechnology, LMU). Adapted from [214].

4 Discussion

4.1 The modulation of proton-sponge activity in oligo(ethanamino)amides

In the transfection process, polymer-based pDNA complexes (polyplexes) [60] are taken up into cells by endocytic routes and thus are exposed to a varying range of different pH values (Scheme 4.1). Opposing requirements have to be considered: on the one hand, polymer basicity provides sufficient positive charges for stabilization of polyelectrolyte nucleic acid complexes at extracellular neutral pH; on the other hand, lower basicity with a shift of pK_a values toward the endosomal acidic pH generates carriers with proton-sponge character. In this respect, endosomal cationization and subsequent membrane destabilization was proposed as mechanism for endosomal escape and a most critical step for the delivery process [55, 130, 136, 215].

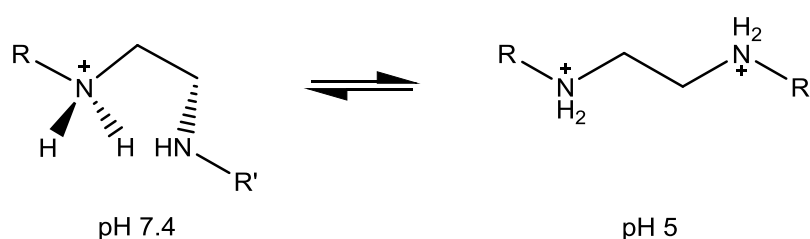
Scheme 4.1 The pH range within the delivery pathway of polymeric transfecting agents



EC, extracellular space; EE, early endosomes; LE, late endosomes; L, lysosomes; NA: nucleic acid, EL: endo-lysosomes. Adapted from [183].

Therefore, different basicities have to be combined in order to meet the requirements of stable nucleic acid (NA) binding and endo-lysosomal (EL) buffering. The titration curves of PLL, PLR and PLH (Figure 3.1) illustrate that each of these polymers only covers a narrow buffering range as a result of its distinct pK_a value and therefore does not strike a balance between high basicity for nucleic acid complexation and an additional endosomal buffer capacity. PLL for instance represents an excellent nucleic acid binder, which mediates cellular uptake of DNA, however fails in gene transfer due to its lack of endosomolytic potency [132, 148]. In contrast, PLH provides enormous endosomal buffer capacity, but insufficient nucleic acid binding at neutral pH [132]. Therefore, several approaches for the combination of the advantages of both polymers have been undertaken, such as histidylation of PLL [132, 216], amination of PLH [217], PLH-graft-PLL copolymers [218] or artificial histidine-lysine peptides [133]. In contrast to the basic polymers with distinct pK_a values, PEI represents an ideal compromise between high basicity for pDNA binding and an additional endosomal buffer capacity, which explains its reputation as highly efficient pDNA transfecting agent. The homogeneous buffering of PEI is based on the repetitive diaminoethane motif, which allows the interaction of neighboring amines (cf. Figure 3.2, 1,2-DAE). The electronic and sterical hindrance by a neighboring protonated group causes a shift of the pK_a toward lower pH, which makes diaminoethanes a beneficial motif for transfecting agents (Scheme 4.2).

Scheme 4.2 Sequential protonation of the diaminoethane motif (adapted from [55] and [219])



In the oligo(ethanamino)amides based on the artificial polyamino acids (Gtt, Stp, Gtp, Sph) the homogeneous repetitive diaminoethane motif of PEI is dissected into a defined number of molecularly precise subunits. Depending on the used polyamino acid building block, these subunits provide two, three or four protonatable diaminoethane nitrogens (at internal positions of the sequence). It turned out that the type of building block and thus the number of protonatable amines within the

In case of even-numbered polyamine units (Gtt, Sph) the protonation state at pH 7.4 offers unprotonated amines with one protonated nitrogen in proximity, which can be protonated in the range down to pH 5. Therefore, different protonation states exist at pH 7.4 and pH 5. In contrast, the alternating distribution of protonated amines at pH 7.4 in the odd-numbered compounds (Stp, Gtp) results in the proximity of two neighboring protonated nitrogens to the unprotonated amines. The subsequent protonation is strongly hindered, since an unfavorable state with three neighboring charged amines is generated and therefore does not occur above pH 5. In consequence, two out of three protonatable Stp (or Gtp) nitrogens are strong bases with highly probable protonation above 7.4, whereas the third is a too weak base to be biologically active. These findings made for oligomers with bis-acylated polyamine units is consistent with the titrations of bare polyamines (cf. Figure 3.3 and 3.4) and their reported pK_a values at the different protonation states [220]. Moreover, Uchida et al. observed an analog odd-even protonation behavior of side chain aminoethylene repeats in N-substituted polyaspartamides used for nucleic acid delivery [65, 221]. Interestingly, opposing effects were found in pDNA and mRNA transfections with these compounds. While an even number of protonatable amines in the side chains was beneficial for pDNA transfections, an odd number mediated sustained mRNA expression. Obviously for mRNA, which is readily degraded in the cytosol, intracellular stability is an additional limiting parameter. In consequence of the lower endosomal buffer capacity, the aminoethylene units with an odd number of protonatable amines exhibit higher charge density at neutral pH, form more stable complexes with mRNA and presumably increase the cytosolic stability. However, for the delivery of pDNA with much higher stability the most critical intracellular step is represented by the endosomal escape and a tuned buffer capacity is favorable.

By integration of histidine into the sequence of oligo(ethanamino)amides the total endosomal buffer capacity can be increased. Depending on the integrated polyamino acid building block (Gtt, Stp/Gtp, Sph), the influence is of greater or lesser extent; in case of low-buffering Stp the effect is most pronounced. Importantly, the increased buffer capacity is caused by a distinctly enhanced protonation around pH 6 in the medium range of the endolysosomal pathway. In all cases the gene transfer efficiency *in vitro* was greatly enhanced by histidylation, independent of the evaluated oligomer topology (four arm structures, PEGylated and un-PEGylated two-arm

structures). In case of PEGylated polyplexes with exclusively ligand dependent cellular uptake, the effect of histidylation could be put down to an improved endosomal escape. The confocal imaging of cells, transfected with histidylated polyplexes, showed a remarkable release of fluorescent calcein from endosomal vesicles into the cytosol, which correlated with an enhanced gene transfer efficiency of the carriers (Figure 3.16 and 3.38). The beneficial effect of histidine incorporation on *in vitro* transfections was also observed in the *in vivo* situation. After the intravenous injection of pDNA polyplexes, a four-arm topology histidine containing oligomer mediated over 30-fold improved transgene expression (approx. 20000-fold above background) in the tumor tissue of Neuro2A tumor bearing mice, compared to its histidine lacking analog.

However, as mentioned before, the endosomal buffer capacity only in part correlates with overall transfection performance. For the rather small oligocations, nucleic acid binding and polyplex stability is a significant parameter and possible bottleneck in transfections. In four-arm oligomers with the Gtt building block (two protonatable amines), which offers the highest buffer capacity, the introduction of stabilizing terminal cysteines has a much higher impact on the transgene expression than histidylation. Nevertheless, also in high-buffering Gtt oligomers the integration of histidine improves gene transfer, although the effect on the total endosomal buffer capacity is minor. Here the redistribution of the endosomal protonation, mediated by histidine, seems to play a role. Gtt is predominantly protonated in the lower range of the endosomal pH, whereas histidine enhances the buffering in the medium ranges around pH 6, which rather represents the pH of early than late endo- or lysosomes [222]. The buffering at an early stage after cellular entry seems to be favorable for the gene transfer. This also explains that the combination of Gtp (three protonatable amines) with Gtt (two protonatable amines), which allowed the gradual adjustment of the buffer capacity between pH 5 and 7.4, failed in pDNA transfections. The use of pyridyl amino acids with lower basicity than histidine did not have a positive effect on endosomal escape either, whereas the analog with histidine mediated remarkable levels of transgene expression. This is consistent with the observation of Funhoff et al. that a basic poly(methacrylate) derivative combining two pK_a values of 9 and 5 condensed DNA into small particles, offered buffer capacity between pH 5 and 7, but failed in gene transfer due to a lack of endosomal escape [138]. The authors

concluded that the validity of the proton-sponge hypothesis was questioned, since the high buffer capacity was no predictor for successful endosomal escape. However, based on the presented data, the definition of the buffer capacity, which is considered beneficial for the endosomal escape, should rather be revisited. It is assumed that only an increase of buffer capacity in the high to medium endosomal pH ranges, representing an early stage of the intracellular delivery pathway (cf. Scheme 4.1), mediates proton-sponge activity in terms of endosomal polyplex release and basic groups with a pK_a below 6 do not seem to be suitable for this purpose. The attempt to introduce an additional buffering nitrogen into the polyamino acid building blocks by using iminodiacetic acid derivatives as dicarboxylic acid part, unfortunately did not result in oligomers with improved protonation characteristics. However, the described synthesis shows a possibility for the introduction of new functionalities into the building blocks without modifying the nucleic acid binding polyamine motif, which might be a useful approach for future developments.

4.2 Targeted and shielded oligo(ethanamino)amides for receptor-specific nucleic acid delivery

The biodistribution and tissue specific delivery of nucleic acids plays an important role for an intended use in cancer therapy. Although in an *in vivo* mouse model a predominant transgene expression in the tumor could be achieved by passive targeting of pDNA polyplexes based on four-arm oligo(ethanamino)amides (cf. Figure 3.12), shielding and active targeting of the nanoparticles are requirements for a smart and adjustable delivery. The solid-phase synthesis using artificial polyamino acids together with α -amino acids and commercially available building blocks allows the assembly of multifunction nucleic acid carriers in a modular fashion. Diverse topologies can be generated and different (chemically or biologically) functional groups can precisely be positioned within the structures. To demonstrate the flexibility of the nucleic acid carrier platform in terms of the compatibility with targeting ligands of different chemical nature, several PEGylated two-arm oligo(ethanamino)amides were assembled. Peptides (B6, cMBP1, cMBP2), a protein (mEGF), carbohydrates (thiogalactose, thio-N-acetylgalactosamine) and small molecules (FolA, MTX) were used as ligands and evaluated for their individual

potency. The studies mostly focused on the screening and evaluation of the targeting ligands as one aspect of a modular optimization process. In selected cases (B6, Fola, cMBP2, MTX) histidylated carriers were additionally used to demonstrate the potential of an optimized ligand/carrier combination.

The peptidic ligands cMBP1 and cMBP2 were readily integrated in the sequence of the PEGylated nucleic acid carriers. Several important findings could be made within the study. First, the nucleic acid carrier platform has demonstrated its potential for the screening and comparison of different targeting ligands. Because of the very efficient shielding due to an appropriate PEGylation, without targeting ligand no considerable interaction, in terms of cell binding or gene transfer, could be observed. Therefore, the activity of the targeted oligomers is strictly ligand dependent. By this means, the more potent c-Met binding peptide cMBP2 was identified. Moreover, the comparison with scrambled sequences in similar carrier structures confirmed the sequence-specificity of cMBP2. Second, the enhancing effect of buffering histidines on endosomal escape could be reconfirmed. Similar as found for the ligands B6 and Fola, histidylation greatly improved the endosomal escape of cMBP2 targeted pDNA polyplexes, as shown by the intracellular calcein release out of endosomes, as well as the enhanced gene transfer efficiency. Importantly, the ligand dependent cellular association and gene transfer was not affected by the presence of histidine in the oligomer backbone. This demonstrates that a separate optimization of different modules, such as ligand, PEGylation or oligomer backbone, is possible with the nucleic acid carrier class. The potential of the identified optimal ligand/carrier combination resulted in the significantly ligand dependent transgene expression *in vivo* after intratumoral injection in the Huh7 xenograft mouse model. For the successful gene delivery to the tumor after systemic administration, a new polyplex formulation procedure with the use of an untargeted Stp-histidine co-formulation oligomer had to be developed. The better compaction of these co-formulation polyplexes resulted in the ligand dependent and tumor-specific transgene expression, which confirmed the tumor homing potential of the cMBP2 ligand as well as the suitability of the used nucleic acid carrier class to mediate targeted gene transfer *in vivo*.

Murine epidermal growth factor (mEGF) was used as a model protein for the conjugation with a PEGylated two-arm oligomer. The strain-promoted alkyne-azide

cycloaddition (SPAAC) allowed the site-specific attachment of the DBCO-functionalized protein at the exposed part of the PEG segment in solution and demonstrated its suitability for the conjugation of targeting ligands, which cannot be integrated during the solid-phase synthesis. It is expected that other proteins can also be coupled to the carriers using the same chemistry. However, the purification procedure presumably has to be adjusted to the individual properties, size and molecular weight of the protein. In case of mEGF, size-exclusion chromatography was suitable to isolate the conjugation product. Importantly, the EGF conjugated oligo(ethanamino)amide retained its nucleic acid binding potency, which had to be verified, since with increasing size of the targeting ligand a sterical hindrance of the relatively small oligocationic core can be expected. The investigations by flow cytometry and live cell imaging revealed a notably fast and efficient cellular uptake of the mEGF-targeted pDNA polyplexes into EGFR expressing Huh7 cells. Likewise observations have been made with EGF-PEI conjugates before. De Bruin et al. reported in detailed kinetic studies that the cellular uptake of EGF targeted polyplexes was strongly accelerated and much more efficient compared to the unmodified PEI polyplexes [83]. In subsequent studies the enhancing effect of EGF could be explained by the activation of EGFR signaling, which triggers a rapid internalization into clathrin-coated vesicles [98, 223]. The EGF-Stp conjugate also showed the potential to mediate transgene expression, however so far only with use of chloroquine as endosomolytic agent.

The synthesis of oligomers with carbohydrate ligands demonstrated the feasibility to combine the carbohydrate building blocks provided by the group of Prof. Hartmann with the nucleic acid carrier platform in one sequential solid-phase synthesis of glyco-functionalized conjugates for gene delivery. The ligand dependent cellular interaction of the PEGylated two-arm oligomers allowed the comparison of the individual ligand potencies and the identification of the most potent candidate. The three multivalent GalS ligands mediated a cell-specific but relatively low cell binding to Huh7 cells. The ligand density and spatial arrangement, modulated by the number of sugar moieties and the introduction of a spacer molecule, did not influence the affinity. However, the GalNAcS ligand mediated strong cell binding and notable transgene expression in transfections with chloroquine. The strong enhancement of ligand potency due to the substitution of GalS by GalNAcS residues correlates with the sugar preference of the

AsGPR, since its affinity for GalNAc is approximately 50-fold higher than for Gal [224, 225]. In combination with an improved nucleic acid carrier, the trivalent GalNAcS ligand is expected to be a potent module for hepatic gene delivery.

The small-molecular drug MTX, which was used in oligo(ethanamino)amide conjugates, takes an exceptional position among the presented targeting ligands, since it served for both folate receptor mediated cellular uptake and an intracellular pharmacologic action. In a combination therapy approach, the assembled oligocationic MTX conjugates were used for the co-delivery of pharmacologically active antifolate ligands and the cytotoxic double-stranded RNA poly(I:C). Combination chemotherapy represents a routine modality in today's cancer treatment. Several combination regimens are established first-line tumor pharmacotherapy in a variety of different malignancies. Motivation for the administration of multiple therapeutics is the fact that different mechanisms of action can trigger additive or even synergistic antitumor effects and evade drug resistance mechanisms [226, 227]. On the one hand this implies the use of drug combinations for hitting different cellular subpopulations in heterogeneous tumors [228], on the other hand hitting different targets within single cells simultaneously, which are supposed to contribute to an enhanced final outcome, e.g. by "crossing the threshold" [229] of triggering tumor cell death. However, the latter strategy requires co-presence of the different agents in the same cell at the same time, which might be problematic in the case of differing pharmacokinetic properties or cellular uptake mechanisms. Since in the presented approach each of both pharmacological entities, MTX and poly(I:C), represents an essential part of the resulting nanoparticles, the spatiotemporal cellular co-delivery can be achieved. However, in contrast to low molecular weight (LMW) MTX, the conjugated γ -carboxamides cannot be metabolically converted in the cytosol into the more active MTX-polyglutamates. Therefore, a synthetic 'a priori' polyglutamylation approach was designed and evaluated. Enhancing effects of synthetic polyglutamylation could be observed in several stages of combined MTX/poly(I:C) activity. A polyglutamylation-degree dependent improvement of DHFR inhibition, as well as increased cytotoxic potency of the conjugates, were observed. The integration of six additional glutamic acid residues caused an almost 13-fold reduction of the EC_{50} value. Although free MTX exhibited the lowest EC_{50} value (5 nM), its potency could be approached by the

hexaglutamylated MTX conjugate (15 nM). This is considered to be a remarkable result for the comparison between a monovalent irreversible MTX conjugate and its native counterpart, which intracellularly gets converted into MTX-polyglutamates. Notably all synthetic MTX conjugates mediated higher maximal cell killing than free LMW MTX. An altered cellular uptake route and potentially evaded efflux mechanisms of the high molecular weight conjugates are considered as possible reasons, which deserve closer attention in future investigations.

The specificity and ligand dependency of the poly(I:C) polyplex uptake into KB cells was shown in two ways. First, the alanine conjugate control sequence **188** lacking any targeting ligand failed in mediating any significant uptake of poly(I:C) polyplexes. Second, co-incubation with free folic acid significantly decreased the cellular uptake levels of both the folate targeted **356** (FolA-Stp) and the tetraglutamylated MTX analogue **640** (4E-MTX-Stp) polyplexes, indicating a folic acid uptake route for both conjugates. Under the folic acid competition conditions the folate conjugate clearly showed higher receptor affinity, which correlates with the much higher FR α affinity for folic acid ($K_d \approx 10$ pM, determined by isothermal titration calorimetry) than for MTX ($K_d \approx 65$ nM, determined by isothermal titration calorimetry) [230]. It is of interest to note that the cellular uptake of MTX polyplexes also showed some dependence on the glutamylation degree, since all polyglutamylated isoforms were superior to the simple MTX conjugate **638** (MTX-Stp). Obviously, in the context of macromolecular MTX γ -carboxy-PEG conjugates, a polyglutamyl chain is favorable over direct PEG attachment without any spacer. The tetraglutamylated conjugate **640** even mediated higher cellular uptake levels of polyplexes than the folate targeted analog, in absence of free folic acid. The remarkably high uptake levels, mediated by the polyglutamylated MTX conjugates, depict the possible use of antifolates as efficient ligands for targeting FR, which is overexpressed in several human cancers [231, 232], due to multivalency on the nanoplex surface [100, 233] and ligand modulation.

At the stage of combined MTX/poly(I:C) toxicity in transfections of KB cells, two important observations were made. First, and in sharp contrast to previous experience with targeted polyethylenimine (PEI) conjugates [39, 89], the new class of well biocompatible sequence-defined oligomers mediated specific poly(I:C) cytotoxicity to a considerable extent only in combination with the cytotoxic MTX ligands. The analogous folate ligand containing oligomer **356**, despite higher uptake

efficiency, did not induce significant poly(I:C) cytotoxicity even when additional free MTX was present during the transfections. Second, the degree of polyglutamylation not only increased the MTX cytotoxicity but also triggered the poly(I:C) dependent cytotoxicity. The antifolate ligands and co-delivered poly(I:C) seem to act synergistically and complement each other. Polyglutamylation of MTX in this context enhanced the combined toxicity and in fact was required for an efficient final outcome. Putting the observations together, obviously the specific separate pharmacological modes of action of polyglutamylated MTX and poly(I:C) contribute to cross a certain threshold level of cytotoxicity required for triggering cell death. In the case of poly(I:C) delivery by PEI conjugates, the inherent cytotoxicity of the polymeric carrier [234, 235] provides such a push toward cell death. Notably, the most effective combined ligand/poly(I:C) cytotoxicity was achieved with the polyglutamylated and histidylated oligomer **672**, which demonstrates the benefit of histidines also in case of poly(I:C) polyplexes and represents another example of the modular optimization of sequence-defined nucleic acid carriers.

Apart from the presented synergistic concept of antifolate/poly(I:C) codelivery, the novel dual-functional MTX ligands, improved by synthetic polyglutamylation, might be useful also in context of other drug delivery systems.

5 Summary

Nucleic acid therapeutics represent an innovative class of biopharmaceuticals with versatile modes of action and high potential for clinical applications. However, only a few examples have so far received marketing authorization. A major hurdle for the development of nucleic acid based drugs is the safe and efficient intracellular delivery. Just like natural viruses, polymer-based nanocarriers have to fulfill several requirements and be multifunctional to pass the separate hurdles of the nucleic acid delivery pathway efficiently. Particularly critical parameters are stable nucleic acid complexation, specific cellular uptake, endosomal escape and intracellular cargo release at the target site. In this work, a recently established solid-phase synthesis platform based on artificial polyamino acids has been used for the modular assembly of multifunctional, sequence-defined nucleic acid carriers. In two separate parts of the thesis, special emphasis has been put on the proton-sponge activity facilitating endosomal escape and receptor-mediated cellular uptake.

In the first part, the protonation characteristics and endosomal buffering of oligo(ethanamino)amides with different polyamino acid building blocks and additional histidines or pyridylalanines were investigated and correlated with the activity in different stages of pDNA delivery. A clear correlation between an even or odd number of protonatable nitrogens in the building blocks and the endosomal protonation could be observed. The integration of histidine increased the endosomal buffer capacity between pH 5 and 7.4 and enhanced transgene expression *in vitro* and *in vivo*. The beneficial effect of 'histidylation' on endosomal release was visualized by imaging of fluorescent calcein, which was co-internalized during transfections with PEGylated, receptor targeted oligomers. In contrast, neither the combination of different polyamino acids nor the integration of pyridylalanines enhanced transgene expression, despite increasing the endosomal buffer capacity. In both cases, the endosomal buffering resulted from a pronounced protonation in the lower pH sub-ranges, whereas histidine mediated buffering in higher ranges around pH 6. The results suggest that the exact localization of the maximal buffering within the endosomal pH range plays an important role for the proton-sponge activity. In this respect, an increased buffering in the early stages of the endosomal pathway seems

to be beneficial for an enhanced proton-sponge activity and endosomal escape of pDNA polyplexes.

In the second part, targeting ligands of different chemical nature were used for the receptor specific nucleic acid delivery. Peptides (cMBP1, cMBP2), a protein (mEGF), multivalent carbohydrates (mimetics of galactose and N-acetylgalactosamine) and small molecules (folic acid, methotrexate derivatives) were conjugated to PEGylated oligo(ethanamino)amides, and their individual suitability was investigated. In all cases, the compatibility with the nucleic acid carrier class could be demonstrated and potent ligands within each group were identified. Moreover, the precise architecture of the compounds allowed detailed structure-activity relationship studies and a stepwise optimization of the multifunctional nucleic acid carriers. By this means, the more potent peptide cMBP2, binding to the hepatocyte growth factor receptor (c-Met/HGFR), was identified in pDNA transfections *in vitro*. In combination with improved histidylated nucleic acid carriers, a cMBP2 dependent and tumor-specific transgene expression *in vivo* could be achieved. A similar modular optimization of ligand and carrier backbone was carried out with a set of antifolate ligands. The antifolate MTX was conjugated to nucleic acid carriers for the co-delivery of cytotoxic poly(I:C) in a cancer combination therapy approach. MTX served as a dual-functional ligand for both a folate receptor-mediated cellular uptake and an intrinsic cytotoxic action. Additionally, MTX polyglutamates, which represent the pharmacologically active forms, were generated by introduction of additional glutamic acid residues during solid-phase synthesis. The synthetic polyglutamylation showed enhancing effects on several stages of combined MTX/poly(I:C) activity. The most effective tumor cell killing *in vitro* was achieved with a polyglutamylated and histidylated nucleic acid carrier, which demonstrated the suitability of histidines to enhance the proton-sponge activity also in case of poly(I:C) polyplexes.

6 Appendix

6.1 Abbreviations

1,2-DAE	1,2-Diaminoethane
1,3-DAP	1,3-Diaminopropane
1,4-DAB	1,4-Diaminobutane
1,5-DAP	1,5-Diaminopentane
1,6-DAH	1,6-Diaminohexane
3PAL	3-(3-Pyridyl)-alanine
4PAL	3-(4-Pyridyl)-alanine
Ac ₂ O	Acetic anhydride
Boc	<i>tert</i> -Butoxycarbonyl protecting group
Boc-IDA	<i>N</i> -(<i>tert</i> -Butoxycarbonyl)iminodiacetic acid
BPEI	Branched polyethylenimine
cMBP	c-Met binding peptide
c-Met	Hepatocyte growth factor receptor
DCC	<i>N,N'</i> -Dicyclohexylcarbodiimide
DCM	Dichloromethane
DCVC	Dry column vacuum chromatography
DETA	Diethylene triamine
DHFR	Dihydrofolate reductase
DIPEA	<i>N,N</i> -Diisopropylethylamine
DMEM	Dulbecco's modified Eagle's medium
DMF	<i>N,N</i> -Dimethylformamide
DNA	Desoxyribonucleic acid
dsRNA	Double-stranded RNA
EDA	Ethylene diamine
EDTA	Ethylendiaminetetraacetic acid
EGF	Epidermal growth factor
EGFR	Epidermal growth factor receptor

ESI-MS	Electrospray ionization mass spectrometry
EtBr	Ethidium bromide
FCS	Fetal calf serum
Fmoc	Fluorenylmethoxycarbonyl protecting group
FoIA	Folic acid
FR	Folate receptor
Gal	Galactose
GalNAc	<i>N</i> -Acetylgalactosamine
Gtp	Glutaryl-tetraethylene pentamine
Gtt	Glutaryl-triethylene tetramine
HBG	Hepes-buffered glucose
HBTU	2-(1H-benzotriazole-1-yl)-1,1,3,3-tetramethyluronium hexafluorophosphate
HEPES	<i>N</i> -(2-hydroxyethyl) piperazine- <i>N'</i> -(2-ethansulfonic acid)
HGF	Hepatocyte growth factor
HMW	High molecular weight
HOBt	1-Hydroxybenzotriazole
IDA	Iminodiacetic acid
ivDde	1-(4,4-dimethyl-2,6-dioxocyclohex-1-ylidene)-3-methylbutyl protecting group
LMW	Low molecular weight
LPEI	Linear polyethylenimine
MeCN	Acetonitrile
MEG	Monoethylene glycol
mEGF	Murine epidermal growth factor
M-IDA	<i>N</i> -(Methyl)iminodiacetic acid
MTBE	Methyl <i>tert</i> -butyl ether
MTT	3-(4,5-dimethylthiazol-2-yl)-2,5-diphenyltetrazolium bromide
MTX	Methotrexate
MWCO	Molecular weight cut-off
N/P	(Protonatable) nitrogen to phosphates ratio
NHS	<i>N</i> -Hydroxysuccinimide

NMP	<i>N</i> -Methyl-2-pyrrolidone
NMR	Nuclear magnetic resonance
PAA	Polyamino acid
pCMVLuc	Plasmid encoding for firefly luciferase under the control of the cytomegalie virus (CMV) promoter
PDI	Polydispersity index
pDNA	Plasmid DNA
PEG	Polyethylene glycol
PEHA	Pentaethylene hexamine
PLH	Poly-L-histidine
PLL	Poly-L-lysine
PLR	Poly-L-arginine
poly(I)	Polyinosinic acid
poly(I:C)	Polyinosinic-polycytidylic acid duplex
PyBOP	Benzotriazol-1-yloxy-tripyrrolidinophosphonium hexafluorophosphate
RLU	Relative light units
RNA	Ribonucleic acid
RP-HPLC	Reversed-phase high performance liquid chromatography
RT	Room temperature
SEC	Size-exclusion chromatography
SPAAC	Strain-promoted alkyne-azide cycloaddition
Sph	Succinyl-pentaethylene hexamine
SPS	Solid-phase synthesis
Stp	Succinyl-tetraethylene pentamine
TBE	Tris-boric acid-EDTA buffer
TEPA	Tetraethylene pentamine
TETA	Triethylene tetramine
TFA	Trifluoroacetic acid
TFE-IDA	<i>N</i> -(Trifluoroethyl)iminodiacetic acid
THF	Tetrahydrofuran
TIS	Triisopropylsilane

6.2 Sequences of peptidic targeting ligands

Peptide	Sequence (N -> C)	References	Chapter
B6	GHKAKGPRK	[104, 126, 175, 236]	3.1.2
cMBP1	YLFSVHWPLKA	[176]	3.2.1
cMBP2	KSLSRHDHIIHH	[177-179]	3.2.1
cMBP2sc1	LHHHDRKSSIIH	*	3.2.1
cMBP2sc2	KSHHRDHIHLHS	*	3.2.1
cMBP2sc3	HHSIHLHKKSD	*	3.2.1
cMBP2sc4	RKIHHLHSHSD	*	3.2.1

* Scrambled sequences of cMBP2 were generated using an online sequence permutation tool (RANDOM.ORG).

6.3 Summary of SPS derived oligomers

ID	Sequence (C -> N)	Topology	Proton. Amines	Chapter
188	A-dPEG ₂₄ -K(Stp ₄ -C) ₂	P-2A	26	3.2.1 - 3.2.4
202	AK(Stp ₄ -C) ₂	2A	26	3.1.4
356	C-Stp ₄ -K(Stp ₄ -C)-dPEG ₂₄ -FolA	P-2A	25	3.2.4
440	A-dPEG ₂₄ -HK[H-(Stp-H) ₄ -C] ₂	P-2A	37	3.2.1
442	K[dPEG ₂₄ -HK(H-(Stp-H) ₄ -C) ₂]-cMBP2	P-2A	37	3.2.1
443	K[dPEG ₂₄ -K(Stp ₄ -C) ₂]-cMBP2	P-2A	26	3.2.1
479	K(5ANV)-dPEG ₂₄ -K(Stp ₄ -C) ₂	P-2A	26	3.2.2
573	AK[HK(H-Stp-H-Stp-H-Stp-HC) ₂] ₂	4A	58	3.1.2
574	AK[HK(H-Stp-H-Stp-H-Stp-HA) ₂] ₂	4A	58	3.1.2
575	AK[AK(A-Stp-A-Stp-A-Stp-AC) ₂] ₂	4A	40	3.1.2
576	AK[AK(A-Stp-A-Stp-A-Stp-AA) ₂] ₂	4A	40	3.1.2
577	AK[HK(H-Gtt-H-Gtt-H-Gtt-HC) ₂] ₂	4A	46	3.1.2
578	AK[HK(H-Gtt-H-Gtt-H-Gtt-HA) ₂] ₂	4A	46	3.1.2
579	AK[AK(A-Gtt-A-Gtt-A-Gtt-AC) ₂] ₂	4A	28	3.1.2
580	AK[AK(A-Gtt-A-Gtt-A-Gtt-AA) ₂] ₂	4A	28	3.1.2
582	AK[K(KH-(KHH) ₃ -KHK) ₂] ₂	4A HK	60	3.1.2
583	C-Stp ₄ -K(Stp ₄ -C)-dPEG ₂₄ -AlexaFluor488	P-2A	25	3.2.4
584	AK[K(KH-(KHH) ₅ -KHK) ₂] ₂	4A HK	84	3.1.2
603	(GalS) ₃ -dPEG ₂₄ -K(Stp ₄ -C) ₂	P-2A	26	3.2.3
604	(GalS) ₆ -dPEG ₂₄ -K(Stp ₄ -C) ₂	P-2A	26	3.2.3
605	(GalS-AEEAc) ₃ -K(Stp ₄ -C) ₂	P-2A	26	3.2.3
606	AK[HK(H-Sph-H-Sph-H-Sph-HC) ₂] ₂	4A	70	3.1.2
607	AK[HK(H-Sph-H-Sph-H-Sph-HA) ₂] ₂	4A	70	3.1.2
608	AK[AK(A-Sph-A-Sph-A-Sph-AC) ₂] ₂	4A	52	3.1.2
609	AK[AK(A-Sph-A-Sph-A-Sph-AA) ₂] ₂	4A	52	3.1.2
610	A-Gtt-A-Gtt-A-Gtt-A	1A	7	3.1.2
611	H-Gtt-H-Gtt-H-Gtt-H	1A	11	3.1.2
612	A-Stp-A-Stp-A-Stp-A	1A	10	3.1.2
613	H-Stp-H-Stp-H-Stp-H	1A	14	3.1.2

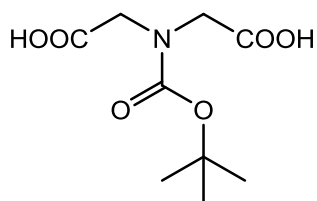
614	A-Sph-A-Sph-A-Sph-A	1A	13	3.1.2
615	H-Sph-H-Sph-H-Sph-H	1A	17	3.1.2
616	A-(dPEG ₂₄) ₂ -HK[H-(Stp-H) ₄ -C] ₂	P-2A	37	3.1.2, 3.2.1
617	B6-(dPEG ₂₄) ₂ -AK[A-(Stp-A) ₄ -C] ₂	P-2A	26	3.1.2
618	B6-(dPEG ₂₄) ₂ -HK[H-(Stp-H) ₄ -C] ₂	P-2A	37	3.1.2
619	K[(dPEG ₂₄) ₂ -FolA]-AK[A-(Stp-A) ₄ -C] ₂	P-2A	26	3.1.2
620	K[(dPEG ₂₄) ₂ -FolA]-HK[H-(Stp-H) ₄ -C] ₂	P-2A	37	3.1.2
638	K(dPEG ₂₄ -MTX)-K(Stp ₄ -C) ₂	P-2A	26	3.2.4
639	K(dPEG ₂₄ -E ₂ -MTX)-K(Stp ₄ -C) ₂	P-2A	26	3.2.4
640	K(dPEG ₂₄ -E ₄ -MTX)-K(Stp ₄ -C) ₂	P-2A	26	3.2.4
641	K(dPEG ₂₄ -E ₆ -MTX)-K(Stp ₄ -C) ₂	P-2A	26	3.2.4
651	(GalNAcS) ₃ -dPEG ₂₄ -K(Stp ₄ -C) ₂	P-2A	26	3.2.3
672	K[(dPEG ₂₄) ₂ -E ₄ -MTX]-HK[H-(Stp-H) ₄ -C] ₂	P-2A	26	3.2.4
689	C-(H-Stp) ₃ -HK[H-(Stp-H) ₃ -C] ₂	3A	43	3.2.1
694	K[(dPEG ₂₄) ₂ -HK(H-(Stp-H) ₄ -C) ₂]-cMBP2	P-2A	37	3.2.1
695	K[(dPEG ₂₄) ₂ -AK(A-(Stp-A) ₄ -C) ₂]-cMBP2	P-2A	26	3.2.1
696	K[dPEG ₂₄ -K(Stp ₄ -C) ₂]-cMBP1	P-2A	26	3.2.1
697	K[dPEG ₂₄ -K(Stp ₄ -C) ₂]-cMBP2sc1	P-2A	26	3.2.1
698	K[dPEG ₂₄ -K(Stp ₄ -C) ₂]-cMBP2sc2	P-2A	26	3.2.1
699	K[dPEG ₂₄ -K(Stp ₄ -C) ₂]-cMBP2sc3	P-2A	26	3.2.1
700	K[dPEG ₂₄ -K(Stp ₄ -C) ₂]-cMBP2sc4	P-2A	26	3.2.1
754	AK(Gtp ₄ -C) ₂	2A	26	3.1.3, 3.1.5
755	AK(IDAtp ₄ -C) ₂	2A	34	3.1.5
756	AK[(M-IDAtp) ₄ -C] ₂	2A	34	3.1.5
757	AK[(TFE-IDAtp) ₄ -C] ₂	2A	34	3.1.5
811	A-3PAL-K[(3PAL-Stp) ₄ -3PAL-C] ₂	2A	37	3.1.4
812	A-4PAL-K[(4PAL-Stp) ₄ -4PAL-C] ₂	2A	37	3.1.4
813	AHK[(H-Stp) ₄ -HC] ₂	2A	37	3.1.4
814	AK[(H-Stp) ₄ -C] ₂	2A	34	3.1.5
815	AK[(Gtp-Gtt) ₂ -Gtp-C] ₂	2A	28	3.1.3
816	AK[(Gtt-Gtp) ₂ -Gtt-C] ₂	2A	26	3.1.3
817	AK(Gtt ₄ -C) ₂	2A	18	3.1.3

Topology abbreviations: 1A, one-arm (linear); 2A, two-arm; P-2A, PEGylated two-arm; 4A, four-arm; 4A HK, four-arm HK peptide. Oligomer **202** was synthesized by Dr. Irene Martin (visiting scientist, IRB Barcelona, Spain). Oligomers **573-580** were synthesized by Dr. Edith Salcher (Pharmaceutical Biotechnology, LMU). Oligomers **582** and **584** were synthesized by Wolfgang Rödl (Pharmaceutical Biotechnology, LMU). Oligomer **689** was synthesized by Dongsheng He (Pharmaceutical Biotechnology, LMU).

6.4 Analytical Data

6.4.1 Building blocks

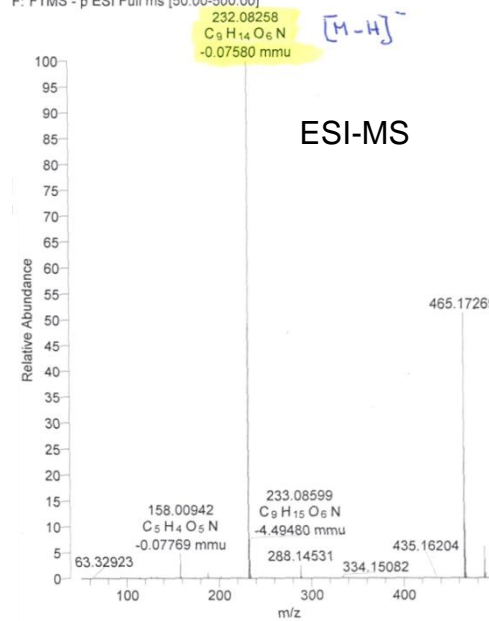
N-(*tert*-Butoxycarbonyl)iminodiacetic acid (Boc-IDA)



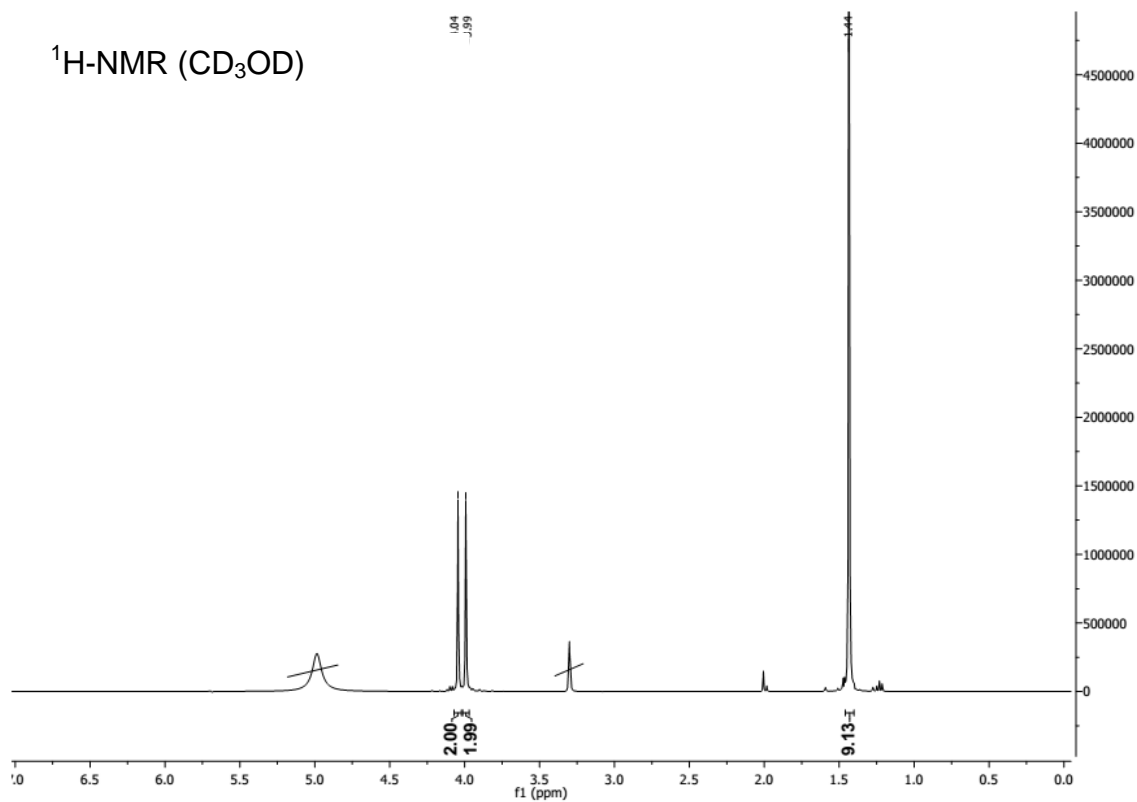
Chemical Formula: $C_9H_{15}NO_6$

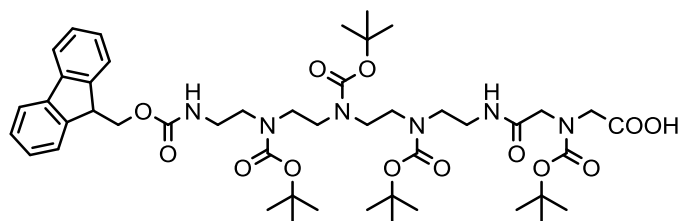
Exact Mass: 233,0899

09-ulaph-Boc-IDA_140930142254 #51-255 RT: 0.53-1.91 AV: 26 NL: 1.05
F: FTMS - p ESI Full ms [50.00-500.00]

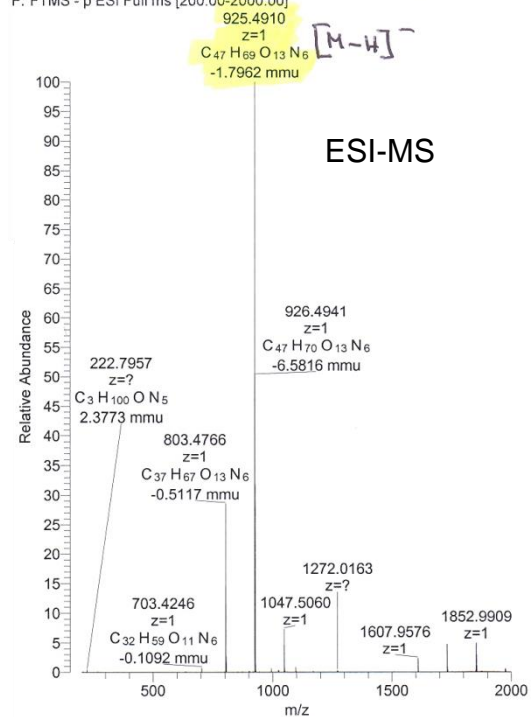
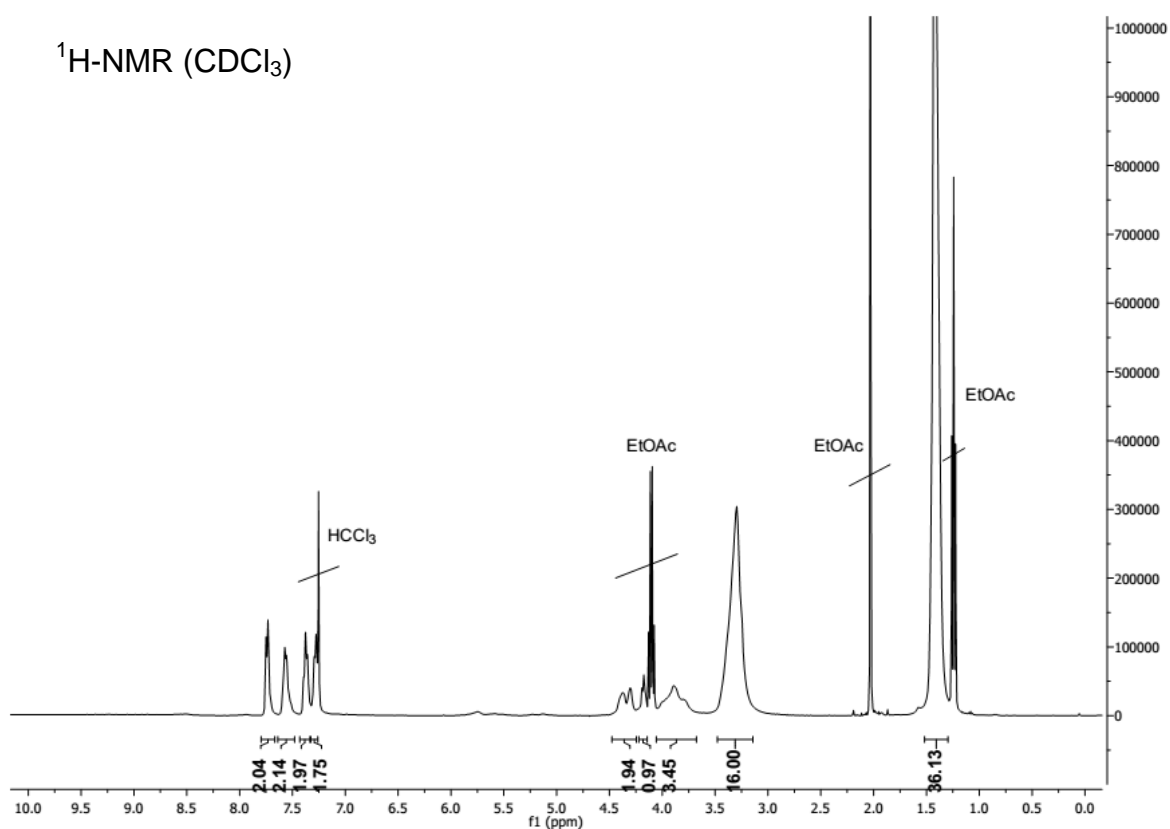


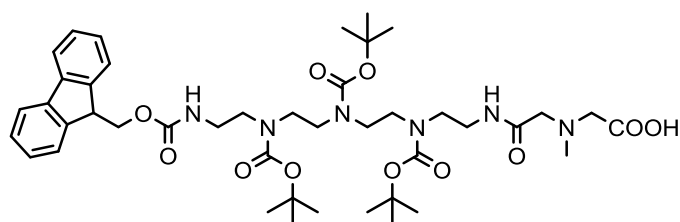
1H -NMR (CD_3OD)



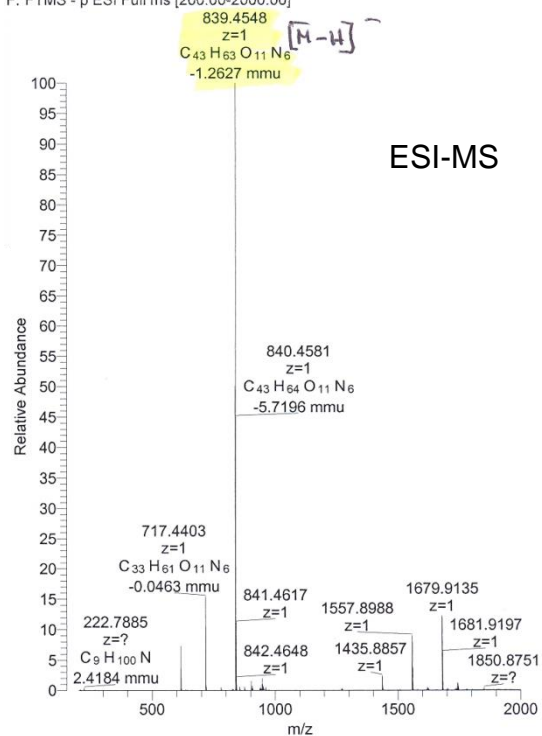
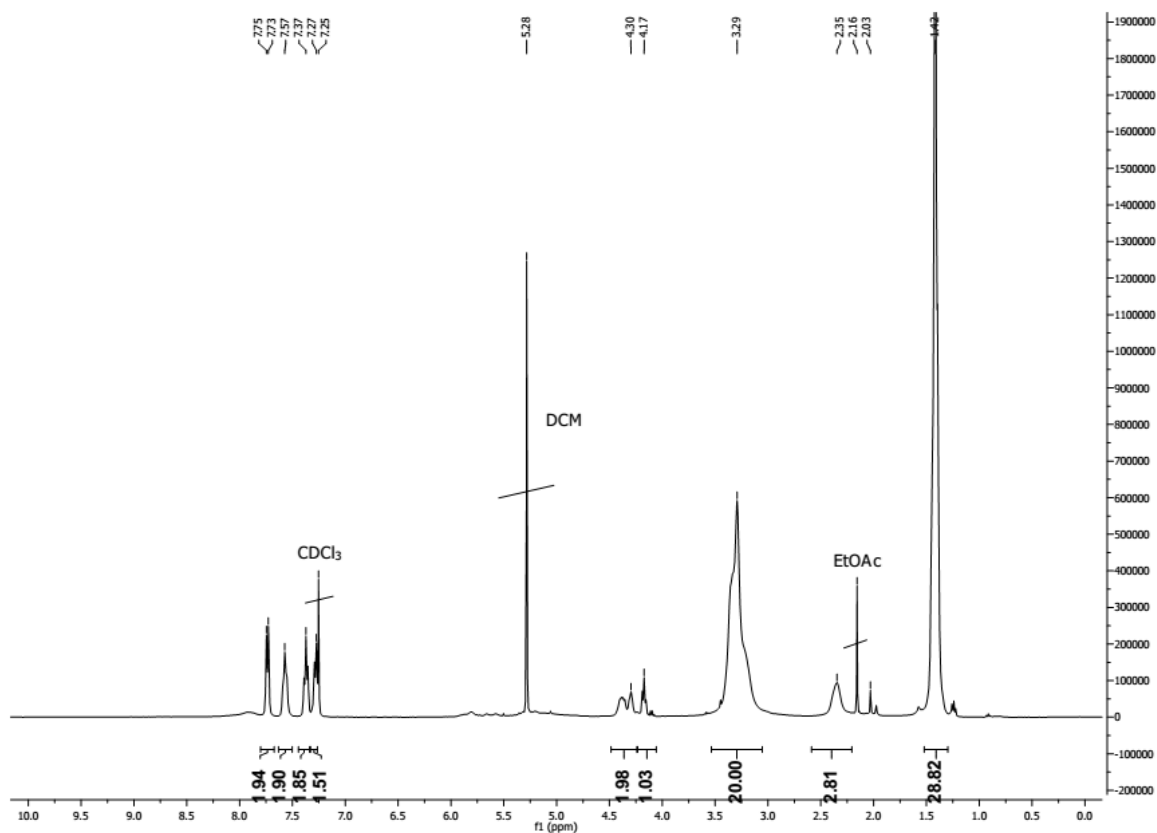
Fmoc-Boc-IDAtp(Boc₃)-OHChemical Formula: C₄₇H₇₀N₆O₁₃

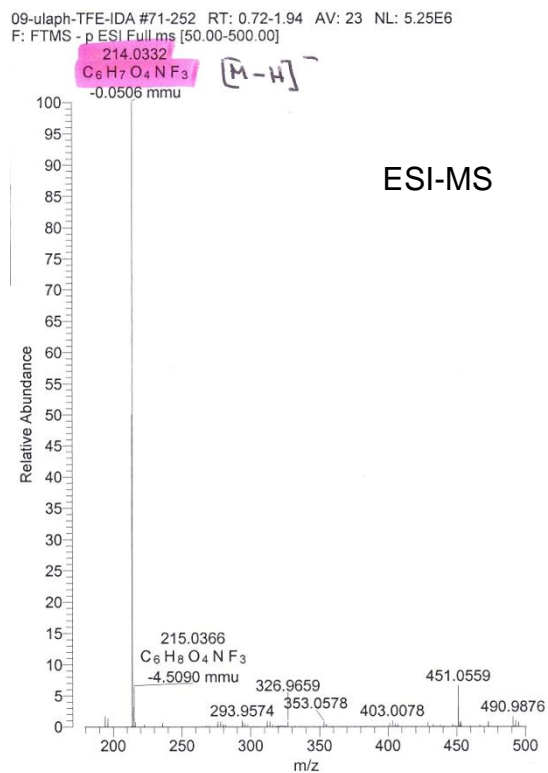
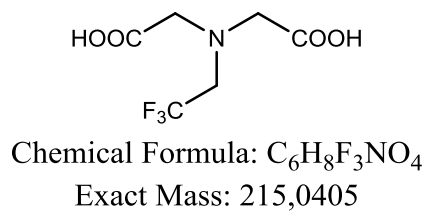
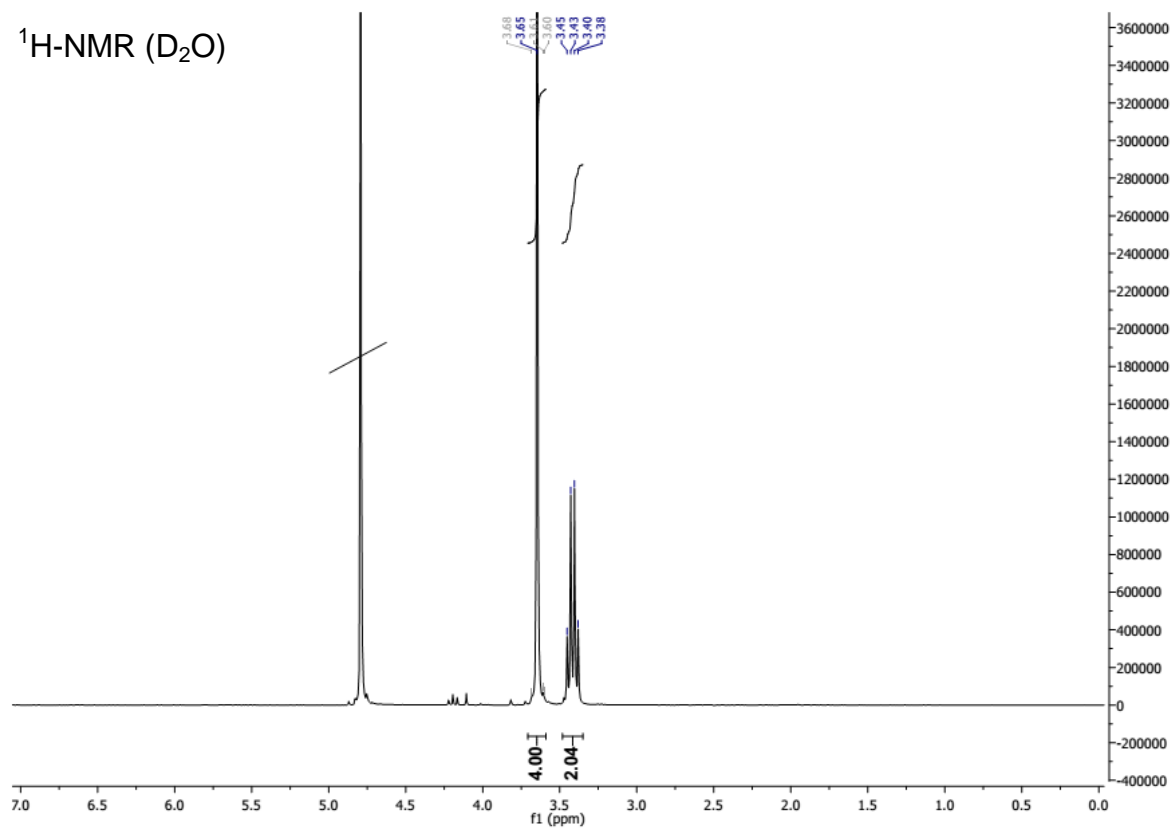
Exact Mass: 926,5001

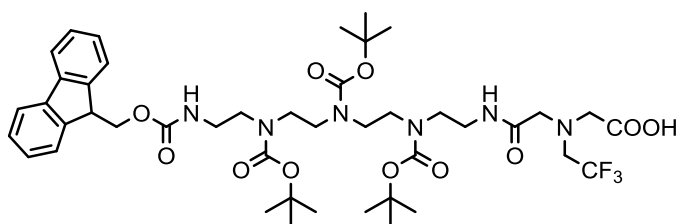
09-ulaph-BIDAtp #59-221 RT: 0.63-1.69 AV: 20 NL: 2.89E6
F: FTMS - p ESI Full ms [200.00-2000.00]¹H-NMR (CDCl₃)

Fmoc-M-IDAtp(Boc)₃-OHChemical Formula: C₄₃H₆₄N₆O₁₁

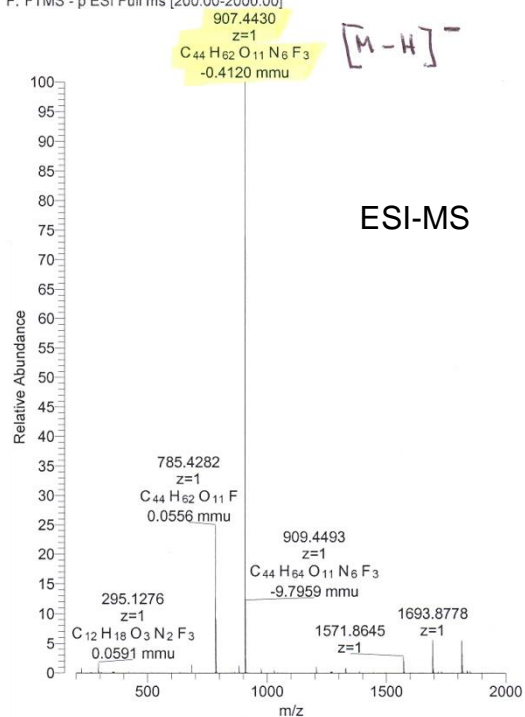
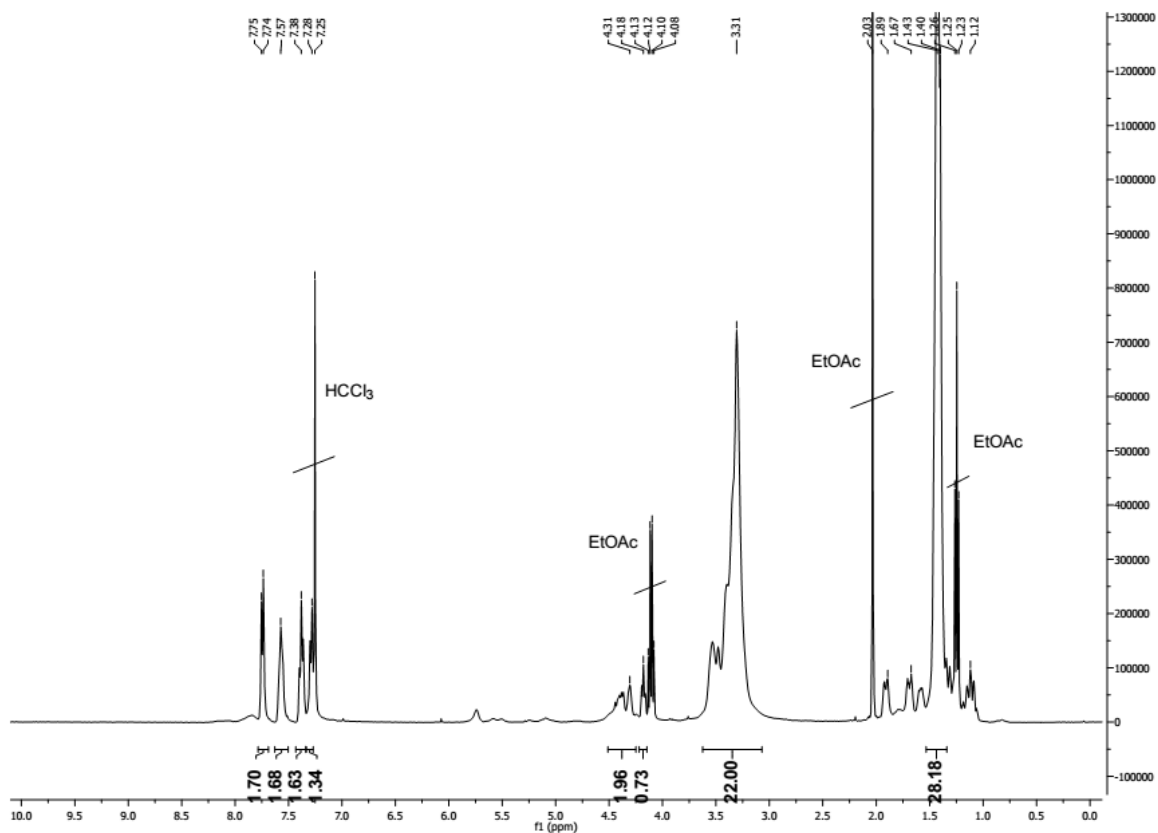
Exact Mass: 840,4633

09-ulaph-MIDAtp #61-219 RT: 0.66-1.70 AV: 19 NL: 1.58E6
F: FTMS - p ESI Full ms [200.00-2000.00]¹H-NMR (CDCl₃)

***N*-(Trifluoroethyl)iminodiacetic acid (TFE-IDA)** **1H -NMR (D_2O)**

Fmoc-TFE-IDAtp(Boc)₃-OHChemical Formula: $C_{44}H_{63}F_3N_6O_{11}$

Exact Mass: 908,4507

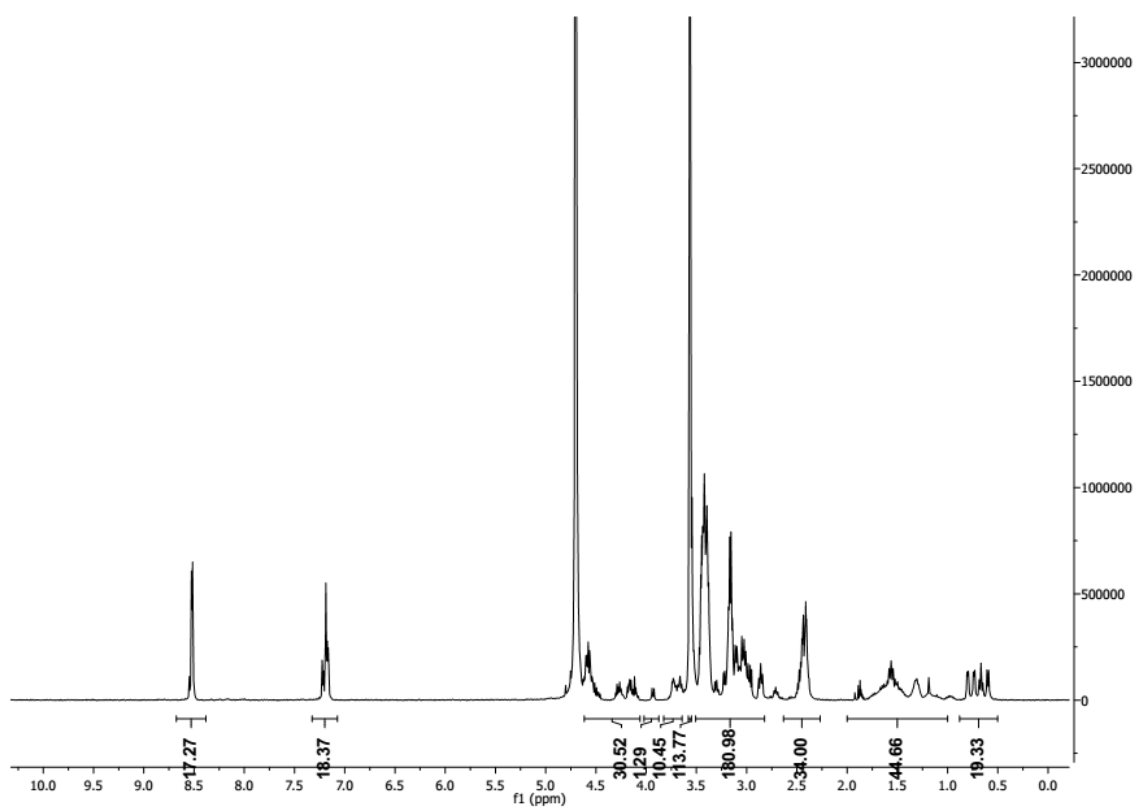
10-ulaph-TFEIDATp #93 RT: 0.79 AV: 1 NL: 6.96E6
F: FTMS - p ESI Full ms [200.00-2000.00] 1H -NMR ($CDCl_3$)

6.4.2 Oligomers

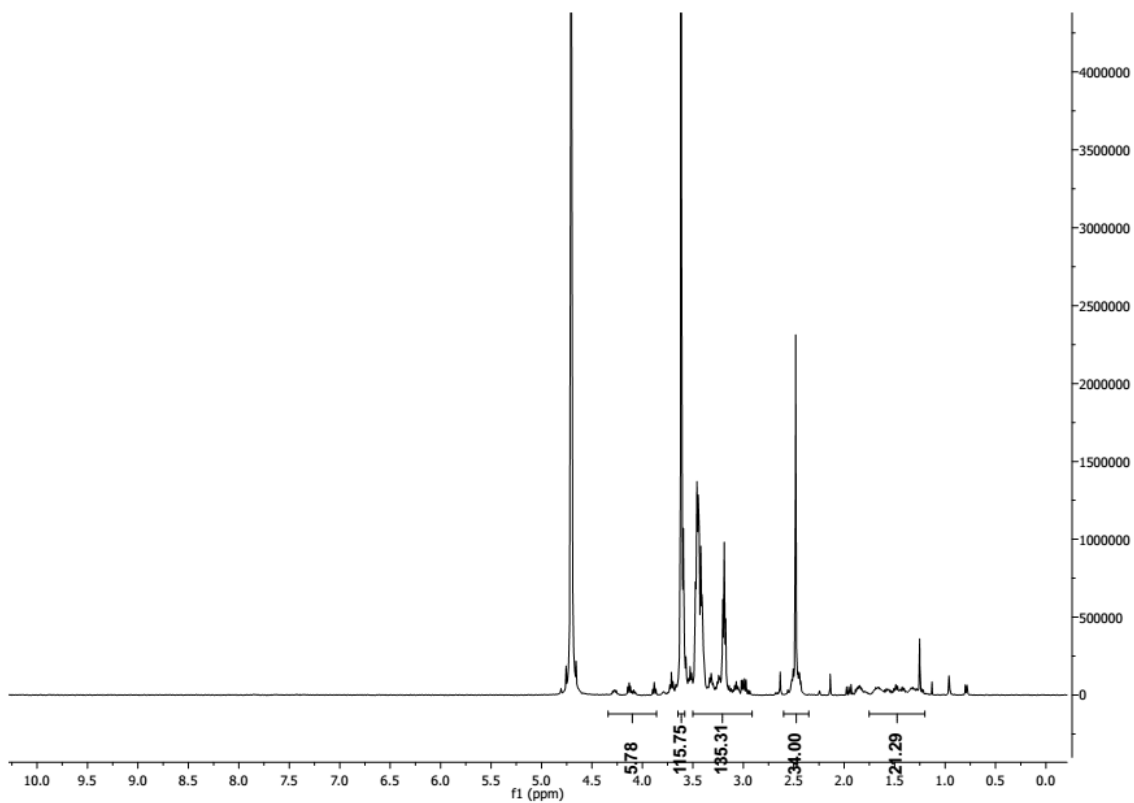
¹H-NMR spectra of key structures

Spectra of oligomers were recorded in deuterium oxide (D₂O).

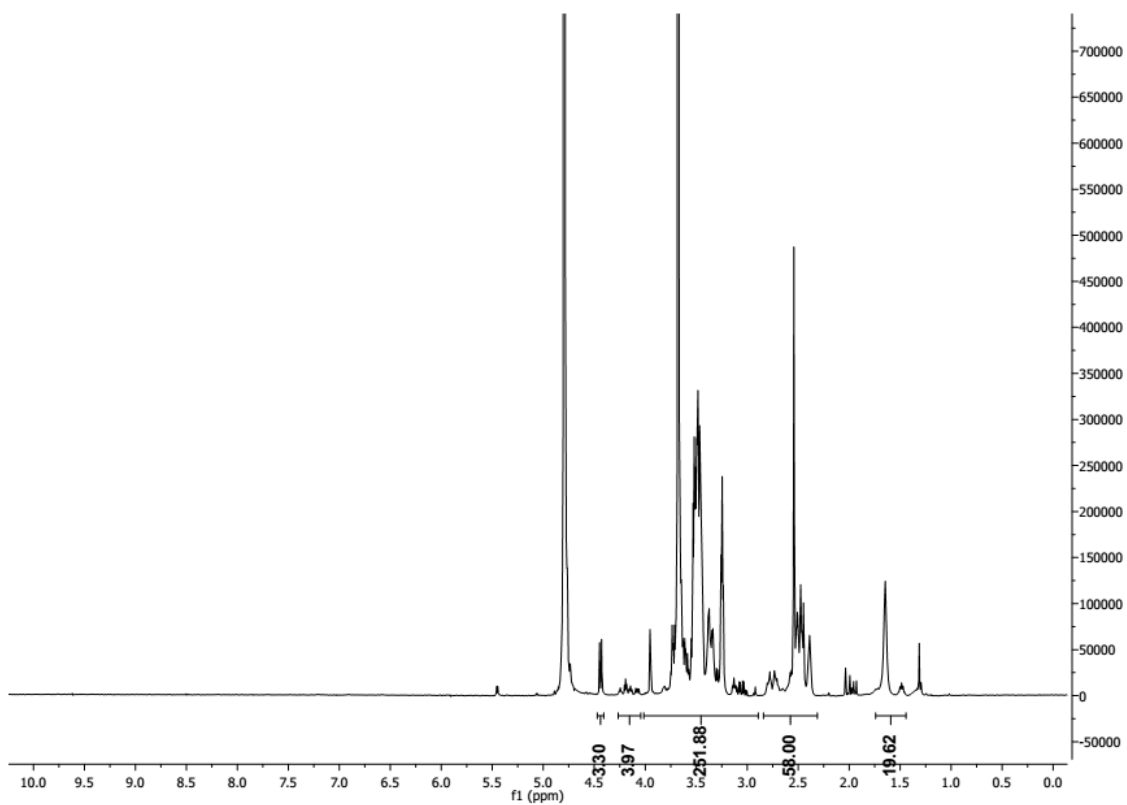
Oligomer **442** / Sequence (C -> N): K[dPEG24-HK(H-(Stp-H)₄-C)₂]-HHHHHDHRSLSK



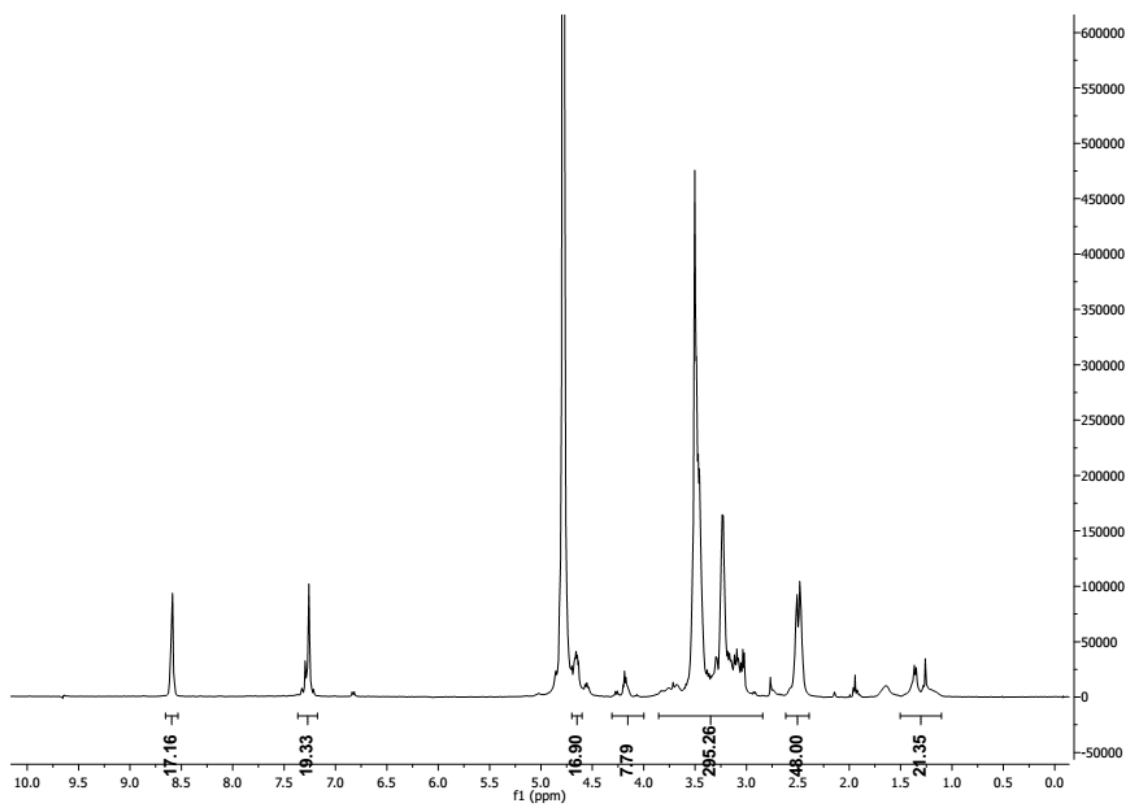
Oligomer **479** / Sequence (C -> N): K(5ANV)-dPEG₂₄-K(Stp₄-C)₂



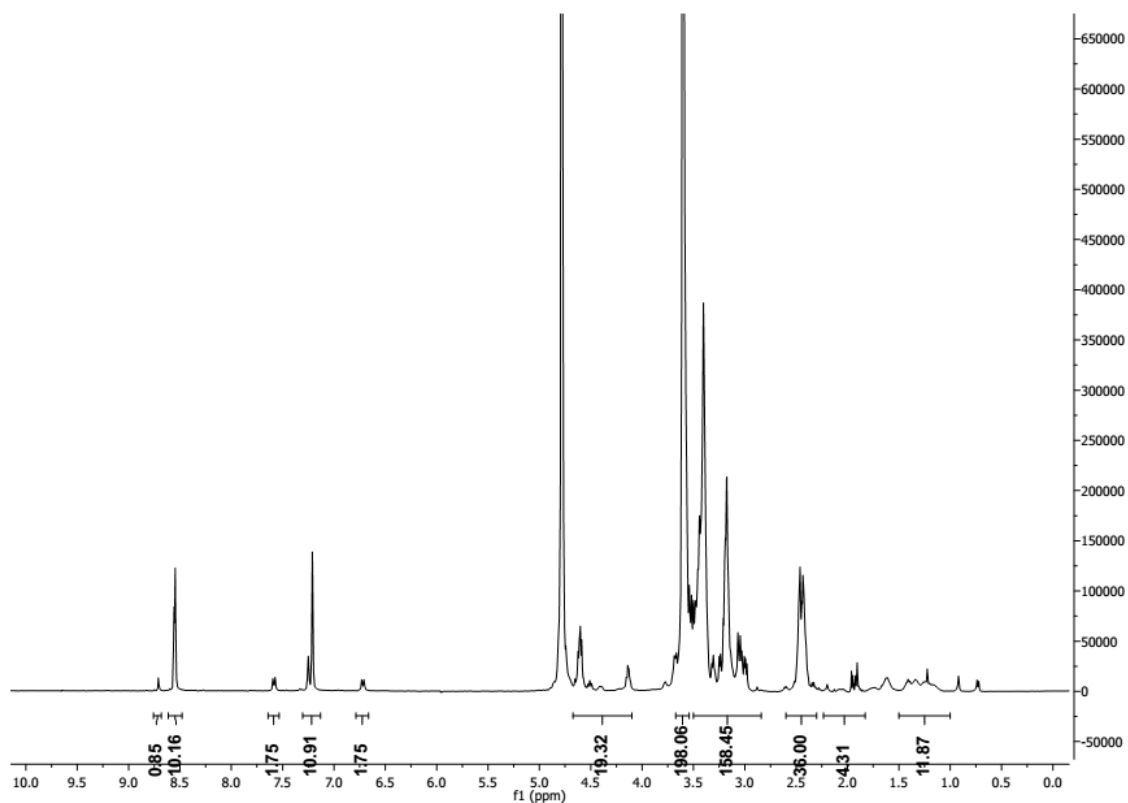
Oligomer **603** / Sequence (C -> N): (GalS)₃-dPEG₂₄-K(Stp₄-C)₂



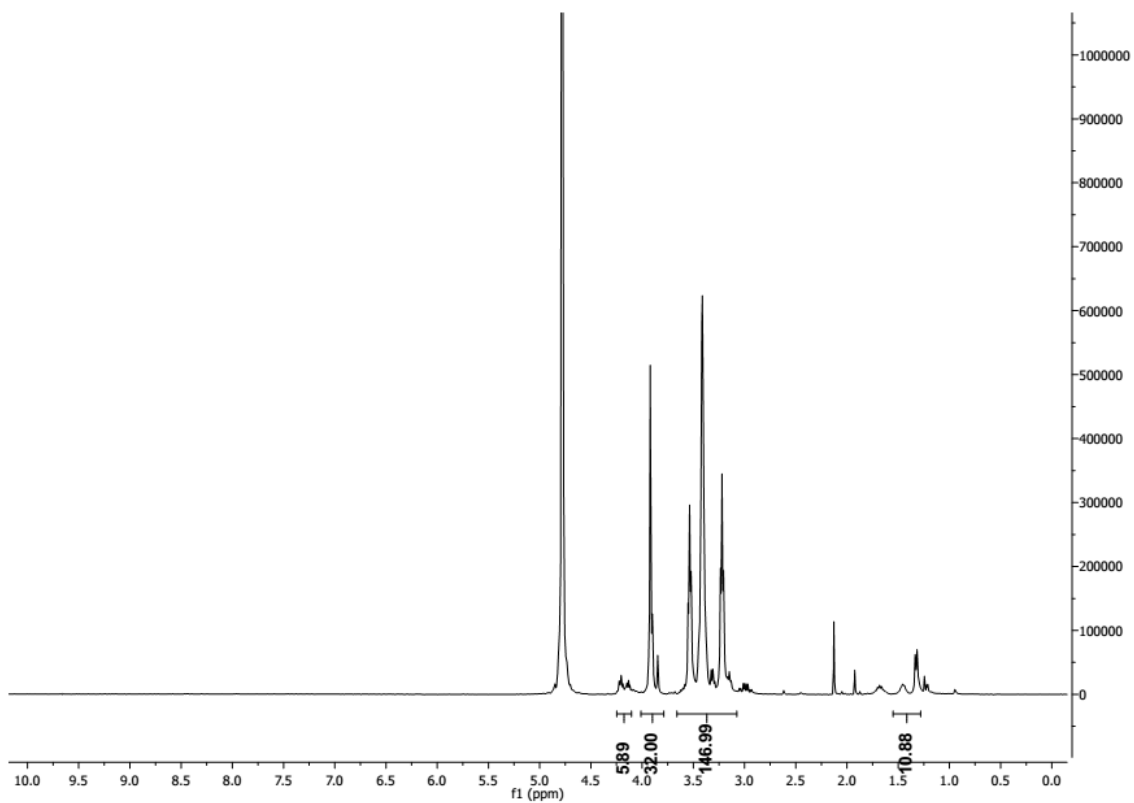
Oligomer **606** / Sequence (C -> N): AK[HK(H-Sph-H-Sph-H-Sph-HC)₂]₂



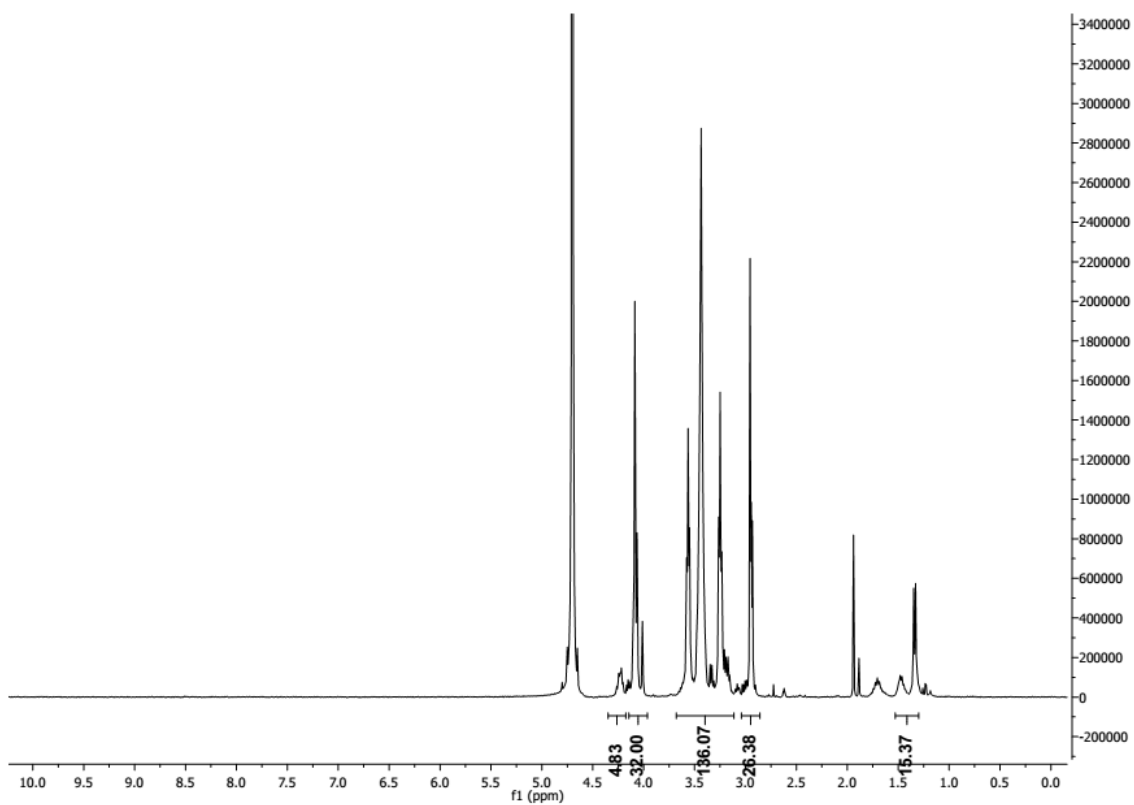
Oligomer **620** / Sequence (C -> N): K[(dPEG₂₄)₂-FolA]-HK[H-(Stp-H)₄-C]₂



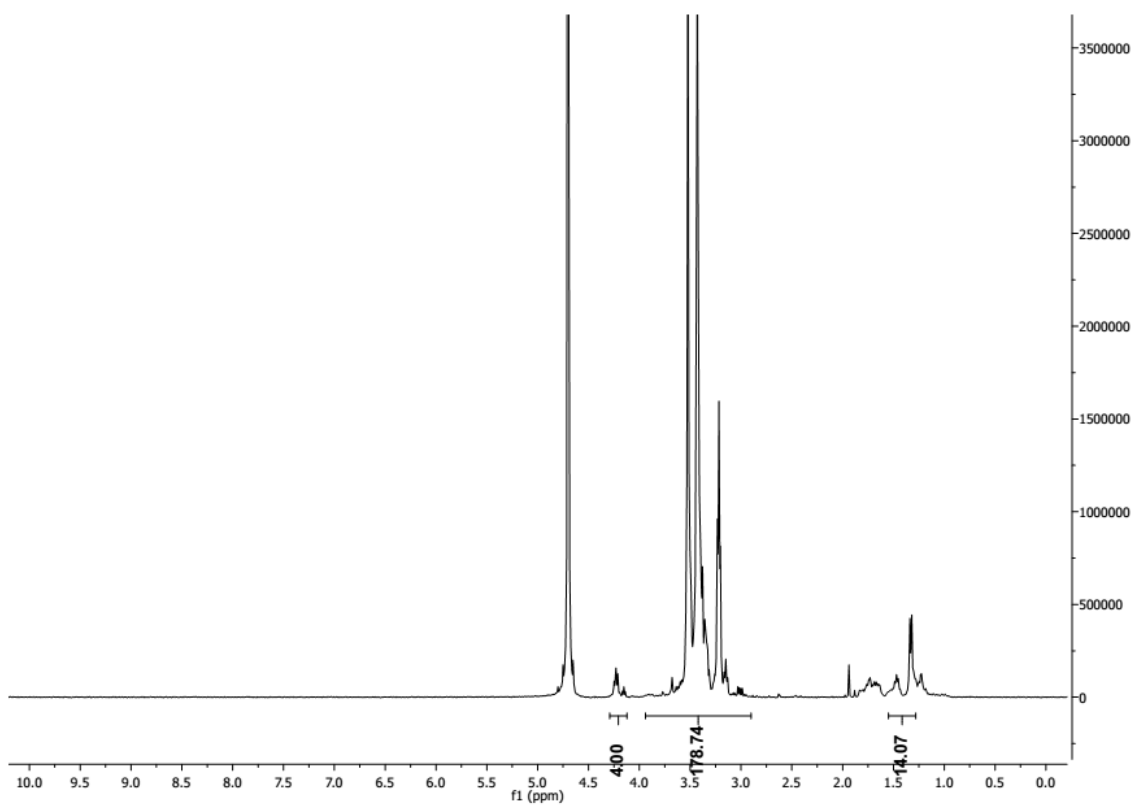
Oligomer **755** / Sequence (C -> N): AK(IDAtp₄-C)₂



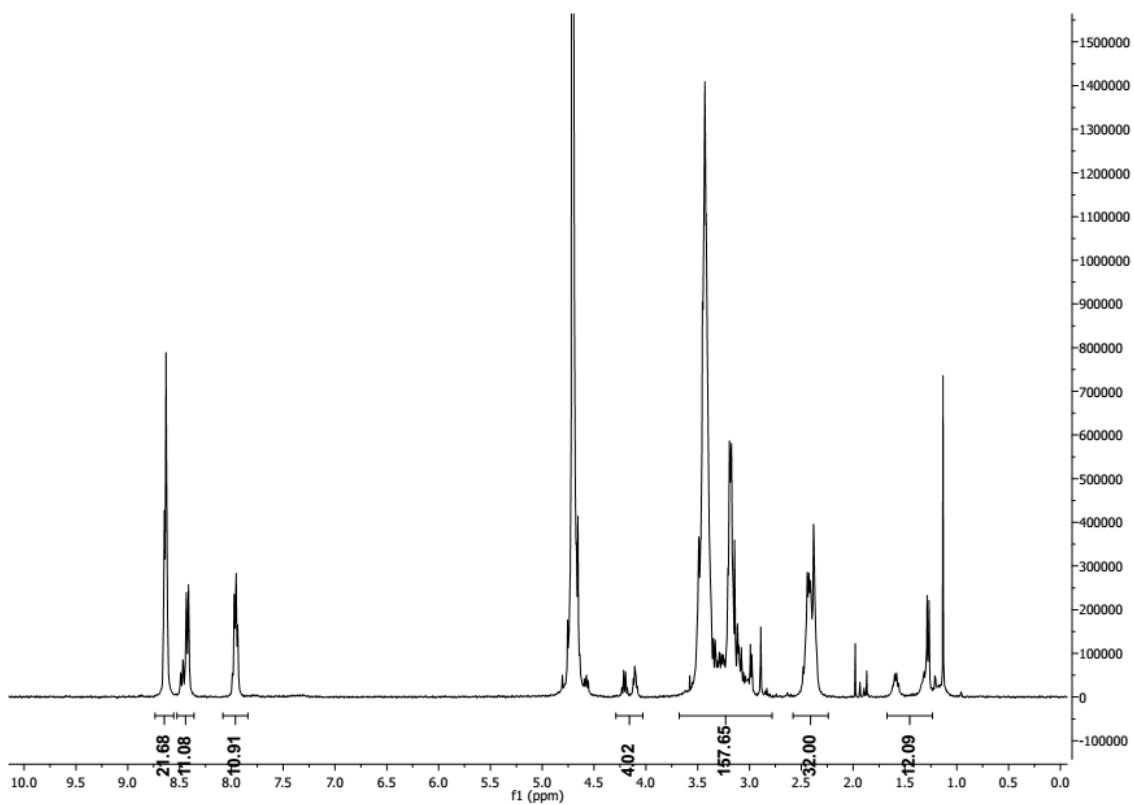
Oligomer **756** / Sequence (C -> N): AK[(M-IDAtp)₄-C]₂



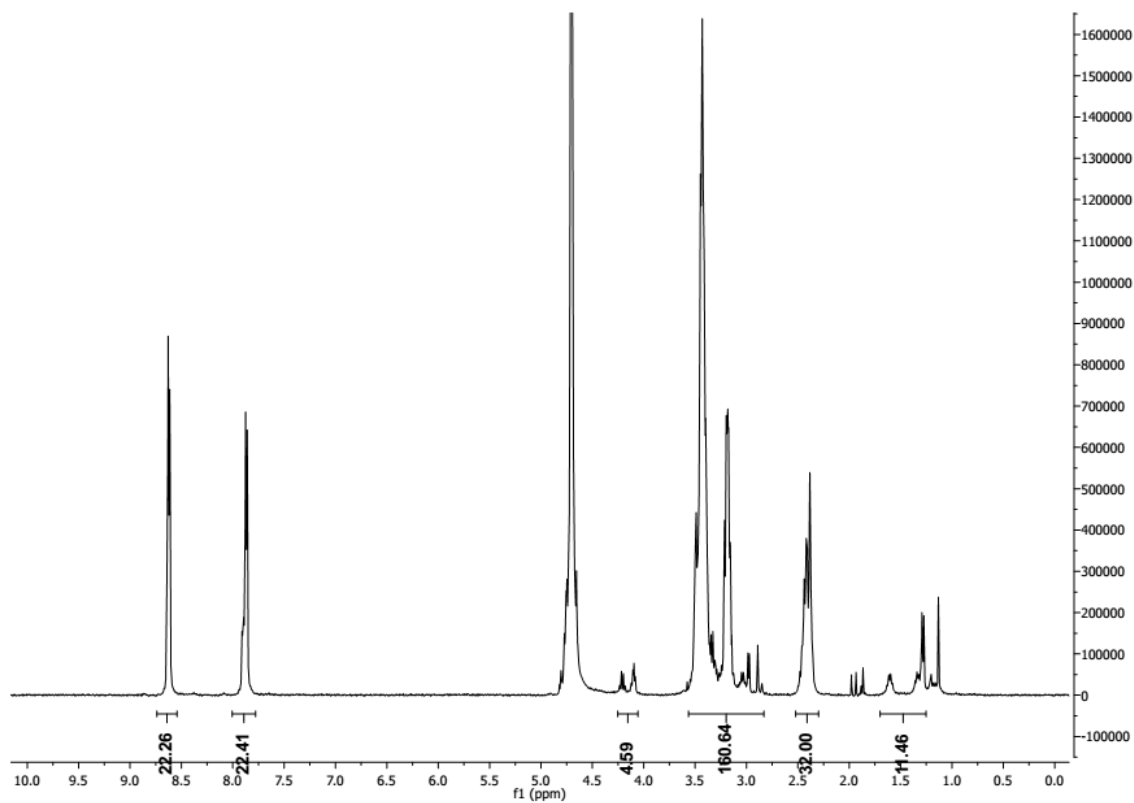
Oligomer **757** / Sequence (C -> N): AK[(TFE-IDAtp)₄-C]₂



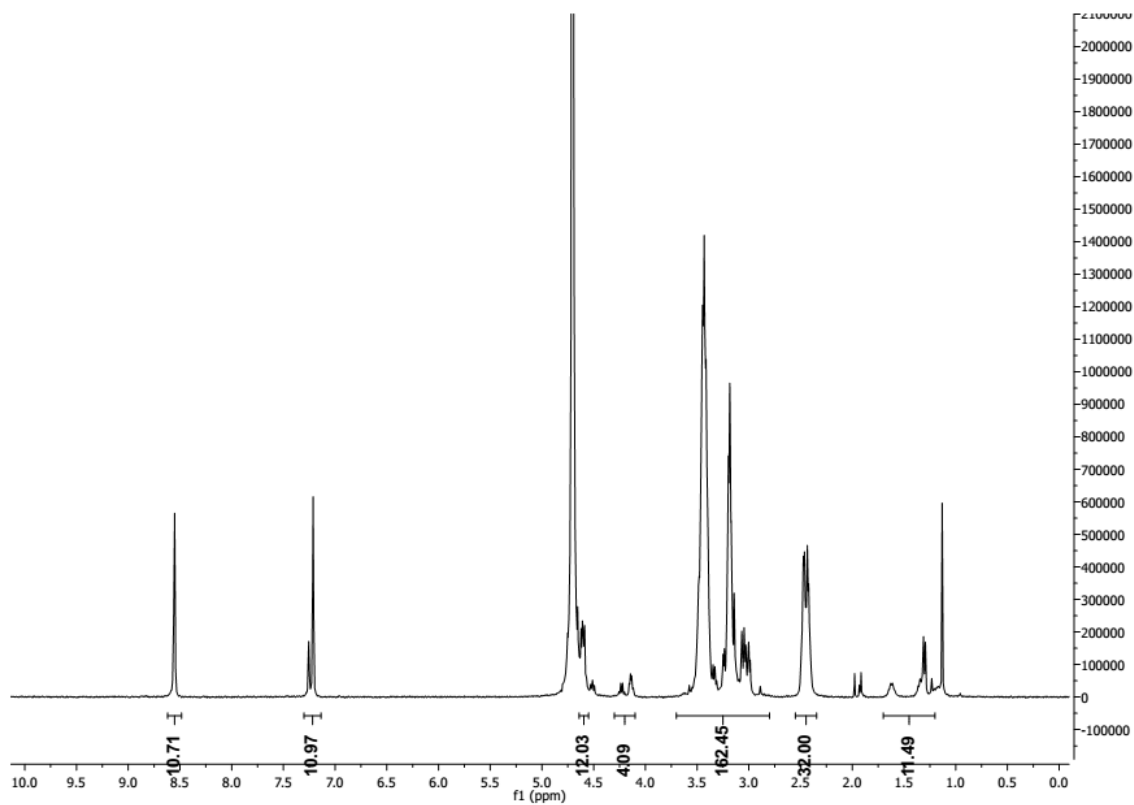
Oligomer **811** / Sequence (C -> N): A-3PAL-K[(3PAL-Stp)₄-3PAL-C]₂



Oligomer **812** / Sequence (C -> N): A-4PAL-K[(4PAL-Stp)₄-4Pal-C]₂



Oligomer **813** / Sequence (C -> N): AHK[(H-Stp)₄-HC]₂



6.4.2.1 Summarized spectral data

Oligomer **188** / Sequence (C -> N): A-dPEG₂₄-K(Stp₄-C)₂

¹H-NMR (500 MHz, D₂O) δ = 1.2-1.5 (m, 9H, βH alanine, βγδH lysine), 2.4-2.6 (m, 34H, -CO-CH₂-CH₂-CO- succinic acid, -CO-CH₂- dPEG₂₄), 2.9-3.5 (m, 134H, -CH₂- TEPA, βH cysteine, εH lysine), 3.63 (s, 98H, -CH₂-O- dPEG₂₄, -CH₂-N- dPEG₂₄), 4.0-4.3 (m, 4H, αH alanine, αH cysteine, αH lysine).

Oligomer **356** / Sequence (C -> N): C-Stp₄-K(Stp₄-C)-dPEG₂₄-FolA

¹H-NMR (400 MHz, D₂O) δ = 1.2-1.5 (m, 6H, βγδH lysine), 1.9-2.1 (m, 4H, βγH glutamic acid), 2.4-2.5 (m, 34H, -CO-CH₂-CH₂-CO- succinic acid, -CO-CH₂- dPEG₂₄), 3.0-3.5 (m, 134H, -CH₂- TEPA, βH cysteine, εH lysine), 3.60 (s, 98H, -CH₂-O- dPEG₂₄, -CH₂-N- dPEG₂₄), 4.0-4.6 (m, 4H, αH amino acids), 6.7-6.8 (d, 2H, Ar-H pteronic acid), 7.5-7.7 (d, 2H, Ar-H pteronic acid), 8.75 (s, 1H, Ar-H pteronic acid).

Oligomer **440** / Sequence (C -> N): A-dPEG₂₄-HK[H-(Stp-H)₄-C]₂

¹H-NMR (500 MHz, D₂O) δ = 1.3-1.7 (m, 9H, βH alanine, βγδH lysine), 2.3-2.6 (m, 34H, -CO-CH₂-CH₂-CO- succinic acid, -CO-CH₂- dPEG₂₄), 3.0-3.5 (m, 156H, -CH₂- TEPA, βH cysteine, βH histidine, εH lysine), 3.63 (s, 98H, -CH₂-O- dPEG₂₄, -CH₂-N- dPEG₂₄), 4.1-4.3 (m, 3H, αH cysteine, αH lysine), 4.5-4.7 (m, 11H, αH histidine), 7.2-7.3 (m, 11H, Ar-H histidine), 8.5-8.7 (m, 11H, Ar-H histidine).

Oligomer **442** / Sequence (C -> N): K[dPEG₂₄-HK(H-(Stp-H)₄-C)₂]-HHHHHDHRSLSK

¹H-NMR (400 MHz, D₂O) δ = 1.0-2.0 (m, 40H, βγH arginine, βγδH isoleucine, βγδH leucine, βγδH lysine), 2.4-2.6 (m, 34H, -CO-CH₂-CH₂-CO- succinic acid, -CO-CH₂- dPEG₂₄), 2.8-3.5 (m, 176H, -CH₂- TEPA, δH arginine, βH aspartate, βH cysteine, βH histidine, εH lysine, βH serine), 3.67 (s, 98H, -CH₂-O- dPEG₂₄, -CH₂-N- dPEG₂₄), 4.0-4.6 (m, 27H, αH amino acids), 7.1-7.3 (m, 16H, Ar-H histidine), 8.5-8.6 (m, 16H, Ar-H histidine).

Oligomer **443** / Sequence (C -> N): K[dPEG₂₄-K(Stp₄-C)₂]-HHHHHDHRSLSK

¹H-NMR (500 MHz, D₂O) δ = 1.0-2.0 (m, 40H, βγH arginine, βγδH isoleucine, βγδH leucine, βγδH lysine), 2.4-2.6 (m, 34H, -CO-CH₂-CH₂-CO- succinic acid, -CO-CH₂-dPEG₂₄), 2.8-3.6 (m, 154H, -CH₂- TEPA, δH arginine, βH aspartate, βH cysteine, βH histidine, εH lysine, βH serine), 3.66 (s, 98H, -CH₂-O- dPEG₂₄, -CH₂-N- dPEG₂₄), 3.9-4.6 (comp, 16H, αH amino acids), 7.24-7.25 (m, 5H, Ar-H histidine), 8.61 (s, 5H, Ar-H histidine).

Oligomer **479** / Sequence (C -> N): K(5ANV)-dPEG₂₄-K(Stp₄-C)₂

¹H-NMR (400 MHz, D₂O) δ = 1.2-1.8 (m, 18H, βγδ 5-azidonorvaline, βγδH lysine), 2.4-2.6 (m, 34H, -CO-CH₂-CH₂-CO- succinic acid, -CO-CH₂- dPEG₂₄), 2.9-3.5 (m, 134H, -CH₂- TEPA, βH cysteine, εH lysine), 3.62 (s, 98H, -CH₂-O- dPEG₂₄, -CH₂-N- dPEG₂₄), 3.9-4.3 (m, 5H, αH 5-azidonorvaline, αH cysteine, αH lysine).

Oligomer **603** / Sequence (C -> N): (GalS)₃-dPEG₂₄-K(Stp₄-C)₂

¹H-NMR (500 MHz, D₂O) δ = 1.4-1.7 (m, 18H, βγδH lysine, βγH 5-mercaptopentanoic acid), 2.3-2.8 (m, 58H, -CO-CH₂-CH₂-CO- succinic acid, -CO-CH₂- dPEG₂₄, αδH 5-mercaptopentanoic acid), 2.9-4.0 (m, 253H, -CH₂- TEPA, -CH₂-O- dPEG₂₄, -CH₂-N- dPEG₂₄, βH cysteine, εH lysine, -CH-O- thiogalactose, -CH₂-O- thiogalactose), 4.0-4.3 (m, 3H, αH lysine, αH cysteine), 4.4-4.5 (d, 3H, -S-CH- thiogalactose).

Oligomer **604** / Sequence (C -> N): (GalS)₆-dPEG₂₄-K(Stp₄-C)₂

¹H-NMR (500 MHz, D₂O) δ = 1.4-1.7 (m, 30H, βγδH lysine, βγH 5-mercaptopentanoic acid), 2.3-2.8 (m, 82H, -CO-CH₂-CH₂-CO- succinic acid, -CO-CH₂- dPEG₂₄, αδH 5-mercaptopentanoic acid), 3.0-4.0 (m, 274H, -CH₂- TEPA, -CH₂-O- dPEG₂₄, -CH₂-N- dPEG₂₄, βH cysteine, εH lysine, -CH-O- thiogalactose, -CH₂-O- thiogalactose), 4.1-4.2 (m, 3H, αH lysine, αH cysteine), 4.4-4.5 (d, 3H, -S-CH- thiogalactose).

Oligomer **605** / Sequence (C -> N): (GalS-AEEAc)₃-K(Stp₄-C)₂

¹H-NMR (500 MHz, D₂O) δ = 1.5-1.7 (m, 18H, βγδH lysine, βγH 5-mercaptopentanoic acid), 2.2-2.8 (m, 58H, -CO-CH₂-CH₂-CO- succinic acid, -CO-CH₂- dPEG₂₄, αδH 5-mercaptopentanoic acid), 3.0-4.1 (m, 283H, -CH₂- TEPA, -CH₂-O- dPEG₂₄, -CH₂-N- dPEG₂₄, βH cysteine, εH lysine, -CH₂- 2-(2-(2-aminoethoxy)ethoxy)acetic acid, -CH-O- thiogalactose, -CH₂-O- thiogalactose), 4.1-4.2 (m, 3H, αH lysine, αH cysteine), 4.4-4.5 (d, 3 H, -S-CH- thiogalactose).

Oligomer **606** / Sequence (C -> N): AK[HK(H-Sph-H-Sph-H-Sph-HC)₂]₂

¹H-NMR (400 MHz, D₂O) δ = 1.1-1.5 (m, 21H, βH alanine, βγδH lysine), 2.3-2.7 (m, 48H, -CO-CH₂-CH₂-CO- succinic acid), 2.8-3.9 (m, 290H, -CH₂- PEHA, βH cysteine, βH histidine, εH lysine), 4.0-4.3 (m, 8H, αH alanine, αH cysteine, αH lysine), 4.6-4.7 (m, 18H, αH histidine), 7.0-7.5 (s, 18H, Ar-H histidine), 8.59 (s, 18H, Ar-H histidine).

Oligomer **607** / Sequence (C -> N): AK[HK(H-Sph-H-Sph-H-Sph-HA)₂]₂

¹H-NMR (400 MHz, D₂O) δ = 1.1-1.7 (m, 33H, βH alanine, βγδH lysine), 2.3-2.6 (m, 48H, -CO-CH₂-CH₂-CO- succinic acid), 2.9-3.9 (m, 282H, -CH₂- PEHA, βH histidine, εH lysine), 3.9-4.3 (m, 8H, αH alanine, αH lysine), 4.5-4.7 (m, 18H, αH histidine), 7.1-7.4 (m, 18H, Ar-H histidine), 8.5-8.7 (s, 18H, Ar-H histidine).

Oligomer **608** / Sequence (C -> N): AK[AK(A-Sph-A-Sph-A-Sph-AC)₂]₂

¹H-NMR (400 MHz, D₂O) δ = 1.2-1.5 (m, 75H, βH alanine, βγδH lysine), 2.4-2.6 (m, 48H, -CO-CH₂-CH₂-CO- succinic acid), 3.0-3.8 (m, 254H, -CH₂- PEHA, βH cysteine, εH lysine), 4.0-4.4 (m, 26 H, αH alanine, αH cysteine, αH lysine).

Oligomer **609** / Sequence (C -> N): AK[AK(A-Sph-A-Sph-A-Sph-AA)₂]₂

¹H-NMR (400 MHz, D₂O) δ = 1.2-1.6 (m, 87H, βH alanine, βγδH lysine), 2.4-2.6 (m, 48H, -CO-CH₂-CH₂-CO- succinic acid), 2.9-3.8 (m, 246H, -CH₂- PEHA, εH lysine), 3.9-4.4 (m, 26H, αH alanine, αH lysine).

Oligomer **610** / Sequence (C -> N): A-Gtt-A-Gtt-A-Gtt-A

$^1\text{H-NMR}$ (500 MHz, D_2O) δ = 1.2-1.6 (m, 12H, βH alanine), 1.7-2.1 (m, 6H, $-\text{CH}_2-\text{CH}_2-\text{CH}_2-$ glutaric acid), 2.2-2.4 (m, 12H, $-\text{CO}-\text{CH}_2-$ glutaric acid), 3.0-3.8 (m, 36H, $-\text{CH}_2-$ TETA), 4.0-4.4 (m, 4H, αH alanine).

ESI-MS: $[\text{M}+2\text{H}]^{2+}$ calcd for $\text{C}_{45}\text{H}_{88}\text{O}_{11}\text{N}_{16}$ 1030.6975; found 1030.6975.
 $[\text{M}+3\text{H}]^{3+}$ calcd for $\text{C}_{45}\text{H}_{88}\text{O}_{11}\text{N}_{16}$ 1031.7053; found 1031.7039.

Oligomer **611** / Sequence (C -> N): H-Gtt-H-Gtt-H-Gtt-H

$^1\text{H-NMR}$ (500 MHz, D_2O) δ = 1.6-1.9 (m, 6H, $-\text{CH}_2-\text{CH}_2-\text{CH}_2-$ glutaric acid), 2.0-2.4 (m, 12H, $-\text{CO}-\text{CH}_2-$ glutaric acid), 2.8-3.9 (m, 44H, $-\text{CH}_2-$ TETA, βH histidine), 4.2-4.7 (m, 4H, αH histidine), 7.2-7.5 (m, 4H, Ar-H histidine), 8.5-8.7 (m, 4H, Ar-H histidine).

ESI-MS: $[\text{M}+2\text{H}]^{2+}$ calcd for $\text{C}_{57}\text{H}_{96}\text{O}_{11}\text{N}_{24}$ 1294.7847; found 1294.7844.
 $[\text{M}+3\text{H}]^{3+}$ calcd for $\text{C}_{57}\text{H}_{96}\text{O}_{11}\text{N}_{24}$ 1295.7925; found 1295.7915.

Oligomer **612** / Sequence (C -> N): A-Stp-A-Stp-A-Stp-A

$^1\text{H-NMR}$ (500 MHz, D_2O) δ = 1.2-1.6 (m, 12H, βH alanine), 2.3-2.7 (m, 12H, $-\text{CO}-\text{CH}_2-\text{CH}_2-\text{CO}-$ succinic acid), 3.0-3.8 (m, 48H, $-\text{CH}_2-$ TEPA), 3.9-4.4 (m, 4H, αH alanine).

ESI-MS: $[\text{M}+2\text{H}]^{2+}$ calcd for $\text{C}_{48}\text{H}_{97}\text{O}_{11}\text{N}_{19}$ 1117.7771; found 1117.7766.
 $[\text{M}+3\text{H}]^{3+}$ calcd for $\text{C}_{48}\text{H}_{97}\text{O}_{11}\text{N}_{19}$ 1118.7850; found 1118.7840.

Oligomer **613** / Sequence (C -> N): H-Stp-H-Stp-H-Stp-H

$^1\text{H-NMR}$ (500 MHz, D_2O) δ = 2.3-2.7 (m, 12H, $-\text{CO}-\text{CH}_2-\text{CH}_2-\text{CO}-$ succinic acid), 2.9-3.8 (m, 56H, $-\text{CH}_2-$ TEPA, βH histidine), 4.2-4.7 (4H, αH histidine), 7.2-7.5 (d, 4H, Ar-H histidine), 8.5-8.7 (t, 4H, Ar-H histidine).

ESI-MS: $[\text{M}+2\text{H}]^{2+}$ calcd for $\text{C}_{60}\text{H}_{105}\text{O}_{11}\text{N}_{27}$ 1381.8643; found 1381.8640.
 $[\text{M}+3\text{H}]^{3+}$ calcd for $\text{C}_{60}\text{H}_{105}\text{O}_{11}\text{N}_{27}$ 1382.8722; found 1382.8710.

Oligomer **614** / Sequence (C -> N): A-Sph-A-Sph-A-Sph-A

$^1\text{H-NMR}$ (400 MHz, D_2O) $\delta = 1.1\text{-}1.5$ (m, 12H, βH alanine), 2.4-2.6 (m, 12H, $-\text{CO-CH}_2\text{-CH}_2\text{-CO-}$ succinic acid), 2.9-3.8 (m, 60H, $-\text{CH}_2\text{-}$ PEHA), 3.9-4.3 (m, 4H, αH alanine).

ESI-MS: $[\text{M}+2\text{H}]^{2+}$ calcd for $\text{C}_{54}\text{H}_{112}\text{O}_{11}\text{N}_{22}$ 1246.9037; found 1246.9034.

Oligomer **615** / Sequence (C -> N): H-Sph-H-Sph-H-Sph-H

$^1\text{H-NMR}$ (400 MHz, D_2O) $\delta = 2.3\text{-}2.6$ (m, 12H, $-\text{CO-CH}_2\text{-CH}_2\text{-CO-}$ succinic acid), 2.9-4.0 (m, 68H, $-\text{CH}_2\text{-}$ PEHA, βH histidine), 4.1-4.7 (m, 4H, αH histidine), 7.0-7.6 (d, 4H, Ar-H histidine), 8.4-8.8 (t, 4H, Ar-H histidine).

ESI-MS: $[\text{M}+2\text{H}]^{2+}$ calcd for $\text{C}_{66}\text{H}_{120}\text{O}_{11}\text{N}_{30}$ 1510.9910; found 1510.9914.
 $[\text{M}+3\text{H}]^{3+}$ calcd for $\text{C}_{66}\text{H}_{120}\text{O}_{11}\text{N}_{30}$ 1511.9988; found 1511.9979.

Oligomer **616** / Sequence (C -> N): A-(dPEG₂₄)₂-HK[H-(Stp-H)₄-C]₂

$^1\text{H-NMR}$ (400 MHz, D_2O) $\delta = 1.3\text{-}1.4$ (m, 9H, βH alanine, $\beta\gamma\delta\text{H}$ lysine), 2.2-2.7 (m, 36H, $-\text{CO-CH}_2\text{-CH}_2\text{-CO-}$ succinic acid, $-\text{CO-CH}_2\text{-}$ dPEG₂₄), 2.9-3.5 (m, 156H, $-\text{CH}_2\text{-}$ TEPA, βH cysteine, βH histidine, ϵH lysine), 3.6-3.7 (s, 200H, $-\text{CH}_2\text{-O-}$ dPEG₂₄, $-\text{CH}_2\text{-N-}$ dPEG₂₄), 4.2-4.3 (m, 4H, αH alanine, αH cysteine, αH lysine), 4.5-4.7 (m, 11H, αH histidine), 7.1-7.3 (m, 11H, Ar-H histidine), 8.4-8.7 (m, 11H, Ar-H histidine).

Oligomer **617** / Sequence (C -> N): KRPGKAKHG-(dPEG₂₄)₂-AK[A-(Stp-A)₄-C]₂

$^1\text{H-NMR}$ (400 MHz, D_2O) $\delta = 1.2\text{-}1.6$ (m, 60H, βH alanine, $\beta\gamma\delta\text{H}$ lysine), 2.3-2.7 (m, 36H, $-\text{CO-CH}_2\text{-CH}_2\text{-CO-}$ succinic acid, $-\text{CO-CH}_2\text{-}$ dPEG₂₄), 2.9-3.6 (m, 146H, $-\text{CH}_2\text{-}$ TEPA, βH arginine, βH cysteine, βH histidine, ϵH lysine, βH proline), 3.64 (s, 200H, $-\text{CH}_2\text{-O-}$ dPEG₂₄, $-\text{CH}_2\text{-N-}$ dPEG₂₄), 4.2-4.3 (m, 25H, αH alanine, αH arginine, αH cysteine, αH glycine, αH histidine, αH proline, αH lysine), 7.24 (s, 1H, Ar-H histidine), 8.5-8.6 (d, 1H, Ar-H histidine).

Oligomer **618** / Sequence (C -> N): KRPGKAKHG-(dPEG₂₄)₂-HK[H-(Stp-H)₄-C]₂

¹H-NMR (400 MHz, D₂O) δ = 1.1-1.6 (m, 27H, βH alanine, βγδH lysine), 2.3-2.7 (m, 36H, -CO-CH₂-CH₂-CO- succinic acid, -CO-CH₂- dPEG₂₄), 2.9-3.5 (m, 168H, -CH₂-TEPA, βH arginine, βH cysteine, βH histidine, εH lysine, βH proline), 3.64 (s, 200H, -CH₂-O- dPEG₂₄, -CH₂-N- dPEG₂₄), 4.2-4.3 (m, 13H, αH alanine, αH arginine, αH cysteine, αH glycine, αH lysine, αH proline), 4.6-4.7 (m, 12H, αH histidine), 7.1-7.4 (m, 12H, Ar-H histidine), 8.5-8.7 (m, 12H, Ar-H histidine).

Oligomer **619** / Sequence (C -> N): K[(dPEG₂₄)₂-FolA]-AK[A-(Stp-A)₄-C]₂

¹H-NMR (400 MHz, D₂O) δ = 1.1-1.5 (m, 45H, βH alanine, βγδH lysine), 1.8-2.0 (m, 4H, βγH glutamic acid), 2.3-2.6 (m, 36H, -CO-CH₂-CH₂-CO- succinic acid, -CO-CH₂-dPEG₂₄), 3.0-3.5 (m, 136H, -CH₂-TEPA, βH cysteine, εH lysine), 3.61 (s, 200H, -CH₂-O- dPEG₂₄, -CH₂-N- dPEG₂₄), 4.0-4.4 (m, 16H, αH alanine, αH cysteine, αH glutamic acid, αH lysine), 6.6-6.8 (d, 2H, pteronic acid), 7.5-7.7 (d, 2H, Ar-H pteronic acid), 8.71 (s, 1H, Ar-H pteronic acid).

Oligomer **620** / Sequence (C -> N): K[(dPEG₂₄)₂-FolA]-HK[H-(Stp-H)₄-C]₂

¹H-NMR (400 MHz, D₂O) δ = 1.0-1.5 (m, 12H, βγδH lysine), 1.8-2.2 (m, 4H, βγH glutamic acid), 2.3-2.6 (m, 36H, -CO-CH₂-CH₂-CO- succinic acid, -CO-CH₂- dPEG₂₄, βH glutamic acid), 2.8-3.5 (m, 158H, -CH₂-TEPA, βH cysteine, βH histidine, εH lysine), 3.61 (s, 196H, -CH₂-O- dPEG₂₄, -CH₂-N- dPEG₂₄), 4.1-4.7 (m, 16H, αH cysteine, αH glutamic acid, αH histidine, αH lysine), 6.7-6.8 (d, 2H, Ar-H pteronic acid), 7.1-7.3 (m, 11H, Ar-H histidine), 7.5-7.6 (d, 2H, Ar-H pteronic acid), 8.5-8.6 (d, 11H, Ar-H histidine), 8.71 (s, 1 H, Ar-H pteronic acid).

Oligomer **638** / Sequence (C -> N): K(dPEG₂₄-MTX)-K(Stp₄-C)₂

¹H-NMR (500 MHz, D₂O) δ = 1.5-1.7 (m, 12H, βγδH lysine), 2.2-2.6 (m, 4H, βγH glutamic acid) 2.5-2.7 (m, 34 H, -CO-CH₂-CH₂-CO- succinic acid, -CO-CH₂- dPEG₂₄), 3.1-3.6 (m, 136H, -CH₂-TEPA, βH cysteine, εH lysine), 3.7-3.8 (m, 98H, -CH₂-O- dPEG₂₄, -CH₂-N- dPEG₂₄), 4.2-4.5 (m, 5H, αH cysteine, αH glutamic acid, αH lysine), 6.9-7.1 (d, 2H, Ar-H MTX), 7.7-7.8 (m, 2H, Ar-H MTX), 8.82 (s, 1 H, Ar-H MTX).

Oligomer **639** / Sequence (C -> N): K(dPEG₂₄-E₂-MTX)-K(Stp₄-C)₂

¹H-NMR (500 MHz, D₂O) δ = 1.2-1.6 (m, 12H, βγδH lysine), 1.7-2.4 (m, 12H, βγH glutamic acid), 2.4-2.6 (m, 34 H, -CO-CH₂-CH₂-CO- succinic acid, -CO-CH₂-dPEG₂₄), 3.0-3.6 (m, 136H, -CH₂- TEPA, βH cysteine, εH lysine), 3.6-3.7 (m, 98H, -CH₂-O- dPEG₂₄, -CH₂-N- dPEG₂₄), 4.0-4.4 (m, 7H, αH cysteine, αH glutamic acid, αH lysine), 6.8-6.9 (m, 2H, Ar-H MTX), 7.6-7.7 (d, 2H, Ar-H MTX), 8.67 (s, 1H, Ar-H MTX).

Oligomer **640** / Sequence (C -> N): K(dPEG₂₄-E₄-MTX)-K(Stp₄-C)₂

¹H-NMR (500 MHz, D₂O) δ = 1.1-1.5 (m, 12H, βγδH lysine), 1.6-2.3 (m, 20H, βγH glutamic acid), 2.4-2.6 (m, 34 H, -CO-CH₂-CH₂-CO- succinic acid, -CO-CH₂-dPEG₂₄), 2.8-3.5 (m, 136H, -CH₂- TEPA, βH cysteine, εH lysine), 3.5-3.6 (m, 98H, -CH₂-O- dPEG₂₄, -CH₂-N- dPEG₂₄), 4.0-4.5 (m, 9H, αH cysteine, αH glutamic acid, αH lysine), 6.7-6.8 (d, 2H, Ar-H MTX), 7.5-7.7 (d, 2H, Ar-H MTX), 8.5-8.6 (d, 1H, Ar-H MTX).

Oligomer **641** / Sequence (C -> N): K(dPEG₂₄-E₆-MTX)-K(Stp₄-C)₂

¹H-NMR (500 MHz, D₂O) δ = 1.2-1.1 (m, 12H, βγδH lysine), 1.6-2.4 (m, 28H, βγH glutamic acid), 2.4-2.6 (s, 34 H, -CO-CH₂-CH₂-CO- succinic acid, -CO-CH₂-dPEG₂₄), 3.0-3.6 (m, 136H, -CH₂- TEPA, βH cysteine, εH lysine), 3.6-3.7 (d, 98H, -CH₂-O- dPEG₂₄, -CH₂-N- dPEG₂₄), 4.1-4.6 (m, 11H, αH cysteine, αH glutamic acid, αH lysine), 6.8-6.9 (d, 2H, Ar-H MTX), 7.6-7.7 (d, 2H, Ar-H MTX), 8.6-8.7 (s, 1H, Ar-H MTX).

Oligomer **651** / Sequence (C -> N): (GalNAcS)₃-dPEG₂₄-K(Stp₄-C)₂

¹H-NMR (500 MHz, D₂O) δ = 1.4-1.7 (m, 18H, βγδH lysine, βγH 5-mercaptopentanoic acid), 1.9-2.0 (s, 9H, -N-CO-CH₃ N-acetylgalactosamine), 2.2-2.8 (m, 58H, -CO-CH₂-CH₂-CO- succinic acid, -CO-CH₂-dPEG₂₄, αδH 5-mercaptopentanoic acid), 3.0-4.0 (m, 250H, -CH₂- TEPA, -CH₂-O- dPEG₂₄, βH cysteine, εH lysine, -CH-O- thiogalactosamine, -CH-N- thiogalactosamine, -CH₂-O- thiogalactosamine), 4.1-4.3 (m, 3H, αH lysine, αH cysteine), 4.4-4.5 (d, 3H, -S-CH- thiogalactosamine).

Oligomer **672** / Sequence (C -> N): K[(dPEG₂₄)₂-E₄-MTX]-HK[H-(Stp-H)₄-C]₂

¹H-NMR (400 MHz, D₂O) δ = 1.1-1.5 (m, 12H, βγδH lysine), 1.6-2.3 (m, 20H, βγH glutamic acid), 2.3-2.6 (m, 36 H, -CO-CH₂-CH₂-CO- succinic acid, -CO-CH₂-dPEG₂₄), 3.0-3.5 (m, 158H, -CH₂- TEPA, βH cysteine, εH lysine), 3.5-3.7 (d, 196H, -CH₂-O- dPEG₂₄, -CH₂-N- dPEG₂₄), 4.1-4.7 (m, 20H, αH cysteine, αH glutamic acid, αH histidine, αH lysine), 6.8-6.9 (d, 2H, Ar-H MTX), 7.2-7.3 (d, 11H, Ar-H histidine), 7.6-7.7 (d, 2H, Ar-H MTX), 8.5-8.6 (d, 11H, Ar-H histidine), 8.61 (s, 1H, Ar-H MTX).

Oligomer **694** / Sequence (C -> N): K[(dPEG₂₄)₂-HK(H-(Stp-H)₄-C)₂]-HHHIHDHRSLSK

¹H-NMR (400 MHz, D₂O) δ = 1.0-2.0 (m, 40H, βγH arginine, βγδH isoleucine, βγδH leucine, βγδH lysine), 2.4-2.6 (m, 36H, -CO-CH₂-CH₂-CO- succinic acid, -CO-CH₂-dPEG₂₄), 2.9-3.5 (m, 176H, -CH₂- TEPA, δH arginine, βH cysteine, βH histidine, εH lysine, βH serine), 3.62 (s, 196H, -CH₂-O- dPEG₂₄, -CH₂-N- dPEG₂₄), 3.9-4.7 (m, 27H, αH amino acids), 7.22 (s, 16H, Ar-H histidine), 8.56-8.57 (m, 16H, Ar-H histidine).

Oligomer **695** / Sequence (C -> N): K[(dPEG₂₄)₂-AK(A-(Stp-A)₄-C)₂]-HHHIHDHRSLSK

¹H-NMR (500 MHz, D₂O) δ = 1.0-2.0 (m, 73H, βH alanine, βγH arginine, βγδH isoleucine, βγδH leucine, βγδH lysine), 2.4-2.6 (m, 36H, -CO-CH₂-CH₂-CO- succinic acid, -CO-CH₂-dPEG₂₄), 2.9-3.6 (m, 154H, -CH₂- TEPA, δH arginine, βH cysteine, βH histidine, εH lysine, βH serine), 3.67 (s, 196H, -CH₂-O- dPEG₂₄, -CH₂-N- dPEG₂₄), 4.0-4.7 (m, 27H, αH amino acids), 7.25-7.30 (m, 5H, Ar-H histidine), 8.61 (s, 5H, Ar-H histidine).

Oligomer **696** / Sequence (C -> N): K[dPEG₂₄-K(Stp₄-C)₂]-AKLPPWHVSFLY

¹H-NMR (500 MHz, D₂O) δ = 1.0-1.9 (m, 53H, βH alanine, βγδH leucine, βγδH lysine, βγH proline, γH valine), 2.4-2.6 (m, 34H, -CO-CH₂-CH₂-CO- succinic acid, -CO-CH₂-dPEG₂₄), 2.9-3.5 (m, 152H, -CH₂- TEPA, βH cysteine, βH histidine, εH lysine, βH phenylalanine, δH proline, βH serine, βH tryptophane, βH tyrosine), 3.66 (s, 98H, -

CH₂-O- dPEG₂₄, -CH₂-N- dPEG₂₄), 4.0-4.6 (m, 16H, αH amino acids), 7.0-7.4 (m, 15H, Ar-H histidine, phenylalanine, tryptophane, tyrosine), 8.61 (s, 1H, Ar-H histidine).

Oligomer **697** / Sequence (C -> N): K[dPEG₂₄-K(Stp₄-C)₂]-HHISSKRDHHHL

¹H-NMR (400 MHz, D₂O) δ = 1.0-2.0 (m, 40H, βγH arginine, βγδH isoleucine, βγδH leucine, βγδH lysine), 2.4-2.6 (m, 34H, -CO-CH₂-CH₂-CO- succinic acid, -CO-CH₂-dPEG₂₄), 2.8-3.6 (m, 156H, -CH₂- TEPA, δH arginine, βH aspartate, βH cysteine, βH histidine, εH lysine, βH serine), 3.66 (s, 98H, -CH₂-O- dPEG₂₄, -CH₂-N- dPEG₂₄), 3.9-4.6 (m, 16H, αH amino acids), 7.24-7.25 (m, 5H, Ar-H histidine), 8.61 (s, 5H, Ar-H histidine).

Oligomer **698** / Sequence (C -> N): K[dPEG₂₄-K(Stp₄-C)₂]-SHLHIHDRHHSK

¹H-NMR (400 MHz, D₂O) δ = 1.0-2.0 (m, 40H, βγH arginine, βγδH isoleucine, βγδH leucine, βγδH lysine), 2.4-2.6 (m, 34H, -CO-CH₂-CH₂-CO- succinic acid, -CO-CH₂-dPEG₂₄), 2.8-3.6 (m, 156H, -CH₂- TEPA, δH arginine, βH aspartate, βH cysteine, βH histidine, εH lysine, βH serine), 3.66 (s, 98H, -CH₂-O- dPEG₂₄, -CH₂-N- dPEG₂₄), 3.9-4.6 (m, 16H, αH amino acids), 7.24-7.25 (m, 5H, Ar-H histidine), 8.61 (s, 5H, Ar-H histidine).

Oligomer **699** / Sequence (C -> N): K[dPEG₂₄-K(Stp₄-C)₂]-DSKHHLRHISHH

¹H-NMR (400 MHz, D₂O) δ = 1.0-2.0 (m, 40H, βγH arginine, βγδH isoleucine, βγδH leucine, βγδH lysine), 2.4-2.6 (m, 34H, -CO-CH₂-CH₂-CO- succinic acid, -CO-CH₂-dPEG₂₄), 2.8-3.6 (m, 156H, -CH₂- TEPA, δH arginine, βH aspartate, βH cysteine, βH histidine, εH lysine, βH serine), 3.66 (s, 98H, -CH₂-O- dPEG₂₄, -CH₂-N- dPEG₂₄), 3.9-4.6 (m, 16H, αH amino acids), 7.24-7.25 (m, 5H, Ar-H histidine), 8.61 (s, 5H, Ar-H histidine).

Oligomer **700** / Sequence (C -> N): K[dPEG₂₄-K(Stp₄-C)₂]-DSHSHLHHHIKR

¹H-NMR (400 MHz, D₂O) δ = 1.0-2.0 (m, 40H, βγH arginine, βγδH isoleucine, βγδH leucine, βγδH lysine), 2.4-2.6 (m, 34H, -CO-CH₂-CH₂-CO- succinic acid, -CO-CH₂-

dPEG₂₄), 2.8-3.6 (m, 156H, -CH₂- TEPA, δH arginine, βH aspartate, βH cysteine, βH histidine, εH lysine, βH serine), 3.66 (s, 98H, -CH₂-O- dPEG₂₄, -CH₂-N- dPEG₂₄), 3.9-4.6 (m, 16H, αH amino acids), 7.24-7.25 (m, 5H, Ar-H histidine), 8.61 (s, 5H, Ar-H histidine).

Oligomer **754** / Sequence (C -> N): AK(Gtp₄-C)₂

¹H-NMR (400 MHz, D₂O) δ = 1.3-1.5 (m, 9H, βH alanine, βγδH lysine), 1.7-1.9 (m, 16H, -CH₂-CH₂-CH₂- glutaric acid), 2.1-2.3 (m, 32H, -CO-CH₂- glutaric acid), 2.9-3.7 (m, 134H, -CH₂- TEPA, βH cysteine, εH lysine), 4.1-4.3 (m, 4H, αH alanine, αH cysteine, αH lysine).

Oligomer **755** / Sequence (C -> N): AK(IDAtp₄-C)₂

¹H-NMR (400 MHz, D₂O) δ = 1.3-1.6 (m, 9H, βH alanine, βγδH lysine), 3.1-3.6 (m, 134H, -CH₂- TEPA, βH cysteine, εH lysine), 3.8-4.0 (d, 32H, -CO-CH₂- IDA), 4.1-4.3 (m, 4H, αH alanine, αH cysteine, αH lysine).

Oligomer **756** / Sequence (C -> N): AK[(M-IDAtp)₄-C]₂

¹H-NMR (400 MHz, D₂O) δ = 1.3-1.5 (m, 9H, βH alanine, βγδH lysine), 2.9-3.0 (m, 24H, -CH₃ M-IDA), 3.0-3.8 (m, 134H, -CH₂- TEPA, βH cysteine, εH lysine), 4.0-4.1 (d, 32H, -CO-CH₂- M-IDA), 4.2-4.3 (m, 4H, αH alanine, αH cysteine, αH lysine).

Oligomer **757** / Sequence (C -> N): AK[(TFE-IDAtp)₄-C]₂

¹H-NMR (400 MHz, D₂O) δ = 1.3-1.5 (m, 9H, βH alanine, βγδH lysine), 2.9-3.9 (m, 182H, -CH₂- TEPA, βH cysteine, εH lysine, -CO-CH₂- TFE-IDA, -CH₂-CF₃ TFE-IDA), 4.1-4.3 (m, 4H, αH alanine, αH cysteine, αH lysine).

Oligomer **811** / Sequence (C -> N): A-3PAL-K[(3PAL-Stp)₄-3PAL-C]₂

¹H-NMR (400 MHz, D₂O) δ = 1.3-1.7 (m, 9H, βH alanine, βγδH lysine), 2.2-2.6 (m, 32H, -CO-CH₂-CH₂-CO- succinic acid), 2.8-3.7 (m, 156H, -CH₂- TEPA, βH cysteine, βH 3-(3-pyridyl)-alanine, εH lysine), 4.0-4.3 (m, 4H, αH alanine, αH cysteine, αH

lysine), 7.9-8.0 (m, 11H, Ar-H 3-(3-pyridyl)-alanine), 8.4-8.5 (m, 11H, Ar-H 3-(3-pyridyl)-alanine), 8.6-8.7 (d, 22H, Ar-H 3-(3-pyridyl)-alanine).

Oligomer **812** / Sequence (C -> N): A-4PAL-K[(4PAL-Stp)₄-4Pal-C]₂

¹H-NMR (400 MHz, D₂O) δ = 1.3-1.7 (m, 9H, βH alanine, βγδH lysine), 2.2-2.5 (m, 32H, -CO-CH₂-CH₂-CO- succinic acid), 2.8-3.7 (m, 156H, -CH₂- TEPA, βH cysteine, βH 3-(4-pyridyl)-alanine, εH lysine), 4.1-4.3 (m, 4H, αH alanine, αH cysteine, αH lysine), 7.8-7.9 (d, 22H, Ar-H 3-(4-pyridyl)-alanine), 8.6-8.7 (d, 22H, Ar-H 3-(4-pyridyl)-alanine).

Oligomer **813** / Sequence (C -> N): AHK[(H-Stp)₄-HC]₂

¹H-NMR (400 MHz, D₂O) δ = 1.2-1.7 (m, 9H, βH alanine, βγδH lysine), 2.3-2.6 (m, 32H, -CO-CH₂-CH₂-CO- succinic acid), 2.8-3.7 (m, 156H, -CH₂- TEPA, βH cysteine, βH histidine, εH lysine), 4.1-4.3 (m, 4H, αH alanine, αH cysteine, αH lysine), 4.5-4.6 (m, 11H, αH histidine), 7.2-7.3 (d, 11H, Ar-H histidine), 8.55 (s, 11H, Ar-H histidine).

Oligomer **814** / Sequence (C -> N): AK[(H-Stp)₄-C]₂

¹H-NMR (400 MHz, D₂O) δ = 1.3-1.8 (m, 9H, βH alanine, βγδH lysine), 2.3-2.6 (m, 32H, -CO-CH₂-CH₂-CO- succinic acid), 2.9-3.7 (m, 150H, -CH₂- TEPA, βH cysteine, βH histidine, εH lysine), 4.0-4.4 (m, 4H, αH alanine, αH cysteine, αH lysine), 4.5-4.6 (m, 8H, αH histidine), 7.2-7.3 (s, 8H, Ar-H histidine), 8.5-8.6 (s, 8H, Ar-H histidine).

Oligomer **815** / Sequence (C -> N): AK[(Gtp-Gtt)₂-Gtp-C]₂

¹H-NMR (400 MHz, D₂O) δ = 1.3-1.5 (m, 9H, βH alanine, βγδH lysine), 1.6-1.8 (m, 20H, -CH₂-CH₂-CH₂- glutaric acid), 2.1-2.3 (m, 40H, -CO-CH₂- glutaric acid), 2.8-3.7 (m, 150H, -CH₂- TEPA, -CH₂- TETA, βH cysteine, εH lysine), 4.1-4.3 (m, 4H, αH alanine, αH cysteine, αH lysine).

Oligomer **816** / Sequence (C -> N): AK[(Gtt-Gtp)₂-Gtt-C]₂

¹H-NMR (400 MHz, D₂O) δ = 1.3-1.5 (m, 9H, βH alanine, βγδH lysine), 1.7-1.9 (m, 20H, -CH₂-CH₂-CH₂- glutaric acid), 2.1-2.3 (m, 40H, -CO-CH₂- glutaric acid), 2.9-3.7 (m, 142H, -CH₂- TEPA, -CH₂- TETA, βH cysteine, εH lysine), 4.1-4.3 (m, 4H, αH alanine, αH cysteine, αH lysine).

Oligomer **817** / Sequence (C -> N): AK(Gtt₄-C)₂

¹H-NMR (400 MHz, D₂O) δ = 1.2-1.5 (m, 9H, βH alanine, βγδH lysine), 1.7-1.9 (m, 16H, -CH₂-CH₂-CH₂- glutaric acid), 2.1-2.3 (m, 32H, -CO-CH₂- glutaric acid), 2.9-3.7 (m, 102H, -CH₂- TETA, βH cysteine, εH lysine), 4.1-4.3 (m, 4H, αH alanine, αH cysteine, αH lysine).

7 References

- [1] J.D. Watson, F.H. Crick, Molecular structure of nucleic acids; a structure for deoxyribose nucleic acid, *Nature*, 171 (1953) 737-738.
- [2] M.H. Wilkins, A.R. Stokes, H.R. Wilson, Molecular structure of deoxyribose nucleic acids, *Nature*, 171 (1953) 738-740.
- [3] R.E. Franklin, R.G. Gosling, Molecular configuration in sodium thymonucleate, *Nature*, 171 (1953) 740-741.
- [4] F.H. Crick, On protein synthesis, *Symposia of the Society for Experimental Biology*, 12 (1958) 138-163.
- [5] F.H. Crick, The origin of the genetic code, *Journal of molecular biology*, 38 (1968) 367-379.
- [6] F. Crick, Central dogma of molecular biology, *Nature*, 227 (1970) 561-563.
- [7] E. Duncan, M. Brown, E.M. Shore, The revolution in human monogenic disease mapping, *Genes*, 5 (2014) 792-803.
- [8] N. Naidoo, Y. Pawitan, R. Soong, D.N. Cooper, C.S. Ku, Human genetics and genomics a decade after the release of the draft sequence of the human genome, *Human genomics*, 5 (2011) 577-622.
- [9] R. Sameek, A.M. Chinnaiyan, Translating genomics for precision cancer medicine, *Annual review of genomics and human genetics*, 15 (2014) 395-415.
- [10] T. Friedmann, R. Roblin, Gene therapy for human genetic disease?, *Science*, 175 (1972) 949-955.
- [11] R.C. Mulligan, The basic science of gene therapy, *Science*, 260 (1993) 926-932.
- [12] Gene Therapy Clinical Trials Worldwide Database provided by the Journal of Gene Medicine, <http://www.wiley.com/legacy/wileychi/genmed/clinical/>, June 2014.
- [13] T. Wirth, N. Parker, S. Yla-Herttuala, History of gene therapy, *Gene*, 525 (2013) 162-169.
- [14] S.R. Eddy, Non-coding RNA genes and the modern RNA world, *Nature reviews. Genetics*, 2 (2001) 919-929.
- [15] J. Sana, P. Faltejskova, M. Svoboda, O. Slaby, Novel classes of non-coding RNAs and cancer, *Journal of translational medicine*, 10 (2012) 103.
- [16] L. He, G.J. Hannon, MicroRNAs: small RNAs with a big role in gene regulation, *Nature reviews. Genetics*, 5 (2004) 522-531.
- [17] P.S. Ray, J. Jia, P. Yao, M. Majumder, M. Hatzoglou, P.L. Fox, A stress-responsive RNA switch regulates VEGFA expression, *Nature*, 457 (2009) 915-919.
- [18] A. Serganov, D.J. Patel, Ribozymes, riboswitches and beyond: regulation of gene expression without proteins, *Nature reviews. Genetics*, 8 (2007) 776-790.
- [19] A. Teixeira, A. Tahiri-Alaoui, S. West, B. Thomas, A. Ramadass, I. Martianov, M. Dye, W. James, N.J. Proudfoot, A. Akoulitchev, Autocatalytic RNA cleavage in the human beta-globin pre-mRNA promotes transcription termination, *Nature*, 432 (2004) 526-530.
- [20] S. Valadkhan, snRNAs as the catalysts of pre-mRNA splicing, *Current opinion in chemical biology*, 9 (2005) 603-608.
- [21] V. Pelechano, L.M. Steinmetz, Gene regulation by antisense transcription, *Nature reviews. Genetics*, 14 (2013) 880-893.
- [22] D. Moazed, Small RNAs in transcriptional gene silencing and genome defence, *Nature*, 457 (2009) 413-420.
- [23] P. Nissen, J. Hansen, N. Ban, P.B. Moore, T.A. Steitz, The structural basis of ribosome activity in peptide bond synthesis, *Science*, 289 (2000) 920-930.

- [24] T. Bratkovic, B. Rogelj, The many faces of small nucleolar RNAs, *Biochimica et biophysica acta*, 1839 (2014) 438-443.
- [25] E. Cusanelli, C.A. Romero, P. Chartrand, Telomeric noncoding RNA TERRA is induced by telomere shortening to nucleate telomerase molecules at short telomeres, *Molecular cell*, 51 (2013) 780-791.
- [26] M.S. Kormann, G. Hasenpusch, M.K. Aneja, G. Nica, A.W. Flemmer, S. Herber-Jonat, M. Huppmann, L.E. Mays, M. Illenyi, A. Schams, M. Griese, I. Bittmann, R. Handgretinger, D. Hartl, J. Rosenecker, C. Rudolph, Expression of therapeutic proteins after delivery of chemically modified mRNA in mice, *Nature biotechnology*, 29 (2011) 154-157.
- [27] N. Bangel-Ruland, K. Tomczak, E. Fernandez Fernandez, G. Leier, B. Leciejewski, C. Rudolph, J. Rosenecker, W.M. Weber, Cystic fibrosis transmembrane conductance regulator-mRNA delivery: a novel alternative for cystic fibrosis gene therapy, *The journal of gene medicine*, 15 (2013) 414-426.
- [28] Y. Wang, H.H. Su, Y. Yang, Y. Hu, L. Zhang, P. Blancafort, L. Huang, Systemic delivery of modified mRNA encoding herpes simplex virus 1 thymidine kinase for targeted cancer gene therapy, *Molecular therapy : the journal of the American Society of Gene Therapy*, 21 (2013) 358-367.
- [29] J.B. Opalinska, A.M. Gewirtz, Nucleic-acid therapeutics: basic principles and recent applications, *Nature reviews. Drug discovery*, 1 (2002) 503-514.
- [30] A. Fire, S. Xu, M.K. Montgomery, S.A. Kostas, S.E. Driver, C.C. Mello, Potent and specific genetic interference by double-stranded RNA in *Caenorhabditis elegans*, *Nature*, 391 (1998) 806-811.
- [31] S.M. Elbashir, J. Harborth, W. Lendeckel, A. Yalcin, K. Weber, T. Tuschl, Duplexes of 21-nucleotide RNAs mediate RNA interference in cultured mammalian cells, *Nature*, 411 (2001) 494-498.
- [32] A. Grunweller, R.K. Hartmann, RNA interference as a gene-specific approach for molecular medicine, *Current medicinal chemistry*, 12 (2005) 3143-3161.
- [33] R. Kole, A.R. Krainer, S. Altman, RNA therapeutics: beyond RNA interference and antisense oligonucleotides, *Nature reviews. Drug discovery*, 11 (2012) 125-140.
- [34] V.J. Schuller, S. Heidegger, N. Sandholzer, P.C. Nickels, N.A. Suhartha, S. Endres, C. Bourquin, T. Liedl, Cellular immunostimulation by CpG-sequence-coated DNA origami structures, *ACS nano*, 5 (2011) 9696-9702.
- [35] M. Sommariva, M. de Cesare, A. Meini, A. Cataldo, N. Zaffaroni, E. Tagliabue, A. Balsari, High efficacy of CpG-ODN, cetuximab and cisplatin combination for very advanced ovarian xenograft tumors, *Journal of translational medicine*, 11 (2013) 25.
- [36] J.E. Talmadge, J. Adams, H. Phillips, M. Collins, B. Lenz, M. Schneider, M. Chirigos, Immunotherapeutic potential in murine tumor models of polyinosinic-polycytidylic acid and poly-L-lysine solubilized by carboxymethylcellulose, *Cancer research*, 45 (1985) 1066-1072.
- [37] I.F. Pollack, R.I. Jakacki, L.H. Butterfield, R.L. Hamilton, A. Panigrahy, D.M. Potter, A.K. Connelly, S.A. Dibrige, T.L. Whiteside, H. Okada, Antigen-specific immune responses and clinical outcome after vaccination with glioma-associated antigen peptides and polyinosinic-polycytidylic acid stabilized by lysine and carboxymethylcellulose in children with newly diagnosed malignant brainstem and nonbrainstem gliomas, *Journal of clinical oncology : official journal of the American Society of Clinical Oncology*, 32 (2014) 2050-2058.
- [38] A. Levitzki, Targeting the Immune System to Fight Cancer Using Chemical Receptor Homing Vectors Carrying Polyinosine/Cytosine (PolyIC), *Frontiers in oncology*, 2 (2012) 4.

- [39] A. Shir, M. Ogris, E. Wagner, A. Levitzki, EGF receptor-targeted synthetic double-stranded RNA eliminates glioblastoma, breast cancer, and adenocarcinoma tumors in mice, *PLoS medicine*, 3 (2006) e6.
- [40] A. Shir, M. Ogris, W. Roedl, E. Wagner, A. Levitzki, EGFR-homing dsRNA activates cancer-targeted immune response and eliminates disseminated EGFR-overexpressing tumors in mice, *Clinical cancer research : an official journal of the American Association for Cancer Research*, 17 (2011) 1033-1043.
- [41] N. Harashima, T. Minami, H. Uemura, M. Harada, Transfection of poly(I:C) can induce reactive oxygen species-triggered apoptosis and interferon-beta-mediated growth arrest in human renal cell carcinoma cells via innate adjuvant receptors and the 2-5A system, *Molecular cancer*, 13 (2014) 217.
- [42] C. Tuerk, L. Gold, Systematic evolution of ligands by exponential enrichment: RNA ligands to bacteriophage T4 DNA polymerase, *Science*, 249 (1990) 505-510.
- [43] A.D. Ellington, J.W. Szostak, In vitro selection of RNA molecules that bind specific ligands, *Nature*, 346 (1990) 818-822.
- [44] A.D. Keefe, S. Pai, A. Ellington, Aptamers as therapeutics, *Nature reviews. Drug discovery*, 9 (2010) 537-550.
- [45] D.H. Bunka, O. Platonova, P.G. Stockley, Development of aptamer therapeutics, *Current opinion in pharmacology*, 10 (2010) 557-562.
- [46] J.C. Burnett, J.J. Rossi, RNA-based therapeutics: current progress and future prospects, *Chemistry & biology*, 19 (2012) 60-71.
- [47] E. Wagner, Biomaterials in RNAi therapeutics: quo vadis?, *Biomaterials Science*, 1 (2013) 804-809.
- [48] P.R. Berthold, T. Shiraishi, P.E. Nielsen, Cellular delivery and antisense effects of peptide nucleic acid conjugated to polyethyleneimine via disulfide linkers, *Bioconjugate chemistry*, 21 (2010) 1933-1938.
- [49] Y. Aoki, T. Nagata, T. Yokota, A. Nakamura, M.J. Wood, T. Partridge, S. Takeda, Highly efficient in vivo delivery of PMO into regenerating myotubes and rescue in laminin-alpha2 chain-null congenital muscular dystrophy mice, *Human molecular genetics*, 22 (2013) 4914-4928.
- [50] E. Wagner, Nucleic Acid Medicines: The Polymer Option, in: S. Kobayashi, K. Müllen (Eds.) *Encyclopedia of Polymeric Nanomaterials*, Springer Berlin Heidelberg, 2014, pp. 1-7.
- [51] D.W. Pack, A.S. Hoffman, S. Pun, P.S. Stayton, Design and development of polymers for gene delivery, *Nature reviews. Drug discovery*, 4 (2005) 581-593.
- [52] H. Yin, R.L. Kanasty, A.A. Eltoukhy, A.J. Vegas, J.R. Dorkin, D.G. Anderson, Non-viral vectors for gene-based therapy, *Nature reviews. Genetics*, 15 (2014) 541-555.
- [53] E. Mastrobattista, M.A. van der Aa, W.E. Hennink, D.J. Crommelin, Artificial viruses: a nanotechnological approach to gene delivery, *Nature reviews. Drug discovery*, 5 (2006) 115-121.
- [54] G.F. Walker, C. Fella, J. Pelisek, J. Fahrmeir, S. Boeckle, M. Ogris, E. Wagner, Toward synthetic viruses: endosomal pH-triggered deshielding of targeted polyplexes greatly enhances gene transfer in vitro and in vivo, *Molecular therapy : the journal of the American Society of Gene Therapy*, 11 (2005) 418-425.
- [55] E. Wagner, Polymers for siRNA delivery: inspired by viruses to be targeted, dynamic, and precise, *Accounts of chemical research*, 45 (2012) 1005-1013.
- [56] S. Uzun, O. Akdemir, G. Hasenpusch, C. Maucksch, M.M. Golas, B. Sander, H. Stark, R. Imker, J.F. Lutz, C. Rudolph, Characterization of tailor-made copolymers of oligo(ethylene glycol) methyl ether methacrylate and N,N-dimethylaminoethyl

methacrylate as nonviral gene transfer agents: influence of macromolecular structure on gene vector particle properties and transfection efficiency, *Biomacromolecules*, 11 (2010) 39-50.

[57] J.C. Kasper, D. Schaffert, M. Ogris, E. Wagner, W. Friess, The establishment of an up-scaled micro-mixer method allows the standardized and reproducible preparation of well-defined plasmid/LPEI polyplexes, *European journal of pharmaceuticals and biopharmaceutics : official journal of Arbeitsgemeinschaft fur Pharmazeutische Verfahrenstechnik e.V.*, 77 (2011) 182-185.

[58] J.C. Kasper, D. Schaffert, M. Ogris, E. Wagner, W. Friess, Development of a lyophilized plasmid/LPEI polyplex formulation with long-term stability--A step closer from promising technology to application, *Journal of controlled release : official journal of the Controlled Release Society*, 151 (2011) 246-255.

[59] V.A. Bloomfield, DNA condensation by multivalent cations, *Biopolymers*, 44 (1997) 269-282.

[60] P.L. Felgner, Y. Barenholz, J.P. Behr, S.H. Cheng, P. Cullis, L. Huang, J.A. Jessee, L. Seymour, F. Szoka, A.R. Thierry, E. Wagner, G. Wu, Nomenclature for synthetic gene delivery systems, *Human gene therapy*, 8 (1997) 511-512.

[61] E. Wagner, M. Zenke, M. Cotten, H. Beug, M.L. Birnstiel, Transferrin-polycation conjugates as carriers for DNA uptake into cells, *Proceedings of the National Academy of Sciences of the United States of America*, 87 (1990) 3410-3414.

[62] P. van de Wetering, J.Y. Cherng, H. Talsma, D.J. Crommelin, W.E. Hennink, 2-(Dimethylamino)ethyl methacrylate based (co)polymers as gene transfer agents, *Journal of controlled release : official journal of the Controlled Release Society*, 53 (1998) 145-153.

[63] P. Erbacher, S. Zou, T. Bettinger, A.M. Steffan, J.S. Remy, Chitosan-based vector/DNA complexes for gene delivery: biophysical characteristics and transfection ability, *Pharmaceutical research*, 15 (1998) 1332-1339.

[64] I. Chemin, D. Moradpour, S. Wieland, W.B. Offensperger, E. Walter, J.P. Behr, H.E. Blum, Liver-directed gene transfer: a linear polyethylenimine derivative mediates highly efficient DNA delivery to primary hepatocytes in vitro and in vivo, *Journal of viral hepatitis*, 5 (1998) 369-375.

[65] H. Uchida, K. Miyata, M. Oba, T. Ishii, T. Suma, K. Itaka, N. Nishiyama, K. Kataoka, Odd-even effect of repeating aminoethylene units in the side chain of N-substituted polyaspartamides on gene transfection profiles, *Journal of the American Chemical Society*, 133 (2011) 15524-15532.

[66] O. Boussif, F. Lezoualc'h, M.A. Zanta, M.D. Mergny, D. Scherman, B. Demeneix, J.P. Behr, A versatile vector for gene and oligonucleotide transfer into cells in culture and in vivo: polyethylenimine, *Proceedings of the National Academy of Sciences of the United States of America*, 92 (1995) 7297-7301.

[67] J. Haensler, F.C. Szoka, Jr., Polyamidoamine cascade polymers mediate efficient transfection of cells in culture, *Bioconjugate chemistry*, 4 (1993) 372-379.

[68] H.S. Choi, W. Liu, F. Liu, K. Nasr, P. Misra, M.G. Bawendi, J.V. Frangioni, Design considerations for tumour-targeted nanoparticles, *Nature nanotechnology*, 5 (2010) 42-47.

[69] F. Yuan, M. Dellian, D. Fukumura, M. Leunig, D.A. Berk, V.P. Torchilin, R.K. Jain, Vascular permeability in a human tumor xenograft: molecular size dependence and cutoff size, *Cancer research*, 55 (1995) 3752-3756.

[70] B. Smrekar, L. Wightman, M.F. Wolschek, C. Lichtenberger, R. Ruzicka, M. Ogris, W. Rodl, M. Kurska, E. Wagner, R. Kircheis, Tissue-dependent factors affect gene delivery to tumors in vivo, *Gene therapy*, 10 (2003) 1079-1088.

- [71] H. Cabral, Y. Matsumoto, K. Mizuno, Q. Chen, M. Murakami, M. Kimura, Y. Terada, M.R. Kano, K. Miyazono, M. Uesaka, N. Nishiyama, K. Kataoka, Accumulation of sub-100 nm polymeric micelles in poorly permeable tumours depends on size, *Nature nanotechnology*, 6 (2011) 815-823.
- [72] M. Piest, J.F. Engbersen, Effects of charge density and hydrophobicity of poly(amido amine)s for non-viral gene delivery, *Journal of controlled release : official journal of the Controlled Release Society*, 148 (2010) 83-90.
- [73] D. Oupicky, M. Ogris, K.A. Howard, P.R. Dash, K. Ulbrich, L.W. Seymour, Importance of lateral and steric stabilization of polyelectrolyte gene delivery vectors for extended systemic circulation, *Molecular therapy : the journal of the American Society of Gene Therapy*, 5 (2002) 463-472.
- [74] M. Neu, O. Germershaus, S. Mao, K.H. Voigt, M. Behe, T. Kissel, Crosslinked nanocarriers based upon poly(ethylene imine) for systemic plasmid delivery: in vitro characterization and in vivo studies in mice, *Journal of controlled release : official journal of the Controlled Release Society*, 118 (2007) 370-380.
- [75] V. Russ, T. Fröhlich, Y. Li, A. Halama, M. Ogris, E. Wagner, Improved in vivo gene transfer into tumor tissue by stabilization of pseudodendritic oligoethylenimine-based polyplexes, *The journal of gene medicine*, 12 (2010) 180-193.
- [76] T. Fröhlich, D. Edinger, V. Russ, E. Wagner, Stabilization of polyplexes via polymer crosslinking for efficient siRNA delivery, *European journal of pharmaceutical sciences : official journal of the European Federation for Pharmaceutical Sciences*, 47 (2012) 914-920.
- [77] A. Philipp, X. Zhao, P. Tarcha, E. Wagner, A. Zintchenko, Hydrophobically modified oligoethylenimines as highly efficient transfection agents for siRNA delivery, *Bioconjugate chemistry*, 20 (2009) 2055-2061.
- [78] S.K. Filippov, C. Konak, P. Kopeckova, L. Starovoytova, M. Spirkova, P. Stepanek, Effect of hydrophobic interactions on properties and stability of DNA-polyelectrolyte complexes, *Langmuir : the ACS journal of surfaces and colloids*, 26 (2010) 4999-5006.
- [79] C. Troiber, D. Edinger, P. Kos, L. Schreiner, R. Klager, A. Herrmann, E. Wagner, Stabilizing effect of tyrosine trimers on pDNA and siRNA polyplexes, *Biomaterials*, 34 (2013) 1624-1633.
- [80] H. Herweijer, J.A. Wolff, Gene therapy progress and prospects: hydrodynamic gene delivery, *Gene therapy*, 14 (2007) 99-107.
- [81] D.L. Lewis, J.A. Wolff, Systemic siRNA delivery via hydrodynamic intravascular injection, *Advanced drug delivery reviews*, 59 (2007) 115-123.
- [82] M. Ogris, P. Steinlein, S. Carotta, S. Brunner, E. Wagner, DNA/polyethylenimine transfection particles: influence of ligands, polymer size, and PEGylation on internalization and gene expression, *AAPS pharmSci*, 3 (2001) E21.
- [83] K. de Bruin, N. Ruthardt, K. von Gersdorff, R. Bausinger, E. Wagner, M. Ogris, C. Bräuchle, Cellular dynamics of EGF receptor-targeted synthetic viruses, *Molecular therapy : the journal of the American Society of Gene Therapy*, 15 (2007) 1297-1305.
- [84] C. Munoz-Pinedo, N. El Mjiyad, J.E. Ricci, Cancer metabolism: current perspectives and future directions, *Cell death & disease*, 3 (2012) e248.
- [85] C.P. Leamon, P.S. Low, Delivery of macromolecules into living cells: a method that exploits folate receptor endocytosis, *Proceedings of the National Academy of Sciences of the United States of America*, 88 (1991) 5572-5576.
- [86] P.S. Low, W.A. Henne, D.D. Doorneweerd, Discovery and development of folic-acid-based receptor targeting for imaging and therapy of cancer and inflammatory diseases, *Accounts of chemical research*, 41 (2008) 120-129.

- [87] M. Kursa, G.F. Walker, V. Roessler, M. Ogris, W. Roedl, R. Kircheis, E. Wagner, Novel shielded transferrin-polyethylene glycol-polyethylenimine/DNA complexes for systemic tumor-targeted gene transfer, *Bioconjugate chemistry*, 14 (2003) 222-231.
- [88] M.E. Davis, The first targeted delivery of siRNA in humans via a self-assembling, cyclodextrin polymer-based nanoparticle: from concept to clinic, *Molecular pharmaceuticals*, 6 (2009) 659-668.
- [89] D. Schaffert, M. Kiss, W. Rodl, A. Shir, A. Levitzki, M. Ogris, E. Wagner, Poly(I:C)-mediated tumor growth suppression in EGF-receptor overexpressing tumors using EGF-polyethylene glycol-linear polyethylenimine as carrier, *Pharmaceutical research*, 28 (2011) 731-741.
- [90] H. Yu, Y. Nie, C. Dohmen, Y. Li, E. Wagner, Epidermal growth factor-PEG functionalized PAMAM-pentaethylenehexamine dendron for targeted gene delivery produced by click chemistry, *Biomacromolecules*, 12 (2011) 2039-2047.
- [91] K. Kunath, T. Merdan, O. Hegener, H. Haberlein, T. Kissel, Integrin targeting using RGD-PEI conjugates for in vitro gene transfer, *The journal of gene medicine*, 5 (2003) 588-599.
- [92] F.M. Mickler, Y. Vachutinsky, M. Oba, K. Miyata, N. Nishiyama, K. Kataoka, C. Bräuchle, N. Ruthardt, Effect of integrin targeting and PEG shielding on polyplex micelle internalization studied by live-cell imaging, *Journal of controlled release : official journal of the Controlled Release Society*, 156 (2011) 364-373.
- [93] Y. Sakurai, H. Hatakeyama, Y. Sato, M. Hyodo, H. Akita, N. Ohga, K. Hida, H. Harashima, RNAi-mediated gene knockdown and anti-angiogenic therapy of RCCs using a cyclic RGD-modified liposomal-siRNA system, *Journal of controlled release : official journal of the Controlled Release Society*, 173 (2014) 110-118.
- [94] M. Spiess, The asialoglycoprotein receptor: a model for endocytic transport receptors, *Biochemistry*, 29 (1990) 10009-10018.
- [95] C. Plank, K. Zatloukal, M. Cotten, K. Mechtler, E. Wagner, Gene transfer into hepatocytes using asialoglycoprotein receptor mediated endocytosis of DNA complexed with an artificial tetra-antennary galactose ligand, *Bioconjugate chemistry*, 3 (1992) 533-539.
- [96] A. Akinc, W. Querbes, S. De, J. Qin, M. Frank-Kamenetsky, K.N. Jayaprakash, M. Jayaraman, K.G. Rajeev, W.L. Cantley, J.R. Dorkin, J.S. Butler, L. Qin, T. Racie, A. Sprague, E. Fava, A. Zeigerer, M.J. Hope, M. Zerial, D.W. Sah, K. Fitzgerald, M.A. Tracy, M. Manoharan, V. Kotliansky, A. Fougerolles, M.A. Maier, Targeted delivery of RNAi therapeutics with endogenous and exogenous ligand-based mechanisms, *Molecular therapy : the journal of the American Society of Gene Therapy*, 18 (2010) 1357-1364.
- [97] T.P. Prakash, M.J. Graham, J. Yu, R. Carty, A. Low, A. Chappell, K. Schmidt, C. Zhao, M. Aghajan, H.F. Murray, S. Riney, S.L. Booten, S.F. Murray, H. Gaus, J. Crosby, W.F. Lima, S. Guo, B.P. Monia, E.E. Swayze, P.P. Seth, Targeted delivery of antisense oligonucleotides to hepatocytes using triantennary N-acetyl galactosamine improves potency 10-fold in mice, *Nucleic acids research*, 42 (2014) 8796-8807.
- [98] F.M. Mickler, L. Mockl, N. Ruthardt, M. Ogris, E. Wagner, C. Bräuchle, Tuning nanoparticle uptake: live-cell imaging reveals two distinct endocytosis mechanisms mediated by natural and artificial EGFR targeting ligand, *Nano letters*, 12 (2012) 3417-3423.
- [99] S. Hong, P.R. Leroueil, I.J. Majoros, B.G. Orr, J.R. Baker, Jr., M.M. Banaszak Holl, The binding avidity of a nanoparticle-based multivalent targeted drug delivery platform, *Chemistry & biology*, 14 (2007) 107-115.

- [100] J.E. Silpe, M. Sumit, T.P. Thomas, B. Huang, A. Kotlyar, M.A. van Dongen, M.M. Banaszak Holl, B.G. Orr, S.K. Choi, Avidity modulation of folate-targeted multivalent dendrimers for evaluating biophysical models of cancer targeting nanoparticles, *ACS chemical biology*, 8 (2013) 2063-2071.
- [101] R. Hennig, K. Pollinger, A. Vesper, M. Breunig, A. Goepferich, Nanoparticle multivalency counterbalances the ligand affinity loss upon PEGylation, *Journal of controlled release : official journal of the Controlled Release Society*, 194C (2014) 20-27.
- [102] S. Kakimoto, T. Moriyama, T. Tanabe, S. Shinkai, T. Nagasaki, Dual-ligand effect of transferrin and transforming growth factor alpha on polyethyleneimine-mediated gene delivery, *Journal of controlled release : official journal of the Controlled Release Society*, 120 (2007) 242-249.
- [103] D. Li, G.P. Tang, J.Z. Li, Y. Kong, H.L. Huang, L.J. Min, J. Zhou, F.P. Shen, Q.Q. Wang, H. Yu, Dual-targeting non-viral vector based on polyethylenimine improves gene transfer efficiency, *Journal of biomaterials science. Polymer edition*, 18 (2007) 545-560.
- [104] Y. Nie, D. Schaffert, W. Rodl, M. Ogris, E. Wagner, M. Gunther, Dual-targeted polyplexes: one step towards a synthetic virus for cancer gene therapy, *Journal of controlled release : official journal of the Controlled Release Society*, 152 (2011) 127-134.
- [105] J.M. Rabanel, P. Hildgen, X. Banquy, Assessment of PEG on polymeric particles surface, a key step in drug carrier translation, *Journal of controlled release : official journal of the Controlled Release Society*, 185 (2014) 71-87.
- [106] M.G. Saifer, L.D. Williams, M.A. Sobczyk, S.J. Michaels, M.R. Sherman, Selectivity of binding of PEGs and PEG-like oligomers to anti-PEG antibodies induced by methoxyPEG-proteins, *Molecular immunology*, 57 (2014) 236-246.
- [107] E.M. Pelegri-O'Day, E.W. Lin, H.D. Maynard, Therapeutic Protein-Polymer Conjugates: Advancing Beyond PEGylation, *Journal of the American Chemical Society*, (2014).
- [108] M. Noga, D. Edinger, W. Rodl, E. Wagner, G. Winter, A. Besheer, Controlled shielding and deshielding of gene delivery polyplexes using hydroxyethyl starch (HES) and alpha-amylase, *Journal of controlled release : official journal of the Controlled Release Society*, 159 (2012) 92-103.
- [109] P. Heller, A. Birke, D. Huesmann, B. Weber, K. Fischer, A. Reske-Kunz, M. Bros, M. Barz, Introducing PeptoPlexes: Polylysine-block-Polysarcosine Based Polyplexes for Transfection of HEK 293T Cells, *Macromolecular bioscience*, (2014).
- [110] V. Subr, C. Konak, R. Laga, K. Ulbrich, Coating of DNA/poly(L-lysine) complexes by covalent attachment of poly[N-(2-hydroxypropyl)methacrylamide], *Biomacromolecules*, 7 (2006) 122-130.
- [111] I. Mellman, R. Fuchs, A. Helenius, Acidification of the endocytic and exocytic pathways, *Annual review of biochemistry*, 55 (1986) 663-700.
- [112] F.R. Maxfield, T.E. McGraw, Endocytic recycling, *Nature reviews. Molecular cell biology*, 5 (2004) 121-132.
- [113] E. Wagner, K. Zatloukal, M. Cotten, H. Kirlappos, K. Mechtler, D.T. Curiel, M.L. Birnstiel, Coupling of adenovirus to transferrin-polylysine/DNA complexes greatly enhances receptor-mediated gene delivery and expression of transfected genes, *Proceedings of the National Academy of Sciences of the United States of America*, 89 (1992) 6099-6103.

- [114] C. Plank, B. Oberhauser, K. Mechtler, C. Koch, E. Wagner, The influence of endosome-disruptive peptides on gene transfer using synthetic virus-like gene transfer systems, *The Journal of biological chemistry*, 269 (1994) 12918-12924.
- [115] C. Dohmen, D. Edinger, T. Fröhlich, L. Schreiner, U. Lachelt, C. Troiber, J. Radler, P. Hadwiger, H.P. Vornlocher, E. Wagner, Nanosized multifunctional polyplexes for receptor-mediated siRNA delivery, *ACS nano*, 6 (2012) 5198-5208.
- [116] D.B. Rozema, K. Ekena, D.L. Lewis, A.G. Loomis, J.A. Wolff, Endosomolysis by masking of a membrane-active agent (EMMA) for cytoplasmic release of macromolecules, *Bioconjugate chemistry*, 14 (2003) 51-57.
- [117] M. Meyer, A. Philipp, R. Oskuee, C. Schmidt, E. Wagner, Breathing life into polycations: functionalization with pH-responsive endosomolytic peptides and polyethylene glycol enables siRNA delivery, *Journal of the American Chemical Society*, 130 (2008) 3272-3273.
- [118] T.B. Wyman, F. Nicol, O. Zelphati, P.V. Scaria, C. Plank, F.C. Szoka, Jr., Design, synthesis, and characterization of a cationic peptide that binds to nucleic acids and permeabilizes bilayers, *Biochemistry*, 36 (1997) 3008-3017.
- [119] W. Li, F. Nicol, F.C. Szoka, Jr., GALA: a designed synthetic pH-responsive amphipathic peptide with applications in drug and gene delivery, *Advanced drug delivery reviews*, 56 (2004) 967-985.
- [120] S.M. Shaheen, H. Akita, T. Nakamura, S. Takayama, S. Futaki, A. Yamashita, R. Katoono, N. Yui, H. Harashima, KALA-modified multi-layered nanoparticles as gene carriers for MHC class-I mediated antigen presentation for a DNA vaccine, *Biomaterials*, 32 (2011) 6342-6350.
- [121] T. Fröhlich, D. Edinger, R. Kläger, C. Troiber, E. Salcher, N. Badgujar, I. Martin, D. Schaffert, A. Cengizeroglu, P. Hadwiger, H.P. Vornlocher, E. Wagner, Structure-activity relationships of siRNA carriers based on sequence-defined oligo (ethane amino) amides, *Journal of controlled release : official journal of the Controlled Release Society*, 160 (2012) 532-541.
- [122] J. Kloeckner, L. Prasmickaite, A. Hogset, K. Berg, E. Wagner, Photochemically enhanced gene delivery of EGF receptor-targeted DNA polyplexes, *Journal of drug targeting*, 12 (2004) 205-213.
- [123] K.G. de Bruin, C. Fella, M. Ogris, E. Wagner, N. Ruthardt, C. Bräuchle, Dynamics of photoinduced endosomal release of polyplexes, *Journal of controlled release : official journal of the Controlled Release Society*, 130 (2008) 175-182.
- [124] M. Zenke, P. Steinlein, E. Wagner, M. Cotten, H. Beug, M.L. Birnstiel, Receptor-mediated endocytosis of transferrin-polycation conjugates: an efficient way to introduce DNA into hematopoietic cells, *Proceedings of the National Academy of Sciences of the United States of America*, 87 (1990) 3655-3659.
- [125] A. Barnard, P. Posocco, S. Pricl, M. Calderon, R. Haag, M.E. Hwang, V.W. Shum, D.W. Pack, D.K. Smith, Degradable self-assembling dendrons for gene delivery: experimental and theoretical insights into the barriers to cellular uptake, *Journal of the American Chemical Society*, 133 (2011) 20288-20300.
- [126] I. Martin, C. Dohmen, C. Mas-Moruno, C. Troiber, P. Kos, D. Schaffert, U. Lachelt, M. Teixido, M. Gunther, H. Kessler, E. Giralto, E. Wagner, Solid-phase-assisted synthesis of targeting peptide-PEG-oligo(ethane amino)amides for receptor-mediated gene delivery, *Organic & biomolecular chemistry*, 10 (2012) 3258-3268.
- [127] V. Sanz, H.M. Coley, S.R. Silva, J. McFadden, Protamine and chloroquine enhance gene delivery and expression mediated by RNA-wrapped single walled carbon nanotubes, *Journal of nanoscience and nanotechnology*, 12 (2012) 1739-1747.

- [128] S.E. Andaloussi, T. Lehto, I. Mager, K. Rosenthal-Aizman, Oprea, II, O.E. Simonson, H. Sork, K. Ezzat, D.M. Copolovici, K. Kurrikoff, J.R. Viola, E.M. Zaghloul, R. Sillard, H.J. Johansson, F. Said Hassane, P. Guterstam, J. Suhorutsenko, P.M. Moreno, N. Oskolkov, J. Halldin, U. Tedebark, A. Metspalu, B. Lebleu, J. Lehtio, C.I. Smith, U. Langel, Design of a peptide-based vector, PepFect6, for efficient delivery of siRNA in cell culture and systemically in vivo, *Nucleic acids research*, 39 (2011) 3972-3987.
- [129] I.A. Khalil, K. Kogure, H. Akita, H. Harashima, Uptake pathways and subsequent intracellular trafficking in nonviral gene delivery, *Pharmacological reviews*, 58 (2006) 32-45.
- [130] J.-P. Behr, The Proton Sponge: a Trick to Enter Cells the Viruses Did Not Exploit, *CHIMIA International Journal for Chemistry*, 51 (1997) 34-36.
- [131] A. Kichler, C. Leborgne, E. Coeytaux, O. Danos, Polyethylenimine-mediated gene delivery: a mechanistic study, *The journal of gene medicine*, 3 (2001) 135-144.
- [132] P. Midoux, M. Monsigny, Efficient gene transfer by histidylated polylysine/pDNA complexes, *Bioconjugate chemistry*, 10 (1999) 406-411.
- [133] Q. Leng, A.J. Mixson, Modified branched peptides with a histidine-rich tail enhance in vitro gene transfection, *Nucleic acids research*, 33 (2005) e40.
- [134] J. Shi, J.G. Schellinger, R.N. Johnson, J.L. Choi, B. Chou, E.L. Anghel, S.H. Pun, Influence of histidine incorporation on buffer capacity and gene transfection efficiency of HPMa-co-oligolysine brush polymers, *Biomacromolecules*, 14 (2013) 1961-1970.
- [135] C.H. Jones, C.K. Chen, A. Ravikrishnan, S. Rane, B.A. Pfeifer, Overcoming nonviral gene delivery barriers: perspective and future, *Molecular pharmaceuticals*, 10 (2013) 4082-4098.
- [136] R.V. Benjaminsen, M.A. Matthebjerg, J.R. Henriksen, S.M. Moghimi, T.L. Andresen, The possible "proton sponge" effect of polyethylenimine (PEI) does not include change in lysosomal pH, *Molecular therapy : the journal of the American Society of Gene Therapy*, 21 (2013) 149-157.
- [137] Z. ur Rehman, D. Hoekstra, I.S. Zuhorn, Mechanism of polyplex- and lipoplex-mediated delivery of nucleic acids: real-time visualization of transient membrane destabilization without endosomal lysis, *ACS nano*, 7 (2013) 3767-3777.
- [138] A.M. Funhoff, C.F. van Nostrum, G.A. Koning, N.M. Schuurmans-Nieuwenbroek, D.J. Crommelin, W.E. Hennink, Endosomal escape of polymeric gene delivery complexes is not always enhanced by polymers buffering at low pH, *Biomacromolecules*, 5 (2004) 32-39.
- [139] M.R. Capecchi, High efficiency transformation by direct microinjection of DNA into cultured mammalian cells, *Cell*, 22 (1980) 479-488.
- [140] H. Pollard, J.S. Remy, G. Loussouarn, S. Demolombe, J.P. Behr, D. Escande, Polyethylenimine but not cationic lipids promotes transgene delivery to the nucleus in mammalian cells, *The Journal of biological chemistry*, 273 (1998) 7507-7511.
- [141] G. Grandinetti, T.M. Reineke, Exploring the mechanism of plasmid DNA nuclear internalization with polymer-based vehicles, *Molecular pharmaceuticals*, 9 (2012) 2256-2267.
- [142] A. Nomani, Z. Hyvonen, E. Pulkkinen, M. Hiekkala, M. Ruponen, Intracellular gene delivery is dependent on the type of non-viral carrier and defined by the cell surface glycosaminoglycans, *Journal of controlled release : official journal of the Controlled Release Society*, 187 (2014) 59-65.
- [143] M.A. Zanta, P. Belguise-Valladier, J.P. Behr, Gene delivery: a single nuclear localization signal peptide is sufficient to carry DNA to the cell nucleus, *Proceedings*

- of the National Academy of Sciences of the United States of America, 96 (1999) 91-96.
- [144] Q. Hu, J. Wang, J. Shen, M. Liu, X. Jin, G. Tang, P.K. Chu, Intracellular pathways and nuclear localization signal peptide-mediated gene transfection by cationic polymeric nanovectors, *Biomaterials*, 33 (2012) 1135-1145.
- [145] M. Tanimoto, H. Kamiya, N. Minakawa, A. Matsuda, H. Harashima, No enhancement of nuclear entry by direct conjugation of a nuclear localization signal peptide to linearized DNA, *Bioconjugate chemistry*, 14 (2003) 1197-1202.
- [146] T. Nagasaki, T. Myohoji, T. Tachibana, S. Futaki, S. Tamagaki, Can nuclear localization signals enhance nuclear localization of plasmid DNA?, *Bioconjugate chemistry*, 14 (2003) 282-286.
- [147] M.A. van der Aa, G.A. Koning, C. d'Oliveira, R.S. Oosting, K.J. Wilschut, W.E. Hennink, D.J. Crommelin, An NLS peptide covalently linked to linear DNA does not enhance transfection efficiency of cationic polymer based gene delivery systems, *The journal of gene medicine*, 7 (2005) 208-217.
- [148] K. Itaka, A. Harada, Y. Yamasaki, K. Nakamura, H. Kawaguchi, K. Kataoka, In situ single cell observation by fluorescence resonance energy transfer reveals fast intra-cytoplasmic delivery and easy release of plasmid DNA complexed with linear polyethylenimine, *The journal of gene medicine*, 6 (2004) 76-84.
- [149] P.M. Klein, E. Wagner, Bioreducible polycations as shuttles for therapeutic nucleic acid and protein transfection, *Antioxidants & redox signaling*, 21 (2014) 804-817.
- [150] S. Bauhuber, C. Hozsa, M. Breunig, A. Gopferich, Delivery of nucleic acids via disulfide-based carrier systems, *Advanced materials*, 21 (2009) 3286-3306.
- [151] D. Soundara Manickam, D. Oupicky, Polyplex gene delivery modulated by redox potential gradients, *Journal of drug targeting*, 14 (2006) 519-526.
- [152] D.L. McKenzie, K.Y. Kwok, K.G. Rice, A potent new class of reductively activated peptide gene delivery agents, *The Journal of biological chemistry*, 275 (2000) 9970-9977.
- [153] M. Breunig, U. Lungwitz, R. Liebl, A. Gopferich, Breaking up the correlation between efficacy and toxicity for nonviral gene delivery, *Proceedings of the National Academy of Sciences of the United States of America*, 104 (2007) 14454-14459.
- [154] D. Schaffert, C. Troiber, E. Wagner, New sequence-defined polyaminoamides with tailored endosomolytic properties for plasmid DNA delivery, *Bioconjugate chemistry*, 23 (2012) 1157-1165.
- [155] E.E. Salcher, P. Kos, T. Frohlich, N. Badgujar, M. Scheible, E. Wagner, Sequence-defined four-arm oligo(ethan amino)amides for pDNA and siRNA delivery: Impact of building blocks on efficacy, *Journal of controlled release : official journal of the Controlled Release Society*, 164 (2012) 380-386.
- [156] L. Wightman, R. Kircheis, V. Rossler, S. Carotta, R. Ruzicka, M. Kurs, E. Wagner, Different behavior of branched and linear polyethylenimine for gene delivery in vitro and in vivo, *The journal of gene medicine*, 3 (2001) 362-372.
- [157] S. Werth, B. Urban-Klein, L. Dai, S. Hobel, M. Grzelinski, U. Bakowsky, F. Czubyko, A. Aigner, A low molecular weight fraction of polyethylenimine (PEI) displays increased transfection efficiency of DNA and siRNA in fresh or lyophilized complexes, *Journal of controlled release : official journal of the Controlled Release Society*, 112 (2006) 257-270.
- [158] G.J. Jeong, H.M. Byun, J.M. Kim, H. Yoon, H.G. Choi, W.K. Kim, S.J. Kim, Y.K. Oh, Biodistribution and tissue expression kinetics of plasmid DNA complexed with

- polyethylenimines of different molecular weight and structure, *Journal of controlled release : official journal of the Controlled Release Society*, 118 (2007) 118-125.
- [159] C. Scholz, P. Kos, E. Wagner, Comb-like oligoaminoethane carriers: change in topology improves pDNA delivery, *Bioconjugate chemistry*, 25 (2014) 251-261.
- [160] R. Tang, R.N. Palumbo, L. Nagarajan, E. Krogstad, C. Wang, Well-defined block copolymers for gene delivery to dendritic cells: probing the effect of polycation chain-length, *Journal of controlled release : official journal of the Controlled Release Society*, 142 (2010) 229-237.
- [161] R.N. Johnson, D.S. Chu, J. Shi, J.G. Schellinger, P.M. Carlson, S.H. Pun, HPMA-oligolysine copolymers for gene delivery: optimization of peptide length and polymer molecular weight, *Journal of controlled release : official journal of the Controlled Release Society*, 155 (2011) 303-311.
- [162] H. Wei, J.A. Pahang, S.H. Pun, Optimization of brush-like cationic copolymers for nonviral gene delivery, *Biomacromolecules*, 14 (2013) 275-284.
- [163] D. Sprouse, T.M. Reineke, Investigating the effects of block versus statistical glycopolyocations containing primary and tertiary amines for plasmid DNA delivery, *Biomacromolecules*, 15 (2014) 2616-2628.
- [164] J.-F. Lutz, Sequence-controlled polymerizations: the next Holy Grail in polymer science?, *Polymer Chemistry*, 1 (2010) 55-62.
- [165] J. Niu, R. Hili, D.R. Liu, Enzyme-free translation of DNA into sequence-defined synthetic polymers structurally unrelated to nucleic acids, *Nature chemistry*, 5 (2013) 282-292.
- [166] R.B. Merrifield, Solid Phase Peptide Synthesis. I. The Synthesis of a Tetrapeptide, *Journal of the American Chemical Society*, 85 (1963) 2149-2154.
- [167] L. Hartmann, E. Krause, M. Antonietti, H.G. Borner, Solid-phase supported polymer synthesis of sequence-defined, multifunctional poly(amidoamines), *Biomacromolecules*, 7 (2006) 1239-1244.
- [168] L. Hartmann, S. Hafele, R. Peschka-Suss, M. Antonietti, H.G. Borner, Tailor-made poly(amidoamine)s for controlled complexation and condensation of DNA, *Chemistry*, 14 (2008) 2025-2033.
- [169] D. Schaffert, N. Badgujar, E. Wagner, Novel Fmoc-polyamino acids for solid-phase synthesis of defined polyamidoamines, *Organic letters*, 13 (2011) 1586-1589.
- [170] D. Schaffert, C. Troiber, E.E. Salcher, T. Frohlich, I. Martin, N. Badgujar, C. Dohmen, D. Edinger, R. Klager, G. Maiwald, K. Farkasova, S. Seeber, K. Jahn-Hofmann, P. Hadwiger, E. Wagner, Solid-phase synthesis of sequence-defined T-, i-, and U-shape polymers for pDNA and siRNA delivery, *Angewandte Chemie*, 50 (2011) 8986-8989.
- [171] D.S. Pedersen, C. Rosenbohm, Dry Column Vacuum Chromatography, *Synthesis*, 2001 (2001) 2431-2434.
- [172] J. Cookson, M.S. Vickers, R.L. Paul, A.R. Cowley, P.D. Beer, Amide functionalised dithiocarbamate ruthenium(II) bis-bipyridyl receptors: A new class of redox-responsive anion sensor, *Inorganica Chimica Acta*, 361 (2008) 1689-1698.
- [173] G.J. Berchet, METHYLIMINODIACETIC ACID, *Organic Syntheses*, 18 (1938) 56.
- [174] E. Kaiser, R.L. Colescott, C.D. Bossinger, P.I. Cook, Color test for detection of free terminal amino groups in the solid-phase synthesis of peptides, *Analytical Biochemistry*, 34 (1970) 595-598.
- [175] H. Xia, B. Anderson, Q. Mao, B.L. Davidson, Recombinant human adenovirus: targeting to the human transferrin receptor improves gene transfer to brain microcapillary endothelium, *Journal of virology*, 74 (2000) 11359-11366.

- [176] P. Zhao, T. Grabinski, C. Gao, R.S. Skinner, T. Giambernardi, Y. Su, E. Hudson, J. Resau, M. Gross, G.F. Vande Woude, R. Hay, B. Cao, Identification of a met-binding peptide from a phage display library, *Clinical cancer research : an official journal of the American Association for Cancer Research*, 13 (2007) 6049-6055.
- [177] K. Kim, Y. Hur, E.K. Ryu, J.H. Rhim, C.Y. Choi, C.M. Baek, J.H. Lee, J. Chung, A neutralizable epitope is induced on HGF upon its interaction with its receptor cMet, *Biochemical and biophysical research communications*, 354 (2007) 115-121.
- [178] E.M. Kim, E.H. Park, S.J. Cheong, C.M. Lee, D.W. Kim, H.J. Jeong, S.T. Lim, M.H. Sohn, K. Kim, J. Chung, Characterization, biodistribution and small-animal SPECT of I-125-labeled c-Met binding peptide in mice bearing c-Met receptor tyrosine kinase-positive tumor xenografts, *Nuclear medicine and biology*, 36 (2009) 371-378.
- [179] E.M. Kim, E.H. Park, S.J. Cheong, C.M. Lee, H.J. Jeong, D.W. Kim, S.T. Lim, M.H. Sohn, In vivo imaging of mesenchymal-epithelial transition factor (c-Met) expression using an optical imaging system, *Bioconjugate chemistry*, 20 (2009) 1299-1306.
- [180] B.W. Bycroft, W.C. Chan, S.R. Chhabra, N.D. Hone, A novel lysine-protecting procedure for continuous flow solid phase synthesis of branched peptides, *Journal of the Chemical Society, Chemical Communications*, (1993) 778-779.
- [181] S.R. Chhabra, B. Hothi, D.J. Evans, P.D. White, B.W. Bycroft, W.C. Chan, An appraisal of new variants of Dde amine protecting group for solid phase peptide synthesis, *Tetrahedron Letters*, 39 (1998) 1603-1606.
- [182] Z. Wang, Zemplén Deacetylation, in: *Comprehensive Organic Name Reactions and Reagents*, John Wiley & Sons, Inc., 2010.
- [183] U. Lächelt, P. Kos, F.M. Mickler, A. Herrmann, E.E. Salcher, W. Rödl, N. Badgujar, C. Bräuchle, E. Wagner, Fine-tuning of proton sponges by precise diaminoethanes and histidines in pDNA polyplexes, *Nanomedicine : nanotechnology, biology, and medicine*, 10 (2014) 35-44.
- [184] R.J.L. Andon, J.D. Cox, E.F.G. Herington, The ultra-violet absorption spectra and dissociation constants of certain pyridine bases in aqueous solution, *Transactions of the Faraday Society*, 50 (1954) 918-927.
- [185] B. Peruzzi, D.P. Bottaro, Targeting the c-Met signaling pathway in cancer, *Clinical cancer research : an official journal of the American Association for Cancer Research*, 12 (2006) 3657-3660.
- [186] C. Birchmeier, W. Birchmeier, E. Gherardi, G.F. Vande Woude, Met, metastasis, motility and more, *Nature reviews. Molecular cell biology*, 4 (2003) 915-925.
- [187] D.L. Jardim, D. de Melo Gagliato, G. Falchook, R. Zinner, J.J. Wheler, F. Janku, V. Subbiah, S.A. Piha-Paul, S. Fu, N. Tannir, P. Corn, C. Tang, K. Hess, S. Roy-Chowdhuri, R. Kurzrock, F. Meric-Bernstam, D.S. Hong, MET Abnormalities in Patients With Genitourinary Malignancies and Outcomes With c-MET Inhibitors, *Clinical genitourinary cancer*, (2014).
- [188] X. An, F. Wang, Q. Shao, F.H. Wang, Z.Q. Wang, Z.Q. Wang, C. Chen, C. Li, H.Y. Luo, D.S. Zhang, R.H. Xu, Y.H. Li, MET amplification is not rare and predicts unfavorable clinical outcomes in patients with recurrent/metastatic gastric cancer after chemotherapy, *Cancer*, 120 (2014) 675-682.
- [189] H. Ozasa, T. Oguri, K. Maeno, O. Takakuwa, E. Kunii, Y. Yagi, T. Uemura, D. Kasai, M. Miyazaki, A. Niimi, Significance of c-MET overexpression in cytotoxic anticancer drug-resistant small-cell lung cancer cells, *Cancer science*, 105 (2014) 1032-1039.

- [190] M.J. Vosjan, J. Vercammen, J.A. Kolkman, M. Stigter-van Walsum, H. Revets, G.A. van Dongen, Nanobodies targeting the hepatocyte growth factor: potential new drugs for molecular cancer therapy, *Molecular cancer therapeutics*, 11 (2012) 1017-1025.
- [191] R.V. Hay, B. Cao, R.S. Skinner, Y. Su, P. Zhao, M.F. Gustafson, C.N. Qian, B.T. Teh, B.S. Knudsen, J.H. Resau, S. Shen, D.J. Waters, M.D. Gross, G.F. Vande Woude, Nuclear imaging of Met-expressing human and canine cancer xenografts with radiolabeled monoclonal antibodies (MetSeek), *Clinical cancer research : an official journal of the American Association for Cancer Research*, 11 (2005) 7064s-7069s.
- [192] A. Petrelli, P. Circosta, L. Granziero, M. Mazzone, A. Pisacane, S. Fenoglio, P.M. Comoglio, S. Giordano, Ab-induced ectodomain shedding mediates hepatocyte growth factor receptor down-regulation and hampers biological activity, *Proceedings of the National Academy of Sciences of the United States of America*, 103 (2006) 5090-5095.
- [193] X. Chen, G. Ding, Q. Gao, J. Sun, Q. Zhang, L. Du, Z. Qiu, C. Wang, F. Zheng, B. Sun, J. Ni, Z. Feng, J. Zhu, A human anti-c-Met Fab fragment conjugated with doxorubicin as targeted chemotherapy for hepatocellular carcinoma, *PLoS one*, 8 (2013) e63093.
- [194] T.H. Nguyen, N. Loux, I. Dagher, C. Vons, K. Carey, P. Briand, M. Hadchouel, D. Franco, J. Jouanneau, R. Schwall, A. Weber, Improved gene transfer selectivity to hepatocarcinoma cells by retrovirus vector displaying single-chain variable fragment antibody against c-Met, *Cancer gene therapy*, 10 (2003) 840-849.
- [195] N.E. Hynes, H.A. Lane, ERBB receptors and cancer: the complexity of targeted inhibitors, *Nature reviews. Cancer*, 5 (2005) 341-354.
- [196] C.R. Chong, P.A. Janne, The quest to overcome resistance to EGFR-targeted therapies in cancer, *Nature medicine*, 19 (2013) 1389-1400.
- [197] S.V. Sharma, D.W. Bell, J. Settleman, D.A. Haber, Epidermal growth factor receptor mutations in lung cancer, *Nature reviews. Cancer*, 7 (2007) 169-181.
- [198] S. Panowski, S. Bhakta, H. Raab, P. Polakis, J.R. Junutula, Site-specific antibody drug conjugates for cancer therapy, *mAbs*, 6 (2014) 34-45.
- [199] T.H. Pillow, J. Tien, K.L. Parsons-Reponte, S. Bhakta, H. Li, L.R. Staben, G. Li, J. Chuh, A. Fourie-O'Donohue, M. Darwish, V. Yip, L. Liu, D.D. Leipold, D. Su, E. Wu, S.D. Spencer, B.Q. Shen, K. Xu, K.R. Kozak, H. Raab, R. Vandlen, G.D. Lewis-Phillips, R.H. Scheller, P. Polakis, M. Sliwkowski, J. Flygare, J.R. Junutula, Site-Specific Trastuzumab Maytansinoid Antibody-Drug Conjugates with Improved Therapeutic Activity through Linker and Antibody Engineering, *Journal of medicinal chemistry*, (2014).
- [200] D. Cretella, F. Sacconi, F. Quaini, C. Frati, C. Lagrasta, M. Bonelli, C. Caffarra, A. Cavazzoni, C. Fumarola, M. Galetti, S. La Monica, L. Ampollini, M. Tiseo, A. Ardizzoni, P.G. Petronini, R.R. Alfieri, Trastuzumab emtansine is active on HER-2 overexpressing NSCLC cell lines and overcomes gefitinib resistance, *Molecular cancer*, 13 (2014) 143.
- [201] A. Schafer, A. Pahnke, D. Schaffert, W.M. van Weerden, C.M. de Ridder, W. Rodl, A. Vetter, C. Spitzweg, R. Kraaij, E. Wagner, M. Ogris, Disconnecting the yin and yang relation of epidermal growth factor receptor (EGFR)-mediated delivery: a fully synthetic, EGFR-targeted gene transfer system avoiding receptor activation, *Human gene therapy*, 22 (2011) 1463-1473.

- [202] T. Blessing, M. Kursa, R. Holzhauser, R. Kircheis, E. Wagner, Different strategies for formation of pegylated EGF-conjugated PEI/DNA complexes for targeted gene delivery, *Bioconjugate chemistry*, 12 (2001) 529-537.
- [203] N. Ruthardt, D.C. Lamb, C. Bräuchle, Single-particle tracking as a quantitative microscopy-based approach to unravel cell entry mechanisms of viruses and pharmaceutical nanoparticles, *Molecular therapy : the journal of the American Society of Gene Therapy*, 19 (2011) 1199-1211.
- [204] G. Ashwell, A.G. Morell, The role of surface carbohydrates in the hepatic recognition and transport of circulating glycoproteins, *Advances in enzymology and related areas of molecular biology*, 41 (1974) 99-128.
- [205] G. Ashwell, J. Harford, Carbohydrate-specific receptors of the liver, *Annual review of biochemistry*, 51 (1982) 531-554.
- [206] S. Kawakami, F. Yamashita, M. Nishikawa, Y. Takakura, M. Hashida, Asialoglycoprotein receptor-mediated gene transfer using novel galactosylated cationic liposomes, *Biochemical and biophysical research communications*, 252 (1998) 78-83.
- [207] M.A. Maier, C.G. Yannopoulos, N. Mohamed, A. Roland, H. Fritz, V. Mohan, G. Just, M. Manoharan, Synthesis of antisense oligonucleotides conjugated to a multivalent carbohydrate cluster for cellular targeting, *Bioconjugate chemistry*, 14 (2003) 18-29.
- [208] C. Managit, S. Kawakami, F. Yamashita, M. Hashida, Effect of galactose density on asialoglycoprotein receptor-mediated uptake of galactosylated liposomes, *Journal of pharmaceutical sciences*, 94 (2005) 2266-2275.
- [209] P.H. Weigel, J.H. Yik, Glycans as endocytosis signals: the cases of the asialoglycoprotein and hyaluronan/chondroitin sulfate receptors, *Biochimica et biophysica acta*, 1572 (2002) 341-363.
- [210] F. Wojcik, S. Lel, A.G. O'Brien, P.H. Seeberger, L. Hartmann, Synthesis of homo- and heteromultivalent carbohydrate-functionalized oligo(amidoamines) using novel glyco-building blocks, *Beilstein journal of organic chemistry*, 9 (2013) 2395-2403.
- [211] F. Wojcik, A.G. O'Brien, S. Gotze, P.H. Seeberger, L. Hartmann, Synthesis of carbohydrate-functionalised sequence-defined oligo(amidoamine)s by photochemical thiol-ene coupling in a continuous flow reactor, *Chemistry*, 19 (2013) 3090-3098.
- [212] M. Meier, M.D. Bider, V.N. Malashkevich, M. Spiess, P. Burkhard, Crystal structure of the carbohydrate recognition domain of the H1 subunit of the asialoglycoprotein receptor, *Journal of molecular biology*, 300 (2000) 857-865.
- [213] D.R. Elias, A. Poloukhine, V. Popik, A. Tsourkas, Effect of ligand density, receptor density, and nanoparticle size on cell targeting, *Nanomedicine : nanotechnology, biology, and medicine*, 9 (2013) 194-201.
- [214] U. Lächelt, V. Wittmann, K. Muller, D. Edinger, P. Kos, M. Höhn, E. Wagner, Synthetic polyglutamylation of dual-functional MTX ligands for enhanced combined cytotoxicity of poly(I:C) nanoplexes, *Molecular pharmaceuticals*, 11 (2014) 2631-2639.
- [215] K. Miyata, N. Nishiyama, K. Kataoka, Rational design of smart supramolecular assemblies for gene delivery: chemical challenges in the creation of artificial viruses, *Chemical Society reviews*, 41 (2012) 2562-2574.
- [216] M. Bello Roufai, P. Midoux, Histidylated polylysine as DNA vector: elevation of the imidazole protonation and reduced cellular uptake without change in the polyfection efficiency of serum stabilized negative polyplexes, *Bioconjugate chemistry*, 12 (2001) 92-99.

- [217] S. Asayama, A. Hamaya, T. Sekine, H. Kawakami, S. Nagaoka, Aminated poly(L-histidine) as new pH-sensitive DNA carrier, *Nucleic acids symposium series*, (2004) 229-230.
- [218] J.M. Bennis, J.S. Choi, R.I. Mahato, J.S. Park, S.W. Kim, pH-sensitive cationic polymer gene delivery vehicle: N-Ac-poly(L-histidine)-graft-poly(L-lysine) comb shaped polymer, *Bioconjugate chemistry*, 11 (2000) 637-645.
- [219] C.K. Choudhury, S. Roy, Structural and dynamical properties of polyethylenimine in explicit water at different protonation states: a molecular dynamics study, *Soft Matter*, 9 (2013) 2269-2281.
- [220] A. Bencini, A. Bianchi, Enrique, M. Micheloni, J.A. Ramirez, Proton coordination by polyamine compounds in aqueous solution, *Coordination Chemistry Reviews*, 188 (1999) 97-156.
- [221] H. Uchida, K. Itaka, T. Nomoto, T. Ishii, T. Suma, M. Ikegami, K. Miyata, M. Oba, N. Nishiyama, K. Kataoka, Modulated protonation of side chain aminoethylene repeats in N-substituted polyaspartamides promotes mRNA transfection, *Journal of the American Chemical Society*, 136 (2014) 12396-12405.
- [222] C.C. Cain, D.M. Sipe, R.F. Murphy, Regulation of endocytic pH by the Na⁺,K⁺-ATPase in living cells, *Proceedings of the National Academy of Sciences of the United States of America*, 86 (1989) 544-548.
- [223] L. Henriksen, M.V. Grandal, S.L. Knudsen, B. van Deurs, L.M. Grovdal, Internalization mechanisms of the epidermal growth factor receptor after activation with different ligands, *PloS one*, 8 (2013) e58148.
- [224] R.T. Lee, Y.C. Lee, Facile synthesis of a high-affinity ligand for mammalian hepatic lectin containing three terminal N-acetylgalactosamine residues, *Bioconjugate chemistry*, 8 (1997) 762-765.
- [225] P.C. Rensen, L.A. Sliedregt, M. Ferns, E. Kieviet, S.M. van Rossenberg, S.H. van Leeuwen, T.J. van Berkel, E.A. Biessen, Determination of the upper size limit for uptake and processing of ligands by the asialoglycoprotein receptor on hepatocytes in vitro and in vivo, *The Journal of biological chemistry*, 276 (2001) 37577-37584.
- [226] G.D. Girnun, E. Naseri, S.B. Vafai, L. Qu, J.D. Szwaya, R. Bronson, J.A. Alberta, B.M. Spiegelman, Synergy between PPAR γ ligands and platinum-based drugs in cancer, *Cancer cell*, 11 (2007) 395-406.
- [227] S. Kummar, H.X. Chen, J. Wright, S. Holbeck, M.D. Millin, J. Tomaszewski, J. Zweibel, J. Collins, J.H. Doroshow, Utilizing targeted cancer therapeutic agents in combination: novel approaches and urgent requirements, *Nature reviews. Drug discovery*, 9 (2010) 843-856.
- [228] P.S. Oak, F. Kopp, C. Thakur, J.W. Ellwart, U.R. Rapp, A. Ullrich, E. Wagner, P. Knyazev, A. Roidl, Combinatorial treatment of mammospheres with trastuzumab and salinomycin efficiently targets HER2-positive cancer cells and cancer stem cells, *International journal of cancer. Journal international du cancer*, 131 (2012) 2808-2819.
- [229] D.E. Fisher, Apoptosis in cancer therapy: crossing the threshold, *Cell*, 78 (1994) 539-542.
- [230] A.S. Wibowo, M. Singh, K.M. Reeder, J.J. Carter, A.R. Kovach, W. Meng, M. Ratnam, F. Zhang, C.E. Dann, 3rd, Structures of human folate receptors reveal biological trafficking states and diversity in folate and antifolate recognition, *Proceedings of the National Academy of Sciences of the United States of America*, 110 (2013) 15180-15188.
- [231] C. Muller, R. Schibli, Prospects in folate receptor-targeted radionuclide therapy, *Frontiers in oncology*, 3 (2013) 249.

- [232] C.P. Leamon, I.R. Vlahov, J.A. Reddy, M. Vetzal, H.K. Santhapuram, F. You, A. Bloomfield, R. Dorton, M. Nelson, P. Kleindl, J.F. Vaughn, E. Westrick, Folate-vinca alkaloid conjugates for cancer therapy: a structure-activity relationship, *Bioconjugate chemistry*, 25 (2014) 560-568.
- [233] T.P. Thomas, B. Huang, S.K. Choi, J.E. Silpe, A. Kotlyar, A.M. Desai, H. Zong, J. Gam, M. Joice, J.R. Baker, Jr., Polyvalent dendrimer-methotrexate as a folate receptor-targeted cancer therapeutic, *Molecular pharmaceuticals*, 9 (2012) 2669-2676.
- [234] S.M. Moghimi, P. Symonds, J.C. Murray, A.C. Hunter, G. Debska, A. Szewczyk, A two-stage poly(ethylenimine)-mediated cytotoxicity: implications for gene transfer/therapy, *Molecular therapy : the journal of the American Society of Gene Therapy*, 11 (2005) 990-995.
- [235] A. Hall, A.K. Larsen, L. Parhamifar, K.D. Meyle, L.P. Wu, S.M. Moghimi, High resolution respirometry analysis of polyethylenimine-mediated mitochondrial energy crisis and cellular stress: Mitochondrial proton leak and inhibition of the electron transport system, *Biochimica et biophysica acta*, 1827 (2013) 1213-1225.
- [236] Z. Liu, X. Gao, T. Kang, M. Jiang, D. Miao, G. Gu, Q. Hu, Q. Song, L. Yao, Y. Tu, H. Chen, X. Jiang, J. Chen, B6 peptide-modified PEG-PLA nanoparticles for enhanced brain delivery of neuroprotective peptide, *Bioconjugate chemistry*, 24 (2013) 997-1007.

8 Publications

Original articles

Kos P, **Lächelt U**, He D, Nie Y, Gu Z, Wagner E. *Dual-targeted polyplexes based on sequence-defined peptide-PEG-oligoaminoamides*. J Pharm Sci. 2014 Sep 29; in press. doi: 10.1002/jps.24194.

Lächelt U, Wittmann V, Müller K, Edinger D, Kos P, Hoehn M, Wagner E. *Synthetic polyglutamylation of dual-functional MTX Ligands for enhanced combined cytotoxicity of poly(I:C) nanoplexes*. Mol Pharm. 2014 Aug 4; 11(8):2631-9. doi: 10.1021/mp500017u.

Zhang CY*, Kos P*, Müller K, Schimpf W, Troiber C, **Lächelt U**, Scholz C, Lamb DC, Wagner E. *Native chemical ligation for conversion of sequence-defined oligomers into targeted pDNA and siRNA carriers*. J Control Release. 2014 Feb 22; 180:42-50. doi: 10.1016/j.jconrel.2014.02.015.

Lächelt U, Kos P, Mickler FM, Herrmann A, Salcher EE, Rödl W, Badgujar N, Bräuchle C, Wagner E. *Fine-tuning of proton sponges by precise diaminoethanes and histidines in pDNA polyplexes*. Nanomedicine NBM. 2014 Jan; 10(1):35-44. doi: 10.1016/j.nano.2013.07.008.

Dohmen C, Edinger D, Fröhlich T, Schreiner L, **Lächelt U**, Troiber C, Rädler J, Hadwiger P, Vornlocher HP, Wagner E. *Nanosized multifunctional polyplexes for receptor-mediated siRNA delivery*. ACS Nano. 2012 Jun 26; 6(6):5198-208. doi: 10.1021/nn300960m.

Martin I, Dohmen C, Mas-Moruno C, Troiber C, Kos P, Schaffert D, **Lächelt U**, Teixidó M, Günther M, Kessler H, Giralto E, Wagner E. *Solid-phase-assisted synthesis of targeting peptide-PEG-oligo(ethane amino)amides for receptor-mediated gene delivery*. Org Biomol Chem. 2012 Apr 28; 10(16):3258-68. doi: 10.1039/c2ob06907e.

Dohmen C, Fröhlich T, **Lächelt U**, Röhl I, Vornlocher HP, Hadwiger P, Wagner E. *Defined Folate-PEG-siRNA Conjugates for Receptor-specific Gene Silencing*. Mol Ther Nucleic Acids. 2012 Jan 31; 1:e7. doi: 10.1038/mtna.2011.10.

Reviews

Lächelt U, Wagner E. *Invading target cells: multifunctional polymer conjugates as therapeutic nucleic acid carriers*, Frontiers Chem. Science Eng. 2011 Jul 19, 5: 275–286. doi: 10.1007/s11705-011-1203-z.

Manuscripts in preparation

Kos P*, **Lächelt U***, Herrmann A, Döblinger M, He D, Wagner E. *cMet-directed compacted polyplexes for tumor-targeted gene transfer in vivo*. Revised manuscript to be submitted.

Patent applications

Dohmen C, Günther M, **Lächelt U**, Schaffert D, Troiber C, Wagner E, *Polymers for Nucleic Acid Delivery*, European Patent Application (WO2011154331 A1).

Meeting abstracts and poster presentations

Lee DJ, **Lächelt U**, Edinger D, He D, Lehto T, Wagner E. *Nanosized Polyplexes with Dual-Functional MTX Ligand for Enhanced Combined Cytotoxicity with therapeutic Eg5 siRNA*. Walk and Talk at the Nanoscale, CeNS Workshop, Venice, Italy (September 2014).

Lächelt U, Kos P, Wagner E. *Sequence-defined nucleic acid carriers combining distinct modules for complexation, shielding, receptor-targeting and endosomal escape*. 3rd Symposium on Innovative Polymers for Controlled Delivery, Suzhou, China (September 2014).

Kos P, **Lächelt U**, Herrmann A, He Dongsheng, Wagner E. *Sequence-defined nanocarriers for c-Met receptor-directed gene transfer in vitro and in vivo*. 17th Annual Meeting of the American Society of Gene & Cell Therapy, Washington, USA (May 2014).

Kos P, **Lächelt U**, Mickler FM, Herrmann A, Wagner E. *Aiming at the bullseye: Pursuing the tumor-addressed gene delivery with sequence-defined nanocarriers comprising novel protein and peptidic targeting ligands*. XIX. Annual Meeting of German Society for Gene Therapy, Ulm, Germany (March 2014).

He D, Müller K, Kos P, Lee DJ, **Lächelt U**, Ernst Wagner. *Cargo-specific optimization of sequence defined non-viral nucleic acid carriers for folate receptor targeted pDNA or siRNA delivery*. XIX. Annual Meeting of German Society for Gene Therapy, Ulm, Germany (March 2014).

Broda E, **Lächelt U**, Mickler F, Wagner E, Bräuchle C. *Influences on cellular adhesion of nanoparticles under blood flow-like conditions*. 58. Annual Meeting of the Biophysical Society, San Francisco, USA (February 2014).

Kos P, Müller K, Zhang CY, Troiber C, **Lächelt U**, Scholz C, Wagner E. *Native chemical ligation for conversion of sequence-defined oligomers of different topologies into targeted pDNA and siRNA Carriers*. Young Ideas in Nanoscience, NIM Workshop, Munich, Germany (November 2013).

Kos P, Müller K, Zhang CY, Troiber C, **Lächelt U**, Scholz C, Wagner E. *Targeted sequence-defined oligomers of different topologies for pDNA and siRNA delivery synthesized via native chemical ligation*. Nanosciences: Great Adventures on Small Scales, CeNS Workshop, Venice, Italy (September 2013).

Lächelt U, Kos P, Herrmann A, Wagner E. *Proton sponge mechanism revisited and revised: Precise polymer DNA complexes for tumor-directed gene transfer*. XIX. Annual Meeting of German Society for Gene Therapy, Hamburg, Germany (February/March 2013).

Troiber C, Fröhlich T, Edinger D, Kläger R, Kos P, **Lächelt U**, Schaffert D, Wagner E. *Nucleic acid carriers for in vitro and in vivo delivery based on sequence-defined T-Shape Polymers*. 15th Annual Meeting of the American Society of Gene & Cell Therapy, Philadelphia, USA (May 2012).

Lächelt U, Dohmen C, Kos P, Martín I, Edinger D, Fröhlich T, Wagner E. *Step by step into the cell: A precise nucleic acid carrier incorporating distinct modules for complexation, shielding, targeting and endosomal escape*. 9th international symposium on polymer therapeutics, Valencia, Spain (May 2012).

Lächelt U, Dohmen C, Martín I, Kos P, Edinger D, Fröhlich T, Wagner E. *Facing barriers: a precise modular nucleic acid carrier to investigate shielding, targeting and endosomolytic performance*. Nanosciences: From Molecular Systems to Functional Materials, CeNS Workshop, Venice, Italy (2011).

9 Acknowledgements

Several appreciated persons made contribution to this thesis, either directly by collaboration and assistance in the lab or indirectly by keeping me happy the whole time. All people supporting me during my PhD study, at work or in my personal circle, deserve my deepest gratitude.

First of all, I would like to thank my supervisor Professor Dr. Ernst Wagner for giving me the opportunity to work on my thesis in his research group. I am deeply grateful for his support and careful guidance during the whole time, but also his encouragement for scientific creativity and the development of own ideas. I have learned much under his supervision.

I would like to thank our collaboration partners Prof. Dr. Christoph Bräuchle, Dr. Frauke Mickler and Ellen Broda for the close collaboration, conducting of sophisticated microscopy techniques and providing excellent imaging data.

Moreover, many thanks to our collaboration partners Prof. Dr. Laura Hartmann and Dr. Felix Wojcik for synthesizing and providing carbohydrate ligands as well as many fruitful discussions.

Special thanks to Petra whom I have been working closely together with during the whole period and who spend a lot of time in the cell culture for testing my (in many cases not working) compounds. Ana, Katharina and Ruth have taken over this job. I appreciate the excellent work of them all.

Many thanks to Annika and Eva for conducting *in vivo* animal experiments, which represent a highly significant part of our work.

I greatly appreciate the efforts of Dr. Martina Ruffer for the organization of all the teaching activities as well as the Christmas party and the traditional 'Weißwurst' and 'Krapfen' breakfast. And please, pass a 'thanks' to St. Nicholas for the steady chocolate supply in December.

Many thanks to our great team of technicians: Anna, Ursula and Melinda for keeping the everyday life in the lab running and making it enjoyable; Miriam for helping with the microscopy experiments and taking care of the administrative business recently;

Wolfgang for peptide synthesis as well as repairing almost any broken computer or scientific instrument and ensuring the technical maintenance; Markus, the 'lord of the mice', for taking care of the animals and creating a great atmosphere by helping with the PhD parties and BBQs; and finally Olga for taking care of the organizational and administrative matters.

Thanks to all the internship students, who helped and assisted in the lab. Especially I would like to thank Valentin for his great work and contribution during his master's thesis. Your help and ideas were essential for the success of our project.

Special thanks to Dongsheng for the oligomer synthesis and his contributions. Since the beginning of my PhD study, there has been a complete turn-over of PhD students. It is a pleasure to work together with all the new colleagues and I appreciate the good team atmosphere. Thanks to all the members of the Wagner lab!

I would also like to thank all the alumni, who gave me a warm welcome and helped to have a good start in the group. Special thanks to David and Christian D., who introduced me into the field and the lab work as well as Edith and Rebekka for their assistance in the corporate projects. Moreover, many thanks to my former lab-mates Kevin and Claudia for a great time together.

I want to thank my whole family and 'family-in-law', as well as my friends for being there and taking care – always. I am deeply grateful for the support of my parents and I appreciate their trust during all periods of my life. Thanks to Stephan and Christian for being my older brothers I can always count on and for teaching me useful things, such as crawling. Many thanks to Albi for his careful and labor-intensive proofreading of my thesis (under Oskar's supervision); very impressive, how fast you got acquainted with the 'chemistry slang'.

Finally, a thousand thanks to my beloved little family! Thank you, Tina, for your continuous support and your patience with a 'nerdy' fellow. This period must have been even more exhausting for you. Thank you, Oskar, for turning us into a little family and being such an enrichment of our life. Every single day, you put a smile on my face and remind me that little wonders exist, which are not scientifically explainable.